FORSCHUNGSZENTRUM ROSSENDORF FZR

WISSENSCHAFTLICH-TECHNISCHE BERICHTE
FZR-271
September 1999
ISSN 1437-322X

Institute of Nuclear and Hadron Physics

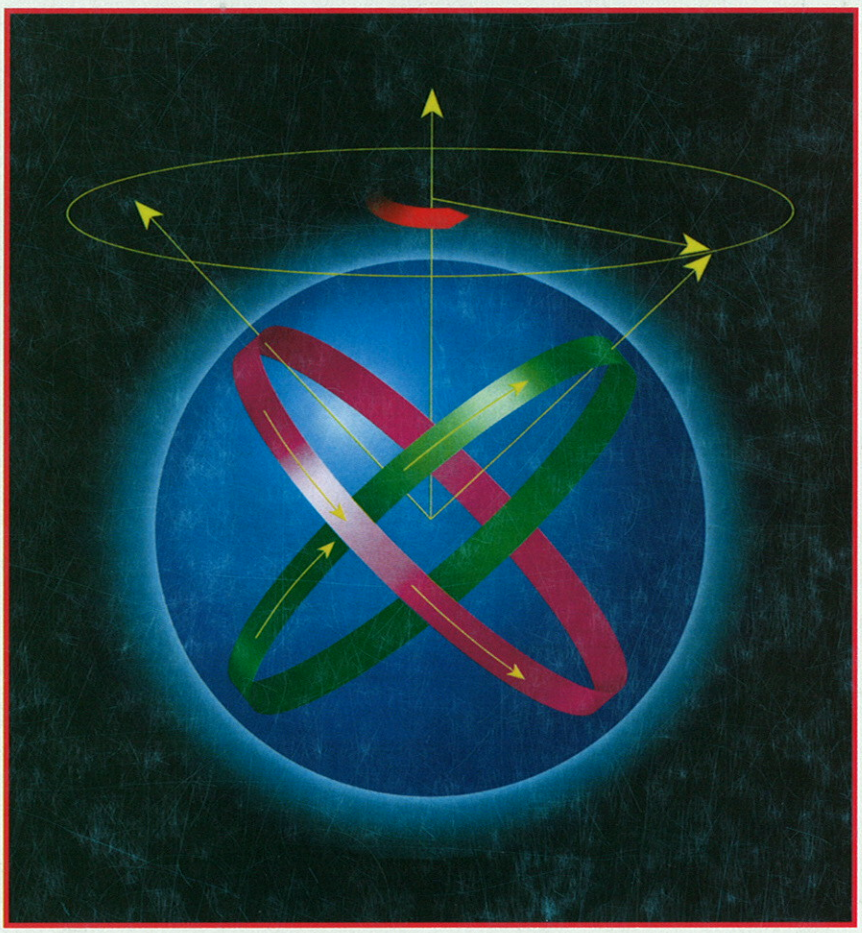

Report
January 1998 - June 1999

Cover Picture:
The cover picture illustrates the Magnetic-Rotation – a fundamentally new mode of nuclear rotation the physical concept of which was developed by the nuclear physics group in Rossendorf. More information on this phenomenon is presented in the contribution „Magnetic Rotation – rethinking nuclear structure" by S. Frauendorf.

The use of this cover picture was permitted by the editoral board of Physics World.

Forschungszentrum Rossendorf e.V.

Postfach 51 01 19
D-01314 Dresden
Bundesrepublik Deutschland

Telefon +49 (3 51) 2 60 22 70
Telefax +49 (3 51) 2 60 37 00
E-Mail E. Grosse@fz-rossendorf.de
Internet http://www.fz-rossendorf.de/FWK/

Als Manuskript gedruckt

FORSCHUNGSZENTRUM ROSSENDORF
WISSENSCHAFTLICH-TECHNISCHE BERICHTE
FZR-271
September 1999

Institute of Nuclear and Hadron Physics

Report

January 1998 - June 1999

Editors:
H.W. Barz, F. Dönau, W. Enghardt, E. Grosse, B. Kämpfer,
H. Prade, M. Schlett, R. Wünsch

Explanation of special symbols:

The letters given in brackets in the following text and used as appendix in the title of the scientific contributions do express our grateful acknowledgement to the funding, sponsoring or grants provided by several institutions.

Research projects were funded by the Federal Ministry of Education and Research BMBF (B), by the German Research Community DFG (D), by the GSI Darmstadt (G), by the KFA Jülich (K) and by the special program HSP III (H) or were sponsored within Scientific agreements with eastern European countries (W).

CONTENTS

Preface

The Forschungszentrum Rossendorf (FZR) at Dresden is a research center devoted to biomedical, environmental, materials, safety and nuclear research; it belongs to the Wissenschaftsgemeinschaft G. W. Leibniz (WGL), one of the German national institutions responsible for extra-university research. Out of the five institutes of the FZR the Institute of Nuclear and Hadron Physics (IKH) is rather strongly engaged in fundamental research related to subatomic systems, but it also investigates and exploits the possibilities for the transfer of experimental and theoretical knowledge and techniques from particle and nuclear physics to other fields of science.

The most remarkable example of such technology transfer is the strong involvement of the Institute in the preparative work for the Radiation Source ELBE presently under construction at Rossendorf. As this instrument is centered around a small superconducting electron accelerator nuclear physicists can well contribute with their experience gained at larger machines elsewhere. The projected electron beam of 1 mA at up to 40 MeV will produce intensive secondary radiation: for the medium and far infrared the free electron laser (FEL) principle will be used, whereas keV-X-rays are produced via electron channeling and MeV photons as bremsstrahlung; from the latter neutron beams of interest for cross section measurements will be generated.

The first chapter of this Report contains contributions on the design work on components of ELBE, especially on the production stations for the different kinds of secondary radiation and on the experimental equipment to be installed for their use.

Hadron Physics at the FZR - as described in the second chapter - is dealing with hadronic interactions as such and also within the hadronic medium formed in collisions between nuclei. Experiments were performed at the COSY proton cooler synchrotron at the Forschungszentrum Jülich (KFA) and at the heavy ion synchrotron SIS at GSI Darmstadt. Theoretical studies performed at the IKH refer to these experiments, to data obtained at higher energy accelerators, and to violent astrophysical events.

The third chapter combines experimental and theoretical research in Nuclear Physics. Here collective excitations of nuclei as well as their interplay to single nucleon degrees of freedom play an important role. Most of the work reported deals with electromagnetic processes in nuclei, with special emphasis on those triggered by impinging bremsstrahlung photons. Attention is also given to studies of nuclear collision dynamics as such collisions may be the source of exotic nuclei whose spectroscopic properties are of interest. They also may be of importance for new nuclear technologies like waste transmutation or accelerator driven fission and spallation; neutrons in the MeV range as will become available as a secondary ELBE beam play an important role in such processes.

Last but not least this Annual Report contains a chapter on Biomedical Research performed by using nuclear technology. The main contribution of the Institute to this field comes from Positron Emission Tomography (PET) and the outstanding achievement here is the successful operation of a PET scanner simultaneously to the tumour treatment with heavy ion beams when a significant number of patients was treated at GSI in 1998 and 1999. The reliability and reproducibility of such radiation therapy is improved considerably by in-situ PET, as developed at the Institute. In the upcoming years

biomedical research will also be performed with the beams coming from ELBE: The quasi-monochromatic X-rays of easily variable energy as produced in electron channeling appear to be an ideal probe for the elementary processes responsible for radiation damage in tissue and a corresponding experimental study is in preparation.

Interesting research in biophysics and biochemistry will also become possible with the tunable FEL-radiation in the infrared as available at ELBE; here discussions with respective specialists and possible future outside users have played an increasing role.

The scientific activities of the institute have benefitted from generous support from various institutions. First of all, we gratefully acknowledge the close and fruitful collaboration with the colleagues from the Technical University (TU) Dresden and many other scientific institutions in Germany and abroad; such contacts are of vital importance for our institute. Specific projects were financially supported by the Federal Ministry for Education and Research (BMBF), the German Research Community (DFG), the Saxon State Ministry for Science and Art (SMWK), Forschungszentrum Jülich and GSI Darmstadt. We express our gratitude to all these as well as to the Executive Board of the Forschungszentrum Rossendorf for its essential support of the ELBE project.

The Radiation Source ELBE

As the ELBE project will be brought into service in the year 2000 great efforts were made to prepare the equipment as well as to design and plan the research projects to be tackled with the radiation from ELBE. The FZR department 'Experimental Facilities and Information Technology' together with the 'New Accelerators' department is setting up the injector and the accelerator, including the building with its important radiation shielding and the cryogenic equipment, and they also prepare the electron beam handling, the diagnostics and the FEL undulator in one of the beam lines. As seen in the floor plan of ELBE there will be a number of stations where the electron beam is used to produce different kinds of secondary radiation.

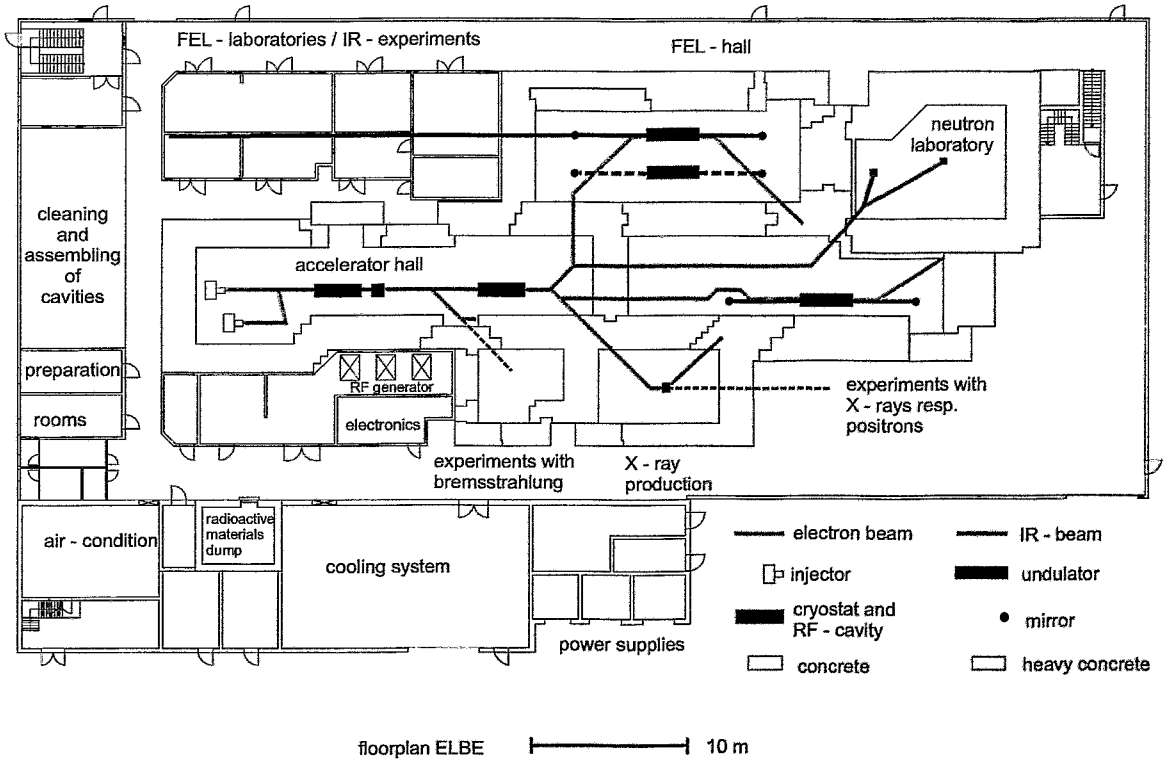

The Institute of Nuclear and Hadron Physics is involved in the realization of four of these stations :

(1) The Free Electron Laser (FEL) hall is designed to house two separate undulators for two different wavelength regimes; on the basis of collaboration agreements between FZR and DESY Hamburg as well as with ENEA Frascati two undulators with different period lengths will become available for ELBE; they allow to produce infrared radiation with wavelengths from 5 to about 100μm.

(2) For the production of quasi-monochromatic X-rays non-conventional photon sources like parametric X-ray and channeling radiation will be exploited. It is expected that channeling radiation will provide the highest intensity; comparable X-ray yields may be obtained from Compton backscattering an intense laser beam off the electrons from ELBE, provided that their brilliance can be further increased in the future.

(3) Bremsstrahlung photons from the 20 MeV stage of ELBE will be used for nuclear spectroscopy. The high electron intensity enables the use of polarized off-axis photons for the determination of the parity of nuclear states in addition to spin and lifetime.
(4) The low emittance of the ELBE beam allows the production of neutrons in a radiator of a few mm in size leading to sub-ns neutron pulses; using a time-of-flight method they will be the basis of energy-dispersive neutron cross section studies related to fusion and fission reactor problems. For this project a collaboration was formed with the FZR Institute of Safety Research and the Institute of Nuclear and Particle Physics of the TU Dresden; the latter has installed the neutron laboratory which allows also other types of experiments with neutrons eventually combining the continuum produced from the ELBE electrons to 14 MeV neutrons from a high power DT-generator.

The following contributions to this Report describe design studies for components of the radiation source ELBE as performed in the Institute of Nuclear and Hadron Physics as well as the plans for the different radiator stations. Studies related to the future research with the different types of radiation will also be presented.
*In the field of research with IR-radiation from FEL's preparatory studies were performed at FELIX (Nieuwegein near Utrecht) and at the ps-FEL center of the Stanford University (California, USA). For future biomedical research with THz- and FIR-radiation groups from several European laboratories (marked by * under collaborations below) have prepared an application for funding through the 5th-EU-framework programme; the radiation in the THz (i.e. mm-) range is available at ENEA Frascati and the 5 μm - 200 μm radiation will be supplied by ELBE.*
Our investigations on non-conventional photon sources are aimed at the development of an compact, intense and tunable source of quasi-monoenergetic X-rays in the energy range between 10 and 100 keV. Theoretical as well as preparatory experimental studies of X-ray emission processes, especially with respect to the possible intensification of channeling radiation in hypersonic superlattices, have been performed.

Collaborations

FEL construction and research with infrared radiation:
- *Stanford University*
- *DESY Hamburg*
- *TU Darmstadt*
- *FELIX Nieuwegein* (Netherlands)*
- *ENEA Frascati* (Italy)*
- *CNRS-LURE Orsay* (France)*
- *University Frankfurt/Main**

Other radiation to be produced at ELBE:
- *TU Dresden*
- *Institute for Safety Research (FZ Rossendorf)*
- *TU Darmstadt*
- *University Mainz*
- *Yerevan Physics Institute (Armenia)*
- *Institute of Applied Problems of Physics Yerevan (Armenia)*
- *Institute of Ion Beam Physics and Material Research (FZ Rossendorf)*

Electron-Bunch Compression by the S-Shaped Beam Transport System

P. GIPPNER, B. FRANCZAK[1], W.A. GILLESPIE[2] AND E.GROSSE

Many advanced applications of the mid infrared (MIR) FEL require short electron bunches with a bunch length in the region of 1 ps. In order to fullfil this requirement we use the beam transport system of fig.1, which guides the electrons from the accelerator hall into the cave as a nonlinear bunch compressor.

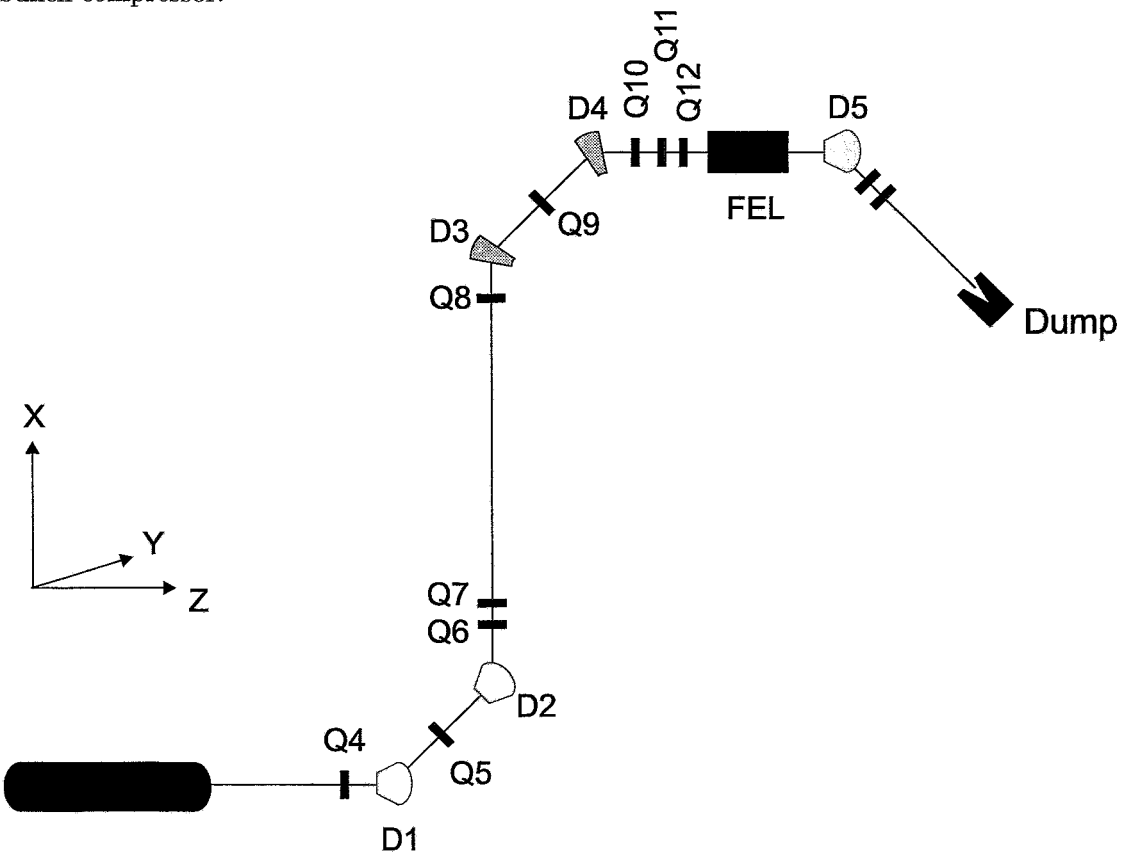

Fig. 1 *The bending system of the MIR-FEL. It consists of the dipole magnets D1...D5, the vertically (Q4,Q6,...) and horizontally (Q5,Q7,...) focusing quadrupoles. The position of the FEL is indicated by a black rectangle.*

The dispersion function of this s-formed system shows that electrons with a momentum $p_+ = p_0 + dp$ (p_0 characterizes the reference particle) have a drift length longer than that of electrons with $p_- = p_0 - dp$. To employ this fact for bunch compression one needs a beam with a $(dz, dp/p)$ correlation as shown in the upper part of fig.2. There the ellipse (a) characterizes the behaviour of the beam in the longitudinal phase space at the exit of the accelerator system. One should emphasize, that dp/p is proportional to the instantaneous energy spread dE/E , whereas dz is proportional to the phase angle $\Delta\Phi$. By careful adjustment of the quadrupole fields the electron bunches moving from the accelerator to the dipole D4 are compressed. The $(dz, dp/p)$ correlation of the bunch is now represented by the erect ellipse. Thereby the bunch length dz is shortened from about 2.9 mm ($\simeq 9.6ps$) to 0.4 mm ($\simeq 1.3ps$).
The compressed bunches exist only on their drift between the dipoles D4 and D5,

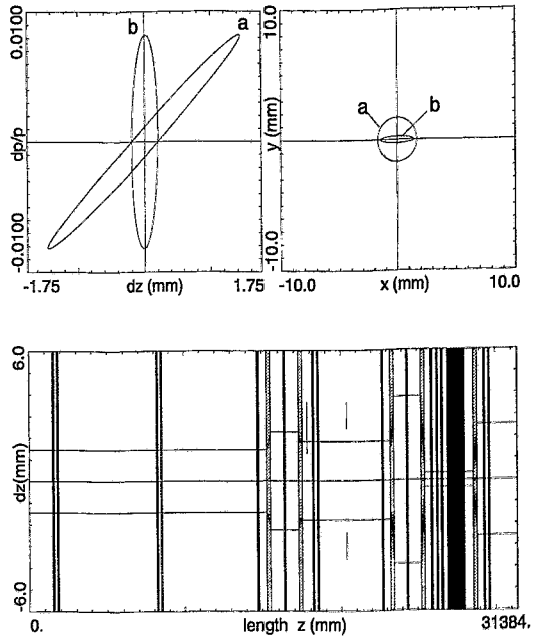

Fig. 2 *The compression of the bunch length at the undulator position for an electron energy of 19.023 MeV.Upper part: the longitudinal ellipses in the phase space (left) and the beam spots (right) at the exit of the accelerator(a) and at the entrance of the undulator(b). Lower part: the bunch length dz as a function of the coordinate z.*

as is demonstrated in the lower part of fig.2. The corresponding calculations were performed with the computer code MIRKO [1] for an electron energy of 19.023 MeV. Additionally we simulated the behaviour of 1900 single particles of the same energy using the code PARMELA [2]. The results of these simulations are shown in fig.3, which compares the longitudinal phase spaces $(\Delta\Phi, \Delta E)$of the electron bunch behind the accelerator and at the entrance of the FEL. A considerable compression of the bunch length could be obtained.

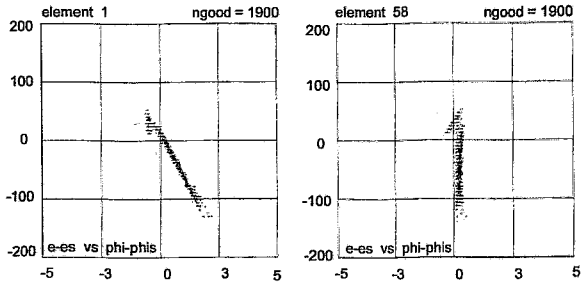

Fig. 3 *Longitudinal phase space $(\Delta\Phi, \Delta E)$ for an initial bunch (left panel) and for the same bunch after compression (right panel).*

[1] *GSI Darmstadt*

[2] *University of Abertay Dundee*

References

[1] B.Franczak, GSI Darmstadt, "MIRKO,Version 6.06, 1998"

[2] L.M.Young, J.H.Billen, Los Alamos National Laboratory, "LA-UR-96-1835"

Electron Beam Diagnostics for the Mid Infrared FEL at ELBE

P.MICHEL

Electron beam diagnostics in a Free Electron Laser facility need similar instrumentation to those of almost any electron accelerator. On the other hand the beam parameters should be optimized to get high and stable laser gain which requires specific diagnostic tools and leads to a different emphasis than usual, such as very short bunch length, the beam β-function in the wiggler, and low average beam loss. Moreover, accurate beam instrumentation is essential for precise operation of any accelerator. The electron beam diagnostics for the MIR FEL [1] at ELBE should enable the setup of the accelerator and beamline elements for a certain lasing mode and to monitor parameter changes during lasing runs. To protect sensitive machine components, and especially to limit activation, the setting up should be carried out at low average beam currents (<0,5μA) which can be achieved by reducing the micropulse repetition rate. That means all diagnostic elements serving this task should have reasonable sensitivity to also work at low beam current. Diagnostics for on-line monitoring should be suitable to operate at high-power cw mode. Table 1 shows the parameters to be measured together with the corresponding instrumentation for setup and monitoring parameters, respectively. In Fig.1 the location of all instrumentation elements of the MIR-beamline is performed. The design is based on the beam line calculations in reference [2].

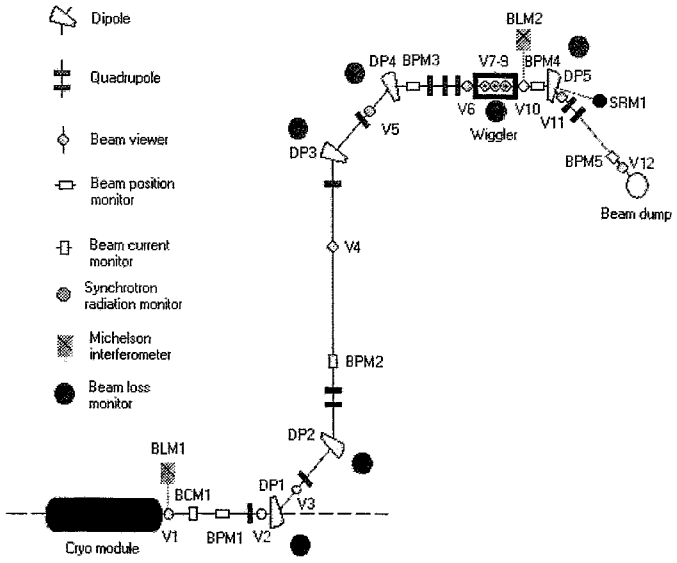

Fig. 1 *Electron beam diagnostic elements of the MIR FEL at ELBE*

Insertable optical transition radiation (OTR) viewers will be used to observe beam profiles and position. Backward scattered OTR is produced on thin (some μm) Al foils and detected by commercial CCD cameras or vidicon tubes. Space resolutions below 100μm and linear response on the current density are the main advantages of this method. Because electrons are scattered in the OTR-foil or the foil can be destroyed at high power deposition, this method is available at low beam currents only. The viewers V2,V3,V4,V5 and V8 are placed at minimum β-function locations with sharp beam spots to find the nominal beam position and to have a strong criterion to compare against the calculated beam envelope. By means of V12 the right beam position for hitting the beam dump can be found. During high power operation the beam position should

be monitored by HF-detectors (BPM1-5). To minimize the emittance grow due to impedance gradients of the beamline, stripline monitors are preferred over resonant TM_{110} cavities.

Table 1

set up parameter	**detector**	**monitor parameter**	**detector**
beam location beam profile	OTR-viewer	beam location	HF-monitor
transverse emittance	OTR-viewer (+ quadrupole)	high beam current	HF monitor beam dump Faraday cup
energy spread	OTR-viewer + dipole	bunch length	SR-monitor
bunch length	OTR-viewer + interferometer	beam loss	photomultiplier tubes
low beam current	beam dump Faraday cup		

V3,V4,V5 and V11 are installed at locations where the beam is dispersive and the β-function in the nondispersive plane has a relative minimum. Consequently these viewers are suitable to measure energy spread. Because the β-function at the wiggler is matched to be nondispersive, the energy spread cannot be measured at this location. The best viewer to reproduce the energy spread at the wiggler is V11. Only the transfer function of DP5 has to be taken into account. The beamspot in the dispersive locations is broadened in the dispersive plane, therefore, the viewer foils show rectangular geometries. To optimize the electron bunch length for lasing it should be measured downstream the accelerator and near the wiggler. For this reason the transition radiation at V1 and V10 will be deflected into polarized Michelson interferometers [3] by switchable mirrors. The coherent transition radiation spectrum at long wavelengths (50μm to 1mm) can be measured, and the electron bunch length as well as, under certain conditions, the longitudinal bunch distribution can be derived [4]. For online monitoring of the bunch length a synchrotron radiation detector could be installed at half of the bending angle of DP5. The viewers V6-V10 are needed to find the precise wiggler axis and to test the β-function at this sensitive region for lasing. The radiators of V7,V8 and V9 are thin Be foils with a hole to reduce radiation and so to protect the wiggler magnets. Although there is enough space between DP2 and DP3, the standard method to measure the beam transverse emittance using the variation of quadrupole k-values is not applicable at V4 location. The dispersion in this region is not zero, and thus the longitudinal and the transverse phase spaces are coupled. As an alternative method the set of 5 beam viewers V6-V10 can be used to image the beam spots and to calculate transverse emittance at the wiggler. The beam current at the end of the beam transport is measured in the beam dump Farrady cup. A TM_{101} resonance cavity (BCM1) just behind the linac cryo-modules should be located for online monitoring of the produced beam current. Because both detectors operate at full beam power, substantial beam losses can be determined from the measured difference. Additional beam loss monitors detecting scattered electrons and photons are located near all dipole magnets and the wiggler.

References

[1] F. Gabriel et. al., The FEL projects at the Rossendorf Radiation Source ELBE (submitted at NIM)

[2] P.Gippner, ELBE Design report 1998, p. 6-8 and this Report p. 5

[3] P.Michel, P.Piot, Design of a Longitudinal Electron Bunch Length Monitor for the Mid Infrared Free Electron Laser at ELBE, this Report p. 9

[4] E.R. Crosson et. al., NIM A385 (1995) 216

Design of a Longitudinal Electron Bunch Length Monitor for the Mid Infrared FEL at ELBE

P. MICHEL, P. PIOT [1]

In high-brightness FEL-driver-accelerators such as ELBE very short bunches are required to achieve the necessary high peak current. The peak current at the wiggler can be estimated from an average beam current, and the longitudinal bunch length measurements. In Fig.1, where the calculated laser gain [1] at 10 μm is plotted versus the bunch length of the electron beam, one can notice the importance of the bunch length on the gain.

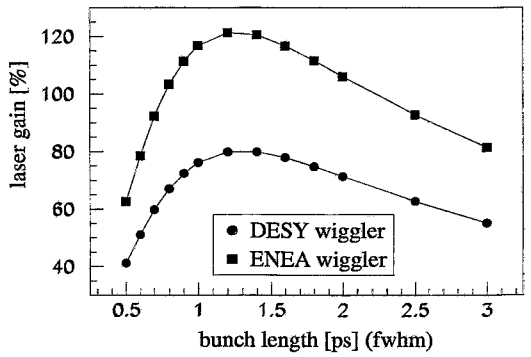

Fig. 1 *Calculated laser gain at 10 μm assuming designed ELBE parameters versus electron bunch length (at fixed $\varepsilon_{long,rms}$ = 60 keVps, $\varepsilon_{trans,rms}$ = 10 π mm mrad) for the DESY wiggler (27 mm period, 33 segments) at E = 27 MeV and the ENEA wiggler (50 mm period, 45 segments) at 40 MeV.*

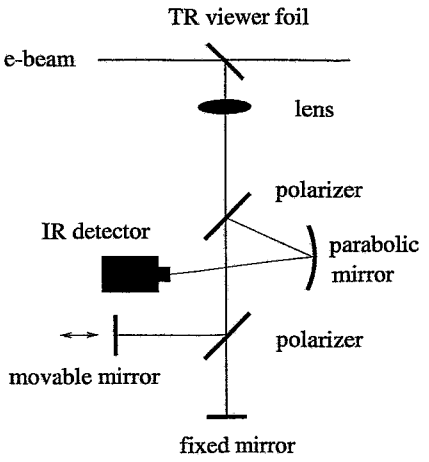

Fig. 2 *Setup of the planned polarized Michelson Interferometer.*

Measurement of the coherent far infrared transition radiation spectrum, by means of an autocorrelation technique [2], allows one to estimate the electron bunch distributions down to the order of ps [3]. This technique is based on the effect that coherent transition radiation is emitted by relativistic electron bunches with wavelengths larger than or comparable to the bunch length. The total emitted radiation energy in this wavelength range is coherently enhanced and dominates the signal. Fig. 2 shows the setup of the planned bunch length monitor. It consists in a insertable Transition Radiation beam viewer and a mm-wave polarizing Michelson Interferometer. A crystalline quartz glass lens is used to collect and collimate the infrared TR beam. A first polarizer is used to linearly polarize the beam along a direction, a second polarizer, that act as a beamsplitter, splits the beam into two perpendicular polarizations. Both parts are reflected on the planar mirrors and focused to the infrared sensitive detector. Because one of the mirrors is movable, the phase between the two beams can be changed thereby providing a means to scan the autocorrelation function. The grids should be made from 20 μm gold coated tungsten wires 50 μm spaced. A room temperature opto-acoustic detector (Golay cell) serves as detector but the suitability of pyroelectric infrared detector should also be assessed. The polarized Michelson Interferometer will be remotely controlled and both control and data taking will be integrated in the main ELBE control system.

[1] *TJNAF, Newport News, Virginia, USA*

References

[1] S.V. Benson, Spreadsheet Code, TJNAF, Newport News, Virginia, USA
[2] U. Happek et. al., Phys. Rev. Letters, 67 (1991) 2692
[3] E.R. Crosson et. al., NIM A385 (1995) 216

Beam Compression for Low Electron Energies

P.GIPPNER

In order to attain a single path gain in the order of 50% beam bunches with a high electron density n are needed. These bunches should be short in the longitudinal phase space and exhibit a large peak value of charge. To demonstrate that our beam line system[1] can provide the undulator with sufficiently short electron bunches we extended our calculations for bunch compression to electron energies of 12 MeV and 15 MeV, where space charge effects play already an important role. For these calculations we used the codes MIRKO[2] and PARMELA[3].
As follows from the figs. 1 and 2, the initial bunches exhibit a long tail of particles with a large phase angle $\Delta\Phi$ for both energies. One may suppress these electrons by a circular diaphragm immediately behind the first arc of our transport system in front of quadrupole Q6 [1]. This gives rise to a loss of particles of about 22% for 12 MeV and 20% for 15 MeV, respectively. This shows the need for sufficient shielding to be introduced locally. After such a suppression the bunches guided to the entrance of the FEL have lengths in the order of about 1.3 ps.

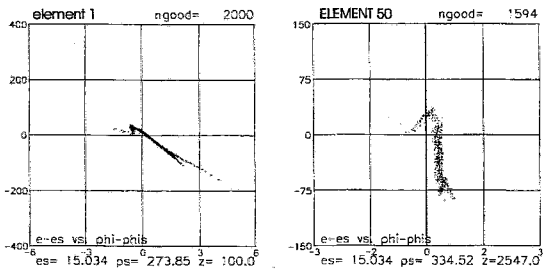

Fig. 1 *Longitudinal phase space* $(\Delta\Phi, \Delta E)$ *for an initial bunch of* $E = 12$ *MeV(left) and for the same bunch after compression(right).*

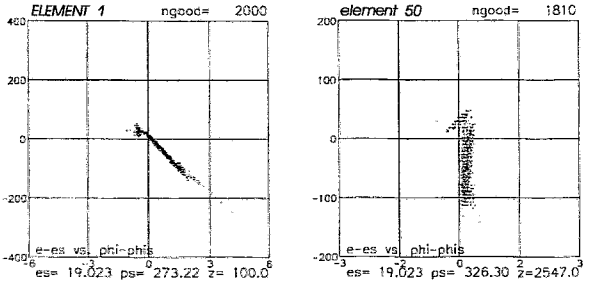

Fig. 2 *Longitudinal phase space* $(\Delta\Phi, \Delta E)$ *for an initial bunch of* $E = 15$ *MeV(left) and for the same bunch after compression(right).*

References

[1] P. Gippner, B. Franczak, this Report p. 5
[2] B. Franczak, GSI Darmstadt, "MIRKO,Version 6.06, 1998",
[3] L.M.Young, J.H.Billen, Los Alamos National Laboratory, "LA-UR-96-1835",

Undulators for ELBE FELs

E. GROSSE, W. SEIDEL AND R. WÜNSCH

Additionally to the production of bremsstrahlung and X-rays ELBE will mainly be used to produce intensive FEL radiation in the infrared range of 5 to 150 μm. For the longer wavelengths an electromagnetic undulator is under consideration, whereas for shorter wavelengths, permanent magnet devices with variable gap will be installed.

Notation		U27*32	U27*64	U50*45	U90*28
Type		hybrid	hybrid	Halbach	electromagnetic
Period	λ_U	2.73 cm	2.73 cm	5 cm	9.0 cm
Number of Periods	N_U	32	64	45	28
Undulator Parameter	K_{rms}	0.3...1.0	0.3...1.0	0.3...2.0	0.8 ...1.2

Table. 1 *Parameters of the undulators considered for ELBE.*

For wavelengths between 3 and 40 μm we plan to install one or two undulator units of the DESY-TTF type [1] with the focusing magnets removed. For longer wavelengths (8 μm$\lesssim\lambda\lesssim$160 μm) a Halbach type undulator built by ENEA/Frascati [2] has been offered to the FZR to be installed at ELBE for some period of time. It is housed in a large vacuum chamber and its widely variable gap should result in undulator parameters below and above one.

Fig. 1 displays the single-pass gain [3] for the considered undulators for the ELBE beam. A beam energy of 20...40 MeV with an constant energy spread of 90 keV and normalized emittance of 7 mm*mrad (both rms) was assumed. Bunches with total charge of 85 pC and rms length of 1.5 ps result in a peak current of 22.6 A. The Rayleigh range of the optical resonator was assumed to be 1 m. The gain was calculated with the degradation factors of ref. [4]. It is by roughly 10-20% smaller than the gain calculated with the reduction factors of ref. [3]. Decreasing the energy spread by a factor of two the gain increases by a factor 2.5 around 20 MeV and by 30% at 40 MeV.

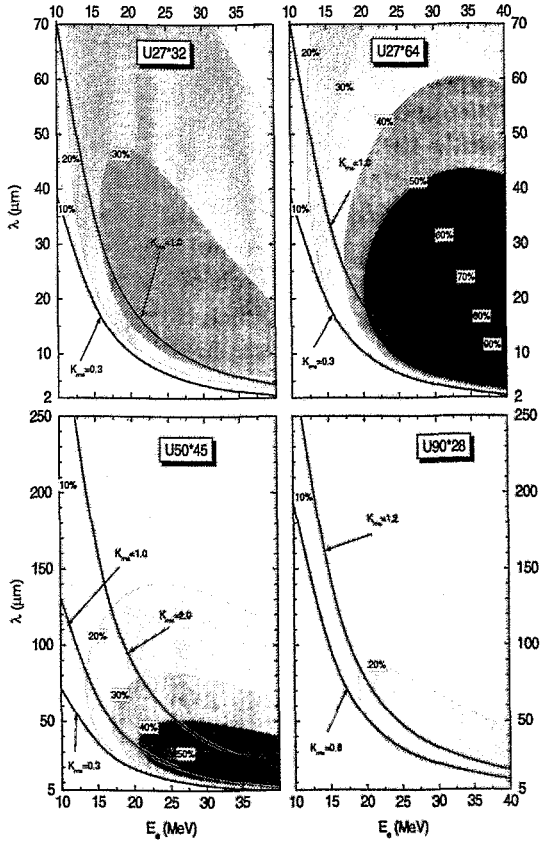

Fig. 1 *Laser single-pass gain calculated for ELBE with the undulators of table 1 as a function of electron beam energy E_e and radiation wavelength λ. The black lines indicate lower and upper limits of the undulator parameter.*

References

[1] J. Pflüger, H. Lu, D. Köster and T. Teichmann, *Nucl. Instr. and Meth.* **A407** (1998) 386-391

[2] F. Ciocci, E. Fiorentino, G.P. Gallerano, A. Renieri and E. Salia, *Nucl. Instr. Meth.* **A 250** (1986) 134-137

[3] G. Dattoli, A. Renieri and A. Torre, *Lectures on the Free Electron Laser Theory and Related Topics*, World Scientific 1993;
U. Bizzarri et al., *Revista del Nuovo Cimento* **10** (1987) 1

[4] S.V. Benson, CEBAF TN #94-065; TJNAF TN #96-037

Optical Power Gain from Simulations versus Small-Signal Gain Formula

R. WÜNSCH

The gain of optical power for a single pass through the undulator of a free electron laser (FEL) can vary over many orders of magnitude in dependence on undulator and beam parameters. If the optical field is not too strong and the gain is sufficiently small (a few ten percent) the small-signal gain characterizes the increase of optical power. However, if the gain exceeds several 10 percent and/or the optical field is larger than a few kW/mm^2 the small-signal gain fails in describing the actual gain. In that case a computer simulation describing the motion of a sufficiently large number of test-electrons controlled by the Maxwell and Lorentz equations should be used to obtain an adequate description of the FEL [1].

In this contribution we investigate the gain of optical power for the 4 undulators [2] considered for ELBE as a function of the optical beam intensity I_0 at undulator entrance. We compare the gain formula of the medium-gain regime [3] including the saturation factor [4] with the results of one-dimensional computer simulations. We consider optimum values of cavity desynchronization and energy detuning. The medium-gain formula includes terms up to third order in the gain parameter. The electron beam is assumed to be monoenergetic. A finite energy spread will be considered in another contribution [5].

To study the influence of different bunch charges Q we combine the calculation for the design value of ELBE (Q=85 pC) with a calculation for a considerably smaller (Q =7 pC) and larger (Q=200 pC, 2 nC) bunch charges. The 7 pC correspond to the S-DALINAC in Darmstadt, while the 2 nC were used at the SASE FEL with the UCLA-KIAE undulator installed at the AFEL linac at LANL. The figure shows that medium-gain formula and saturation factor reproduce the result of the simulation sufficiently well up to bunch charges of 200 pC. At 2 nC and weak optical field ($I_0 \lesssim 50\,\mathrm{kW/mm^2}$) the gain is much larger as predicted be the gain formula. Increasing the optical power the gain is remarkably stronger reduced than predicted by the saturation factor.

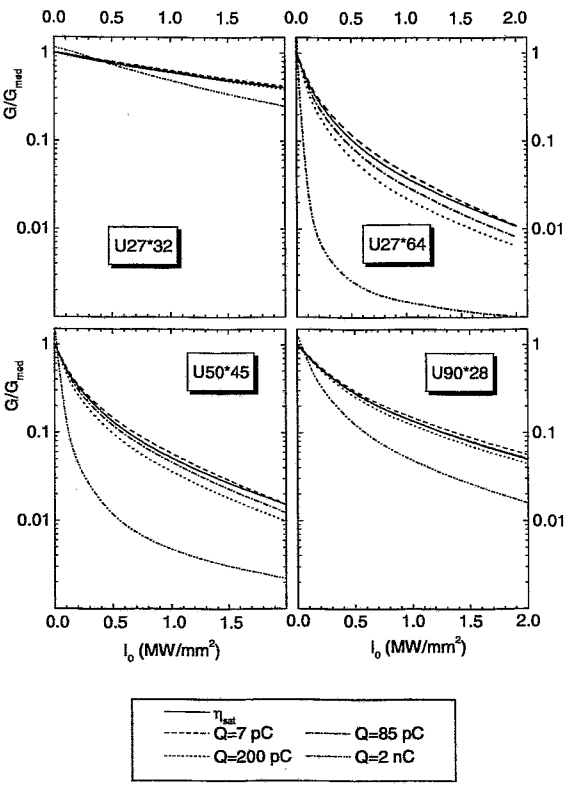

Fig. 1 *Ratio between the gain G obtained by means of a one-dimensional simulation code and the gain formula G_{med} in the medium-gain regime as a function of the initial optical intensity I_0 for the four undulators considered for ELBE. Each calculation was performed with* 1000 *test-electrons of exactly* 20 *MeV energy (σ_{E}=0), undulator parameter K_{rms}=1.0 and* 4 *values of the bunch charge Q. η_{sat}* shows the saturation factor according to eq. (6.2) on page 328 of ref. [4].

References

[1] J.B. Murphy and C. Pellegrini, *Free Electron Laser Handbook*, Vol. 6 eds. W.B. Colson, C. Pellegrini and A. Renieri (North-Holland, Amsterdam, 1990) Chap. 2

[2] E. Grosse, W. Seidel and R. Wünsch, this Report p. 11

[3] G. Dattoli et al., Nucl. Instr. Meth. **A285** (1989) 108

[4] G. Dattoli A. Renieri and A. Torre, *Lectures on the Free Electron Laser Theory and Related Topics*, World Scientific, Singapore, 1993

[5] R. Wünsch, this Report p. 14

The Gain Curves for the Elbe FEL

R. WÜNSCH

If the gain of optical power in a free electron laser (FEL) is sufficiently small (a few percent per pass) Madey's first theorem (see e. g. [1]) can be applied according to which the gain is proportional to the first derivative of the corresponding line-shape function of the spontaneously emitted spectrum with respect to the detuning parameter ν

$$G(\nu) \sim -\frac{d}{d\nu}\left(\frac{\sin\frac{\nu}{2}}{\nu/2}\right)^2 . \tag{1}$$

It has a zero at ν=0 and a maximum at ν=2.606. If the gain is larger it may remarkably deviate from Madey's prediction (1).

By means of a one-dimensional numerical simulation code basing on the solution of Maxwell and Lorentz equations for an appropriate number of test-electrons we have calculated the single-pass gain G as a function of the energy detuning parameter $\nu = 2n\pi N_U(1-\lambda_n/\lambda)$, which describes the deviation of the laser wavelength λ from the resonant wavelength λ_n for the n-th harmonic determined by $\lambda_n = (1+K_{rms}^2)\lambda_U/(2n\gamma^2)$. Here, γ is the electron energy in units of its rest mass, K_{rms} is the undulator parameter, N_U the number of undulator periods with length λ_U, and n is the harmonic number at which the laser lases. Besides the design value of ELBE with micropulse charge Q=85 pC we consider a smaller (7 pC) and a larger pulse charge (200 pC) and compare their gain with Madey's prediction (1). The electron beam is assumed to be monoenergetic.

At small charges (7 pC) Madey's curve is almost exactly reproduced by the simulation (fig. 1). For the beam of ELBE (85 pC) the gain $G(\nu)$ starts to deviate and the curves become unsymmetric. At larger bunch charges (200 pC) the effect is even more pronounced. At positive detuning ν the actual gain is larger than Madey's prediction, at negative values it is smaller. The larger the gain is the bigger is the deviation. Unlike Madey's prediction an energy transfer is possible at resonance energy (ν=0). The position of maximum gain at $\nu \approx 2.6$ is nearly unshifted in all cases.

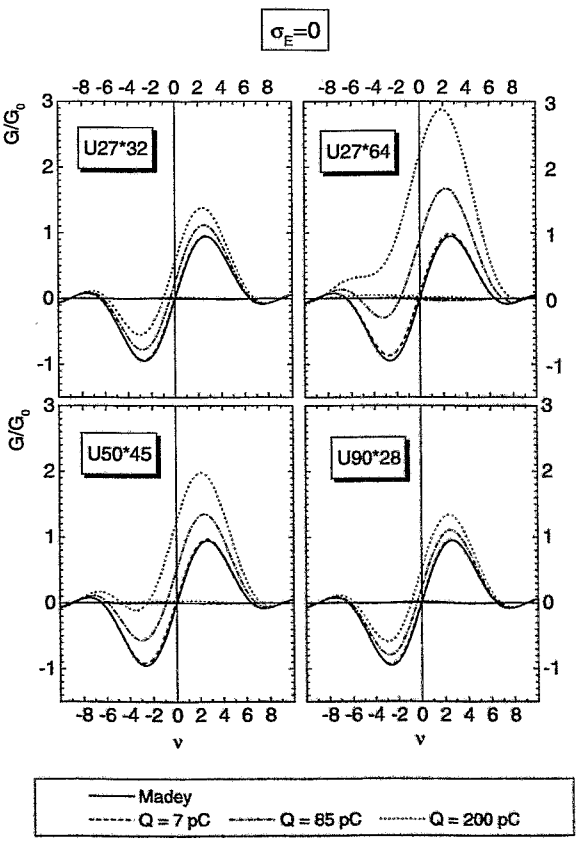

Fig. 1 *Single-pass gain G obtained by means of a one-dimensional simulation code divided by the small-signal gain G_0 as a function of the detuning parameter ν for the undulators of ELBE [2] and various bunch charges. The bunch length is assumed to be 1.5 ps (rms). The simulations have been performed with* 1000 *test-electrons with an energy of exactly* 20 *MeV (σ_E = 0), undulator parameter K_{rms} = 1.0 and* 3 *values of the bunch charge Q. Additionally Madey's prediction (1) is shown.*

References

[1] J.B. Murphy and C. Pellegrini, *Free Electron Laser Handbook*, Vol. 6
eds. W.B. Colson, C. Pellegrini and A. Renieri (North-Holland, Amsterdam, 1990) Chap. 2
[2] E. Grosse, W. Seidel and R. Wünsch, this Report p. 11

FEL Gain for a Warm Electron Beam

R. WÜNSCH

In a preceding contribution [1] we compared the single-pass gain G for a monoenergetic beam obtained in a one-dimensional simulation with the corresponding gain formulae in the medium-gain regime. Now we investigate its dependence on the energy spread of the electron beam. According to Dattoli's formula [2] the gain for a beam with rms energy spread σ_{E} differs from the gain for a monoenergetic beam with the same energy E_{e} by the reduction factor

$$\eta_{\mathrm{E}} = 1/(1+1.7n^2\mu_{\mathrm{E}}^2) \qquad \text{with} \qquad \mu_{\mathrm{E}} = 4N_{\mathrm{U}}\sigma_{\mathrm{E}}/E_{\mathrm{e}}, \tag{1}$$

where N_{U} is the number of undulator periods and n the harmonic number at which the laser lases. Alternatively to Dattoli's formula a more sophisticated approach to the gain reduction due to electron energy spread is used in the literature [3]. We compare both approaches with each other and with the results of the simulation code.

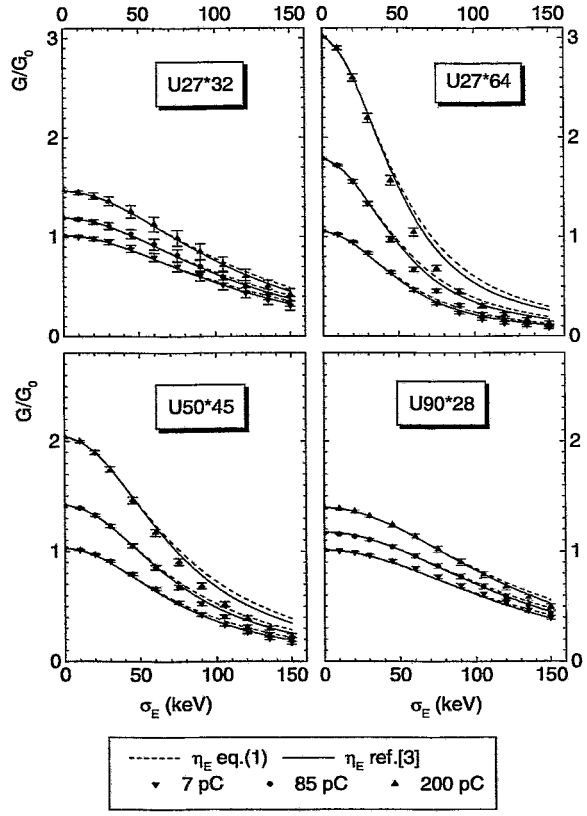

Fig. 1 shows the ratio G/G_0 for the undulators designed for ELBE as a function of the energy spread σ_E. The 10^9 electrons of a bunch produced by the linac of ELBE are represented by 10000 test-electrons with an energy distribution according to σ_E. Additionally to ELBE with $Q = 85\,pC$ we study bunch charges of 7 and 200 pC. The figures show that the gain degradation obtained by the simulation code is sufficiently well reproduced by both approximations. Only for larger bunch charges (Q=200 pC) and energy spread $\sigma_{\mathrm{E}} \gtrsim 80$ keV the degradation factors start to systematically underestimate the actual gain reduction.

The deviation at $\sigma_{\mathrm{E}} = 0$ from one, in particular for larger bunch charges, illustrates the deviation from the small-signal regime and the importance of the nonlinear terms in the medium-gain regime.

Moreover fig. 1 shows that the gain can remarkably be risen by reducing the energy spread from the designed value of roughly 90 keV to 30–50 keV.

Fig. 1 *Ratio between the single-pass gain G obtained by means of a one-dimensional simulation code and the small-signal gain G_0 as a function of the rms energy spread σ_{E} of the electron beam for the undulators considered for ELBE [4]. The simulation has been performed for* 10000 *test-electrons with a Gaussian energy distribution with mean value $E_{\mathrm{e}} = 20\,MeV$ and variance σ_E. The undulator parameter is fixed to $K_{\mathrm{rms}} = 1.0$. The error bars indicate the statistical errors of the simulation. The lines show the gain degradation according to eq. 1 (broken lines) and ref. [3] (full lines).*

References

[1] R. Wünsch, this Report p. 12
[2] G. Dattoli, T. Letardi, J.M.J. Madey and A. Renieri, *IEEE J. Quantum Electron.* QE-**20** (1984) 637
[3] S.V. Benson, TJNAF TN #96-037
[4] E. Grosse, W. Seidel and R. Wünsch, this Report p. 11

Beam Matching for the MIR-FEL Project

P.GIPPNER AND G.WÜSTEFELD[1]

In order to obtain within the undulator a maximum overlap between the electron beam and the electromagnetic field accumulated in the optical resonator, the electron beam should be matched to the beta function of the undulator. An example of an optimum beam matching was mentioned by W.A.Gillespie et al. [1]. For demonstrating the matching procedure for our MIR-FEL project [2] we simulated a FEL by a set-up of permanent magnets with the following parameters:

$\lambda_u = 27mm$	undulator period,
$g = 12mm$	gap width,
$B_0 = 0.562T$	maximum magnetic field in the middle plain,
$D = 6.75mm$	width of the dipoles in z-direction,
$N_u = 40$	number of periods,
$L_u = 1080$	length of the whole undulator.

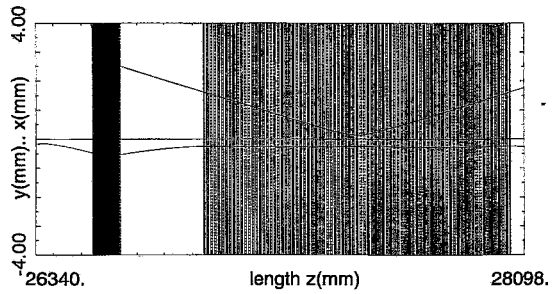

Fig. 1 *Electron beam matching for our MIR-FEL model.*

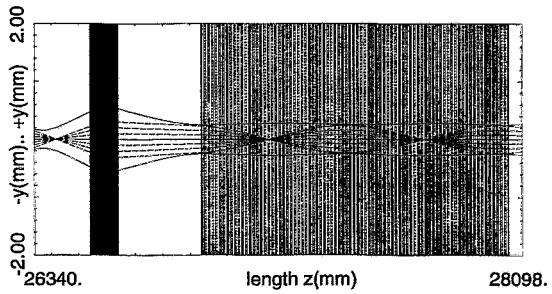

Fig. 2 *Vertical electron envelopes of a matched beam through the undulator. The dashed lines show single particle trajectories.*

Our calculations show that an optimum matching is attained when the $\sigma - matrix$ at the undulator entrance fullfils the conditions

$\sigma_{34} = 0$	waist in the (y,z)-plain,
$\sigma_{33} = \epsilon_y\sqrt{2}\rho_0$	half of the beam width in the (y,z)-plain.

Thereby, ϵ_y represents the geometric emittance in y-direction, whereas the radius of curvature ρ_0 is defined by the equation $p = e\rho_0 B_0$. Since ϵ_y scales inversely proportional with p, and ρ_0 is proportional to p, the given expression for σ_{33} should be independent of the electron momentum. The results of the matching procedure are given in fig.1, which shows the dimensions of a matched beam within the undulator in the (x,z)- and the (y,z)-plain, respectively. Fig.2 presents the behaviour of the beam in the (y,z)-plain in a better scale. It can clearly be seen, that the betatron oscillations of the envelopes are suppressed to a great extend and only the single electrons exhibit oscillations within a envelope "tube" of lower than 1 mm diameter.
The calculations were performed using the computer codes MIRKO [3] and PARMELA [4] by consideration of the space charge effects. The results of PARMELA demonstrate that the ellipses in the phase spaces (x,x') and (y, y') stay unchanged through the undulator, when the space charge is not included in the calculations.

[1] *BESSY II, Berlin*

References

[1] W.A.Gillespie et al., NIM A250(1986)233
[2] F.Gabriel et al., accepted for publication in NIM A
[3] B.Franczak, GSI Darmstadt, MIRKO,Version 6.06, 1998
[4] L.M.Young, J.H.Billen, Los Alamos National Laboratory, LA-UR-96-1835

A Prototype of a "Passive" Tunable Undulator for ELBE

P.GIPPNER, W.SEIDEL AND A.SCHAMLOTT

Tuning an undulator the correction of the fringe fields by additional coils or by movable magnets has to be done to attain a proper matching of the electron beam into the wiggle field. In order to make tuning more convenient, we tried to find a fringe field for an undulator (of hybrid type), which allows the variation of the gap without additional correction elements. Such an undulator matching may be called a "passive" one. Thereby the elongation of the electrons for a given energy should be nearly independent on the gap width g, whereas the displacement Δ and the slope of the electron trajectory at the undulator exit should be as small as possible.

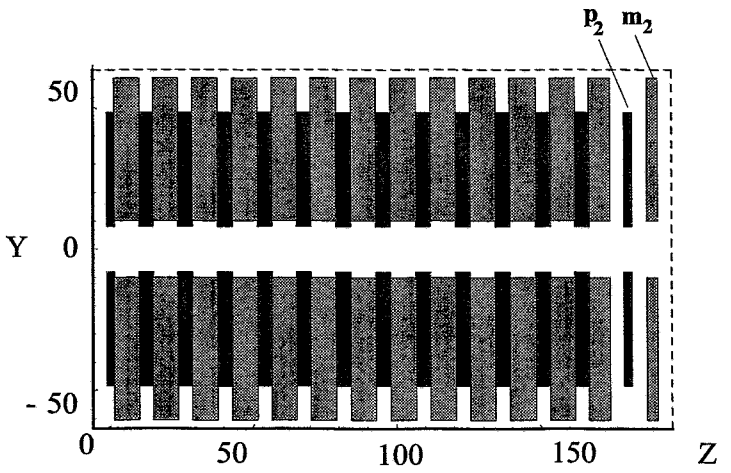

Fig. 1 *Half of the geometry of a model for a "passive" undulator. The grey rectangles represent NdFeB permanent magnets, the black details show poles of decarburized iron. On the left hand side only the half of the central pole is visible. The symbols p_2 and m_2 denote poles and magnets of reduced thicknesses mounted at the same girder like the rest of the structure.*

The geometry of a model for a "passive" undulator simulated with the code RADIA [1] is shown in fig. 1. The dimensions of the iron poles and the permanent magnets are the same as for the TESLA-Test-Facility (TTF) at DESY [2]. The undulator period is $\lambda_u = 27.3$ mm. It was assumed that all permanent magnets have the remanent magnetization of $M_r = 1.12\ T$.
The undulator was adjusted for a gap width of g = 16 mm by variation of the distance between the border magnets m_2 and the poles p_2 . Accordingly we calculated the field component $B_y(0,0,z)$ in the middle plane varying the gap parameter in the intervall 10 mm $\leq$ g $\leq$ 22 mm. The trajectories of reference electrons with an energy of $E_{kin} = 20.0\ MeV$ were achieved by twofold integration.
These trajectories are shown in fig. 2 for seven different gaps. As can be seen the mean values $\bar{x}$ of the electron elongation are nearly independent on g and lie at about 0.2 mm. Finally the fig. 3 demonstrates that the displacements Δ at the undulator exit as a function of g are only small. Both parameters, $\bar{x}$ as well as Δ, should be compatible with the properties of the optical resonator.

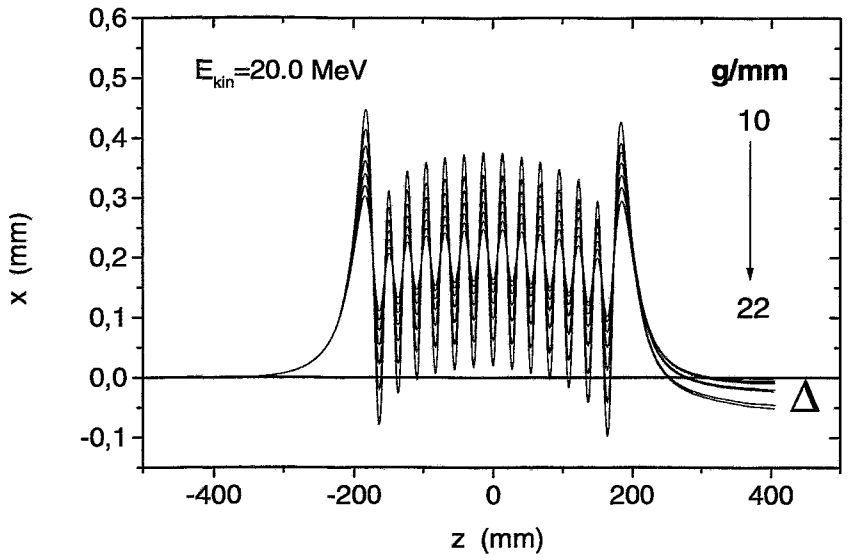

Fig. 2 *Trajectories of reference electrons with $x_0 = 0$ mm, $\Theta_0 = 0$ degr and $E_{kin} = 20.0$ MeV in the middle plane of the studied "passive" undulator. The results for g = 10 mm, 12 mm, 14 mm, ... 22 mm are superimposed.*

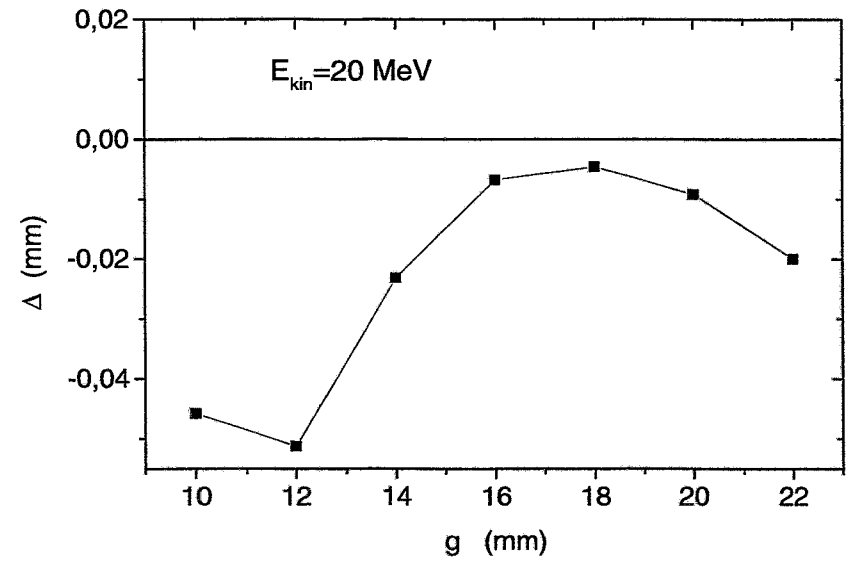

Fig. 3: *The displacement Δ of the electron trajectories as a function of the gap width g. The incidence energy of the reference electron was $E_{kin} = 20.0$ MeV.*

References

[1] P. Elleaume, O. Chubar and J. Chavanne, J. Synchrotron Rad. 5 (1998) 481-484
[2] B. Faatz, J. Pflueger and Y.M. Nikitina, Nucl.Instr.Meth. A375 (1996) 618-625

Field Measurements for the ENEA Permanent Magnet Undulator

P.GIPPNER, G.P. GALLERANO[1], U. WOLF, A.SCHAMLOTT, A. DORIA[1] AND E. GIOVENALE[1]

The ENEA FEL experiments done in the early eighties were aimed at the generation of laser light in the IR region[1]. The undulator is characterized by a period of $\lambda_u = 50$ mm, a length of $L_u = 2250$ mm, a working gap of $h_u = 13 - 24$ mm and a remanent field of $B_r = 9.5$ kG. The field distribution of this Halbach type undulator was recently measured in order to be sure that the permanent magnets, mounted at ENEA in 1984, did not suffer considerable defects. The measured magnetic field component $B_y(0,0,z)$ in the middle plane as well as the first and second field integrals for a 20 MeV electron are shown in fig. 1. Superimposing a weak homogeneous magnetic field of $B_0 = -1.32$ G the trajectory cling to the undulator axis resonably well.

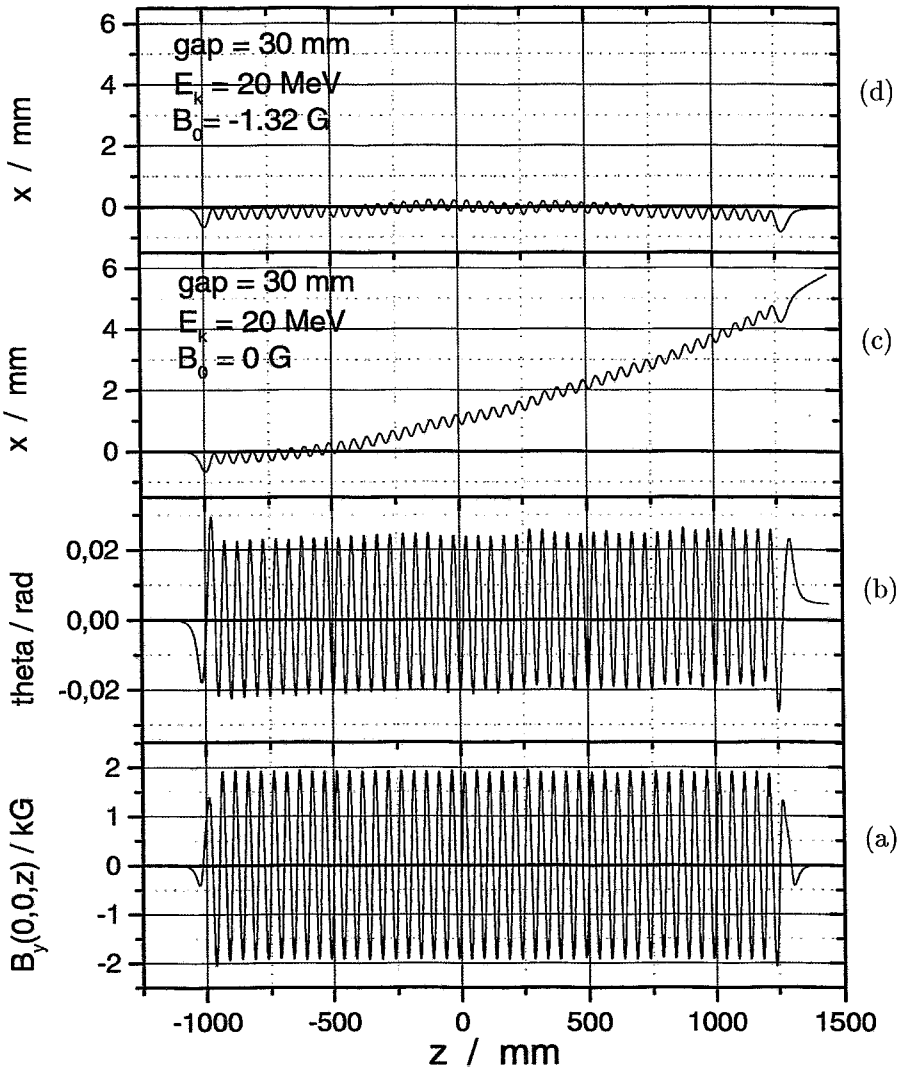

Fig. 1 *The measured field component $B_y(0,0,z)$ (a), the first integral (b) of this component, which is proportional to the angle Θ of the moving electron relative to the z-axis, and the trajectory of this electron (c). The trajectory closely follows the z-axis by addition of a constant field B_0 = -1.32 G to $B_y(0,0,z)$ (d).*

[1] *ENEA, Frascati, Italy*

References

[1] F. Ciocci et al., Nucl. Instr. Meth. A 250 (1986) 134-137

Considerations on the resonator of the ELBE FELs

D. Reppel, W. Seidel, U. Steegmüller, R. Wünsch

The FZ-Rossendorf wants to build up a free-electron-laser user facility at the ELBE project. Some investigations on the design of the optical resonator of the MIR-FEL in the wavelength range from 5 to 30 μm have already been made. A resonator consists of two mirrors of a given radius of curvature between which the optical power that is built up by the laser medium is amplified at each round trip. The stability of a resonator is determined by the g-parameter, defined by $g = 1 - L/R$ (where L is the length of the cavity and R is the mirror radius of curvature). For a symmetric resonator g^2 must be smaller than 1 [1]. The optical cavity length of the ELBE-FELs is determined by the repetition rate of the electron bunches from the accelerator. In this way the cavity length was fixed at 12.68 m. The Rayleigh range should be between $1/\sqrt{12}$ and $1/2$ of the undulator length [2]. The first value leads to a minimum mode volume in the undulator region and hence to a high small-signal gain, the second one minimizes the field size at undulator exit.

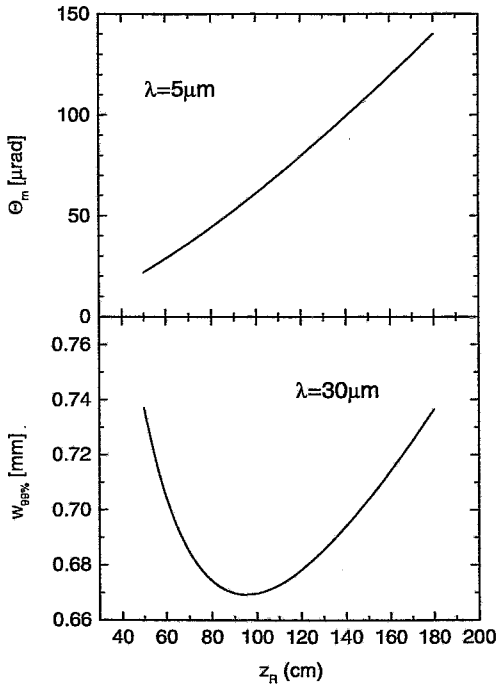

Fig. 1 *Angular tolerance Θ_m of the resonator mirrors (upper panel) and beam radius $w_{99\%}$ for 99% energy transmission at undulator exit (lower panel) as a function of the Rayleigh range z_R each at the most critical wavelength.*

The beam tube of the undulator we want to use has a length of 190 cm and an internal transverse dimension of 1 cm × 4 cm. It acts as an aperture, especially for longer wavelengths. The transverse mode size of the beam is a function of the Rayleigh range. An examination of the dependence of the optical mode size on the Rayleigh range z_R for the longest wavelength of the MIR-FEL of 30 μm leads to a minimum value at the undulator exit if $z_R = 95$ cm (Fig.1). In this case the losses due to diffraction are minimized but the optical beam radius is still bigger then the spacing left by the aperture. We are still examining the influence of this restriction of space on the mode structure. A Rayleigh range of 95 cm leads to a mirror radius of curvature of 6.478 m and a g-parameter of -0.956, with $g^2 = 0.914$. The angular tolerance, that is the maximum angular tilt of a mirror is given by $\Theta_m < \sqrt{2\lambda/\pi L} * (1-g)^{\frac{1}{4}} * (1+g)^{\frac{3}{4}}$. It is defined that way that the tilted optical axis still lies within the transverse mode volume of the optical field [1]. With the parameters above, one obtains $\Theta_m = 56.9$ μrad for the most critical wavelength of 5 μm.

References

[1] C. Brau, "Free-electron Lasers", (Academic Press, San Diego, CA, 1990) chap. 7

[2] S. Benson, "Optical cavities for free electron lasers" Nucl. Instr. and Meth. A304 (1991) 774

Considerations for IR-Absorption Experiments at the ELBE FELs

M.WENZEL, W.SEIDEL, E.GROSSE

Infrared absorption measurements for material sciences or biological investigations will be one of the most important types of future experiments at the ELBE Free Electron Lasers (FEL).

The Cavity Ring Down Spectroscopy (CRDS) is an ultrasensitive absorbance measurement technique. Light from a pulsed laser enters an optical cavity and rings down due to losses from the cavity mirrors and from the sample inside the cavity. The most important property of this method is: measuring the rate of absorption and not the amount makes the result independent from intensity fluctuations of the light source. The multiple reflections in the cavity produce long path lengths, which increases the sensitivity of the method. For these reasons the CRDS is especially useful for trace gases and thin films.

The intensity at the output of the cavity after n round trips of the light will be

$$I(t_0 + nt_R) = I(t_0)R^{2n},$$

where $I(t_0)$ is the initial intensity of the light, t_R the round trip time, R the mirror reflectivity, and where the losses in the cavity are induced only by the mirror reflectivity. In that case we find an exponential decay

$$I(t_0 + nt_R) = I(t_0)e^{-nt_R/\tau_0}$$

with the decay constant $\tau_0 = \frac{t_R}{2(1-R)}$. Note, that the absorption sensitivity here is direct a function of the mirror reflectivity. The round trip time can be found by $t_R = \frac{2L_C}{c}$, with the velocity of the light c and the length of the cavity L_C.
Introducing a sample into the cavity the decay will be influenced by the absorbance α and the thickness l of the sample, too. The ring down decay constant is then

$$\tau = \frac{t_R}{2((1-R) + \alpha l)}.$$

Knowing the sample thickness, the absorbance α can be easily determined using this expression. First results of this technique were presented in [1].
A considerable enhancement of the signal-to-noise ratio for this method is attained with Pulse-Stacking (PS) in the ring down cavity. To that end the cavity round trip time is selected to be - by a small integer factor - smaller than the pulse repetition time of the beam coming from the FEL. Thus the cavity length is just an integer fraction of the FEL resonator length, making the PS-CRDS a technique very well suited to be combined with a FEL with its high repetition rate and its wide wavelength range.
Experimental requirements are a very fast detector and a fast data acquisition system, a good vacuum system around the optical cavity, highly reflective cavity mirrors and eventually an optical beam shutter system, e.g. a semiconductor switch with a synchronized Titan-Sapphire-Laser or acusto-optical modulators.

References

[1] A.J.Ramponi, F.P.Milanovich,T.Kan and D.Deacon, Applied Optics 27 (1988), 4906

Metal Meshes as Reflectors in the Infrared

M. WENZEL, K. NIELSEN[1], E. CROSSON[2], W. SEIDEL, E. GROSSE

Strip gratings and metal meshes are used as partial reflectors and filter elements at submillimeter wavelengths. For the realization of flat reflectors no supporting substrate is needed resulting in broad band reflectivity and output coupling. The application of these meshes for the infrared region as laser mirrors seems to be possible and is proved in this work.

Using the Free Electron Laser FIREFLY of the Hansen Experimental Physics Laboratory (HEPL) at Stanford University, we measured the transmission and reflectivity of an inductive mesh (Ni, 2000 lines/inch, lattice constant $g = 13\mu$m) in the wavelength region from 35 μm to 55 μm. We compare the results with calculated transmission and reflectivity values in dependence on the wavelengths. The calculations are based on an equivalent circuit transmission-line model cited first in [1].

The transmission was investigated with two calibrated detectors and a beamsplitter, whereas one of the detectors measured the incoming intensity of the light, the other one the transmitted intensity. For the measurement of the reflectance we used the Cavity Ring Down Technique. A cavity with two meshes as cavity mirrors surrounded by a vacuum system was necessary. The ring down time in the cavity depends only on the length of the cavity L_C and on the reflectivity R of the cavity mirrors, under the assumption that no other intensity losses appear inside the cavity. From the exponential decay time τ_0 of the intensity after the end of the light pulse the reflectivity R can be found: $\tau_0 = \frac{t_R}{2(1-R)}$, with the round trip time $t_R = 2L_C/c$ (c is the velocity of the light).

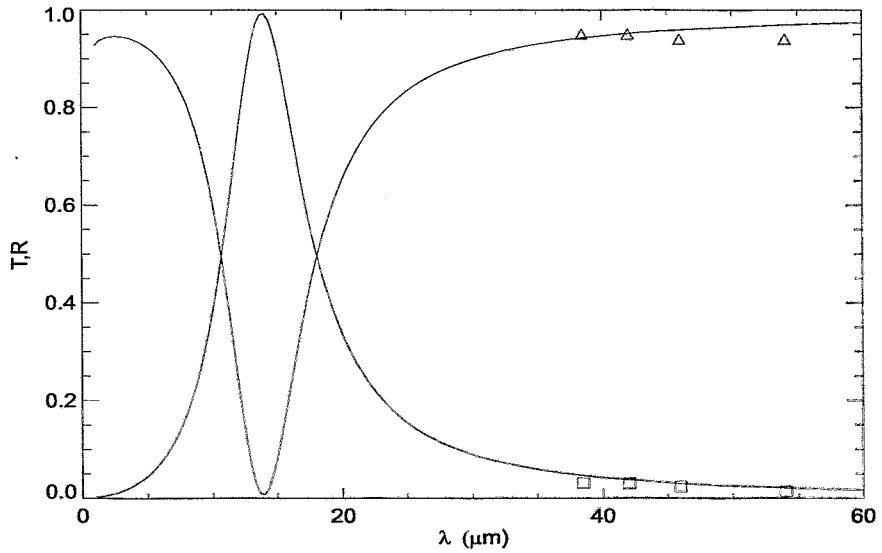

Fig. 1 *Measured transmittances (triangles) and reflectivities (squares) of a metal mesh in comparison with calculated values in dependence of the wavelength.*

As it can be seen in Fig. 1, the agreement for the investigated wavelengths ($\lambda \gg g$) of the experimental and the theoretical values is good. The minimum in the transmittance at about 13 μm can be explained with $\lambda \sim g$ in this region. Metal meshes can be used as mirrors in the far infrared region. For applications in the mid infrared region, however, meshes with smaller grid periods are necessary but not available up to now.

[1] *Universität Marburg*
[2] *HEPL, Stanford*

References

[1] L.B.Whitbourn and R.C.Compton, *Applied Optics* **24** (1985), 217

Optimization of the ELBE Injector for the Production of Electron Beams with Minimum Transverse Emittance

U. LEHNERT

For radiation physics and radiation biology experiments an electron beam with a normalized transverse RMS emittance of less than 1 π mm mrad and an average current of 100 μA is required. This requirement can be met by cutting down the 1 mA average current delivered by the cw thermionic RF gun [1,2] with two diaphragms in the injector beam path, thus reducing the initial 1.2 π mm mrad transverse emittance to less than 0.5 π mm mrad before the entrance of the accelerator cavities.

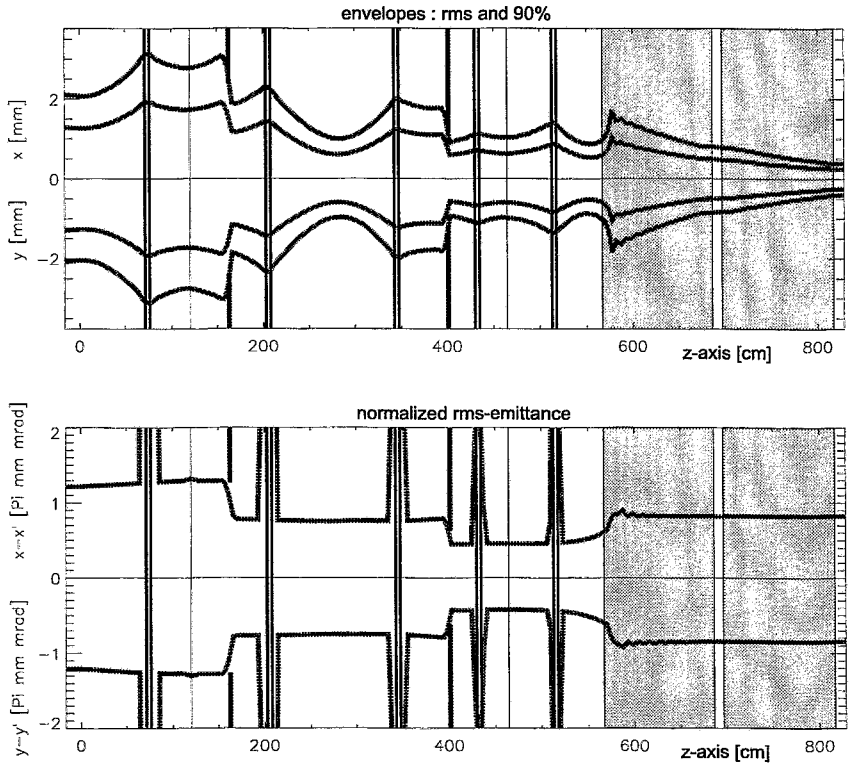

Fig. 1 *Envelope and transverse emittance of a 100 μA electron beam in the ELBE accelerator; double lines mark the positions of solenoid magnets, single lines mark the positions of the two bunchers, diaphragms are shown as thick lines and the accelerator cavities are underlaid grey.*

The proposed design was developed using the PARMELA [3] code. Figure 1 shows the computed beam properties within the ELBE accelerator. Solenoid fields and RF phases of bunchers and cavities have been adapted to the smaller space charge of the reduced electron current and optimized to achieve a minimum possible transverse emittance of the beam at the accelerator exit. With these settings an 18 MeV electron beam with a normalized transverse RMS emittance of 0.75 π mm mrad and an energy spread of less than 100 keV can be produced.

References

[1] F. Gabriel ed.; FZR Internal Design Report (1995)
[2] D. Janssen, P. von Stein; Nuclear and Hadron Physics and Project ELBE, Annual Report (1996)
[3] L.M. Young; Los Alamos National Laboratory (1996) LA-UR-96-1835

Design of the Beam Transport System for the Radiation Physics Cave at ELBE

U. LEHNERT

The beamline, which transports the accelerated electrons to the radiation physics target chamber has to be achromatic in order to conserve the transverse emittance of the electron beam. Additionally, it has to provide a versatile focusing of the beam onto the target allowing to achieve either a minimal beam spot size or a minimal beam divergence.

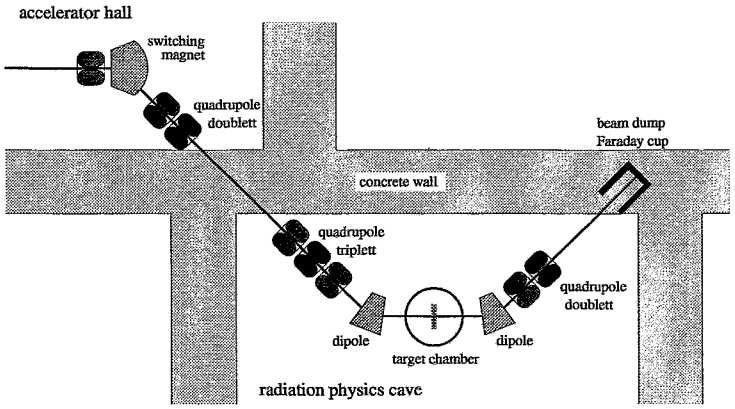

Fig. 1 *The placement of electron optical elements on the radiation physics beamline*

The general outline of the design is shown in figure 1. Its main features have to meet given special limitations. The center of the beamline from the switching magnet to the first dipole lies inside a concrete wall and is not accessible for optical elements, preventing a symmetrical design. In order to provide enough space for experimental setups the beamline segments between the dipoles and the target chamber are kept very short, precluding the insertion of quadrupoles in these positions. Thus, all necessary focusing has to be provided by the first dipole and the preceding quadrupole triplet.

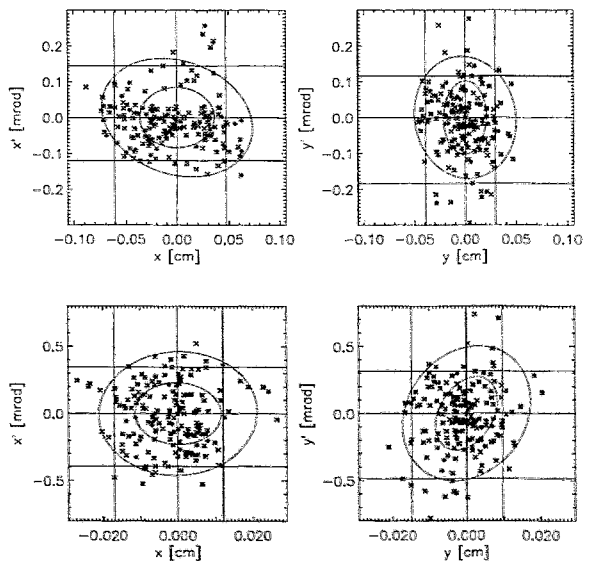

Fig. 2 *The transverse phase space at the target position for an 18 MeV electron beam with an initial emittance of 0.8 π mm mrad*

a) for minimal divergence of the electron beam

b) for minimal beam spot size and a maximum allowed divergence of 1 mrad

RMS and 90% phase space ellipses are shown.

As shown in figure 2, the requirements of a narrow focusing and a low divergence, conserving the low initial emittance of the beam, can be met with the proposed design.

Energy Resolution of a CCD Camera for X-ray Detection [B]

W. Neubert, B. Naumann, W. Enghardt and W. Wagner

Channeling radiation (CR) detected at zero degree with respect to the beam axis is always accompanied by the continuous bremsstrahlung spectrum. In order to get a reasonable effect-to-background ratio an energy resolution of the X-ray detector better than 10% is required. Connected with this task we investigated the properties of a thermoelectrically cooled CCD camera [1]. The Be entrance window (200 μm) and the thickness of the silicon chip fix the mostly efficient registration range from $\simeq$ 4 keV to $\simeq$ 15 keV (see below, Fig.3). The camera was irradiated by a ^{55}Fe source and fluorescence X-rays. The 1152 times 1242 pixels (each 22.5 μm^2) were read out by a 200 kHz ADC and the following histogramming over the full frame provides the pulse height distribution. The energy resolution has been measured as function of the cooling temperature (see Fig.1). The theoretical limit was attained within the range -55°C $\leq T \leq$ -50°C corresponding to an energy resolution of $\sigma \simeq$ 120 eV. The section of the pulse height spectrum of Fig.2 demonstrates the resolved K_α and K_β lines.

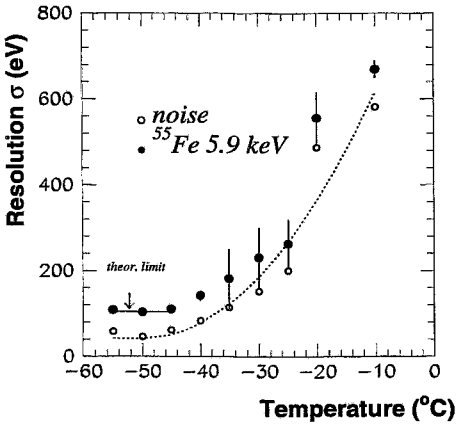

Fig. 1 *Energy resolution of the CCD camera vs. cooling. Dots: measured energy resolution of K X-rays from a ^{55}Fe source, open circles: width of the thermal noise distribution.*

The energy resolution of the CCD camera in the expected energy range of CR is shown in Fig.3. Outside the narrow effective range there is an increasing contribution of noise from the dark current which deteriorates the attainable energy resolution.

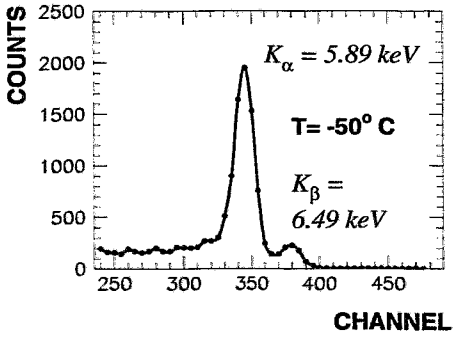

Fig. 2 *X-ray spectrum of a uncollimated ^{55}Fe source, obtained after background subtraction and histogramming over the whole sensitive area of the CCD camera.*

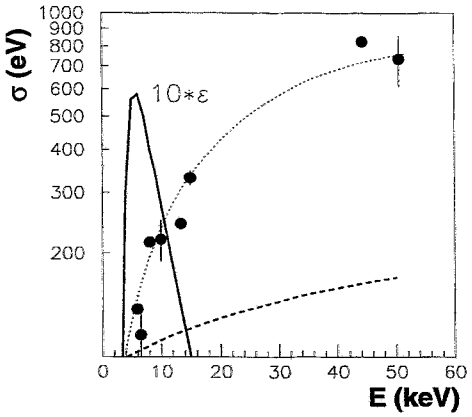

Fig. 3 *Energy resolution of the CCD camera vs. X-ray energy. Black dots: line width obtained from Gaussian fits to the K_α and K_β lines excited by an ^{241}Am source in radiators of Fe,Cu,Rb and Tb, solid curve: detection efficiency [1], dotted line: fit for experimental data, dashed line: theoretical limit of the energy resolution.*

References

[1] TE/CCD Operation Manuals, Princetown Instruments, May 1997

GEANT Simulations of Experimental Setups for Channeling Radiation [B]

W. NEUBERT, B. NAUMANN, P. GIPPNER, V.V. MOROKHOVSKI[1] AND J. FREUDENBERG [1]

Channeling radiation is always affected by bremsstrahlung which is not only produced by the electron beam penetrating the crystal but also by scattered electrons which interact with the construction materials. In order to localize the most important interaction areas and sources of bremsstrahlung at the low-energy experimental area at S-DALINAC Monte-Carlo simulations using a realistic geometry have been performed with the GEANT program package [1]. The results of simulations carried out for incident 9 MeV electrons on a 100 μm diamond crystal are presented in Fig.1. Multiscattering of the electrons spreads the beam and produces the most important background in the narrow exit tubes of the goniometer and magnet chamber compared to smaller contributions from the beam dump (see right part of Fig.1).

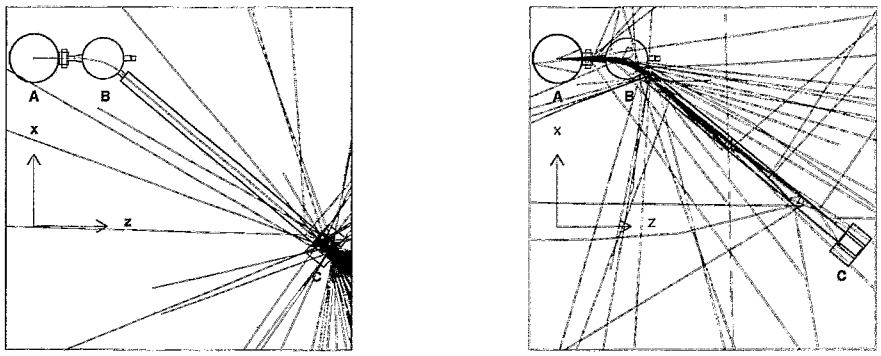

Fig. 1 *Particle tracking starting just in front of the target in the center of the goniometer chamber (A) through the bending magnet (B) to the beam dump (C), left: 10 trigger events (e^-), interaction by bremsstrahlung and knock-on electrons, right: 30 events with additional multiscattering and energy loss in the crystal, red lines: electrons, blue dashed lines: photons.*

In preparation of experiments at the radiation source ELBE similar considerations have been performed in order to optimize the design of the corresponding setup. The Rossendorf goniometer chamber is shown in Fig.2. We used the beam parameters provided by the code MIRKO [2] for the projected beam line at the target position x=0.58 mm and y=0.24 mm corresponding to a phase space ellipse which contains 90 % of the intensity of the 20 MeV electron beam. The distribution in the transversal phase space supplies $x' = y' = 1.3$ mrad. After transmission of the diamond crystal (80 μm) the beam size is broadened by the above mentioned interactions but fits into the exit tube of the goniometer chamber. Only $\simeq 0.2$ % of the electrons stacked into the surrounding material, but this portion rises to $\simeq 8$ % in the following narrow tube (CF 42); thus an increased beam line diameter as compared to the standard size is indicated. Simulations of the bremsstrahlung spectra generated in the beam line material are in progress.

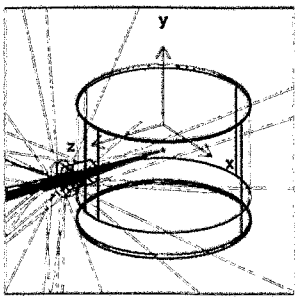

Fig. 2 *Beam tracking including multiscattering, energy loss and generation of knock-on electrons.*

[1] *Institut für Kernphysik der TU Darmstadt, 64289 Darmstadt,Schlossgartenstr.9*

References

[1] GEANT - CERN Program Library W5013, March 1994.
[2] B.J. Franczak, code MIRKO (Version 6.06-V 1998), GSI Darmstadt.

Resonant Channeling Radiation in a Hypersonic Field [W]

L.Sh. Grigorian[1], A.R. Mkrtchyan[1], B.V. Khachatryan[1],
H.F. Khachatryan[1], H. Prade, W. Wagner

Electromagnetic processes are substantially influenced by the medium [1]. The planned application of channeling of relativistic electrons in single crystals for the production of quasi-monochromatic X-radiation at ELBE initiated the investigation of effects which can be used for a stimulated enhancement of the intensity of this radiation. It has already been shown that an intensification of the radiation emission should take place when the crystal is excited by an appropriate hypersonic wave [2]. The optimization of this effect, however, requires the fundamental understanding of the mechanism of such external stimulation.

The description of the channeling process at the energies E of interest (E $\leq$ 100 MeV) needs a quantum mechanical treatment. For simplicity, the case of planar positron channeling in a longitudinal hypersonic field has been considered. In adiabatic approximation and neglecting the spin degree of freedom, the Dirac equation for the wave function φ_E of the positron channeled in an acoustic superlattice takes the form

$$\left[(E-U)^2 - m_0^2 + \hbar^2\Delta + \frac{\hbar^2}{E-U+m_0}(\nabla U)\nabla\right]\varphi_E = 0 \qquad (1)$$

where m_0 the rest mass of the positron. The acoustically modified crystal potential

$$U(x,z) = U_0 \cos k_s z + bx^2(1+\mu\cos k_s z), \qquad (2)$$

contains the amplitudes U_0 and μ depending on the power of the hypersound, the parameter b of the non-affected crystal potential $U(x) = bx^2$, and $k_s = 2\pi/\lambda_s$ is the wave number of the hypersound propagating along the z-coordinate which coincides with the direction of positron motion. The x-coordinate is taken to be normal to the channeling plane. To solve eq.(1) the function φ_E is expanded in a series of functions $S_n(x)$ which describe the oscillations of the positron in the transverse plane. For small values of the potential U the function φ_E becomes a superposition of only three states with momenta $p_z = (p_n - \hbar k_s\ ,\ p_n\ ,\ p_n + \hbar k_s)$ with p_n being the momentum in the state n.

A resonance appears in the amplitudes of the wave function if the wave length of the hypersound λ_s approaches the critical value $c\pi/\omega_E$ related to the frequency $\omega_E = \sqrt{2b/E}$ of the transverse oscillation of the positron. This resonance condition is formally the same as it has been found earlier within a classical description [2].

The probability of radiative transitions consists of five terms with frequencies

$$\omega_{res} \approx \frac{\Omega_{fi} - 2\nu\omega_E}{1-\beta_{\|}\cos\vartheta}, \qquad \nu = 0,\ \pm1,\ \pm2, \qquad (3)$$

where Ω_{fi} is the non-affected frequency. For $\nu = -1,\ -2$ the emission of a photon may be accompanied with an *increase* of the transversal energy of the positron ($\Omega_{fi} < 0$). To achieve resonance, the frequency of the hypersound must be of the order of 10 GHz.

A verification of resonant electron-channeling radiation at ELBE is of fundamental interest.

[1] *Institute of Applied Problems of Physics, Yerevan, Rep. of Armenia*

References

[1] M.L. Ter-Mikaelian, High-Energy Electromagnetic Processes in Condensed Media, J. Wiley and Sons Inc., New York, 1972.

[2] A.R. Mkrtchyan et al., Phys. Lett. A115 (1986) 410; Phys. Lett. A126 (1988) 528.

Parametric X-Radiation from Piezoelectric Crystals [W]

W. WAGNER, A.R. MKRTCHYAN[1], H. BACKE[2], N. CLAWITTER[2], F. HAGENBUCK[2], O. KETTIG[2], G. KUBE[2], W. LAUTH[2], V.K. MIRZOYAN[1], A.H. MKRTCHYAN[1], H. PRADE, S.P. TAROYAN[1]

Parametric X-radiation (PXR) spectra and angular distributions from the piezoelectric crystals SiO_2, $LiNbO_3$ and KH_2PO_4 have been measured for the first time at an electron energy of 855 MeV at the Mainz microtron facility MAMI.

The crystals were mounted on a goniometer situated inside a vacuum chamber and adjusted by scanning of planar channeling radiation so as to fulfill the condition for axial channeling along a main crystal axis. Then they were rotated around the vertical goniometer axis to a glancing angle of Θ_B=22.5°. The PXR was measured using a small 300 μm thick SiLi detector positioned under 45° with respect to the electron beam axis at a distance of about 6 m.

In these measurements an original two-dimensional registration method was applied where the PXR energy spectrum was registered simultaneously with the monotonously changing rotation angle Ω of the crystal around the horizontal goniometer axis. This allows one to obtain a complete picture of PXR reflexes from the crystal.

It is known that PXR induced in a crystal by traversing relativistic electrons is emitted in conformity with the Bragg equation for the respective crystal planes. It can, therefore, be interpreted as a diffraction of electromagnetic waves accompanied with the moving electron. Hence, in these measurements we observed PXR reflexes from all crystal planes (i.e. elements of crystal symmetry) for which the Bragg law was fulfilled.

One of the PXR matrices measured for a 0.81 mm thick quartz crystal is shown for illustration in Fig. 1. In honor of the Armenian scientist Alpik R. Mkrtchyan we have named this figure *Alpikogramme* ©.

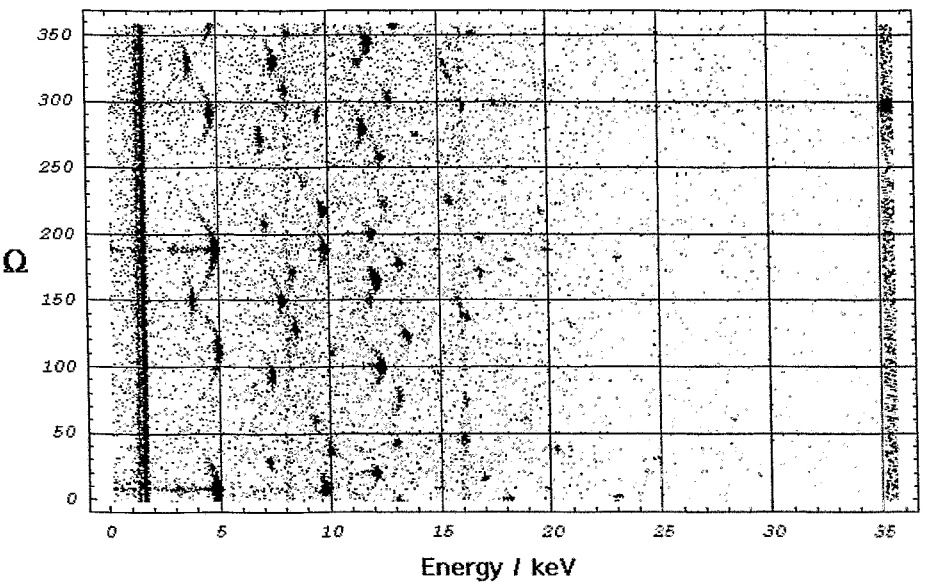

Fig. 1 *Alpikogramme of a 0.81 mm thick quartz crystal. The rotation angle (Ω) is given in degrees. Reflexes of equidistant energy spacing represent the different orders of diffraction.*

Similar to other crystallographic representations like, e.g., the Lauegramme, Debyegramme or Fjudgevaragramme, the Alpikogramme represents a set of PXR reflex groups each consisting of n reflexes where n is determined by symmetry elements of the given crystal. It can be used to obtain a three-dimensional view of the crystal.

[1] *Institute of Applied Problems of Physics of NAS, Yerevan, Armenia*
[2] *Johannes-Gutenberg-Universität Mainz, Institute of Nuclear Physics, Mainz, Germany*

X-Ray Diffraction on Piezocrystalline Specimen in the Presence of an Acoustic Field

W. WAGNER, W. MATZ[1], V.K. MIRZOYAN[2], A.H. MKRTCHYAN[2], A.R. MKRTCHYAN[2], H. PRADE, N. SCHELL[1]

The dynamic diffraction of X-rays on piezoelectric single crystals excited by acoustic vibrations was studied at the Rossendorf Beam Line (ROBL) [1] of the ESRF in Grenoble. Earlier investigations using characteristic X-rays showed that for crystals of $\mu t < 1$ (μ - linear absorption coefficient, t - crystal thickness) a nearly complete transfer of monoenergetic X-rays can be achieved resembling a total mirror reflection [2].

A parallel beam (horizontal divergence $\leq 5"$) of monochromatic synchrotron radiation ($E = 17keV, \Delta E/E \approx 10^{-4}$) was scattered by a quartz single crystal of X-cut. The crystal was mounted in Laue geometry on a 6-axes goniometer for precise adjustment to fulfill the Bragg condition for the $(10\bar{1}1)$ plane. Longitudinal standing ultrasonic waves of wavelength $\lambda = 2t$ were excited in the crystal forming a quasi-static acoustic superlattice.

To investigate the effect of ultrasound on X-ray diffraction we measured the intensities of the diffracted and the transmitted beam around the Bragg angle in dependence on the magnitude of the ultrasonic vibrations. Examples of such spectra are presented in Fig. 1.

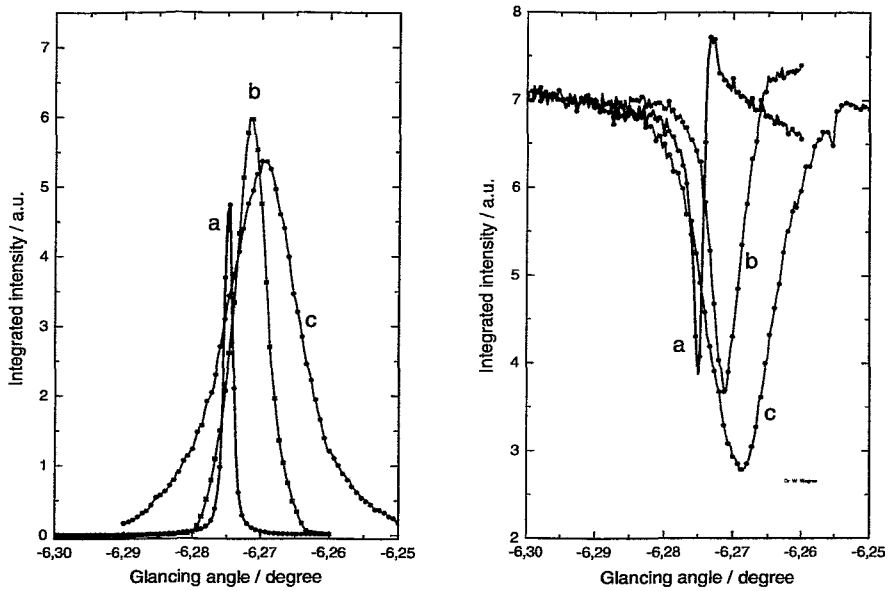

Fig. 1 *Pattern of diffracted (left panel) and transmitted (right panel) beam without ultrasound (a) and for two values of the magnitude of ultrasonic vibrations (b, c).*

The intensity of the diffracted beam (curve a on the left panel) increases with increasing magnitude of ultrasonic vibrations up to saturation (curve b), and the width of the reflex also increases steadily (b, c). In this way, the integrated reflecting power could be increased by a factor of about ten. The results are in qualitative agreement with calculations performed in the framework of the dynamical diffraction theory [3]. The reverse picture is observed for the transmitted beam (right panel). Additionally, a decrease of the linear absorption coefficient has been found.

[1] *Institute of Ion-Beam Physics and Materials Research FZ Rossendorf*
[2] *Institute of Applied Problems of Physics of NAS Yerevan, Armenia*

References

[1] W. Matz *et al.*, FZR-256, Forschungszentrum Rossendorf, 1999.
[2] A.R. Mkrtchyan *et al.*, JETP Lett. 9(19) (1983) 1181.
[3] R.G. Gabrielyan *et al.*, phys. stat. sol. 92 (1985) 361.

Parametric X-ray Detection at S-DALINAC using a CCD Camera [B]

U. Lehnert, W. Neubert, U. Nething, V. Morokhovskyi[1] and S. Fritzler[2]

The thermoelectrically cooled CCD-camera described in [1] was used at S-DALINAC to detect parametric X-rays (PXR) from 8 MeV electrons penetrating a silicon crystal. As this camera does not contain a mechanical shutter, special precautions are necessary to prevent the chip from being irradiated during readout time. Therefore, the electron beam of the accelerator was gated using the status signals from the camera controller. The radiation was collimated down to 5.0*10^-6 sr solid angle at an angle of 44° to the forward direction. Thus, a circular region with approximately 1 cm diameter was irradiated on the CCD. For each angular position of the crystal one image frame from the CCD was analyzed. The number of events in the peak as well as the peak energy are plotted in figure 1 showing the characteristic distribution for parametric X-rays. The obtained spectra compare very well with those measured at the same position using a Si(Li) detector.

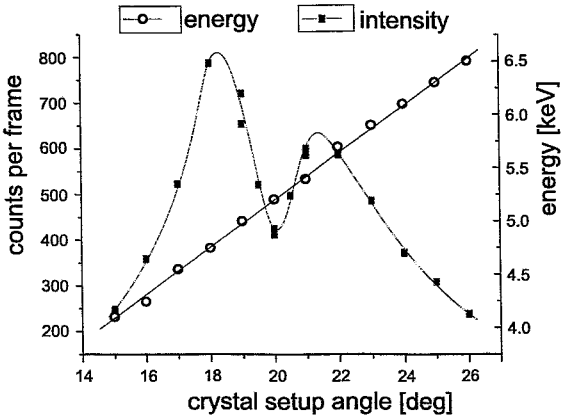

Fig. 1 *The angular distribution of PXR intensity and energy measured with the CCD camera*

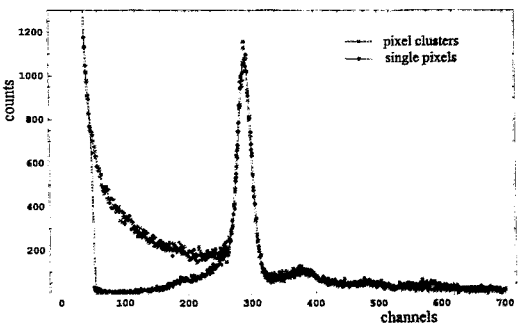

Fig. 2 *The accumulated charge in single pixels and in clusters of pixels of the CCD-camera irradiated with PXR from the (111) plane of a Si crystal at an energy of 4.8 keV*

The shape of an X-ray line in the pulse height distribution shows a rather prominent low-energetic shelf (see figure 2). This shelf originates from events where the signal charge from one X-ray photon is spread over two or more neighboring pixels. In order to correct for this effect, a cluster recognition algorithm was applied that sums up the charge collected in all adjacent pixels that exceed the noise threshold. To prevent the generation of excessive pileup by this algorithm, the total irradiation of the CCD has to be low so that the true events are spatially well separated.

With this experiment the operability of the CCD camera in an accelerator synchronized mode and in a high noise high radiation background environment has been demonstrated, thus showing its usability for future imaging applications.

[1] *Kharkov Institute of Physics and Technology, 310108 Kharkov, Ukraine*
[2] *TU Darmstadt, Institut für Kernphysik*

References

[1] W. Neubert, B. Naumann, W. Enghardt, W. Wagner:
Energy Resolution of a CCD Camera for X-ray Detection; this Report p. 24

Compton Scattering of Laser Light off the ELBE Electron Beam

H.W. Barz and E. Grosse

High energy photons can be produced by scattering laser light off relativistic electron beams (i.e. Compton backscattering). A photon with energy E_{ph} which is scattered off an electron with a much larger energy of $E_e = \gamma m_e c^2$ gets a maximum energy of $E_C \simeq 4\gamma^2 E_{ph}$ in the direction of the electron when Compton scattered. Fig. 1 illustrates the double differential cross section $d\sigma/d\Omega dE_C$ near the maximum energy for the scattering of 2.36 eV (green) laser light off a 40 MeV electron beam which will be generated at the ELBE facility. For this case the maximum energy of the scattered photon amounts to 59.24 keV. The finite energy width ΔE_e and the angular width $\Delta\Theta_e$ of the beam leads to an broadening of the peak cross section of $d\sigma/d\Omega \simeq 320\ \gamma^2$ mb/sr over an energy range ΔE_C where the relative spread $\Delta E_C/E_C$ is given by combining $\gamma^2\Delta\Theta_e^2$ and $2\Delta E_e/E_e$ with the electron beam having an angular spread of 0.07 mrad and an energy spread of 25 keV. As shown in Fig. 1 the rather sharp angle-energy correlation results from the high brilliance of the beam.

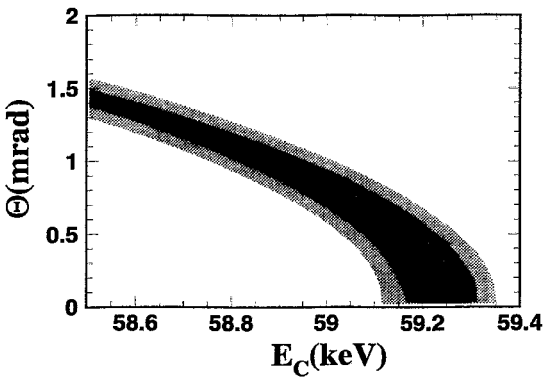

Fig. 1 *Contour plot of the double differential cross section $d\sigma/d\Omega dE_C$ for the production of keV photons by scattering laser light off a 40 MeV electron beam. The width of the band in the plot results from an rms angular spread of 0.07 mrad and an rms energy spread of 25 keV of the electron beam (the different areas denote cross sections above 3, 6, and 9 b/eV/sr, respectively).*

The effective cross for generating photons sensitively depends on the required energy resolution and the opening angle allowed for the backscattered photons: For a 1 % rms energy resolution a cross section of about 12 mb out of the total one of 600 mb is usable. The yield of backscattered photons is inversely proportional to the size of the cross section of the overlap zone of laser and electron beams. If it is in the mm^2 range a 2W laser light will result in a rate of 10^3 Compton scattered photons per second for the above mentioned energy resolution. A very interesting possibility is to use the free electron laser (FEL) light within the undulator by doubling the frequency of the electron bunch emission and scatter the light off every second bunch. As there is a considerably higher power than in a standard laser an intensity of 10^7/s of 6 keV photons can be produced at using an IR FEL laser of 5μm wavelength.

Estimates of the Landau-Pomeranchuk-Migdal and Ter-Mikaelian Effects [B]

B. KÄMPFER, O.P. PAVLENKO[1], W. MÜLLER[2]

A charged particle, traversing an amorphous material, suffers multiple scatterings, and as a consequence it radiates photons. At relativistic energies, where the Lorentz factor $\gamma \gg 1$, the separation of the particle and the emitted photon occurs over a large longitudinal distance, called formation length. If the emission process is disturbed, the emitted radiation will be reduced due to destructive interferences (often referred to as Landau-Pomeranchuk effect). The emission process can be interrupted either by multiple scattering of the particle (Landau-Pomeranchuk-Migdal effect (LPM)) or by scattering of the photon in the medium (Ter-Mikaelian effect (TM)). For a rough qualitative estimate of these effects one may employ the approach of Galitsky and Gurevich [1], where the radiation spectrum is $dI/d\omega = q(dI/d\omega)|_{BH}$ with $(dI/d\omega)|_{BH} \approx const$ as Bethe-Heitler (BH) spectrum. The suppression factor is the ratio of the coherence length in medium to that one in vacuum. It reads in suitable variables for $\omega \gg \omega_0$

$$q = 2\frac{\eta}{\xi}\left(\sqrt{(1+\xi)^2 + \frac{\xi}{\eta}} - (1+\xi)^2\right), \tag{1}$$

where $\xi = \gamma\omega_0/\omega$, $\eta = \gamma_{LPM}/\gamma$ and $\gamma_{LPM} = \frac{1}{4}\omega_0 X_0 m^2/E_s^2$; $\omega_0 \approx 60$ - 80 eV is the plasma frequency, $X_0 \approx 1$ cm stands for the radiation length (for copper $\cdots$ lead), and $E_s \approx 21$ MeV denotes the radiation constant. The normalized radiation spectrum is displayed in fig. 1.

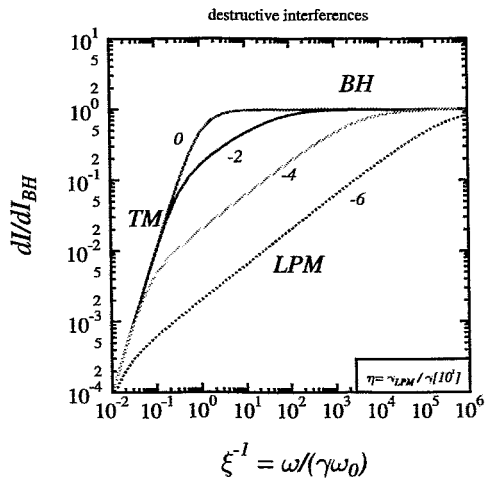

Fig. 1 *Normalized radiation spectrum as a function of ξ^{-1} for various values of α in $\eta = 10^{\alpha}$. The low-frequency part is bounded by the TM spectrum with $q = 1/\xi^2$, while the hard part is the BH regime with $q = 1$. For sufficiently large particle energies $\gamma > \gamma_{LPM} \approx 10^3$, in the intermediate frequency range $\eta < \xi < 1/\eta^{1/3}$ the proper LPM spectrum appears with $q = 2\sqrt{\eta/\xi}$. We consider here electrons with mass $m = 0.5$ MeV.*

The design energy of the electron accelerator ELBE, $\gamma_{ELBE} = 80$, is far below γ_{LPM}, therefore $\eta \gg 1$. The dielectric suppression by the longitudinal density effect à la TM sets in at $\xi = 1$, i.e. $\omega < \omega_{TM} \approx 5$ keV. In this region, however, a measurement of the radiation spectrum may be hampered by the resonant interaction processes with atoms. Also the transition radiation and finite size effects of the target material need to be removed [2]. At considerably larger beam energies (say at 1 GeV and above) the turn-over to the TM regime happens at sufficiently large frequencies ($\sim$ 150 keV) to have an access to the plasma frequency ω_0 for various materials by measuring the suppressed continuum spectrum and comparing it with the full theory [3].

[1] *Institute of Theoretical Physics, Kiev, Ukraine* [2] *Institut für Theoretische Physik, TU Dresden*

References

[1] V.M. Galitsky, I.I. Gurevich, Nuovo Cimento XXXII (1964) 396
[2] Anthony et al., Phys. Rev. D 56 (1997) 1373
[3] A.B. Migdal, Phys. Rev. 103 (1956) 1811
R. Baier et al. Nucl. Phys. B 478 (1996) 577
B.G. Zakharov, hep-ph/9805271

Set-Up for Nuclear Resonance Fluorescence (NRF) Experiments at ELBE [B]

K.D. SCHILLING, R. SCHWENGNER, L. KÄUBLER, F. DÖNAU

NRF experiments using unpolarized as well as linearly polarized bremsstrahlung represent a powerful tool for precise and systematic investigations of the structure of stable nuclei and for a model-independent determination of lifetimes in the fs-region. In order to efficiently perform such experiments, a high beam intensity and stability as well as excellent background conditions are needed in combination with highly efficient Ge detectors. All this is planned to be realized in a special beam station at the new ELBE radiation source.

The set-up design is schematically displayed in Fig. 1. The electron beam is transported by a non-dispersive dipole/quadrupole magnet system and focused onto a thin (25-100 μm Al) bremsstrahlung radiator. The steering coils in front of the radiator enable the incidence polar and azimuthal angles of the electron beam to be changed in order to optimize the generation of linearly polarized photons. After passing through the thin radiator the electrons are finally deflected by a 45° dipole magnet into the beam dump. The (off-axis) bremsstrahlung photons produced in the radiator will be collimated and directed onto the scattering (NRF) target located approximately 4 m downstream in the experimental hall. This geometry will ensure favourable background conditions. The γ-rays scattered off the NRF target are detected with EUROBALL Cluster modules (see e.g. [1]) representing very powerful instruments for NRF experiments in the energy region of interest (about 5 to 10 MeV).

A 1.6 m thick wall of heavy concrete blocks separates the beam area from the electron beam line with radiator chamber and beam dump. This shielding and the especially constructed 2.3 m long collimator (with a slightly increasing aperture and made from pure Al, selected because of its high neutron separation energy of 13 MeV) will efficiently reduce the undesired photon and neutron background. The actual beam energy (up to about 13 MeV) will be carefully adapted to the neutron separation energies of the radiator and collimator materials in order to avoid resp. minimize neutron production. By utilizing average beam currents of the order of 500 μA in the cw-regime, photon fluxes of 5×10^7 photons per MeV $\cdot$ s for 7 MeV photons at $E_{e-} = 10$ MeV can be expected at the NRF interaction area. The energy deposition in the radiator foil does thereby not exceed 30 W.

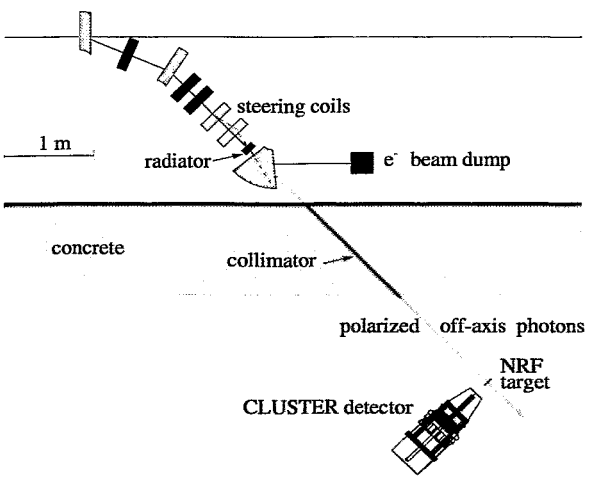

Fig. 1 *Polarized bremsstrahlung facility at ELBE.*

References

[1] R. Schwengner et al., Nucl. Phys. A 620 (1997) 277.

Considerations for the Bremsstrahlung-Photon Radiator at ELBE

A. WAGNER, F. DÖNAU, E. GROSSE, L. KÄUBLER, K. D. SCHILLING, H. SCHNARE, R. SCHWENGNER

One major area of research of the new ELBE facility [1] will be devoted to nuclear spectroscopy studies by means of Nuclear Resonance Fluorescence (NRF) experiments using polarized photons. In these experiments the nucleus of interest will be exited by resonant absorption of photons from a continuous spectrum of polarized Bremsstrahlung-photons. The subsequent decay of excited states will then reveal information about the excitation energy, angular momentum, parity, and lifetime. The use of real photons will result preferentially in magnetic and electric dipole excitations which can be studied in regions even at high level densities. For the determination of parities of the exited states at energies below 5 MeV unpolarized photons and a Compton-polarimeter can be used while at higher energies polarized photons from off-axis Bremsstrahlung-production will be a suitable tool. These experiments will greatly benefit from the high duty factor and the high electron beam intensity available at the ELBE facility. In order to obtain the optimal radiator configuration the photon fluxes produced with two different radiator materials were calculated using the program library GEANT [2]. Figure 1 shows the number of photons Φ_γ emitted into a forward cone with an opening angle of 20 mrad for photon energies below and above 5 MeV. It can be seen that Φ_γ for both radiators almost saturates above thicknesses of 200 μm making thicker radiators unfavorable as they lead to an increased energy deposition and small angle scattering. Due to the higher density and atomic charge of Niobium the high-energy photon flux produced in a Niobium radiator exceeds the flux from an Aluminum radiator by a factor of three to ten. The higher available photon flux combined with the high melting point favors the use of Niobium as a radiator material for electron energies in the range of 10 MeV. Additionally, Niobium will cause less harm to the superconducting accelerator cavities in case of radiator sputtering. For higher electron energies which will be used to generate photons above 7 MeV Aluminum is a more suitable material due to its higher neutron separation energy of 13 MeV (see table 1) causing less unwanted neutron background radiation. The lower melting point of Aluminum compared to Niobium can partly be compensated by the higher heat conductivity if a proper radiator geometry and cooling system is chosen to remove excessive heat.

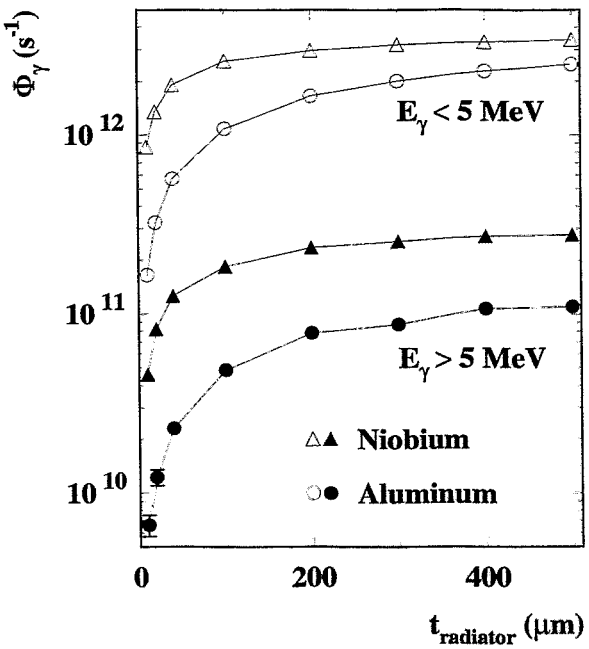

Fig. 1 *Photon flux produced into a forward cone with $\Delta\vartheta = 20$ mrad by an 1 mA electron beam of 10 MeV kinetic energy impinging onto an Aluminum (circles) or Niobium (triangles) radiator of different thickness $t_{radiator}$. The open (full) symbols show the integrated flux up to (above) photon energies of 5 MeV. Lines are drawn to guide the eye.*

Table 1 *Melting point temperatures, heat conductivities, and neutron separation energies for three different radiator materials.*

Element	T_m [K]	λ [W/mK]	S_n [keV]
Ta	3290	57	7577
Nb	2750	54	8831
Al	934	235	13058

References

[1] E. Grosse, Phys. Bl. 54 (1998)Nr. 4, pp 342

[2] CERN Program Library Long Writeup Q121, CERN, Geneva (CH)

Calculation of Neutron Production using FLUKA

B. Naumann and E. Grosse

For the estimation of activation and background neutron radiation in physics experiments at ELBE the knowledge of the photoneutron production in structural components of the electron accelerator is required. Detailed calculations of such processes are especially important as at ELBE it is planned to use the neutrons generated from the electron beam [1]. For time of flight studies sub-nanosecond neutron pulses may be obtained [2]. In traditional nuclear physics transport codes as EGS4 [3], GEANT [4] or MCNP [5] photonuclear reactions are not implemented and the neutron production can only be approximated in a two-stage technique by converting a bremsstrahlung photon fluence into a neutron source, as described in [6].
Thus the Monte Carlo radiation transport program FLUKA [7] was implemented for simulating not only electromagnetic interactions of photons and electrons, but also photonuclear reactions and the subsequent neutron propagation. The present status of the FLUKA photonuclear cross-section database is documented in detail in [8]. The photonuclear cross-sections from the FLUKA database were compared with experimental data from [9] for various materials with nuclei of $6 \leq Z \leq 73$ and a good agreement was found for nuclei with $Z \geq 13$.

Using the program FLUKA tracking calculations of the full particle cascade in irradiated materials have been done for the neutron production in various beam dump materials [10]. Here the emitted neutron yield per incident electron and the energy deposition in various materials with widely different Z are presented for 50 MeV electrons (see Fig.1).

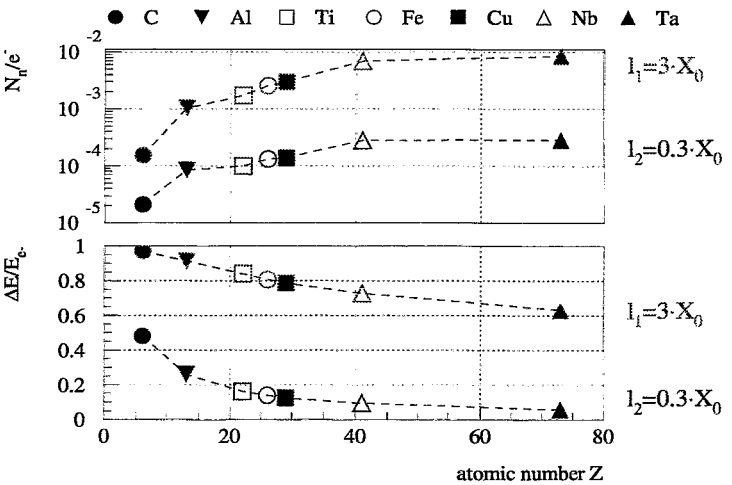

Fig.1 *Z-dependence of neutron production and deposited energy in materials bombarded with a pointlike beam of 50 MeV electrons.*

For these calculations the size of the target was scaled with the radiation length X_0, the radius of the cylindrical target being X_0 and its depth $0.3 \cdot X_0$ or $3 \cdot X_0$, respectively. The smooth Z dependence of both plotted quantities, when scaled with their radiation length, allows a straightforward interpolation to other materials.

References

[1] H. Freiesleben et al., Neutrons at ELBE, Annual report 1997, FZR-215 (1998)14.
[2] B. Naumann and E. Grosse, this Report p. 35
[3] W. R. Nelson et al., The EGS4 Code System, SLAC-Report-265 (1985).
[4] GEANT, CERN Program Library W5013 (1994).
[5] J. F. Briesmeister, Editor, MCNP, Version 4A, LA 12625 M (1993).
[6] B. Naumann and W. Neubert, this Report p. 37
[7] A. Fasso et al., Proc. of the 8th Int. Conf. on Rad. Shielding, Arlington (1994)643-649.
[8] A. Fasso et al., Proc. of the III Spec. Meeting on Shielding Aspects, Sendai (1997)61-74.
[9] EXFOR-Database of the IAEA, http://iaeand.iaea.or.at/exfor.
[10] B. Naumann et al., Strahlfänger für maximale Energien an ELBE, FZR Report FZR-267 (1999).

FLUKA Simulations for a Pulsed Neutron Beam at ELBE

B. NAUMANN AND E. GROSSE

Experiments with a pulsed neutron beam can be performed at ELBE allowing the study of the energy dependence of cross sections using the time of flight technique. Measurements with a neutron beam generated from a pulsed electron beam of 30 MeV hitting a tantalum radiator have been simulated using the particle transport program FLUKA [1]. The purpose of these calculations is to optimize the geometry of the neutron radiator. Calculations have been carried out for three rotation symmetric radiators as shown in fig. 1. The radiator thickness seen by the electron beam equals the radiation length in tantalum $X_0 = 4.1$ mm. The large radiator has an apex angle of about 15° corresponding to the electron distribution caused by small angle scattering. The emitted neutron beam will be used at a reaction target arranged perpendicular to the electron beam direction. The time of flight and the kinetic energy of the neutrons have been simulated; because of the rotational symmetry a 30 mrad ring detector surrounding the radiator at 90° could be introduced to obtain good statistics. The energy spectra of the neutrons leaving the radiator surface and entering the ring detector are shown in fig. 2; the total number of neutrons per electron are also indicated. Calculations with the program MCNP [2,3] confirm these results. The neutron emission times directly at the surface of the radiator are displayed in fig. 3 indicating the possibility for obtaining sub-ns neutron pulses.

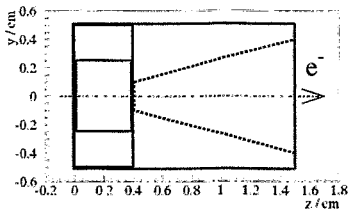

Fig.1 *Radiator shapes.*

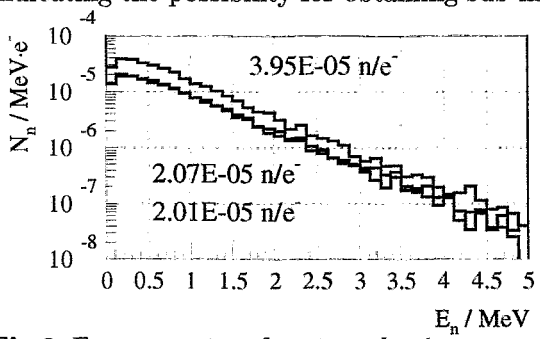

Fig.2 *Energy spectra of neutrons leaving the radiator (per incident electron).*

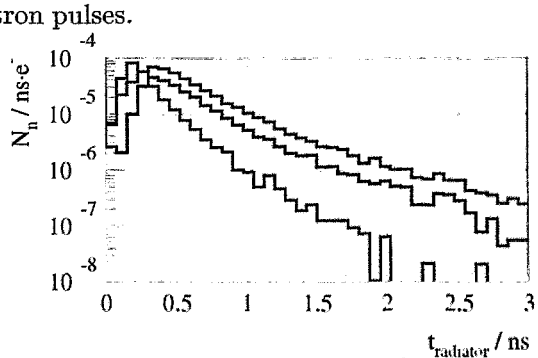

Fig.3 *Time spectra of neutrons at the radiator surface (per incident electron).*

The energy dependence of the arrival time of the neutrons when entering the ring detector after a flight path of 1 m is shown in fig. 4 for one radiator geometry (d = 5 mm). For a detector time resolution of 300 ps and a flight path of 1 m (resp. 3 m) a neutron energy resolution $\Delta E/E$ of 0.8% (resp. 0.3%) can be obtained for neutrons of 1 MeV kinetic energy.

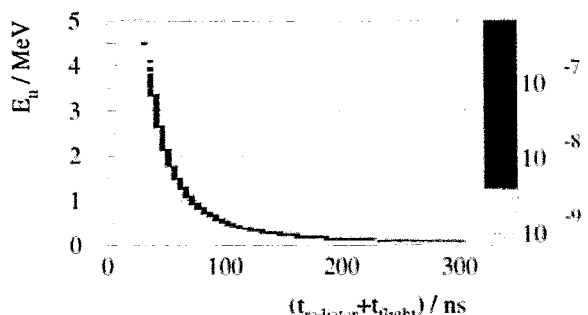

Fig.4 *Energy dependence of the time for neutrons entering the ring detector.*

References

[1] A. Fasso *et al.*. . Proc. of the III Spec.Meeting on Shielding Aspects, Sendai .1997. 61-74.
[2] J. F. Briesmeister, Editor, MCNP , Version 4A, LA 12625 M, Nov. 1993.
[3] A. Rogov and K. Noack, Institute of Safety Research FZR, private communication.

A Possible Beam Dump Design for Intense Electron Beams

B. NAUMANN, W. NEUBERT, H. PRADE AND D.PRÖHL[1]

Experiments at the radiation source ELBE require beam dumps fulfilling the safety conditions up to the maximum electron beam current of $\simeq$ 1 mA. The construction materials have to meet requirements as low specific energy deposition, heat resistance combined with sufficient thermal conductivity, modest neutron production rate and a low level of produced long-living nuclides. Here, we present a possible layout for a power dissipation of 50 kW. The core is proposed to be built from purified graphite covered by a water cooled copper coating.

The construction shown in Fig. 1 was imaged by a corresponding GEANT geometry including the material parameters [1]. The origin of the electron beam characterized by a spatial distribution of $\sigma_{x,y}$ =2 mm and a divergence of $\sigma_{x',y'}$=12 mrad was assumed to be at a distance of 2 m in front of the entrance of the graphite core. Under these conditions, the incident beam strikes completely the cone-shaped hole of the beam dump.

section	$\Delta E/E_{kin}$ [%]	ΔP [kW]
beam line	0.072	0.036
Al separation foil ($50\mu m$)	0.049	0.024
graphite core	92.175	46.087
copper coating (20 mm)	3.271	1.635
Fe shielding plate (15 cm)	3.973	1.987
concrete wall	0.459	0.230
air gap	$8.0{\cdot}10^{-4}$	$4.0{\cdot}10^{-4}$

Table 1 *Energy deposition in the dump materials*

The slowing-down of the electrons and the production of bremsstrahlung as well as the associated energy release were simulated with the GEANT 3.21 package. In this way, we calculated the energy deposition in all construction materials involved (see Table 1). The power dissipation in the graphite core is plotted in Fig. 2. Dose calculations were performed with a cubic water phantom (l = 20 cm) which was positioned at the downstream position 2.20 m, i.e. 20 cm backward the simulated beam origin. The expected dose from the photons and electrons backscattered by the graphite core amounts to 9 Gy/h provided that the incident beam current is 1 mA. A complete representation of the Monte Carlo simulations is published in [2].

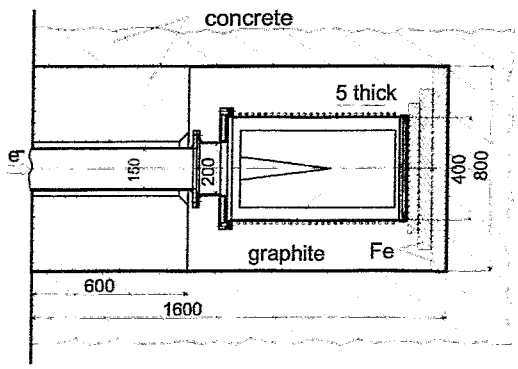

Fig. 1 *Construction of the beam dump (the vacuum separation foil (Al) mentioned in Table 1 is placed in front of the concrete wall).*

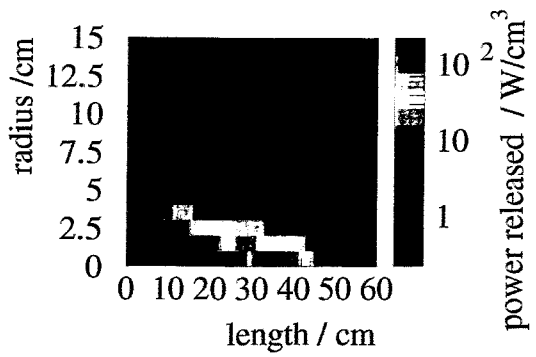

Fig.2 *Power released in the graphite core.*

[1] *Department of Research and Information Technology*

References

[1] GEANT - CERN Program Library W5013, March 1994

[2] B. Naumann, W. Neubert, D. Pröhl, FZR Report FZR-267, Juli 1999.

Calculation of the Activation of Beam Dump Materials

B. Naumann and W. Neubert

The GEANT 3.21 program package allows to calculate the bremsstrahlung photon yields in electron-nucleus interactions [1] but not secondary reactions induced by photons like (γ,n). In order to calculate the activation of different dump materials (e.g. C, Al, Cu, Cr, Ni, Mn, Fe) by such processes a special procedure explained in the following has been performed. In these calculations the corresponding (γ,n)-cross sections are required. Most of these data are available in [2,3], the cross section of iron was taken from [4]. The saturation activity of a given radioactive nucleus is calculated by

$$\left.\frac{dN}{dt}\right|_{t \to \infty} = I \cdot N_Z \int_0^{E_{\gamma,max}} \mathcal{F}_\gamma(E_\gamma)\, \sigma_{\gamma,n}(E_\gamma) dE_\gamma, \qquad (1)$$

where I is the beam current and N_Z is the number of stable nuclei in the probe irradiated by the photon fluence $\mathcal{F}_\gamma$. In a first approximation, the fluence $\mathcal{F}_\gamma$ was calculated as the number of photons per energy bin which transmit the surface of the considered probe. The known half-life of the isotope allows to calculate the activity N(t) at a given time.

Furthermore, activation by radiative capture of the complementary produced neutrons has also been taken into account by using the (n,γ) cross section data from [9]. The calculation of the neutron production in the graphite core of the beam dump are based on simulations with the MCNP program package ([5]), which were found to be in agreement with estimates in [6]. The obtained neutron yield was transformed into an energy spectrum (Watt distribution)

$$W(E_n) = C \cdot e^{-a \cdot E_n} \cdot \sinh(b \cdot E_n)^{1/2}.$$

The parameters a and b were obtained from fits to the photoneutron spectra of C, Cr and Au reported in [7].

Additionally, the production rate of radioactive nuclei induced by the radiative neutron capture was calculated in analogy to equation (1), where $\mathcal{F}_\gamma(E_\gamma)$, $\sigma_{\gamma,n}(E_\gamma)$ and dE_γ were replaced by $\mathcal{F}_n(E_n)$, $\sigma_{n,\gamma}(E_n)$ and dE_n, respectively.

We considered the activity of ^{60}Co which is assumed to be produced in the energy domain of the ELBE accelerator mainly via the reaction ^{63}Cu(n,α)^{60}Co by photoneutrons. In the calculations we used cross sections available in [8,9]. A saturation activity of about $2.1 \cdot 10^{12}$ Bq is expected for the 2 cm thick copper coating provided for cooling of the beam dump core as presented in [1]. The production of ^{24}Na in the reaction ^{27}Al(n,α)^{24}Na calculated by the same method yields a similar activity.

A complete representation of the results is given in [10].

References

[1] B. Naumann et al., A Possible Beam Dump Design for Intense Electron Beams, this Report p. 36
[2] S. S. Dietrich and B. L. Berman, Atomic and Nuclear Data Tables, 38 (1988) 199.
[3] EXFOR Data basis, http://www.nea.fr./html/dbdata/x4.
[4] S. Costa et al., Nuovo Cimento 51B (1967) 199.
[5] H. Kumpf, FZR Internal report, Institute of Safety Research, 17.6.1998.
[6] W. P. Swanson , IAEA Technical Reports Series No.188, Vienna 1979.
[7] M. Barbier, Induced Radiactivity, North Holland Publishing Company, Amsterdam 1969.
[8] P. Jessen et al., Nuclear Data A1 (1966) 103.
[9] ENDF (evaluated nuclear data files) of the NDS online Data Service, http://www-nds.iaea.org/.
[10] B. Naumann, W. Neubert and D. Pröhl, FZR Report FZR-267, Juli 1999.

Hadron Physics

The research topics of the hadron physics department are strangeness and electromagnetic radiation from colliding hadron systems. These probes allow insights in the properties of hadrons and nuclear matter as formed in heavy-ion collisions in the 1 GeV region. In particular, we are interested in in-medium modifications of hadrons. The KaoS collaboration at GSI/Darmstadt has detected an abnormal enhancement of anti-kaon production (relative to kaon production) in heavy-ion collisions at equivalent beam energies. Most interpretations of this effect point to an anti-kaon mass reduction (sometimes interpreted as indication of partial restoration of chiral symmetry in dense nuclear matter). This finding is corroborated by a specific momentum dependence of the anti-kaon–to–kaon ratio and azimuthal anisotropies as measured by the FOPI and KaoS collaborations. Very recent measurements at KaoS focus on kaon and anti-kaon detection in reactions with various beam and target combinations to get a systematic mass and energy dependence. Last year a series of experiments with a proton beam has been performed. These investigations are going to be continued with the ANKE spectrometer at COSY/Jülich in a supplementary phase space region. Especially the reaction $p + {}^{12}C \rightarrow K^{\pm} + X$ will be studied. In-medium effects are expected to be different in such hadron-induced reactions, where no compression of matter takes place.

With the 4π detector FOPI at SIS also hidden strangeness is measurable, e.g., in ϕ production which is identified via the kaon–anti-kaon decay channel.

Complementary to the mentioned measurements of hadron spectra in heavy-ion collisions one needs a detailed knowledge of hadron reactions in the same energy region. For instance, the first measurements with the time of flight spectrometer TOF at COSY are devoted to the strangeness production in the reaction $pp \rightarrow p\Lambda K^+$ and to bremsstrahlung in the reaction $pp \rightarrow pp\gamma$, thus extending the data base by providing cross sections of elementary hadron reactions.

While selected hadron channels, in particular the above mentioned anti-kaons, are sensitive to in-medium effects, a direct measurement of spectral functions is desirable. This goal can be accomplished via the dielectron decay channel of light vector mesons. Indeed, the upcoming HADES project at SIS is aimed at verifying the predicted in-medium properties of ρ, ω and ϕ mesons in a nuclear environment. To ensure a participation in this future development, the third drift chamber plane for the HADES experiment is built in the detector laboratory in Rossendorf. The envisaged physical programme covers a large range of reactions at various target nuclei bombarded by heavy ions, protons and pions as delivered by the synchrotron SIS.

The mentioned detector systems are multi-purpose installations. Therefore, a much wider set of various interesting aspects has been explored and reported in a series of publications. It should be emphasized that the mentioned investigations are performed in comparatively large collaborations, in particular with German university groups, as listed below. Our well equipped detector laboratory allows us to support these groups by building large detector components, such as previously parts of the HELITRON for FOPI, the BARREL for TOF, the side wire chambers for ANKE, and now drift chambers for HADES. These activities represent an important part of our work.

The theory group in the hadron physics department is accompanying these experimental activities. Predictions and interpretations of selected topics in the realm of strange and rare electromagnetic probes are provided. Some of these calculations refer to the energy range covered by the experiments performed with FZR participation, others deal with various phenomenological aspects of the quark-gluon plasma, as a state with chiral

symmetry restoration in strongly interacting matter, produced in high-energy heavy-ion reactions. Whereas the investigations on dense and hot hadronic matter as produced in medium-energy collisions are of strong interest for the understanding of astronomical objects like supernovae and neutron stars, the quark-gluon phase transition studies are of relevance for more violent scenarios (e.g. bigbang).

Collaborations

ANKE: Univ. Münster, FZ Jülich, Univ. Giessen, Univ. Bonn, Univ. Köln, Univ. Erlangen-Nürnberg, Fachhochschule München, FZ Rossendorf, JINR Dubna (Russia), Univ. Tblisi (Georgia), Petersburg Nuclear Physics Institute (Russia), ITEP Moscow (Russia), Russian Academy of Science Moscow (Russia), ECN-Nuclear Energy (Netherlands), Jagellonian Univ. Cracow (Poland), Moscow State University (Russia), Univ. College London (England), Soltan Institute for Nuclear Studies (Poland).
spokesperson: K. Sistemich

FOPI: Univ. Heidelberg, GSI Darmstadt, FZ Rossendorf, IPNE Bucharest (Romania), KFKI Budapest (Hungary), Univ. Blaise Pascal Clermont (France), ITEP Moscow (Russia), Kurchatov Institute Moscow (Russia), Korea Univ. Seoul (Korea), IReS Strasbourg (France), Univ. Warsaw (Poland), RBI Zagreb (Croatia),
spokesperson: N. Herrmann

HADES: Univ. Frankfurt, TU München, Univ. Giessen, GSI Darmstadt, FZ Rossendorf, Institute of Physics Bratislava (Slovakia), LNS Catania (Italy), Univ. Blaise Pascal Clermont (France), Jagellonian Univ. Cracow (Poland), JINR Dubna (Russia), INFN Milano (Italy), ITEP Moscow (Russia), Russian Academy of Science Moscow (Russia), MEPhI Moscow (Russia), Univ. of Cyprus (Cyprus), Institute de Physique Nucleaire d'Orsay (France), Nuclear Physics Institute Rez (Tschechia), Univ. of Santiago de Compostela (Spain), Univ. of Valencia (Spain),
spokesperson: J. Friese

KaoS: TU Darmstadt, Univ. Frankfurt, Univ. Marburg, GSI Darmstadt, Jagellonian Univ. Cracow (Poland)
spokesperson: P. Senger

TOF: Univ. Bochum, FZ Jülich, Univ. Bonn, TU Dresden, Fachhochschule Jülich, Univ. Tübingen, Univ. Erlangen-Nürnberg, FZ Rossendorf, IUCF Bloomington (USA), INFN Torino (Italy), SINS Warsaw (Poland),
local organizer: E. Roderburg

Medium Effects in Kaon and Antikaon Production in C+C Collisions [B,G]

F. Laue[1], C. Sturm[2] and the KaoS Collaboration

Recent experiments on kaon and antikaon production in nucleus-nucleus collisions found a large K^-/K^+ ratio [1], a vanishing in-plane flow of K^+ mesons [2] and an enhanced out-of-plane emission of K^+ mesons [3]. These effects have been attributed to modifications of kaon and antikaon properties in dense nuclear matter [4,5].

Here we report on the first comparative measurement of the K^+ and K^- production in nucleus-nucleus collisions at beam energies near and below the free NN thresholds. Figure 1 shows the data taken in C+C collisions as function of the excess energy [6]. The excess energy is defined as $\sqrt{s}$ - $\sqrt{s_{th}}$ with $\sqrt{s_{th}}$ = 2.55 GeV (kaons) and 2.86 GeV (antikaons) being the threshold energy in the nucleon-nucleon system. The kaon and antikaon multiplicities per participating nucleon nearly fall on the same curve (open and full symbols). This result is in contrast to the parameterizations of the nucleon-nucleon data (lines) which are fitted to the available proton-proton data and averaged over the isospin channels. We have calculated the multiplicities from the production cross sections via $M_K = \sigma_K/\sigma_R$ with the total reaction cross section σ_R=0.95 b for C+C and σ_R=47 mb for p+p. The average number of participants is assumed to be $<A_{part}>$=6 for C+C (according to a geometrical model) and $<A_{part}>$=2 for p+p. The large difference in the K^+/K^- ratio for C+C and p+p provides strong experimental evidence for an enhanced antikaon production in nucleus-nucleus collisions. The systematic uncertainties of the experimental data partly cancel when looking differentially at K^-/K^+ ratios. Figure 2 presents the K^-/K^+ cross section ratio as a function of the c.m. kinetic energy of the K mesons for C+C collisions at 1.8 AGeV. The K^-/K^+ ratio steeply decreases with increasing kinetic energy of the K mesons in contradiction to relativistic transport calculations [8] which predict a constant K^-/K^+ ratio if in-medium mass modifications of the K mesons are neglected.

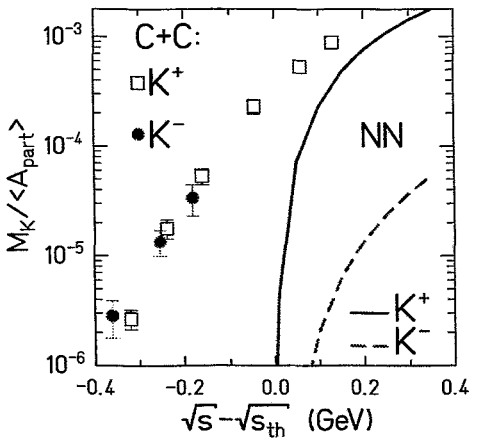

Fig. 1 *Kaon and antikaon multiplicity per participating nucleon as a function of the excess energy for C+C collisions (open squares: K^+, full dots: K^-) [6]. The lines correspond to parameterizations of the cross sections for K meson production in nucleon-nucleon collisions (solid line: K^+, dashed line: K^-) [7].*

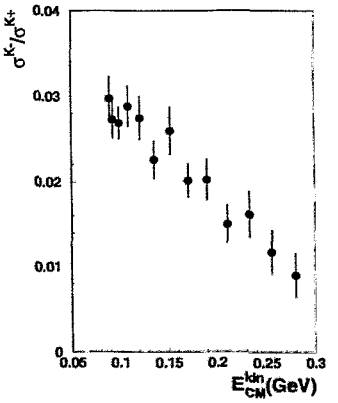

Fig. 2 *K^-/K^+ ratio as function of the kinetic energy of K mesons in the center of mass system for C+C collisions at 1.8 AGeV [6].*

[1] *GSI Darmstadt,* [2] *TU Darmstadt, Institut für Kernphysik*

References

[1] R. Barth et al., Phys. Rev. Lett. 78 (1997) 4007
[2] J. Ritman et al., Z. Phys. A352 (1995) 355
[3] Y. Shin et al., Phys. Rev. Lett. 81 (1998) 1576
[4] G.Q. Li et al., Phys. Lett. B329 (1994) 149
[5] W. Cassing et al., Nucl. Phys. A614 (1997) 415
[6] F. Laue et al., Phys. Rev. Lett. 82 (1999) 1640
[7] A. Sibirtsev et al., Z. Phys. A359 (1997) 101
[8] E. Bratkovskaya and W. Cassing, priv. comm.

Probing the Nuclear Equation of State by Kaon Production in Nucleus-Nucleus Collisions [B,G]

C. Sturm[1] and the KaoS Collaboration

The equation of state of nuclear matter (EOS) plays an important role to understand the stability of neutron stars and the dynamics of a supernova explosion. The formation of a dense nuclear fireball in nucleus-nucleus collisions provides the possibility to study nuclear matter properties at high baryon density. In particular, the azimuthal emission pattern of nucleons and subthreshold kaon production are observables which are expected to be sensitive to the EOS. Subthreshold kaon production is related to collective processes in nuclear matter. These processes are strongly enhanced at high baryon density which is obtained in central collisions. Due to strangeness conservation K^+ mesons leave the interaction zone without being reabsorbed. According to transport calculations [1,2], the relative K^+ yield obtained in Au+Au collisions at 1 AGeV is about two times larger for a soft EOS than for a stiff one. The normalized K^+ yield is a sensitive probe of the EOS and is predicted to increase with increasing mass of the collision system and with decreasing beam energy [2,3].

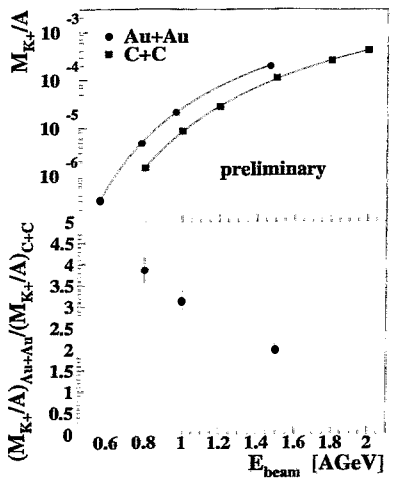

Fig. 1 *upper part: Excitation functions of the K^+ multiplicity per nucleon for Au+Au und C+C reactions as function of the beam energy; solid lines are fits to the data. lower part: The ratio of measured K^+ multiplicities in Au+Au and C+C systems.*

Therefore, the excitation functions for K^+ production in Au+Au collisions should be different from the one in C+C collisions: the cross section ratio $\sigma^{K^+}_{Au+Au}(E_{beam})/\sigma^{K^+}_{C+C}(E_{beam})$ is expected to increase with decreasing beam energy E_{beam} for a soft EOS (for a stiff EOS this ratio would remain constant). In order to study this effect we have performed a systematic measurement of K^+ production as a function of beam energy in C+C and Au+Au collisions using the Kaon Spectrometer (KaoS) at SIS. The measurements have been performed at various laboratory angles in order to study the kaon polar angle distribution which was found to be slightly forward-backward peaked. The total cross sections σ_{K^+} are calculated by integrating the fit results over momentum and extrapolating to 4π taking into account the nonisotropic emission. The inclusive K^+ production multiplicities are determined by $M_{K^+} = \sigma_{K^+}/\sigma_R$ with $\sigma_R = 4\pi(1.2 \times A^{1/3})^2$ fm^2. In the upper part of Fig. 1 the K^+ multiplicities per nucleon as measured in C+C and Au+Au collisions are shown as a function of the beam energy. The lower part of Fig. 1 presents the ratio of the measured K^+ multiplicities per nucleon for three beam energies. The kaon multiplicities are not measured at exactly the same beam energies. We have corrected this effect by shifting the Au+Au data in energy according to the fit. It can clearly be seen that the ratio increases with decreasing beam energy. However, this cannot be considered yet as a proof for a soft EOS. The steeper excitation function for K^+ meson production in C+C collisions may also result from the smaller size of the colliding system and thus the smaller total energy available for particle production. A detailed analysis of these data using state of the art transport models should clarify this question and put further constraints on the compressibility of nuclear matter.

[1] *TU Darmstadt, Institut für Kernphysik*

References

[1] J. Aichelin and C.M. Ko, Phys. Rev. Lett. 55 (1985) 2661
[2] G.Q. Li and C.M. Ko. Phys. Lett. B349 (1995) 405
[3] C. Hartnack et al., Nucl. Phys. A580 (1994) 643

About the p_t Dependence of Kaon Squeeze-Out for Low p_t [B,G]

C. PLETTNER, R. KOTTE, W. NEUBERT, D. WOHLFARTH, AND THE FOPI COLLABORATION

With the drift chamber Helitron charged kaons at midrapidity for small transverse momenta ($100\,\mathrm{MeV/c} < p_t < 250\,\mathrm{MeV/c}$) can be measured [1]. For the system ^{96}Ru + ^{96}Ru at an incident energy of 1.69 A·GeV the high number of identified K^+ mesons permits the investigation of the azimuthal distribution $dN/d\phi$ (ϕ being the angle with respect to the reaction plane ϕ_R) in dependence on the transverse momenta p_t. The anisotropy of kaon emission is quantified by the out-of-plane ratio R'_N [2]. $R'_N > 1$ means preferential out-of-plane emission, $R'_N < 1$ preferential in-plane flow. The precision $d\phi_R$ of the reaction plane determination varies with the centrality of the heavy ion reaction. For semicentral events $d\phi_R$ amounts to 29°, for central and peripheral collisions it increases to 34°. GEANT simulations have shown that the background in the mass region of K^+ mesons for velocities close to the center of mass velocity is due to protons. Using the output of IQMD simulations as an event generator for GEANT, the effect of the detector acceptance on the Squeeze-Out signal has been studied.

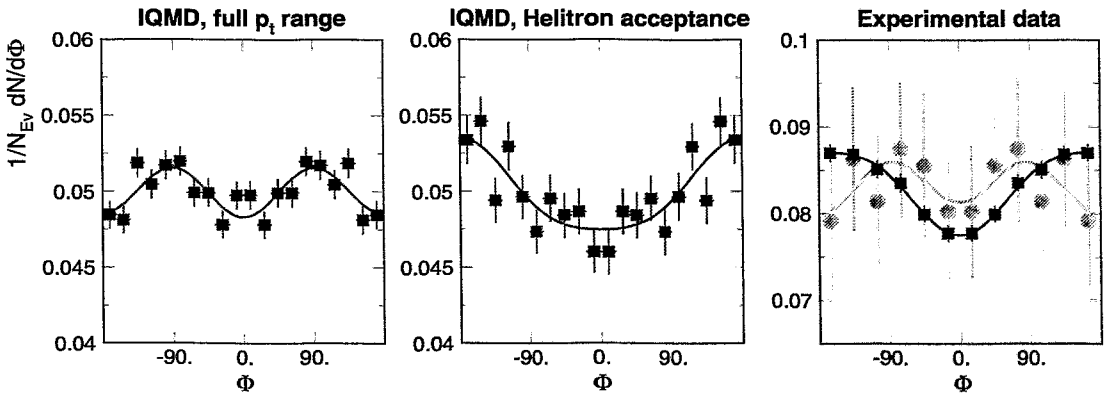

Fig 1. *Symmetrized azimuthal distributions $dN/d\phi$ of protons (squares) and kaons (dots) at midrapidity ($0.35 < y/y_{proj} < 0.65$). The curves correspond to Fourier fits (cf. [2.3]). The left panel shows the result of IQMD calculations with no additional constraints in p_t. In the middle panel $dN/d\phi$ within the geometrical acceptance of the Helitron is plotted. The right panel gives the experimental data.*

Especially at ±180° the proton distributions are distorted due to the limited Helitron acceptance (see fig. 1). It affects also the azimuthal distributions of kaons because of the high proton background. Depending on the transverse momentum range, the proton contamination of the kaon signal lies between 42% and 71%. Fortunately, the value of R'_N does not depend very sensitively on the amount of the subtracted background. In table 1 the corrected values R_N for protons and kaons are given. RQMD calculations of Wang et al. [4] have shown, that only by including a density dependent kaon potential into the transport model such a variation of R_N with p_t can be explained.

Table 1. *Preliminary out-of-plane emission ratios R_N (corrected for the precision of the reaction plane determination) for semicentral events.*

p_t [MeV/c]	125±25	175±25	225±25
protons	1.005±0.017	1.016±0.015	1.017±0.010
K^+	1.25±0.06	0.95±0.06	0.82±0.2

References

[1] C. Plettner et al., this Report p. 44
[2] N. Bastid and the FOPI collaboration, Nucl. Phys. A 622 (1997) 573
[3] P. Crochet and the FOPI collaboration, Nucl. Phys. A 624 (1997) 755
[4] Z.S. Wang, A. Fässler, C. Fuchs, U. Mahesware, and D. Kosov, Phys. Rev. C 57 (1998) 3284

Midrapidity Ratio of Charged Kaons at Low Transverse Momenta [B,G]

C. Plettner, R. Kotte, W. Neubert, D. Wohlfarth, and the FOPI collaboration

In summer 1996 the FOPI collaboration measured with its 4π covering detector system [1] at GSI, Darmstadt, the products of the heavy ion reaction ^{96}Ru + ^{96}Ru/$^{96}ZrO_2$ at an energy of 1.69 A·GeV. For each system approximately 4 million central events have been written on tape. The main components of the FOPI detector system are two radial symmetric drift chambers, the Central Drift Chamber (CDC) and the Helitron, sitting inside a superconducting solenoid with a maximum magnet field of 0.6 T. They cover the polar angle range from 33° to 140° and from 15° to 26°, respectively. Both drift chambers are capable of identifying pions and hydrogen isotopes. However, for kaon identification the velocity information from time-of-flight scintillation detectors, namely the Plastic Barrel and the Plastic Wall, becomes essential.

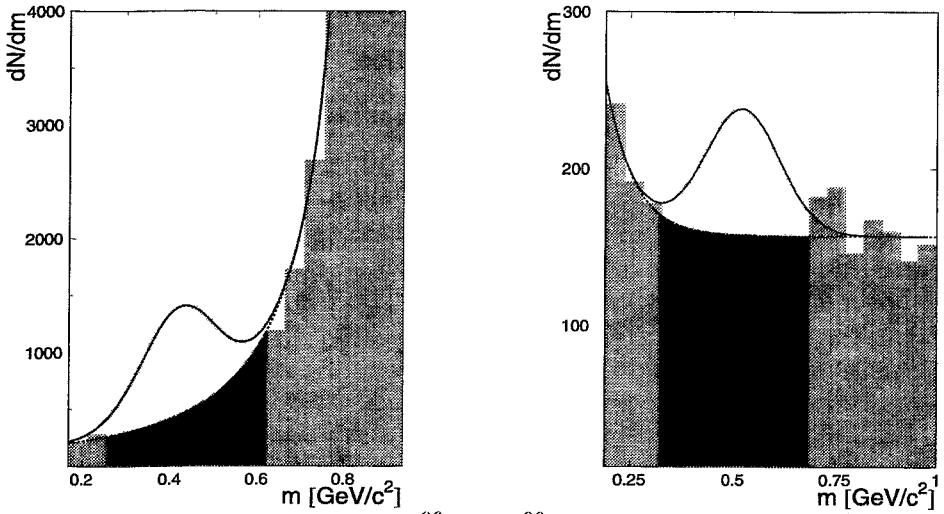

Fig 1. *Mass spectra of the reaction ^{96}Ru + ^{96}Ru @ 1.69A·GeV for K^+ mesons (left panel) and K^- mesons (right panel). The black areas represent the background and the light grey areas the remaining kaons and anti-kaons.*

K^+ and K^- identification with the CDC/Barrel detector combination is well settled and several papers on strangeness physics have been published or are on their way [2,3.]. In ref. [4] it has been shown that K^+ mesons can be separated from the data using Helitron together with Plastic Wall information. It is obvious from fig. 1, that also a clear K^- signal can be digged out from the data. Thus, we are able to determine the K^-/K^+ ratio at midrapidity ($0.35 < y/y_{proj} < 0.65$) for transverse momenta between 100 MeV/c and 250 MeV/c. The efficiency for K^+ identification has been estimated to 33^{+12}_{-8}%. The crucial point of the analysis is the treatment of the background. With the background approximation plotted in fig. 1 we get 3935 K^+ mesons and 371 K^- mesons. The preliminary ratio is (9.4 ± 2.8)%. The error depends mainly on uncertainties in the background determination. This result would give, according to RBUU calculations [5], a strong hint for in-medium modifications of K meson properties in hot and dense nuclear matter.

References

[1] J. L. Ritman, Nucl. Phys. (Proc. Suppl.) B 44 (1995) 708
A. Gobbi and the FOPI collaboration, Nucl. Instr. Meth. A 324 (1993) 156
[2] D. Best and the FOPI collaboration, Nucl. Phys. A 625 (1997) 307
[3] K. Wiśniewski and the FOPI collaboration, submitted to Phys. Rev. Lett.
[4] C. Plettner et al., Annual Report 1997, FZR-215 (1998) 22
[5] G.Q. Li and G.E. Brown, Phys. Rev. C 58 (1998) 1698

$\phi(1020)$ Vector Meson Reconstruction with the Helitron/Plastic Wall Detector Combination of FOPI [B,G]

C. Plettner, R. Kotte, W. Neubert, D. Wohlfarth,
and the FOPI collaboration

Nowadays, yields and phase space distributions of charged K mesons as well as of neutral vector mesons (like $\rho(770)$, $\omega(783)$ and the $\phi(1020)$) decaying into pairs of charged mesons or leptons play a crucial role in the investigation of possible modifications of particle properties in hot and dense nuclear matter produced in heavy-ion collisions.

Here, we present data which are taken with the Helitron/Plastic Wall combination of the 4π detector system FOPI at GSI [1]. Similar to the analysis performed within the acceptance of the detector combination of Central Drift Chamber and Plastic Barrel [2] we investigated pairs of charged K mesons within the common acceptance of the forward drift chamber Helitron and the Plastic Wall [3].

Almost $7 \cdot 10^6$ central collisions comprising about 15% of the total cross section have been scanned for the reaction ^{96}Ru+^{96}Ru at 1.69 A·GeV beam energy. Kaons with velocities $0.4 < \beta < 0.8$ have been analyzed within the polar angle range of $15^o < \theta < 28^o$. About 520 events have been found containing both a K^+ and a K^- candidate. The deduced distribution of invariant masses of K^+/K^- pairs is given in fig. 1 together with the corresponding background distribution (upper part). The lower part gives the difference spectrum (dots) together with a fit applying a Breit-Wigner distribution (full line).

Fig. 2 shows the distributions of K mesons as well as K^+/K^- pairs in the plane of normalized transverse momentum $p_t^0 = (p_t/A)/(p/A)^{cm}_{proj}$ vs. normalized rapidity $y^0 = (y - y_{cm})/y_{cm}$. (For symmetric collisions at 1.69 A·GeV beam energy one has $(p/A)^{cm}_{proj} = 0.890$ GeV/c and $y_{cm} = 0.845$.)

A preliminary analysis (including efficiency corrections and Monte Carlo estimates of the detector acceptance) yields a ϕ-to-K^- ratio of $\sigma_\phi/\sigma_{K^-} = 0.57 \pm 0.29(stat.) \pm 0.20(syst.)$ indicating that the decay of intermediate $\phi(1020)$ mesons contributes substantially (i.e. due to the branching ratio of $\Gamma_{\phi \to K^+K^-}/\Gamma_{tot} = 0.491$ with about 30%) to the subthreshold K^- production cross section.

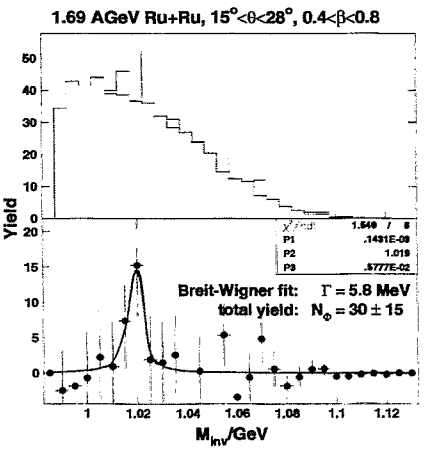

Fig. 1 *Upper panel: The invariant mass distribution of pairs of K^+ and K^- mesons (full histogram). The hatched histogram shows the uncorrelated background (mostly misidentified protons) obtained via event mixing techniques. Lower panel: The corresponding distribution after background subtraction.*

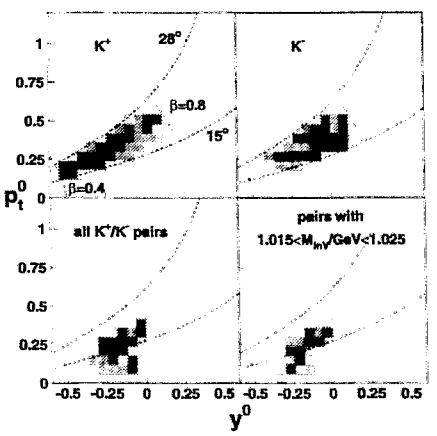

Fig. 2 *The distribution of K^+ and K^- mesons (upper panel) in the plane of normalized transverse momentum vs. rapidity. Lower panel: The same for K^+/K^- pairs without (left part) and with (right part) a gate around the $\phi(1020)$ mass. No background subtraction has been performed. The dashed and dotted lines give the polar angle limits and the upper velocity threshold, respectively.*

References

[1] A. Gobbi et al., Nucl. Instr. Meth. A 324 (1993) 156; J. Ritman, Nucl. Phys. B 44 (1995) 708

[2] N. Herrmann for the FOPI collaboration. Nucl. Phys. A 610 (1996) 49c

[3] C. Plettner et al., thesis TU Dresden (1999) and this Report

Antikaon and Kaon Production near Threshold in Proton-Nucleus Collisions [B,G]

W. Scheinast, R. Barth[1], I. Böttcher[4], D. Brill[3], M. Dębowski, F. Dohrmann, A. Förster[2], E. Grosse*, B. Kamys[5], P. Koczoń[1], B. Kohlmeyer[4], F. Laue[1], M. Mang[1], M. Menzel[4], L. Naumann, H. Oeschler[2], F. Pühlhofer[4], Ch. Schneider, E. Schwab[1], P. Senger[1], Y. Shin[3], J. Speer[2], H. Ströbele[3], Ch. Sturm[2], G. Surówka[5], F. Uhlig[2], A. Wagner[6], W. Waluś[5]

In August/September 1998 the KaoS collaboration performed an experiment on K^+ and K^- production in pA collisions using the Kaon Spectrometer [1] and the first proton beam at GSI. Data for three targets was taken at different beam energies around the kaon and antikaon production threshold. The K^+ and K^- production yield was measured at up to five different laboratory angles (see Table 1), thus a wide range of phase space was covered.

Table 1: *Range of kaon emission angles (passed in 8° steps) for beam energy and target material. For the K^- statistics the estimated total numbers are shown.*

	K^+		K^-		K^- statistics		
	C, Au	Ni	C, Au	Ni	C	Ni	Au
1.6 GeV	40° - 64°	40°	–	–	–	–	–
2.5 GeV	32° - 64°	40°	32° - 56°	40°	4400	1000	5700
3.5 GeV	32° - 56°	–	32° - 56°	–	13000	–	12000

In addition to the usual time-of-flight condition a new kind of trigger was used during this measurement. It consists of a programmable unit that attempts to reconstruct reasonable tracks detected in three scintillator hodoscopes [2]. This method improves background suppression by about one order of magnitude. Because of the reduced background it was possible to raise the beam intensity by the same factor, which led to the highest detection rates ever seen in a KaoS experiment. Figure 1 gives an example of K^- and K^+ counts for the highest beam energy used.

The analysis of the data has begun recently and is still in progress.

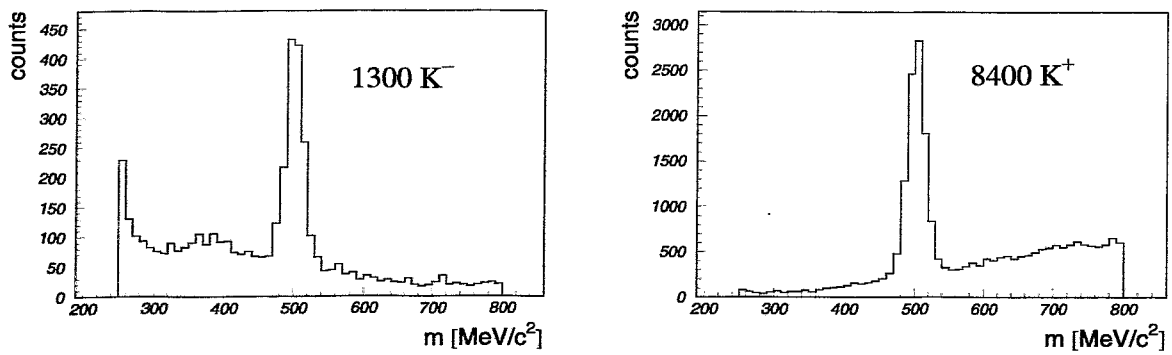

Fig. 1 *K-meson mass spectra for p+Au at beam energy of 3.5 GeV. This data was taken within 1 h (K^-) and 12 min (K^+), respectively.*

[1] *GSI Darmstadt*
[2] *TU Darmstadt, Institut für Kernphysik*
[3] *Universität Frankfurt, Institut für Kernphysik*
[4] *Universität Marburg, Physikalisches Institut*
[5] *Jagiellonian University Cracow, Institute of Physics, Poland*
[6] *GSI, now at Michigan State University, NSCL, USA*
* *FZR and TU Dresden, Institut für Kern- und Teilchenphysik*

References

[1] P. Senger et al., Nucl. Inst. and Meth. A 327 (1993) 393
[2] M. Menzel et al., Annual Report 1997, FZR-215 (1998) 21

Analysis of K^+ Data from ANKE [B,K]

M. Debowski, H. Müller, Ch. Schneider, and ANKE Collaboration

The measurement of K^+ mesons is an important tool in studies of the properties of nuclear matter. Because of their $\bar{s}$-quark content the interaction of the K^+ mesons in the nuclear medium is relatively weak, thus once produced they leave the nuclear medium without being reabsorbed. The ANKE spectrometer has been designed for the detection of rare kaon events produced in proton-nucleus collisions at beam energies far below the free N-N threshold for K^+ production (1.58 GeV proton kinetic energy). It is one of the internal beam experiments installed in the COSY ring in Jülich.

The major advantage of the spectrometer is the coverage of the forward emission angles. With the standard magnetic field setting particles with momenta 0.1–0.6 GeV/c can be detected.

In the first half of 1999 first production runs on the subthreshold kaon production in p+C collisions have been performed at proton beam energies of 2.3, 2.0, 1.8, 1.5, 1.2 and 1.0 GeV. Luminosities of $(1\text{-}2)\cdot 10^{32}\mathrm{cm}^{-2}\cdot\mathrm{s}^{-1}$ were obtained with a carbon-strip target (polycrystalline diamond, d=4μm).

The challenge in the experiment is the kaon identification. At these low bombarding energies the ratio of K^+ mesons to other particles is up to $1/10^6$. Kaons can be very efficiently identified by using the information from telescope detectors especially designed for the K^+ identification [1] combined with the TOF between the Start and Stop counters. However, at lowest beam energies these criteria were insufficient for a clean K^+ identification due to the background of rescattered ejectiles. The additional information from wire chambers was necessary to reduce the enormous background. Beside of the precise information on the particle momentum and its emission angle, the wire chambers allow to distinguish between particles emitted from the target and those rescattered on the magnet frame. Figure 1 shows the strong correlation of the vertical positions in the two wire chambers (MWPC1/2) for particles coming directly from target. The dots aside the diagonal result from particles which were rescattered on their way to the telescopes. A cut put on the *good* events reduces the background drastically in the kaon-region and thus makes the kaon-peak visible. The preliminary result of the 1 GeV run is shown in Fig. 2. In spite of the very low kaon production cross section at this energy, it is possible to identify K^+ mesons.

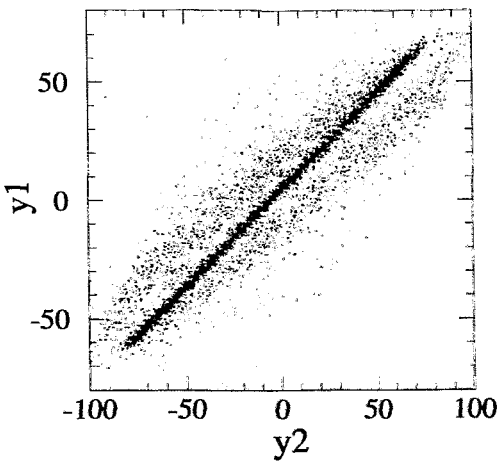

Fig. 1 *Dependence of the vertical hit position in MWPC1 - y1 and MWPC2 - y2. The band on the diagonal corresponds to good tracks, the dots outside the band are background particles.*

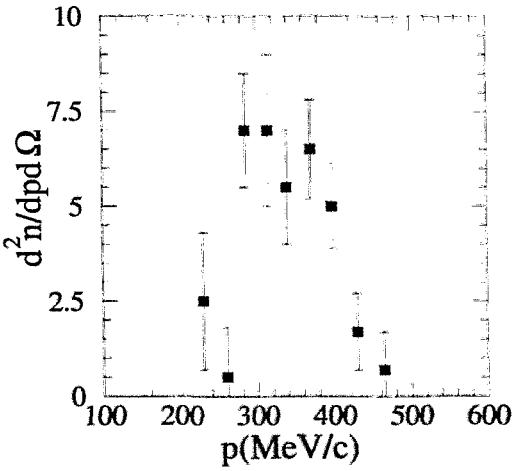

Fig. 2 *Kaon momentum spectrum at 1 GeV proton kinetic energy. The data are corrected for the angular and momentum acceptance but not corrected for the kaon detection efficiency.*

References

[1] see `http://ikpd15.ikp.kfa-juelich.de:8085/doc/Publications.html`

Commissioning of the MWPCs at ANKE [B]

CH. SCHNEIDER, M. FREITAG, J. HUTSCH, M. SOBIELLA AND ANKE COLLABORATION

The spectrometer ANKE was installed in one of the straight sections of the cooler synchrotron COSY Jülich in May 1998. During the first beam times the detectors and the data acquisition system were tested with proton and pion ejectiles from proton induced reactions on carbon and polyethylene targets. In the commissioning phase pions from the reaction $pp \rightarrow d\pi^+$ were used to calibrate the apparatus. Part of the beam time was spent on the program of K^+ detection in proton nucleus collisions below the free NN-threshold. Data were taken for proton on carbon at 2.3, 1.8, 1.5 and 1.2 GeV.

In the Kaon detection system of the ANKE spectrometer a particle track is measured by two multi wire chambers with dimension 1.4 x 0.5 m and 2.0 x 0.9 m, constructed in the detector laboratory of the FZ Rossendorf [1]. The chamber read-out electronic has been developed in a cooperation of the Rutherford Appleton Laboratory, the ZEL Jülich and the FZ Rossendorf. It is a chamber mounted high integrated system which bases on the Chips RAL118 and RAL111 [2]. The information from the chamber is essential for the momentum determination and the understanding of the background which is a major step in the selection of the kaons. During the commissioning of ANKE the RAL system was tested for the first time with real beam conditions. Therefore the properties of the MWPCs together with the readout system can be studied with the opportunity of a high particle flux crossing the chambers under different angles.

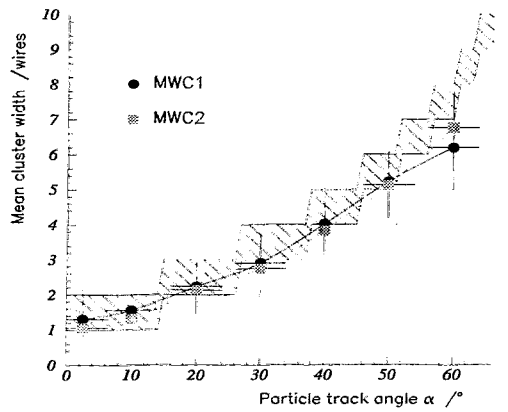

Fig. 1 *Measured cluster width as a function of the particle track angle.*

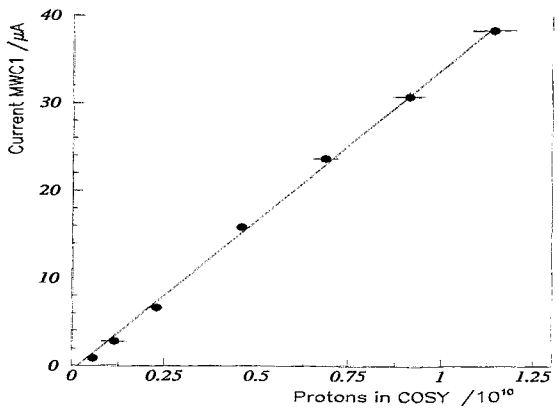

Fig. 2 *Rate capability of the wire chambers.*

Previous investigations have shown that if a particle crosses a MWPC under a large angle, signals from all hit wires can only be detected with a certain probability. It is therefore necessary to apply procedures to reconstruct the hit patterns in a proper way [1]. An appropriate quantity to prove the expected interplay of the chamber signals, the electronics, the data readout and the hit reconstruction is the number of hit wires as a function of the particle crossing angle. This is shown in fig. 1. The hatched area between the upper and lower step functions shows the expected behavior from pure geometrical considerations. For both chambers it is well demonstrated that the MWPCs and the data readout and analysis works properly. A high rate capability of the MWPC is required if ANKE is operated with a fast kaon production trigger in the near future. In fig. 2 the loading current of MWPC1 is shown as a function of the COSY intensity for the reaction proton (1.8 GeV) on carbon. With the chosen gas mixture of $Ar : C0_2 = 70\,\% : 30\,\%$ it is possible to run the MWPCs up to an intensity of $1.15 \cdot 10^{10}$ protons at these conditions.

References

[1] Ch. Schneider, Untersuchung der Subschwellenerzeugung von Kaonen am COSY-ANKE-Spektrometer, Ph. D. thesis, Technische Universität Dresden (1997)

[2] M. French et al., NIM A324(1993) 511

Recent Results on pp Bremsstrahlung and Associated Strangeness Production with the COSY-TOF Spectrometer [B,K]

S. Dshemuchadse, P. Michel, K. Möller, B. Naumann, L. Naumann, A. Schamlott and the Cosy-Tof Collaboration

Motivated by the lack of data on elementary proton-proton reactions the reactions $pp \rightarrow pp\gamma$ and $pp \rightarrow pK^+\Lambda$ were studied with the TOF spectrometer at the COSY accelerator in Jülich. The differential cross section of the first reaction, the pp bremsstrahlung, was measured in a kinematically complete experiment at a beam momentum of 797 MeV/c. A plot of the obtained missing mass spectrum is shown in Fig. 1 and compared to a Monte Carlo simulation.

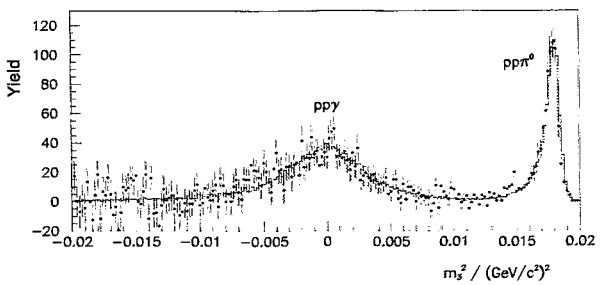

Fig. 1 *Missing mass spectrum of the pp bremsstrahlung (dots) and Monte Carlo simulation (solid line)*

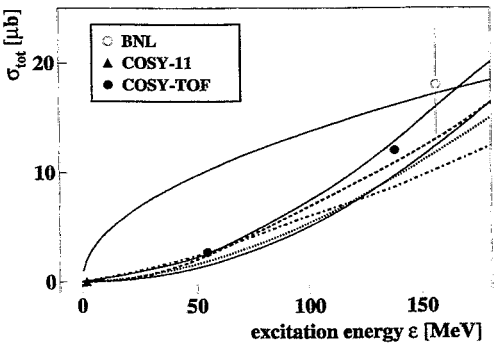

Fig. 2 *Cross sections of the $pp \rightarrow pK^+\Lambda$ reaction. The curves correspond to different theoretical models (cf. [2])*

Although the measurement was performed with the TOF spectrometer not yet completely upgraded to its designed 2π (lab) solid angle acceptance (the actual acceptance amounted to approximately 1 sr), also angular distributions and Dalitz plots were obtained [1]. From the Dalitz plots it turned out that no proton proton final state interaction (FSI) is observed for the $pp \rightarrow pp\gamma$ reaction. The reason for the absence of FSI is currently under investigation.
In another kinematically complete experiment the associated strangeness was investigated at beam momenta 2.50 GeV/c and 2.75 GeV/c. The total cross sections (Fig. 2) for these momenta were extracted to be (2.7 ± 0.3) μb and (12.0 ± 0.4) μb. respectively. Also angular and momentum distributions were measured for this reaction. Furthermore Dalitz plots and missing mass distributions for the different 2-body subsystems were deduced [2]. The missing mass distributions follow roughly phase space. The question whether the observed small deviations from the phase space distributions can be attributed to resonance behavior in one of the two particle subsystems can be answered only by the next measurement with the full upgrade of the TOF spectrometer available. Also the Λ-polarization was measured in dependence on the transverse momentum in the cms using the self-analyzing property of the weak decay $\Lambda \rightarrow \pi^- p$.
More accurate and comprehensive data on the $pp\gamma$ reaction were taken by the end of 1998 with the full upgrade of the TOF spectrometer (i.e., the BARREL detector built in Rossendorf and the RING detector built in Jülich) and a polarized proton beam (extracted for the first time). The data analysis is in progress.

References

[1] R. Bilger et al., Phys. Lett. B 429 (1998) 195
[2] R. Bilger et al., Phys. Lett. B 420 (1998) 217

Hidden Strangeness in the Reaction $NN \to NN\phi$ [B]

A.I. Titov[1], B. Kämpfer, V.V. Shklyar[1]

Recently [1] we have shown that polarization observables of the reaction $pp \to pp\phi$ are sensitive to a hidden strangeness component in the proton. Such investigations are motivated by the observation of an apparent violation of the OZI rule in $\bar{p}p \to \phi X$ reactions, which can be resolved by the assumption of a substantial $s\bar{s}$ admixture in the proton. Furthermore, with respect to forthcoming HADES experiments the basic features of the elementary reaction $NN \to NN\phi(\to e^+e^-)$ need to be understood. The reaction $pp \to pp\phi(\to K\bar{K})$ is also accessible at COSY.

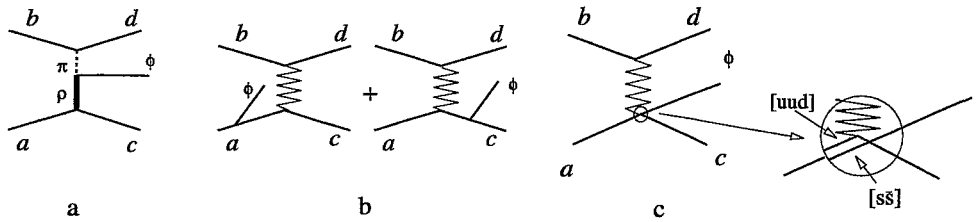

Fig. 1 *Diagrammatic representation of processes of the ϕ production.*

In the one-boson-exchange model we have calculated [2] the tree level diagrams displayed in fig. 1. The main contribution comes from the internal meson conversion 1a. The emission from external legs, 1b, can be microscopically interpreted as coupling of the ϕ to the virtual kaon cloud surrounding the nucleon. The process 1c is the knock-out of the $s\bar{s}$ component. In diagrams 1b and 1c the π, σ, ρ and ω mesons are exchanged. For details of parameter fixing and a discussion of uncertainties related to unknown phase relations we refer the interested reader to [2]. In figs. 2 and 3 we show the spin density matrix and the decay asymmetry (threshold predictions are depicted by the long-dashed lines). One can see a strong modification of the anisotropy for $\phi \to e^+e^-$ decays by the knock-out mechanism at small angles θ. This effect is smaller for K^+K^- decays and depends on the strangeness weight b^2.

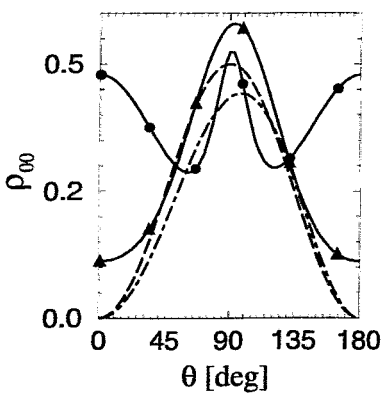

Fig. 2 *The spin density matrix element ρ_{00} for the reaction $pp \to pp\phi$ at 0.1 GeV above threshold for different channels and for an imaginary two-body T matrix. Contribution from the OBE channel 1a: dot-dashed line, ϕ bremsstrahlung channel 1b: triangle markers, ϕ shake-off 1c: dot markers.*

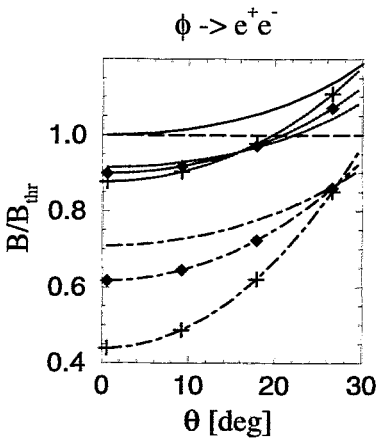

Fig. 3 *The asymmetry of $\phi \to e^+e^-$ decays normalized to the threshold value for an imaginary two-body T matrix. Solid, dotted and dot-dashed lines correspond to b^2=0., 0.01 and 0.05. A positive value of the phase factor a_1 [2] (real phase) is marked by crosses (diamonds).*

[1] *Bogoliubov Theoretical Laboratory, JINR Dubna, 141980 Dubna, Russia*

References

[1] A.I. Titov, B. Kämpfer, V.V. Shklyar, FZR-202 (1997)
[2] A.I. Titov, B. Kämpfer, V.V. Shklyar, Phys. Rev. C 59 (1999) 999

Soft Hadron Production in *pp* Collisions [B]

H. MÜLLER

Soft hadron production is a non-perturbative process the understanding of which is at present based to a large extent on phenomenological models. The ROC model [1] is an attempt to describe soft hadron production in the whole center-of-mass energy region from threshold up to several tens of GeV, where the complete hadronic interaction is dominated by soft production. At still higher energies new phenomena like high-p_t jets occur and make the interaction picture more complicated.

The model is based on the assumption that the relative cross section of each possible final state is given by its statistical weight, which is, however, modified by applying empirical transition matrix elements as additional weights and cuts in the phase space.

The production process is assumed to proceed via intermediate states called fireballs or clusters. They are created in a first stage of the interaction and have their origin in the complicated internal partonic structure of the two interacting hadrons. In dependence on the impact parameter and the collision energy a varying number of fireballs is produced. The probability of creating a definite number of fireballs is in the present version of the ROC model parameterized by a negative binomial distribution. The well known facts of limited transverse momenta of the produced particles and the observation of so called leading particles are implemented by distributing the produced fireballs in longitudinal phase-space the dimensions of which are fixed by two parameters, the mean transverse momentum of the fireballs and the mean longitudinal momentum of the two leading fireballs. The fireballs are characterized by two parameters, a temperature Θ and a radius R, which determine the relative energy and the mean multiplicity of the particles in which the fireballs decay. Particle production is assumed to proceed via the creation of quark-antiquark pairs which are subsequently randomly combined to form the resulting hadrons. The suppression of strangeness production relative to up and down quarks is taken into account by one further parameter.

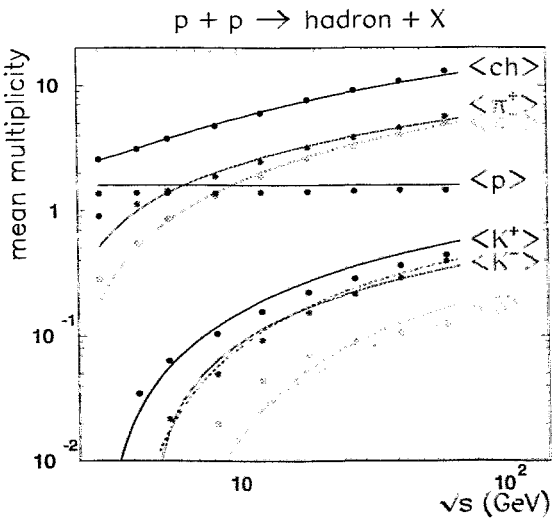

Fig. 1 *Mean multiplicities as a function of the center-of-mass energy. Full and dashed curves are fits [2] to experimental data, points are model results.*

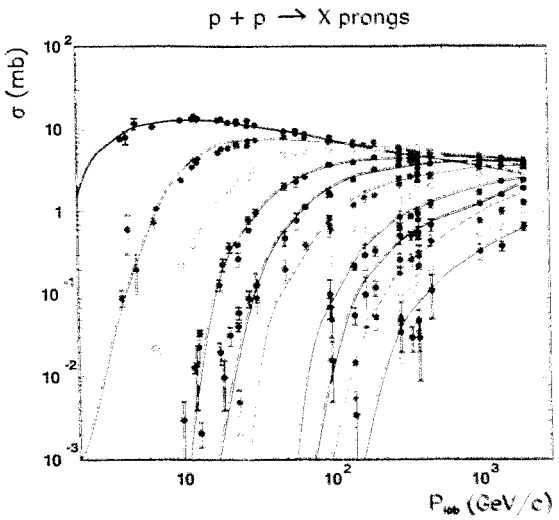

Fig. 2 *Topological cross sections as a function of the laboratory momentum. Points represent experimental data [3], full curves model results for the reaction pp → X prongs (X=4,6.....26)*

Thus, there are altogether seven free parameters adapted by considering a large variety of available data. Since the parameters are highly correlated, it is difficult to define an optimal parame-

ter set. In the present version the parameters have been fixed at the highest energy considered ($\sqrt{s} = 63\ GeV$). The energy dependence of the mean multiplicity of charged particles has been reproduced by slight chances (not more than about 10 %) of Θ and R. All the other parameters remain unchanged. In this way a huge amount of data in a wide energy region can be quite well reproduced. For instance, in Figs. 1 and 2 the energy dependence of the calculated multiplicities of various particles and of the topological cross sections are compared with experimental data. In both cases the reproduction of the data is quite satisfactory.

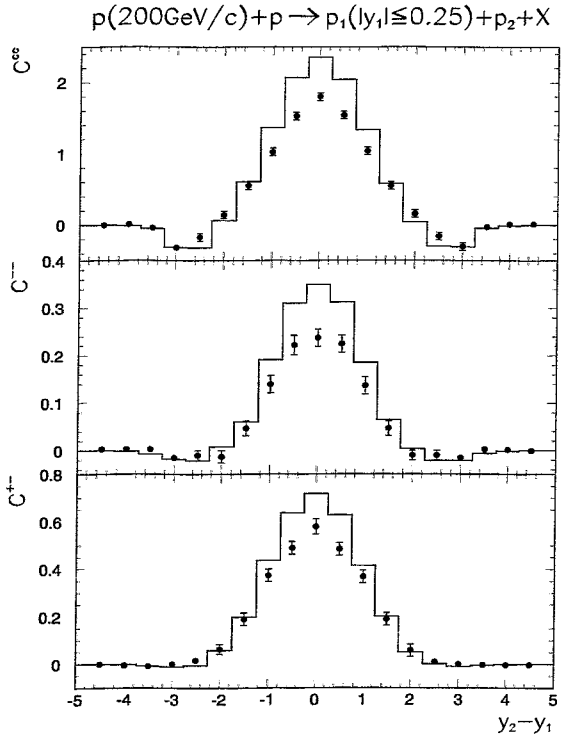

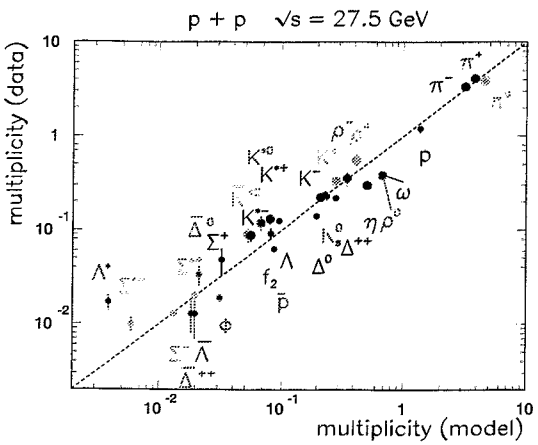

Fig. 3 *Measured multiplicities versus model results. Data are from [4] and [5]. Well reproduced values lie near the dashed line.*

Fig. 4 *Inclusive two-particle correlation functions for charged-charged (C^{cc}), negative-negative (C^{--}) and positive-negative (C^{+-}) particles as a function of the rapidity difference $y_2 - y_1$ when $\mid y_1 \mid \leq 0.25$. Points are experimental data taken from [6], histograms show the model calculations.*

Fig. 3 shows the multiplicities of produced particles at 27.5 GeV. With the exception of $\Lambda^* = \Lambda(1520)$ the points lie in the vicinity of the dashed line, which is defined by the equality of measured and calculated multiplicities.

Correlation coefficients $C(y_1, y_2) = \rho_2(y_1, y_2) - \rho_1(y_1)\rho_1(y_2)$ with $\rho_1(y) = \sigma^{-1} d\sigma/dy$ and $\rho_2(y_1, y_2) = \sigma^{-1} d^2\sigma/dy_1 dy_2$ being the one and two-particle rapidity densities are shown in Fig. 4. The peaks in Fig. 4 indicate that the particles are not randomly distributed. Instead, there is an increased probability to find a second particle near the rapidity value of the first one. This is a direct experimental proof of the fireball hypothesis. The model results tend to overestimate the correlation indicating that the fireball parameters Θ and R must be further optimized.

References

[1] H. Müller, Z. Phys. A 355 (1996) 223
[2] A.M. Rossi et al., Nucl. Phys. B 84 (1975) 269
[3] Landolt-Börnstein, New Series I/12b, Springer-Verlag Berlin Heidelberg 1988
[4] M. Aguilar-Benitez et al., Z. Phys. C 50 (1991) 405
[5] H. Kichimi et al., Phys. Rev. D 20 (1979) 37
[6] J. Whitmore, Phys. Rep. 27 (1976) 187

Thermal Particle Production at SIS? [B]

Gy. Wolf[1], H.W. Barz, B. Kämpfer

The dynamics of heavy-ion collisions up to bombarding energies of 2 A·GeV is quite successfully described by transport approaches of the BUU type. These models are usually very involved. and there is a natural desire to understand the experimental data within simpler models. Among those approaches the thermal models play an important role. At SPS and AGS energies the final particles abundances are very successfully described within thermal models. Recently several authors [1,2] were aiming to describe the particle ratios also at SIS energies.
In order to study to what an extent the assumptions of the thermal equilibrium is realized in heavy ion collisions at SIS energies we perform calculations within our transport model [3]. First we study the relaxation process towards chemical and thermal local equilibrium. For this purpose we enclose nuclear matter in a box with a volume of 5000 fm^3. The initial state consists of two currents of homogeneous matter flowing against each other. The initial parameters are chosen to reproduce realistic conditions for freeze out, namely density $\rho = 0.5\rho_o$ and energy per baryon $\epsilon = e/\rho - m_{proton} = 140$ MeV.

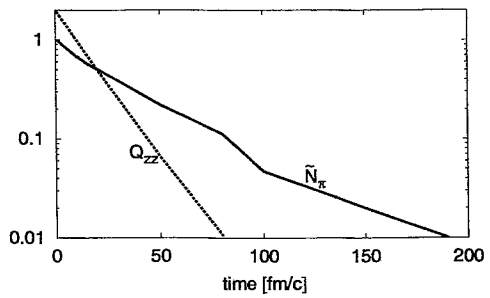

Fig. 1 *The evolution towards equilibrium of the anisotropy Q_{zz} (dashed line) and the relative pion number $\tilde{N}_\pi$ (solid line) for nuclear matter enclosed in a box.*

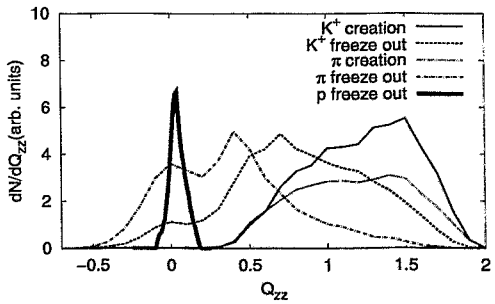

Fig. 2 *Unnormalized probabilities for particle creation and freeze-out as a function of the local anisotropy.*

In fig. 1 we show the time evolution of the relative pion number defined by $\tilde{N}_\pi = 1 - n^\pi(t)/n^\pi_{eq}$ and the anisotropy defined as the quadrupole moment of the stress tensor $Q_{zz} = \frac{2T_{zz} - T_{xx} - T_{yy}}{T_{zz} + T_{xx} + T_{yy}}$. We find an exponential decay of the anisotropy, and the pion number also nearly exponentially approaches its equilibrium value. The corresponding relaxation times are about 15 (30) fm/c for the anisotropy (pion number). For kaons the approach towards chemical equilibrium would even be much slower since the relevant cross sections are much smaller.
Let us now consider a BUU calculation of central collisions of Au+Au at 1 A·GeV. In fig. 2 we show the dependence of the creation and the freeze-out of protons, pions and kaons as a function of the local anisotropy ("creation" of a particle means its production [i.e. for pions it is the moment when the pion created for the first time, its subsequent reabsorption and reemission are considered as elastic collisions], and "freeze-out" means the particle suffers the last collision [for pions the moment of their last emission]). The baryons are very well thermalized, while pions and kaons are created at a substantially larger anisotropy, and even their freeze-out takes place at a locally non-equilibrated stage.

[1] *KFKI RMKI, H-1525 Budapest, POB 49, Hungary*

References

[1] R. Averbeck, nucl-ex/9803001
[2] J. Cleymans, H. Oeschler and K. Redlich, Phys. Rev. C 59 (1999) 1663, J. Phys. G (1999) 281c
[3] Gy. Wolf, W. Cassing, U. Mosel, Nucl. Phys. A 552 (1993) 549

Status of the Production of Large Trapezoidal Drift Chambers for the HADES Experiment [B]

F. Dohrmann, W. Enghardt, E. Grosse, L. Naumann, M. Sobiella
and the HADES-Collaboration

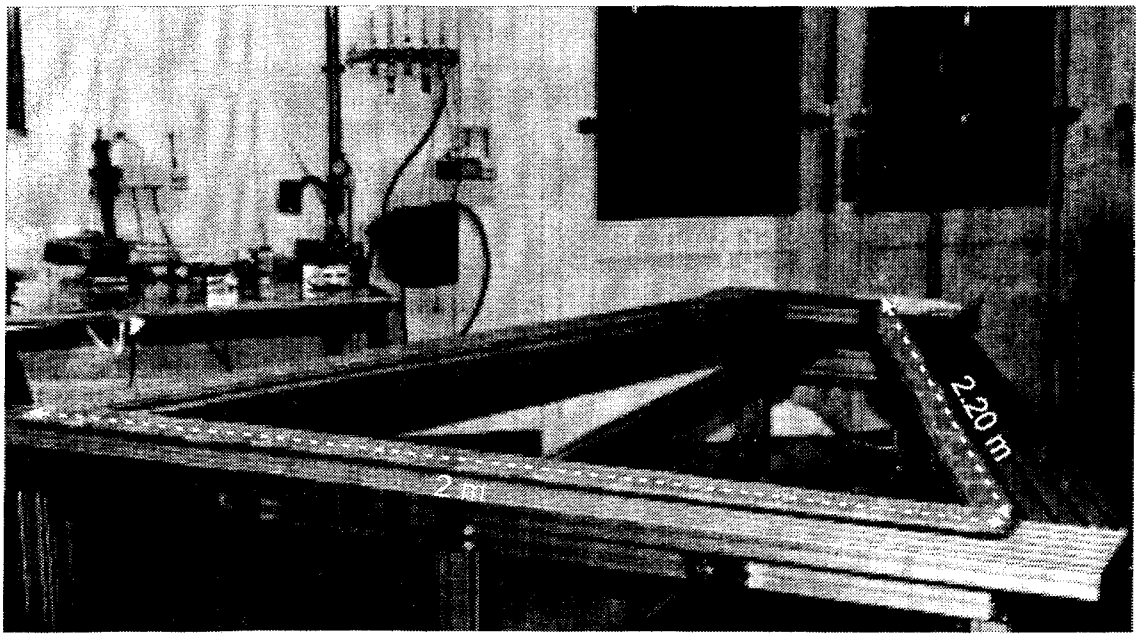

Fig. 1 *A MDC III frame on a trapezoidally shaped table. Readout pads have to be glued into the frame before winding. Note the size of the frame.*

The setup of the high acceptance di-electron spectrometer HADES at GSI, Darmstadt, has begun in 1998. The large superconducting magnet as well as both mainframes have been installed [1]. A pion production target was operated successfully in the HADES beamline. First experiments investigating the properties of vector mesons in dense nuclear matter are scheduled for 1999 [2].

At the detector laboratory of the FZ Rossendorf the final design of the *large* trapezoidal low-mass drift chambers (cf. figure 1) of the HADES tracking system has been developed. Being the second largest tracking plane (MDC III) of the spectrometer it consists of 6 modules with an active area of $\sim 2.2\,\mathrm{m}^2$ and a drift cell size $8 \times 12\,\mathrm{mm}^2$. Each module has 6 drift cell layers, i.e. 6 anode and 7 cathode frames. Since the size of the frames is enormous, they have to be assembled from four pieces. The frames consist of Stesalit material (Stesalit EP107-G118-40, $Y = 30\,\mathrm{GPa}$). Both the machining and the gluing of the frames have been done at a small company (Kossmann, 78532 Tuttlingen, Germany) which had already proven to be well equipped for manufacturing another of the HADES tracking planes (MDC I) for the detector laboratory of GSI Darmstadt [2]. Meanwhile, the entire set of frames for all 6 detector modules has been delivered to Rossendorf. Al-wires (80 and 100 μm diameter) for cathode and field wires and tungsten wires (20 μm) have been ordered. Readout pads for the wires have been developed and have been delivered. The production of the modules has started in the beginning of 1999. A first module is expected to be completed in fall 1999.

References

[1] C. Garabatos et al. Nucl. Phys. B 61B. (1998) 607
[2] The HADES collaboration, proposal presented to GSI, August 1998
[3] GSI Scientific Report 1997, GSI 98-1, p 185

A Model of the Dilepton Spectrum from ω Meson Decays Applicable to HADES Experiments [B,W]

B. KÄMPFER, O.P. PAVLENKO[1]

The current CERES experiments at CERN and the starting HADES measurements at GSI have initiated a great deal of activities in understanding the behavior of hadrons in dense hadronic matter. In spite of these activities there is so far no commonly accepted understanding of properties of hadrons in a dense nuclear environment. In particular, according to the Brown-Rho scaling hypothesis [1] the vector meson masses should universally drop in the matter with increasing density of the medium. At the same time several analyses of the meson masses based on an effective Lagrangian which combine chiral SU(3) dynamics with vector meson dominance [2] show different in-medium modifications of the ρ and ω masses: the ρ meson mass changes only slightly in comparison with the corresponding modification of ω mass. The last approach is also in agreement with QCD sum rule analyses if one replaces the simple delta function approximation of the spectral function [3] by the full spectrum.

All the above mentioned theoretical estimates assume the vector mesons to be at rest relative to the surrounding medium, i.e., the phase space of the produced dileptons from meson decays is restricted by $\vec{q} = 0$, where $\vec{q}$ is the momentum of lepton pair. On the other hand the dilepton rates dN/d^4q, planned to be measured in HADES experiments, depend on the full four-momentum q^μ providing very important experimental information on the in-medium current-current correlation function in a wide kinematical region of q^μ.

In order to analyze the full dilepton spectra from meson decays measured with HADES we will use, in a first attempt, the simple model of spherically symmetrical collective flow of nuclear matter. In Boltzmann approximation for the thermal distribution of ω mesons we get the following expression for the dilepton spectrum from meson decays

$$\frac{dN}{d^4q} = \frac{V_d q_0 T_d}{(2\pi)^3 \gamma v q} \exp\left(-\frac{q_0\gamma}{T_d}\right) \sinh\left(\frac{\gamma v q}{T_d}\right) A(q). \qquad (1)$$

where the function $A(q)$ denotes the HADES acceptance [4]. q_0 is the energy of the decaying meson and $q = |\vec{q}|$, and v stands for the averaged radial flow velocity. The values of the ω meson decay temperature T_d and the corresponding matter volume V_d are obtained within the hydrodynamic model [5] under the assumption of approximately constant profiles of temperature and density at the meson decay instant $t_d = 1/\Gamma_\omega$, where in-medium modifications of the ω meson width Γ_ω are to be included.

The goal of such a model is to take into account the effect of radial flow which has proven important in heavy-ion collisions at SIS energies. Indeed, eq. (1) demonstrates that the dilepton spectrum depends on the flow properties of matter due to boosting the various contributions to a common reference frame. Results of numerical simulations will be reported elsewhere.

[1] *Institute of Theoretical Physics, Kiev, Ukraine*

References

[1] G.E. Brown, M. Rho, Phys. Rev. Lett. 66 (1991) 2720
[2] G. Chanfray, R. Rapp, J. Wambach, Phys. Rev. Lett. 76 (1996) 368
F. Klingl, N. Kaiser, W. Weise, Nucl. Phys. A 624 (1997) 527
[3] S. Hatsuda, S.H. Lee, Phys. Rev. C 46 (1992) R34
[4] F. Dohrmann, FZR-258 (1999)
[5] B. Kämpfer, O.P. Pavlenko, Z. Phys. C 62 (1994) 491

Quark Propagator and Dilepton Production in the Quark-Gluon Plasma [B]

A. Peshier, M. Thoma[1]

As an experimental probe of the quark-gluon plasma, virtual photons decaying into lepton pairs have been proposed since they are emitted from the fireball without further interaction. We will argue on general grounds by considering in-medium properties of quarks, that the thermal dilepton spectrum of deconfined matter features distinct structures which may provide a unique signal for the experimental creation of this new state of matter.

The influence of the plasma on the properties of particles is described by the selfenergy, which has for the light quarks the general form $\Sigma(p_0,p) = -a\not{p} - b\gamma_0$, with a, b being functions of the energy p_0 and momentum p. The exact propagator $S = (S_0^{-1} - \Sigma)^{-1}$ can be decomposed into helicity eigenstates corresponding to the propagating excitations: a particle mode q_+ and an antiparticle-hole excitation q_- called plasmino. The dispersion relations $\omega_\pm(p)$ of both fermionic modes are given by the poles of the propagator and can be expressed by the functions a and b. As a general feature resting only on isotropy arguments, both branches can be shown to have the same rest energy $\omega_\pm(0)$ and opposite slope at vanishing momentum. On the other hand, both branches approach the light cone for hard momenta, $\omega_\pm(p) \to p$. Consequentely, the dispersion relation starting with the negative slope (the plasmino branch, as it turns out) has a minimum at a non-vanishing momentum [1]. This argument shows that the non-trivial minimum found previously in perturbative calculations, as well as in an effective non-perturbative approach taking the gluon condensate into account [2], is a general feature of the quark propagator.

The existence of this minimum has interesting consequences on the spectrum of emitted lepton pairs. These are produced by electromagnetic transitions between the branches, $q_+ \to q_-\gamma^*$, or by annihilation, $q_\pm\bar{q}_\pm \to \gamma^*$. For zero 3-momentum of the lepton pair, e. g., the first process contributes for invariant masses M smaller than the maximum of the energy difference $E(p) = \omega_+(p) - \omega_-(p)$ of the two branches, where it terminates with a van-Hove singularity caused by the diverging density of states $\sim (dE(p)/dp)^{-1}$. Similarily, the plasmino annihilation channel opens at $M = 2\omega_-(p_{\min})$ with a second van-Hove singularity due to the dip in the plasmino branch. At $M = 2\omega_\pm(0)$ the quark annihilation sets in, which dominates at large invariant mass. Due to the close relation to the plasmino dip, the dilepton rate obtained from the exact dispersion relation is thus expected to have similar peaks and gaps as calculated in the approach [2], cf. Fig. 1. Although other effects as, e. g., bremsstrahlung will smear out these singularities, it will be worthwhile looking for distinct structures of the dilepton rate at invariant masses below 1 GeV as a strong indication of the presence of collective excitations of deconfined quarks.

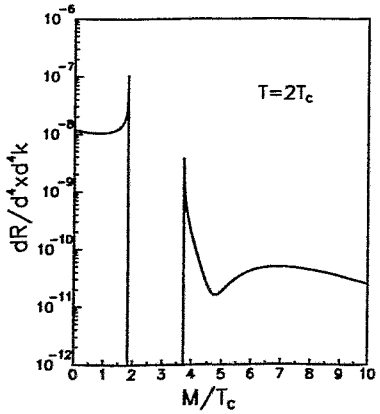

Fig. 1 *The dilepton production rate at vanishing 3-momentum as calculated in [2].*

[1] *Institut für Theoretische Physik, Universität Giessen*

References

[1] A. Peshier and M.H. Thoma, hep-ph/9907268
[2] A. Schäfer and M.H. Thoma, Phys. Lett. B **451** (1999) 195

Interpreting the Dilepton Excess in Relativistic Heavy-Ion Reactions by a Unique Thermal Source [B,W]

K. GALLMEISTER, B. KÄMPFER, O.P. PAVLENKO[1]

Recently the NA50 collaboration launched the interpretation of the observed excess of dimuons in the intermediate mass region, seen in the reaction Pb(158 A·GeV) + Pb, as abnormally enhanced open charm production; the NA38 data of the reaction S(200 A·GeV) + U is similarly interpreted. In contrast, the dielectron excess in the low-mass region, observed in the reaction Pb(158 A·GeV) + Au by the CERES collaboration, is quite naturally explained by secondary processes which can be interpreted as thermal dilepton radiation from the fire ball. Also previous interpretations of the low-mass dielectron excess in the reaction S(200 A·GeV) + Au (CERES) and the intermediate-mass dimuon excess in the reaction S(200 A·GeV) + W (HELIOS-3) as thermal dileptons successfully describe the data.

Desirable is, of course, a unique interpretion of all of the mentioned measurements. As a first step we have parameterized the CERES excess by a simple thermal source function (see fig. 1). The same source function is shown [1] to describe also the NA50 measurements (see fig. 2).

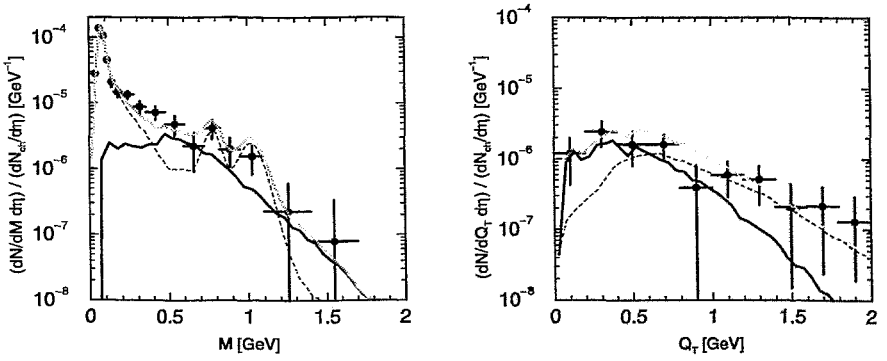

Fig. 1 *The preliminary CERES data for the reaction Pb(158 A·GeV) + Au and the hadronic cocktail (dashed lines) and the thermal yield (full curves). The sum of the cocktail and the thermal yield is shown by the grey curves. Left panel: the invariant mass spectrum, right panel: the transverse momentum spectrum for the mass bin 0.25 ··· 0.68 GeV.*

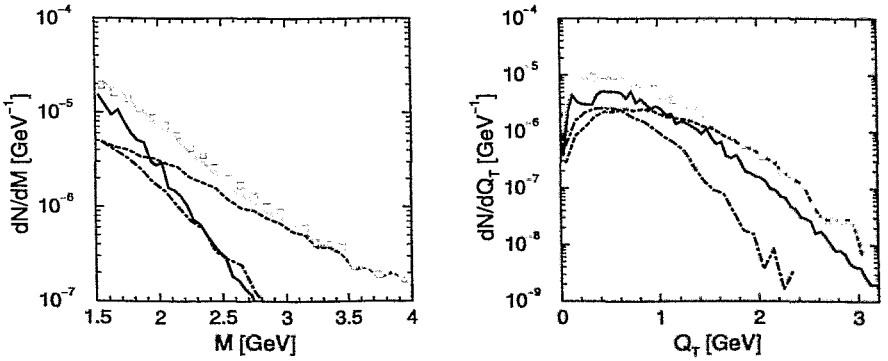

Fig. 2 *The reconstructed measurements of the NA50 collaboration (see [1] for details) indicated by open squares in comparison with the thermal yield (full curves), the Drell-Yan contribution (dashed curves) and the contribution of open charm decays (dash-dotted curves). The sum of these contributions is displayed by the grey curves. Left panel: the continuum invariant mass spectrum, right panel: the transverse momentum spectrum for the mass bin 1.5 ··· 2.5 GeV.*

[1] *Institute of Theoretical Physics, Kiev, Ukraine*

References

[1] K. Gallmeister, B. Kämpfer, O.P. Pavlenko, hep-ph/9908269

Dileptons, Charm and Bottom at RHIC and LHC [B]

K. GALLMEISTER, B. KÄMPFER, O.P. PAVLENKO[1]

To get information on the hottest stages of deconfined matter during heavy–ion collisions, dileptons as a penetrating probe are one of the most favourable messengers. With increasing beam energy also other production channels for dileptons gain importance, especially the correlated semileptonic decays of open charm and bottom mesons.

We have studied the systematics of these rates and the Drell–Yan (DY) process with increasing energy $\sqrt{s}$ from SPS to the future colliders RHIC and LHC for the intermediate mass region, where the thermal signal is expected to be best visible [2]. There is no preferable energy region for observing the thermal signal of deconfined matter. When going to very high energy $\sqrt{s}$ the thermal signal exceeds the DY yield, however the charm and bottom contributions become even stronger (see fig. 1).

Kinematical cuts superimposed to the detector acceptance open a window for the thermal signal. One possibility is to look at the double differential rate $dN/dM_\perp^2 dQ_\perp^2$ (where $M_\perp$ is the transverse mass and $Q_\perp$ is the transverse momentum) within a narrow $M_\perp$ range and a suitably adjusted single–lepton transverse momentum cut $p_\perp^{\min}$ [1]: The thermal signal, obeying the so–called $M_\perp$–scaling, extends nearly up to the kinematical boundary, whereas the background is suppressed for larger $Q_\perp$–values. Another possibility is to use only an increased $p_\perp^{\min}$–cut. Then the background in the invariant mass spectrum becomes suppressed (fig. 2) [2]. The thermal signal shows a 'plateau', while the DY yield has a threshold like behavior at $M = 2p_\perp^{\min}$. Also the charm and bottom contributions are strongly suppressed below this value of M.

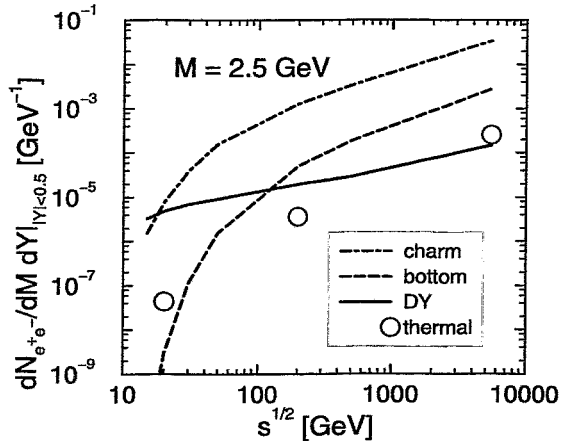

Fig. 1 *The dependence of dileptons from the lowest-order processes (DY and correlated semileptonic decays of open charm and bottom mesons) and the thermal source (only purely deconfined matter) on $s^{1/2}$.*

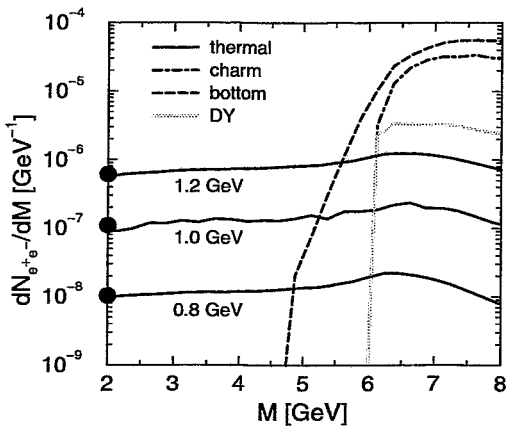

Fig. 2 *The invariant mass spectra of dileptons from the DY process, charm and bottom decays, and thermal emission at LHC within the ALICE acceptance. The single-electron low transverse momentum cut is $p_\perp^{\min} = 3$ GeV. The fat dots indicate the estimates of the low-M thermal plateau as described in [2]. The labels at the thermal curves indicate initial temperatures.*

[1] *Institute for Theoretical Physics, 252143 Kiev - 143, Ukraine*

References

[1] K. Gallmeister, B. Kämpfer, O.P. Pavlenko, Phys. Rev. C 57 (1998) 3276
[2] K. Gallmeister, B. Kämpfer, O.P. Pavlenko, Eur. Phys. J. C 8 (1999) 473

Thermodynamics of Deconfined Matter at Finite Chemical Potential [B]

A. Peshier, B. Kämpfer, G. Soff[1]

The available lattice QCD calculations are presently constrained to vanishing chemical potentials μ of the quarks. In contrast, the equation of state of deconfined matter is calculated at finite values of the temperature T at $\mu = 0$ for pure SU(3) gluon gauge fields and for the four flavor case with small quark masses. We have extended [1] our previous quasi-particle model [2] to extrapolate the lattice QCD results at $\mu = 0$ to finite values of μ. The model is based on an ansatz for the pressure which contains the contributions of the quasi-particles and a mean field term. The resulting expression for the entropy density looks formally as that one of a superposition of ideal gases, however, the quasi-particles are explicitly temperature and density dependent. A selfconsistency condition results in an equation which transports the information from the T axis into the $T - \mu$ plane (see fig. 1). Our model does not cover the transition to confined matter. However, there is a region where the effective coupling strength becomes large (see fig. 2). In this region the confinement transition is expected.

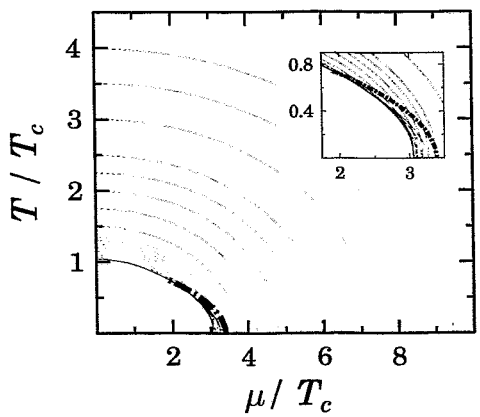

Fig. 1 *The characteristics resulting from the self-consistency condition for the four flavor case with effective coupling adjusted to lattice QCD results at $\mu = 0$. At leading order the characteristics are curves of constant coupling strength. The pressure is negative in the region at the left hand side of the dash-dotted line, thus excluding the intersecting characteristics.*

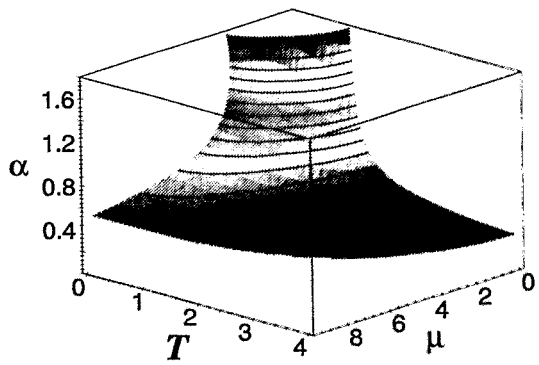

Fig. 2 *The effective coupling strength α as a function of T and μ for the four flavor plasma. The rapid increase of α is considered as indication of the onset of the confinement transition.*

We have extended the equation of state to the realistic case of two light flavors and a medium-heavy flavor corresponding to the strange quark and extracted the resulting equation of state for $T = 0$. Invoking β stability and local charge neutrality by an admixture of degenerate electrons one arrives at an equation of state relevant for purely deconfined quark stars. Within a reasonable range of parameters we find that such objects have masses much less than one solar mass. Therefore, in contrast to earlier estimates relying on a bag model equation of state, pure quark stars or quark cores in neutron stars are very light.

[1] *Technische Universität Dresden*

References

[1] A. Peshier, B. Kämpfer, G. Soff, hep-ph/9906305
[2] A. Peshier et al., Phys. Lett. B 337 (1994) 235, Phys. Rev. D 54 (1996) 2399.
B. Kämpfer et al., J. Phys. G 23 (1997) 2001c

Tadpole Resummed ϕ^4 Thermodynamics [B]

A. Peshier, B. Kämpfer

Finite temperature quantum field theory is the framework to describe hot and dense quantum systems as the quark-gluon plasma (QGP). This state of matter, presumably attainable in relativistic heavy-ion collisions, is characterized by a strong coupling strength. Hence, the quantitative description of properties of the QGP requires nonperturbative methods. In the following, a consistent analytical approach is outlined for the ϕ^4 model field theory with the Lagrangian $\mathcal{L} = \frac{1}{2}(\partial_\mu\phi)(\partial^\mu\phi) - \frac{g_0^2}{4!}\phi^4$, and a possible extension to QCD is pointed out.

Our approach [1] is based on the functional Luttinger-Ward formulation of thermodynamics as originally derived in condensed matter physics. With $T\sum\!\!\!\!\!\!\int$ denoting the finite temperature phase space integration, the thermodynamic potential of the scalar theory reads $\Omega = \frac{1}{2}VT\sum\!\!\!\!\!\!\int [\ln(-\Delta^{-1}) + \Delta\Pi] + \Omega'$ where Π and $\Delta = (\Delta_0^{-1} - \Pi)^{-1}$ denote the exact selfenergy and propagator, respectively. The functional Ω' can be decomposed into the selfenergy skeleton contributions. Owing to the fundamental stationary property $\delta\Omega/\delta\Pi = 0$ there is a close relation between Ω and Π, which in leading order with $\Omega' \approx \Omega'_1 = -3$  yields for the selfenergy the approximation $\Pi_1 = 12$  $= 12\left(\frac{-g_0^2}{4!}\right) T\sum\!\!\!\!\!\!\int \Delta_1$. Renormalizing g_0^2 by introducing the physical coupling $g^2 =$ 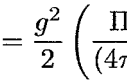 $=$ 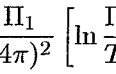 $+ 12$  at a momentum scale $\sim T$, Π_1 is determined by

$$\Pi_1 = \frac{g^2}{2}\left(\frac{\Pi_1}{(4\pi)^2}\left[\ln\frac{\Pi_1}{T^2} - 1\right] + \frac{1}{2\pi^2}\int_0^\infty dp\,\frac{p^2}{\omega_p}\,n_B(\omega_p/T)\right), \tag{1}$$

where $\omega_p = (\Pi_1 + p^2)^{\frac{1}{2}}$, and $n_B(x) = [\exp(x) - 1]^{-1}$ is the Bose function. The pressure, which is related to the thermodynamic potential by $p = -\Omega/V$, is approximated by

$$p_1 = -\frac{T}{2\pi^2}\int_0^\infty dp\,p^2 \ln\left(1 - \exp\{-\omega_p/T\}\right) + \frac{\Pi_1}{8\pi^2}\left[\int_0^\infty dp\,\frac{p^2}{\omega_p}\,n_B(\omega_p/T) + \frac{\Pi_1}{16}\right] \tag{2}$$

and displayed in fig. 1. The approximations (1. 2) represent complete resummations of all diagrams with a tadpole topology. In contrast to the perturbative results, even for large values of g, p_1 as shown in fig. 1 has a smooth behavior and does not deviate much from the free limit.

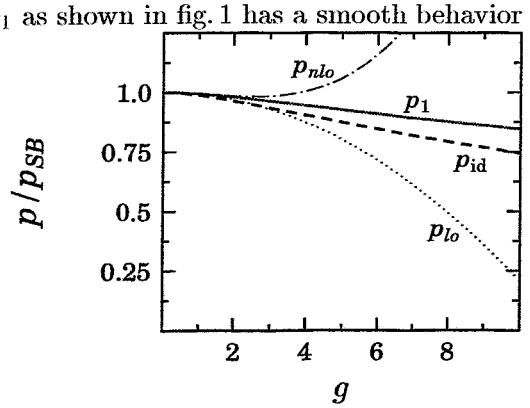

Fig. 1 *The pressure p_1, eq. (2), and the ideal gas contribution $p_{\rm id}$ (the first term in eq. (2)) which looks like an ideal gas of quasiparticles with mass $\sqrt{\Pi_1}$ as determined by eq. (1) as functions of the coupling strength g in units of $p_{\rm SB} = \frac{\pi^2}{90}T^4$. For comparison, the leading and next-to-leading order perturbative results are shown as well.*

Confirmed by other nonperturbative approaches to the ϕ^4 theory, this general behavior is also found in lattice simulations of the QGP. Indeed, an effective quasiparticle model motivated by the structure of (2) reproduces, with suitable selfenergy approximations, available lattice data. Moreover, this nonperturbative model allows predictions [2] beyond lattice calculations.

References

[1] A. Peshier, B. Kämpfer, O.P. Pavlenko, G. Soff, Europhys. Lett. 43 (1998) 381

[2] B. Kämpfer, O. P. Pavlenko, A. Peshier, M. Hentschel, G. Soff, J. Phys. G 23 (1997) 2001c

Induced Soft Gluon Radiation in a QCD Medium [B]

B. KÄMPFER, O.P. PAVLENKO[1], W. MÜLLER[2]

The soft gluon radiation induced by energetic partons propagating through a medium of quarks and gluons is of great interest now, since the radiative energy loss and corresponding stopping power of quark or gluon jets might serve as a probe of the quark-gluon plasma formation in ultrarelativistic heavy-ion collisions. It was recently shown that the Landau–Pomeranchuk–Migdal effect plays a very important role for the formation of gluon bremsstrahlung in a QCD medium. At the same time it is well-known from electrodynamics that the radiation can be modified not only by multiple scatterings of the radiating particle but also by the medium polarization, i.e. the emitted photon is affected. It was firstly pointed out by Ter-Mikaelian [1] that the dielectric polarization of the medium can also cause a loss of coherence, suppressing in this way the emission process.

The strong reduction of the formation length, reflecting the suppression of radiation due to the dielectrical effect, can be seen in electrodynamics by the following simple qualitative estimates. In the high-frequency approximation the dielectrical "constant" becomes $\varepsilon = 1 - \omega_p^2/\omega^2$, where ω_p is the plasma frequency. In a medium the dispersion relation between energy ω and momentum $\vec{k}$ becomes $\omega = |\vec{k}|/\sqrt{\varepsilon}$ in contrast to the vacuum dispersion relation $\omega = |\vec{k}|$ (we use units with $\hbar = c = 1$). As a result the "vacuum" formation length $l_f = 2\gamma^2/\omega$ is reduced to $l_f = 2\omega/\omega_p^2$ in the interval $\omega_p \ll \omega \ll \gamma\omega_p$, where γ is the Lorentz factor of the radiating particle.

Due to the long-range properties of color forces one can expect that the polarization of a QCD medium is also important for the induced gluon radiation. In a recent note [2] we have considered the influence of the QCD medium polarization on the induced soft gluon emission and demonstrated the existence of the non-Abelian analogue to the Ter-Mikaelian effect. We treated the gluon radiation for single scattering of a fast parton and have shown that, due to the polarization of the surrounding medium, the resulting gluon spectrum in the small transverse momentum region is considerably suppressed and the infrared divergence is regularized by the gluon mass. This result is extended to multiple scatterings in a QCD medium.

Our approach is based on the quasi-Abelian diagrams displayed in fig. 1, which provide the main contribution to the radiation amplitude in a certain phase space region [2] in the $A^+ = 0$ gauge [3]. It should be emphasized that a complete analysis of the Ter-Mikaelian effect in QCD needs the consideration of interferences between gluon production and rescattering amplitudes, i.e. much more diagrams than displayed in fig. 1.

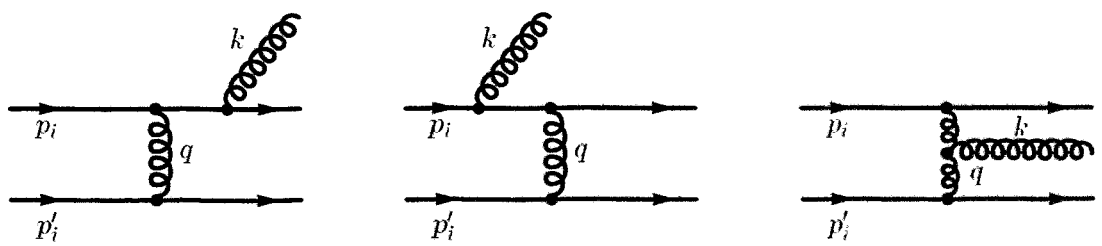

Fig. 1 *Feynman diagrams for radiation in a single scattering via a one-gluon exchange process.*

[1] *Institute of Theoretical Physics, Kiev, Ukraine* [2] *Institut für Theoretische Physik, TU Dresden*

References

[1] M.L. Ter-Mikaelian, *High-Energy Electromagnetic Processes in Condensed Media*, John Wiley & Sons, New York 1972

[2] B. Kämpfer, O.P. Pavlenko, hep-ph/9906258

[3] W. Müller, Diploma thesis, TU Dresden 1999

Effect of Opaqueness in Two-Pion Correlations in Relativistic Heavy-Ion Collisions [B]

H.W. Barz

Measurements of correlations of pions as a function of their relative momenta are used to determine the source size in heavy ion reactions using the Hanbury-Brown and Twiss effect. If pions are rescattered within the hot nuclear source they are emitted from a relatively small surface region which is determined form their mean free path [1]. This effect will reduce the apparent radius of the source if the correlation function $C_2(K,q)$ is measured in outward direction, i.e. if the difference of the momenta of the two pions $\mathbf{q} = \mathbf{p} - \mathbf{p}'$ is parallel to the average pair momentum $\mathbf{K} = \frac{1}{2}(\mathbf{p} + \mathbf{p}')$. To investigate this effect quantitatively we introduce into the equation of motion for the pions an absorptive potential.
The correlation function C_2 is essentially determined by the square of the density matrix $\rho(\mathbf{p},\mathbf{p}')$ which is given by the overlap of the pion wave functions and the source function $S(\mathbf{r},\mathbf{v})$

$$\rho(\mathbf{p},\mathbf{p}') = e^{-(\omega-\omega')^2\tau^2/2}\langle\psi_{\mathbf{p}} \mid S(\mathbf{r},\mathbf{v}) \mid \psi_{\mathbf{p}'}\rangle\,, \tag{1}$$

where ω, ω' denote the pion energies, τ is the life time of the source which depends also on the velocity field $\mathbf{v}$. For details see ref. [2]. The wave functions $\psi_{\mathbf{p}}$ are obtained by solving the Klein-Gordon equation with a potential U

$$U = U_{Coulomb} + i\frac{p}{\omega}\frac{1}{2\lambda}\,. \tag{2}$$

The mean free path λ is estimated from the baryonic density and the pion-nucleon cross-section mainly governed by the Δ resonance. Due to the thermal motion the width of the Δ resonance is increased to about 250 MeV. Using a Gaussian source distribution characterized by a radius R_0 the calculated correlation function C_2 still has the typical Gaussian shape $\sim exp(-q^2R^2_{HBT})$ but with an apparent radius R_{HBT}. Fig. 1 shows the obtained radii for an ideal uncharged source (left panel) and also the common influence of opaqueness, flow and charge (right panel). The charge leads to an increase of the sideward radius for negative pions while the flow reduces all the observed radii with growing momentum of the pion pair. The influence of the opaqueness destroys the correlation of the emission time τ with the difference between outward and sideward radius.

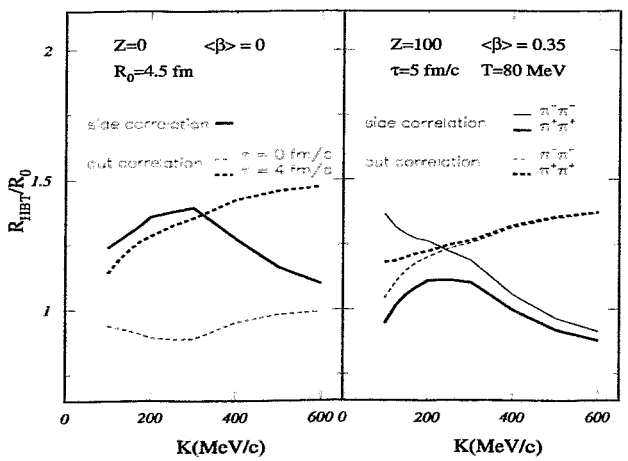

Fig. 1 *Ratios of HBT radii to the geometrical radius extracted from sideward and outward correlations as a function of the average momentum K of the pion pair. The left panel shows the pure opaqueness effect while the right panel shows in addition the influence of Coulomb and velocity field in the source.*

References

[1] H. Heiselberg and A.P. Vischer, Eur. Phys. J. **C1** (1998) 593
[2] H.W. Barz. Phys. Rev. **C53** (1996) 2536, **C59** (1999) 2214

Pion Exchange Effects in Elastic Backward Proton-Deuteron Scattering [B]

L.P. KAPTARI[1], B. KÄMPFER, S.M. DORKIN[2] S.S. SEMIKH[1]

In a recent work [1] we have studied relativistic effects and polarization observables in elastic proton - deuteron (pd) backward scattering. This approach is based on the impulse approximation, i.e., the one-nucleon exchange diagram shown in fig. 1, and a realistic deuteron wave function obtained as solution of the Bethe-Salpeter (BS) equation. The comparison of some observables (such as cross section, polarization transfer and tensor analyzing power) with available experimental data shows that some gross features are satisfactorily well described, but there are still remarkable deviations in detail. Therefore, one might argue that one has to go beyond the impulse approximation to get better agreement with data. As first extension we are going to include the triangle diagrams displayed in fig. 1. Such improvements are necessary since at COSY-TOF the elastic backward scattering reaction $\vec{p}d \to \vec{p}(180^o)d(0^o)$ will be measured in near future with polarized proton beams (approved COSY proposal 68.1). In this experiment the proton-proton polarization transfer can be measured. As example of our calculations [2] we exhibit in fig. 2 the proton and the deuteron polarization transfer.

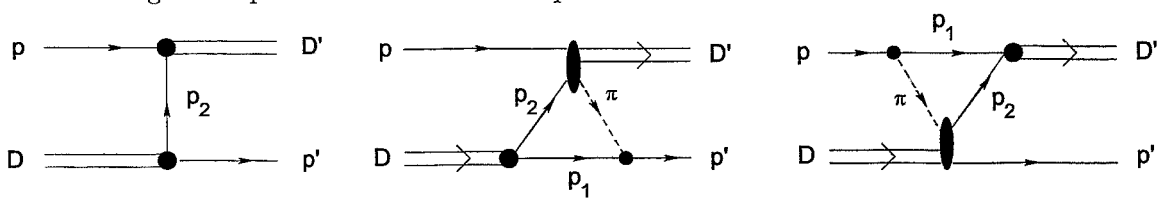

Fig. 1 *The one-nucleon (left diagram) and the one-pion exchange graphs for the elastic pd reaction.*

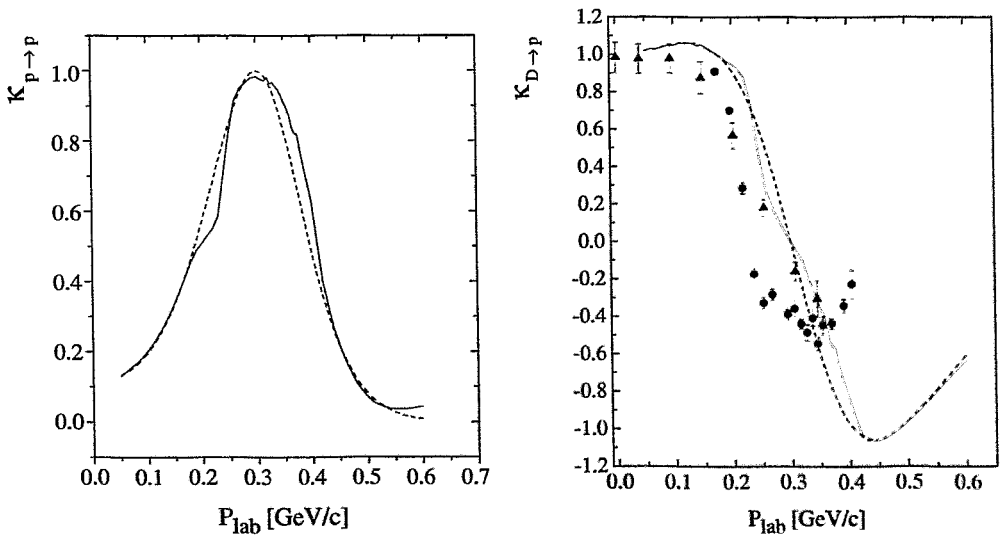

Fig. 2 *The polarization transfer for the elastic pd backward scattering. Left panel: The vector-vector polarization transfer coefficient from the initial proton to the final proton: dashed line: contribution of the one-nucleon exchange mechanism: solid line: the full BS result. Right panel: deuteron to proton polarization transfer $\kappa_{D\to p}$: dashed line: the contribution of the one-nucleon exchange mechanism: solid line: the result of computation within the BS approach, including contributions from the triangle diagram: experimental data: circles - for the elastic backward scattering, triangles - measured in the deuteron break up reactions.*

[1] *Bogoliubov Laboratory of Theoretical Physics, JINR Dubna* [2] *Far-Eastern State University, Vladivostok, Russia*

References

[1] L.P. Kaptari, B. Kämpfer, S.M. Dorkin, S.S. Semikh, Phys. Rev. C 57, 1097 (1998)
[2] L.P. Kaptari, B. Kämpfer, S.M. Dorkin, S.S. Semikh, nucl-th/9812064

On the Sequence of Proton and Composite Particle Emission in Central Reactions of Ru+Ru at 400 $A \cdot$ MeV [B,G]

R. Kotte, H. W. Barz, W. Neubert, C. Plettner, D. Wohlfarth,
and the FOPI collaboration

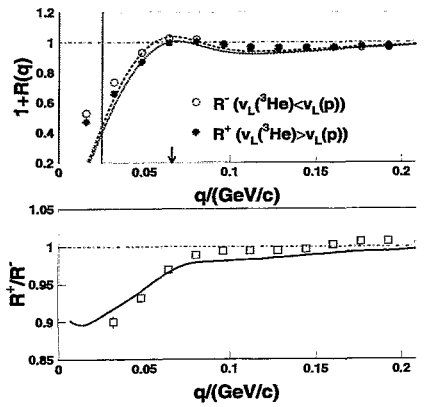

Fig. 1 *Upper panel: Forward (full dots) and backward (open dots) longitudinal experimental correlation functions of ^{3}He-p pairs. The arrow marks the position of a resonance due to the decay of the particle-unbound ground state of ^{4}Li ($J^\pi = 2^-$, $\Gamma = 6$ MeV). The full and dashed lines give the corresponding model predictions with the true (apparent) time delay of $\tau_{^3He} - \tau_p = 11.7$ (4.5) fm/c. The hatched area indicates the unreliable region. Lower panel: Forward/backward ratio of experimental (squares) and theoretical (line) correlation functions.*

Small-angle correlations of pairs of light charged particles produced in central collisions of ^{96}Ru + ^{96}Ru at a beam energy of 400 A·MeV are investigated with the FOPI detector system at GSI Darmstadt [1]. In order to determine the space-time differences in the emission of nonidentical particles, we follow the recipe of Lednický et al. [2] who proposed to measure the ratio of longitudinal correlation functions R(q) + 1 of particles having the relative momentum $\mathbf{q} = \mu(\mathbf{v}_1 - \mathbf{v}_2)$ parallel and anti-parallel to the pair velocity $\mathbf{v}_{12} = (\mathbf{p}_1 + \mathbf{p}_2)/(m_1 + m_2)$, where $\mathbf{v}_{1,2}$ and $\mathbf{p}_{1,2}$ are the velocities and momenta of particles 1,2 in the source frame, and $\mu = m_1 m_2/(m_1 + m_2)$ is their reduced mass. The forward and backward correlation functions are defined by the cuts on the angle ζ between $\mathbf{q}$ and $\mathbf{v}_{12}$, $\cos\zeta > 0$ and $\cos\zeta < 0$, respectively. This choice selects pairs with the longitudinal velocity component v_L of particle 1 being larger or smaller than the corresponding value of particle 2. A central source is selected by a cut on large charged-particle multiplicities in the outer Plastic Wall which comprises about 8 % of the total cross section. The comparison of the correlations with the corresponding results of a final-state interaction model delivers quantitative estimates of the apparent emission times [3]. Time differences as short as 1 fm/c $\approx 3 \cdot 10^{-24}$ sec are resolved. The strong collective expansion of the participant zone found in central collisions introduces not only an apparent reduction of the source radius (see also ref. [4]) but also a modification of the emission time differences which is strongest for large differences of the particle masses. After correcting for both effects, for the first time [3] a complete sequence of the emission times of p, d, t, ^{3}He, and α particles is presented (cf. table 1). Here, the source radius is fixed by fitting the p-p and d-d correlation functions with a Gaussian source of zero lifetime and radius $R_0 = 5.7$ fm.

Figure 1 shows, as an example, the result for ^{3}He-p pairs. Obviously, the particles experience a stronger final state interaction if $v_L(^3\mathrm{He}) > v_L(p)$. This is only possible if the ^{3}He particles are emitted later than the protons. The flow correction increases the apparent emission time difference by about 7 fm/c.

Table 1 *The emission time sequence of p, d, t, ^{3}He, and α particles derived from the ratios R^+/R^- for all ten combinations of nonidentical particles.*

particle	p	d	α	t	^{3}He
time/(fm/c)	0	6.3 ± 0.8	7.7 ± 0.9	8.5 ± 0.9	11.1 ± 0.8

References

[1] A. Gobbi et al., Nucl. Instr. Meth. A 324 (1993) 156; J. Ritman, Nucl. Phys. B 44 (1995) 708
[2] R. Lednický, V.L. Lyuboshitz, B. Erazmus, and D. Nouais, Phys. Lett. 373 (1996) 30
[3] R. Kotte, H. W. Barz et al. (FOPI collaboration), Eur. Phys. J. A, 6 (1999) 185
[4] R. Kotte et al., Z. Phys. A 359 (1997) 47

Fragmentation of ^{12}C and ^{27}Al by 1 GeV Protons Comparison of Experimental Data with Model Calculations [W]

L.N. ANDRONENKO[1], M.N. ANDRONENKO[1], W. NEUBERT AND D.M. SELIVESTROV[1]

Fragment production by 1 GeV protons interacting with targets from Be to Au was investigated in ref. [1,2]. An incident proton initiates a cascade of successive NN and πN collisions leaving target residues with excitation energies sufficient to undergo clusterization. These processes are well described by the Intra-Nuclear Cascade (INC) model coupled with the Statistical Multifragmentation Model (SMM) as far as medium-weight target nuclei are considered [3,4]. Here, we compare inclusive data (measured at $\Theta_{lab} = 30°$ and 126°) available for light nuclei with corresponding calculations. The results demonstrate that (i) composite particle production by coalescence has minor influence on the findings presented below and that (ii) the calculated kinetic energy spectra of fragments with $Z \geq 2$ are steeper (i.e. equivalent to *lower* apparent temperatures) compared with the experimental ones. The consideration of preequilibrium emission of light charged particles does not improve the reproduction. For lighter target-nuclei the data differ more and more from an equilibrated scenario implemented in the model. We present here two examples. Fig. 1 shows the charge distributions of the fragments obtained from C and Al targets. In case of Al the almost exact reproduction of the shape of the Z distribution by the model points to predominant thermal production. The kinetic energy spectra of selected fragments (with fixed Z) and of separated isotopes also show a rather good agreement (fig. 2). However, with regard to the carbon target the relative yields are not consistent with the results of the model. But we mention the nearly correct description of the slopes of the He isotopes (fig. 3). Especially, the exceptional behaviour of ^3He (also observed in other reactions) is surprisingly well reproduced.

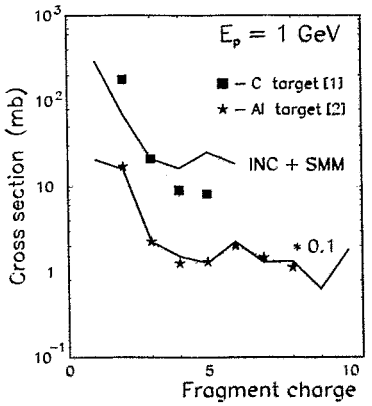

Fig. 1 *Fragment charge yields, solid lines: calculations normalized to data at Z=3.*

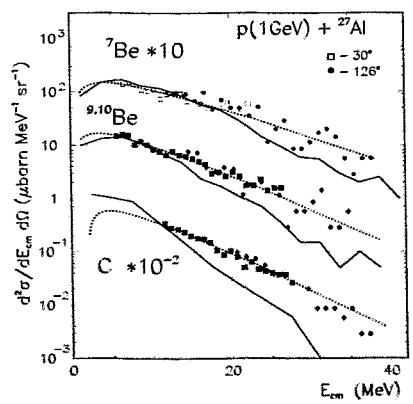

Fig. 2 *Kinetic energy spectra, dots: data, dashed lines: moving source fits, solid lines: model calculations.*

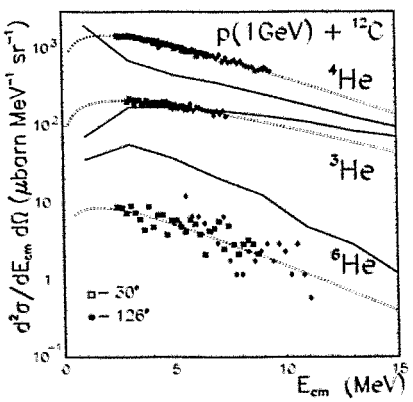

Fig. 3 *Kinetic energy spectra, notations are the same as in fig 2.*

[1] *St. Petersburg Nuclear Physics Institute, 188350 Gatchina, Russia*

References

[1] L.N. Andronenko et al., PNPI Research Report 1996-1997, p. 237
[2] A.A. Kotov et al., Nucl. Phys. A 583 (1995) 575
[3] A.S. Botvina et al., Nucl. Phys. A 507 (1990) 649
[4] W. Neubert et al., FZR Annual Report 1994, p. 92

Application of Pulse Shape Analysis to Isotope Separation in Bragg Curve Spectroscopy [W]

M.N. Andronenko[1] and W. Neubert

Flash-ADC's as integral part of a setup designed for fragmentation studies in p+A reactions [1] allow to register the complete pulse shape of the current signal generated in the Bragg Ionization Chambers (BIC). The separation of certain isotopes becomes possible by the simultaneous measurement of the TOF, range and energy loss, which can be additionally verified by using redundant quantities. Here we report on a refinement of isotope separation. As mentioned in [2], the current signal from the BIC as image of the Bragg curve is influenced by the apparatus response (especially by the amplifiers shaping times). Thus, the Bragg peak height (BP) depends for a given Z also on the mass A. This fact was used to improve the Z resolution, moreover it allows resolving isotopes of light nuclei like Li and Be, too. Our method used is based on the generation of a *reference shape* as already demonstrated in [3]. In analogy, we derived a set of *reference shapes* for the isotopes produced in p+^{12}C interactions (fig. 1). The pulse shapes exhibit perceptible differences of both the BP and the shape itself over the whole pulse duration if different isotopes are involved. If the relationship of a registered pulse shape to a given Z was recognized during the data processing then the most probable *reference shape* was selected by the χ^2 criterion which allows to specify the *range* and determination of the mass number. In fig. 2 we show the obtained energy spectra of ^9Be and ^{10}Be (right panel) the separation of which was not feasible by usual methods (left panel). The smallest possible χ^2 as measure of the quality of a registered pulse can also serve as a condition for a dynamic data reduction to remove events distorted by noise or pile-up as well as a criterion to search for rare events during the acquisition process.

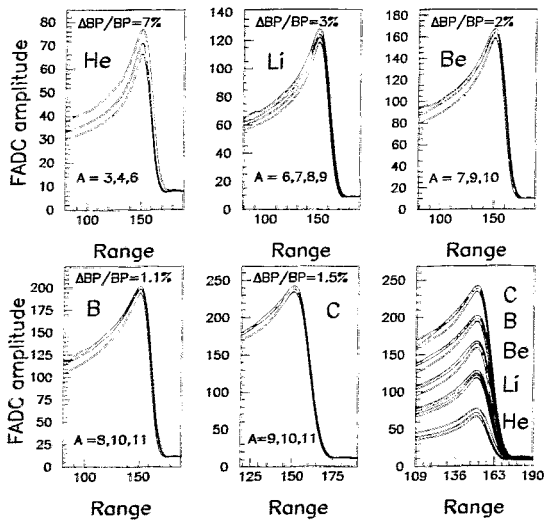

Fig. 1 *Reference shapes for He, Li, Be, B and C.*

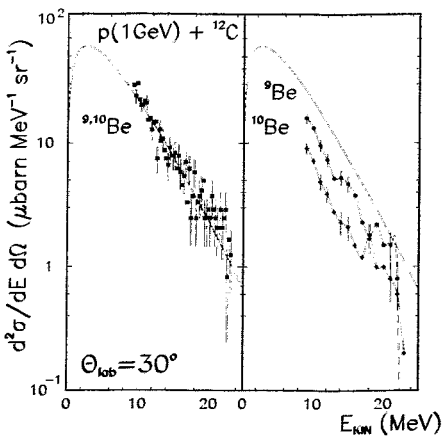

Fig. 2 *Kinetic energy distributions of Be isotopes.*

[1] *St. Petersburg Nuclear Physics Institute, 188350 Gatchina, Russia*

References

[1] L.N. Andronenko et al., Preprint PNPI-2217, Gatchina 1998
[2] N.J. Shenhav and H. Stelzer., Nucl. Instr. Meth. 228 (1985) 359 and Ch. Schulz, Diploma work, TU Berlin 1995
[3] M.N. Andronenko et al., Annual report 1996, FZR-179, p.102

Nuclear Physics

The activities in the nuclear physics department can be shortly characterized as follows:

- *The experimental and theoretical studies of* **nuclei at high spin** *concentrated on the phenomena related with the spin orientation and the breaking of the discrete mirror symmetries of deformed nuclear shapes in conjunction with rotational degrees of freedom. Among the topics treated by our group the leading one has been the magnetic rotation which is also due considerable attention paid to this phenomenon in physics community. The effort to develop new theoretical methods for the restoration of broken symmetries and to include quantum corrections were successful.*

- *The design of the experimental set-up for a polarized photon beam at the ELBE accelerator has been worked out. This facility will enable us to realize the* **nuclear resonance fluorescence** *experiments at our home institution. Compared to the measurements performed up to now in collaboration at the SDALINAC in Darmstadt and at the DYNAMITRON in Stuttgart the photon energy range for the excitation of dipole states can be extended and the parity identification at high excitation energy is possible.*

- *We participated in an ISOL type experiment at the Unilac of the GSI Darmstadt aiming at the properties of proton-rich* **exotic nuclei**. *The measurements included the available mass separation technique and the coincident recording of β-delayed γ-rays with the Rossendorf CLUSTER Detector and GSI segmented Clover detector. The next experiments planned in collaboration with GSI concern N=Z nuclei around mass number A=70 where both the on-line mass separator at Unilac and the fragment separator at SIS will be used.*

- *The bulk of data measured during the experiment series in 1995-1997 at the Dubna U400m cyclotron with the FOBOS detector is still not fully evaluated. In the ongoing analysis new information on the reaction process in the Fermi energy region was gained.*

Below the physical content of the reports is summarized.
Symmetry breaking in many body quantum systems is a subject of general interest in physics. In high spin states the presence or breaking of symmetries expresses through its particular type of band structure and its decay pattern. The magnetic rotation, for instance, is a regular rotational band with strong magnetic dipole transitions and extremely weak quadrupole cross-over transitions. Since the latter feature signals the nearly spherical shape of the nucleus one is asking how it can quantum-mechanically rotate? The tilted axis cranking (TAC) theory has predicted the appearance of magnetic rotation in several mass regions. Indeed, in evaluating the data obtained in an experiment with the GASP spectrometer, this peculiar rotational mode was confirmed in the weakly deformed $^{82,84}Rb$ nuclei. It is not observed in the odd neighbor ^{83}Rb showing that this phenomenon might be quite fragile. The magnetic rotation should transform into the familiar type of collective rotation when the nuclear system becomes deformed. This question was the specific goal of the experimental investigations concerning the nature of a dipole band in ^{79}Br. The analysis has shown that the ^{79}Br seems to be a transitional case in between magnetic and collective rotation as indicated by the observation of sizeable electric cross over (E2) transitions simultaneously with the magnetic dipole (M1)

transitions.
We developed a contour integration method to account for the correlation energy gain due to small amplitude quantum oscillations about a classically stable mean field state. This method is applicable to nuclei and clusters and it allows us to include really the large configuration spaces needed for the treatment of practical cases. The proposed state mixing approach enables one to treat the tunneling process of a nuclear system from a given potential energy minimum to another minimum. The approach describes e.g. the continuous change of a finite many-body system from one symmetry type to another one which might exemplify similar transition phenomena in other domains of physics.
Experiments, firstly at the MP Tandem in Heidelberg and later at the large γ-array EUROBALL at Legnaro, were performed to observe nuclei with $N \approx Z$ around the mass number A=70. The weak production channel for this proton rich nuclides require the simultaneous measurement of charged particles and neutrons in coincidence with the emitted γ-rays. Here, for the first time the Rossendorf Silicon Detector Ball (RoSiB) was successfully employed together with the EUROBALL neutron wall which was crucial for selecting the reaction channels. The collected EUROBALL data implied surprising results for the isotopes $^{72,73}Br$. In particular, the band structures of ^{73}Br obtained with the high sensitivity of the EUROBALL spectrometer achieve with the value $\hbar\omega$ =1.8 MeV a new limit of rotational frequency that is higher than any value observed before in nuclei. The interpretation of those structures, in particular their stability is a challenging task for the theory.
In preparation to our planned measurements with Bremsstrahlung at the ELBE accelerator (γ, γ') experiments on the semi-magic N=50 isotones ^{88}Sr and ^{87}Rb were performed at the S-DALINAC in Darmstadt and at the DYNAMITRON in Stuttgart, respectively, in collaboration with our partner groups at the universities. The emphasis of the Darmstadt experiment was on the parity determination for the dipole states by using a set-up of two EUROBALL CLUSTER detectors as Compton polarimeters. The physical question behind these experiments concerns the systematic search for two-phonon dipole states in N=50 isotones which can be firmly assigned only if the parity is determined. The planning for our polarized Bremsstrahlung source at ELBE aims at the parity measurements in the higher excitation energy region E =6-10 MeV where the Compton polarimeter becomes ineffectient. Presently, the set-up of the polarized Bremsstrahlung at ELBE is optimized for giving high enough intensity and to reduce the photon background from scattering and the effects of possible neutron production.
In continuing the analysis of FOBOS data the independent measurement of velocity and energy for heavy fragments at FOBOS allowed one to apply a refined separation of the reaction channels for the fission process by using a new parametrization for the data analysis. This leads to a more consistent understanding of the complex dynamics of the heavy-ion induced reactions in energy region 10-100 MeV/A investigated in these FOBOS experiments.
With regard of the magnetic susceptibility of Aluminum clusters the results demonstrate the useful application of the nuclear many body methods to cluster physics.

As already mentioned in the preface all the described achievements express also the successful and continuous cooperation with the university groups, in particular with the German spectroscopy groups at Cologne, Göttingen, Darmstadt and Bonn, as well as the support coming from groups experimenting with us at the EUROBALL and the GASP spectrometer in Legnaro. Starting our common investigations of exotic nuclei at the GSI Darmstadt it was very important to get the help and encouragement from the nuclear physics groups at the Unilac and SIS.

Spontaneous Symmetry Breaking in Rotating Nuclei

S. FRAUENDORF[1]

The concepts of spontaneous symmetry breaking are applied to the rotating mean field of nuclei. The description is based on the tilted axis cranking model, which takes into account that the rotational axis can take any orientation with respect to the deformed density distribution. The appearance of rotational bands in nuclei is analyzed [1], focusing on weakly deformed nuclei at high angular momentum. The quantization of the angular momentum of the valence nucleons leads to new phenomena. Magnetic rotation represents the free quantized rotation of a magnetic dipole in a near spherical nucleus. Band termination is a consequence of the restricted amount of angular momentum readily accessible. The discrete symmetries of the mean field Hamiltonian provide a classification scheme of rotational bands, both in weakly and strongly deformed nuclei. New symmetries result from the combination of the spatial symmetries of the density distribution with the vector of the angular momentum. We analyze in detail the case of three mirror planes. Most bands correspond to rotation about a principal axis and about an axis tilted within a plane. If the angular momentum vector lies outside all three planes, the chiral symmetry is broken, the consequences of which are discussed. A brief survey of the cases with two and one mirror planes is given.

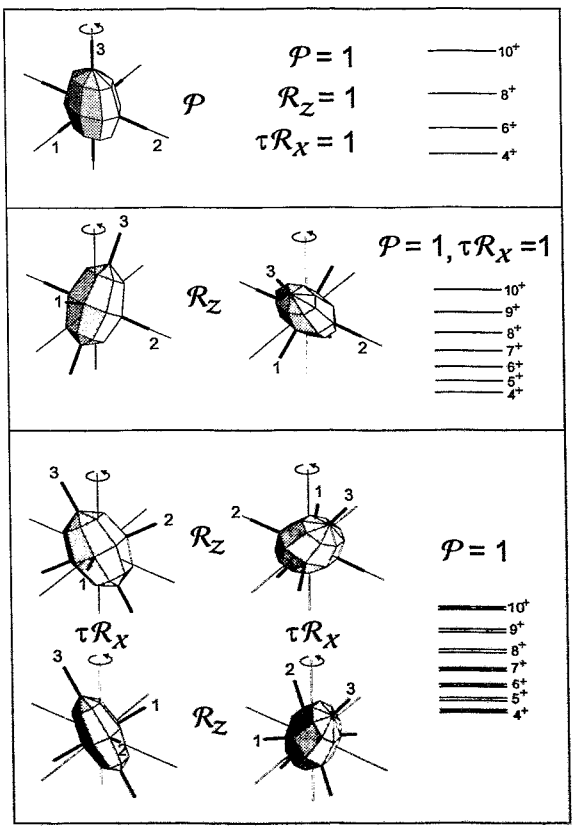

Fig. 1 *The discrete symmetries of the mean field of a rotating triaxial reflection symmetric nucleus (three mirror planes). The mean field is represented by its density distribution. A polyhedron is used to make the symmetries better visible. The axis of rotation (z) is marked by the circular arrow. It coincides with the angular momentum $\vec{J}$. The figure illustrates the reorientation of the mean field by the three symmetry operations, which leave the two body routhian invariant. If an operation does not ensue a reorientation this is indicated by the identity. Equivalent operations are also indicated. The structure of rotational band associated with each symmetry type is illustrated on the right side. (Note the change of chirality induced by $\mathcal{R}_x\mathcal{T}$ in the lowest panel.)*

[1] *on leave of absence at Department of Physics, University of Notre Dame, IN 46556, USA*

References

[1] S. Frauendorf, Rev. Mod. Phys. , submitted

Magnetic Rotation - Rethinking Nuclear Structure

S. FRAUENDORF[1]

Until recently it was thought that regular rotational bands appeared only in nuclei with a substantial deformation, whereas near-spherical nuclei always emitted irregular pattern of γ-rays. However, in the early 1990s very regular pattern of γ-rays - and hence possible evidence for rotation - were detected from nuclei that were known to be almost perfect spheres. The γ-rays do not have electric quadrupole character (E2) but magnetic dipole (M1). Hence, they must be emitted from a rotating magnetic dipole.

The figure on the front page illustrates this exotic type of quantal rotor, which was suggested in [1]. The new mode called "Magnetic Rotation" is generated by just a few proton particles and neutron holes (or vice versa) outside a closed shell core, which remains passive. The active nucleons move on orbits with a high angular momentum, which are similar to the current loops shown in the figure. They interact via the exchange phonons of surface vibrations. Since the interaction is attractive between the proton particles, their current loops and, as a consequence, their angular momenta align themselves to the long vector $\vec{j}_\pi$. The same holds for the neutron holes, which align to $\vec{j}_\nu$. The repulsive interaction between the particles and holes tries to keep the current loops of the protons and neutrons as much separated as possible. Hence, the energy has a minimum for an angle of 90^o between $\vec{j}_\pi$ and $\vec{j}_\nu$ which defines the bottom of the rotational band. The higher members of the band are generated by gradually aligning $\vec{j}_\pi$ with $\vec{j}_\nu$. This process has been dubbed the "shears" mechanism because it resembles the closing of a pair of shears with a spring that tries to keep it open. Like classical gyroscopes, the blades of the shears must rotate in order to compensate for the torque exerted by the spring.

The two blades have very different magnetic moments because the protons are charged but the neutrons not and their spin moments have opposite signs. Therefore, the cross arrangement of the current loops generates a large transversal component μ_{perp} of the magnetic dipole moment, which permits to specify the orientation angle. Magnetic rotation is the quantized motion of μ_{perp}, which is observed as regular bands of strong $M1$ transitions. The transversal dipole moment becomes shorter when the shears close. Therefore, the rate of magnetic dipole radiation, which is proportional to μ^2_{perp}, decreases with increasing angular momentum.

Magnetic rotation was discovered in the Pb - isotopes, but predicted to exist in a number of other mass regions as well [2]. Within the period of this report, magnetic rotation was found in ^{82,84}Rb [3], ^{110}Cd [4] and ^{106,108}Sn [5,6]. Magnetic rotation in its purest form appears in ^{106}Sn, the deviations of which from the spherical shape are less than 5%. The experiment [3] was carried out by the FZR group at the GASP spectrometer in Legnaro. Our contribution to the work [4-6] consists in the theoretical interpretation.

Fig. 1 See front page

Magnetic rotation. The high-j proton particles and neutron holes form current loops embedded in in near spherical mass distribution of the nucleus. These current loops as well as the associated transverse magnetic moment μ_{perp} allow us to specify the angle of a rotation around the axis $\vec{J}$. The total angular momentum J increases by the gradual alignment of the particle and hole angular momenta $\vec{j}_p$ and $\vec{j}_n$.

[1] *on leave of absence at Department of Physics, University of Notre Dame, IN 46556, USA*

References

[1] S. Frauendorf, Nucl. Phys. A 557 (1993) 259c
[2] S. Frauendorf, Z. Phys. A 358 (1997) 163
[3] H. Schnare et al., Phys. Rev Lett. 82 (1999) 4408
[4] R. Clark et al., Phys. Rev Lett. 82 (1999) 3220
[5] D. Jenkins et al., Phys. Lett. B 428 (1998) 23
[6] D. Jenkins et al., Phys. Rev Lett. , in print

Study of Magnetic Rotation in ^{82}Rb and ^{84}Rb within the TAC Model [B]

R. Schwengner, H. Schnare, S. Frauendorf, F. Dönau, L. Käubler, H. Prade, A. Jungclaus[1], K. P. Lieb[1], C. Lingk[1], S. Skoda[2], J. Eberth[2], G. de Angelis[3], A. Gadea[3], E. Farnea[3], D.R. Napoli[3], C. A. Ur[3] and G. Lo Bianco[4]

In our study of Rb isotopes [1.2] we have observed regular magnetic dipole ($M1$) bands in the odd-odd nuclei $^{82}Rb_{45}$ and $^{84}Rb_{47}$ that show the typical characteristics of magnetic rotation. Therefore, we have interpreted these bands in the framework of the tilted-axis cranking (TAC) model [3]. In the calculations, the configuration $\pi(fp)\ \pi(g_{9/2}^2)\ \nu(g_{9/2})$ has been adopted, which is the lowest-lying four-quasiparticle ($4qp$) configuration with negative parity for $Z = 37$ and $N = 45, 47$. Equilibrium deformations of $\epsilon_2 = 0.16$ and $\epsilon_2 = 0.14$ were obtained for the adopted $4qp$ configuration in ^{82}Rb and ^{84}Rb, respectively. The nuclei turn out to be soft with respect to γ deformation with a tendency to positive values in ^{82}Rb but negative values in ^{84}Rb. Thus, values of $\gamma = 20°$ and $\gamma = -15°$ have been used for ^{82}Rb and ^{84}Rb, respectively. The dependence of the spin on the rotational frequency for the $M1$ bands in ^{82}Rb and ^{84}Rb is given in the upper panels of Fig. 1. It shows that the calculated curves follow well the experimental regular behaviour. Experimental and calculated ratios of transition strengths $B(M1)/B(E2)$ are compared in the lower panels of Fig. 1. The ratios calculated for the proposed $4qp$ configuration in ^{82}Rb are in excellent agreement with the experimental values. In ^{84}Rb the behaviour of the experimental $B(M1)/B(E2)$ ratios is fairly well described in the calculation up to $\hbar\omega = 0.7$ MeV, whereas the upbend above $\hbar\omega = 0.7$ MeV cannot be described with the chosen $4qp$ configuration.
This TAC-model description proves the applicability of the concept of magnetic rotation to the $M1$ bands in ^{82}Rb and ^{84}Rb and provides the first evidence of this novel rotational mode in the mass region around $A = 80$ [4].

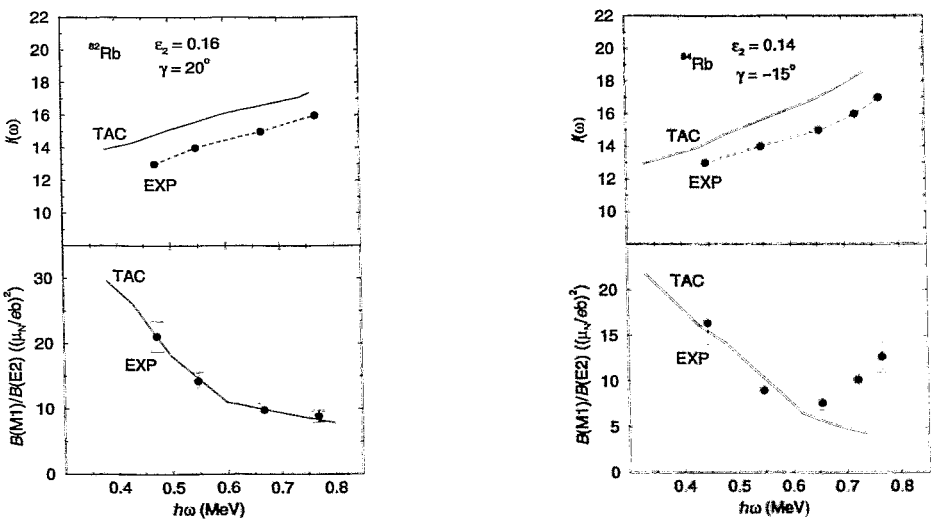

Fig. 1 *Experimental and calculated spins (top) and $B(M1)/B(E2)$ ratios (bottom) as a function of the rotational frequency for the $M1$ band in ^{82}Rb (left) and ^{84}Rb (right).*

[1] *II. Physikalisches Institut, Universität Göttingen.* [2] *Institut für Kernphysik, Universität zu Köln*
[3] *INFN, Laboratori Nazionali di Legnaro,* [4] *INFN, Sezione di Milano*

References

[1] H. Schnare et al., Annual Report 1997, FZR-219 (1998) 46
[2] R. Schwengner et al., Annual Report 1997, FZR-219 (1998) 48
[3] S. Frauendorf, Nucl. Phys. A 557 (1993) 259c
[4] H. Schnare et al., Phys. Rev. Lett. 82 (1999) 4408

^{79}Br - a Transitional Nucleus between Magnetic and Collective Rotation [B]

R. Schwengner, T. Servene, H. Schnare, J. Reif, G. Winter, L. Käubler, H. Prade, F. Dönau, S. Frauendorf, S. Skoda[1], J. Eberth[1], H.G. Thomas[1], F. Becker[1], B. Fiedler[1], S. Freund[1], S. Kasemann[1], T. Steinhardt[1], O. Thelen[1], T. Härtlein[2], C. Ender[2], F. Köck[2], P. Reiter[2], D. Schwalm[2]

In our study of the nucleus ^{79}Br we have investigated in particular the magnetic dipole ($M1$) band starting with a $13/2^-$ state at 2393 keV [1,2]. This $M1$ band coexists with collective electric quadrupole ($E2$) bands which are built on low-lying $5/2^-$ and $9/2^+$ states and correspond to a quadrupole deformation of the nucleus of $\beta_2 \approx 0.2$. In contrast to this, $M1$ bands representing magnetic rotation [3] have been observed so far only in nearly spherical nuclei at high spin, while the low-spin structure of those nuclei is irregular [4].

We have interpreted the $M1$ band in ^{79}Br in the framework of the tilted-axis cranking (TAC) model [5]. In the calculations, the low-lying three-quasiparticle ($3qp$) configuration $\pi(g_{9/2})\ \nu(g_{9/2})\ \nu(fp)$ has been assumed. For this configuration an equilibrium deformation of $\epsilon_2 = 0.20$ and a shallow minimum of the γ deformation in a range of about $-20° \leq \gamma \leq +20°$ were obtained. Experimental and calculated $B(M1)$ and $B(E2)$ transition strengths and the $B(M1)/B(E2)$ ratios are compared in Fig. 1. The $B(M1)$ transition strengths (top panel) calculated for $\gamma = 0$ and $\gamma = +20°$ reproduce the behaviour of the experimental values in the range of $0.4 \leq \hbar\omega \leq 0.6$ MeV. The increase of the experimental $B(M1)$ values above $\hbar\omega \approx 0.6$ MeV cannot be described with the chosen $3qp$ configuration but point to a configuration change. The experimental $B(E2)$ values (middle panel) tend to decrease with increasing frequency and may also indicate the termination of the $3qp$ configuration at $\hbar\omega \approx 0.6$ MeV. The calculated $B(E2)$ values for $\gamma = 0$ reproduce the experimental values at $\hbar\omega = 0.45$ MeV.

The magnitude and the decrease of the experimental and calculated $B(M1)$ values as a function of $\hbar\omega$ shows that the $M1$ band includes a strong magnetic component and the particle spins align along the axis of the total spin with increasing rotational frequency (shears mechanism). On the other hand, collective rotational spin contributes as well to the total spin at higher frequency. Thus, the TAC description reflects the transitional character of this band which includes components of both magnetic and collective rotation. The increase of the $B(M1)$ strengths and decrease of $B(E2)$ strengths above $\hbar\omega = 0.6$ MeV may arise from a band crossing of proton orbitals and is currently investigated within the TAC model.

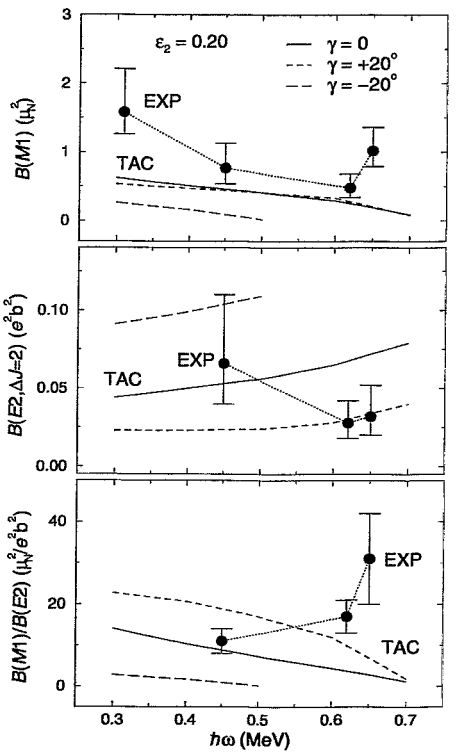

Fig. 1 *Experimental and calculated $B(M1)$ and $B(E2)$ transition strengths as a function of the rotational frequency for the $M1$ band in ^{79}Br.*

[1] *Institut für Kernphysik, Universität zu Köln*
[2] *MPI für Kernphysik Heidelberg*

References

[1] T. Servene et al., Annual Report 1996, FZR-179 (1997) 69
[2] T. Servene et al., Annual Report 1997, FZR-215 (1998) 50
[3] S. Frauendorf et al., Conf. on Physics of large γ-ray detector arrays, Berkeley, LBL-35687 (1994) 52
[4] H. Schnare et al., Phys. Rev. Lett. 82 (1999) 4408
[5] S. Frauendorf, Nucl. Phys. A 557 (1993) 259c

Integral Representation of the Random Phase Approximation Correlation Energy

F. DÖNAU, D. ALMEHED AND R.G. NAZMITDINOV[1]

The Random Phase Approximation (RPA) enables one to account for the quantized small amplitude motion not included into the static Mean Field (MF) treatment of the nuclear or cluster systems. These quantal fluctuations lead not only to series of collective excitations like rotation and vibrations but give rise also to typical correlations in the ground state which change its properties. The correlation energy gain in RPA can be formally written as

$$E_{corr} = \frac{1}{2}\Big[\sum_{\nu}\omega_{\nu} - \sum_{i<j}(e_i + e_j)\Big]. \tag{1}$$

where ω_ν are the RPA eigen frequencies and e_i denote the mean field (quasiparticle) energies of the Hamiltonian. Since the number of the RPA eigen frequencies might be quite large as, for instance, in heavy nuclei of the order 10^4 and none of the eigen frequencies can be neglected, the calculation of the correlation energy E_{corr} is rather difficult even for separable interactions. We propose to apply the following contour integral representation [1]

$$\frac{1}{2\pi i}\oint dz\, g(z)\,\frac{F'(z)}{F(z)} = \sum_{\nu} g(\omega_{\nu}) - \sum_{i<j} g(e_i + e_j) \tag{2}$$

where $g(z)$ is an arbitrary complex function which is analytical in the enclosed integration region and $F(z)$ is the defining function of the RPA dispersion relation $F(\omega) = 0$ the zeros of which provide the frequencies ω_ν. The correlation energy (1) is obtained by setting $g(z) = z$. The integration formula is also appropriate to calculate other important quantities of the system as, for instance, the level density or the transition densities. The poles of the derivative $F'(z)$ are the two quasiparticle energies $E_\mu \equiv e_i + e_j$ such that the spectral function $\frac{F'(z)}{F(z)}$ has the poles symmetrically around the real x-axis as shown in fig. 1.

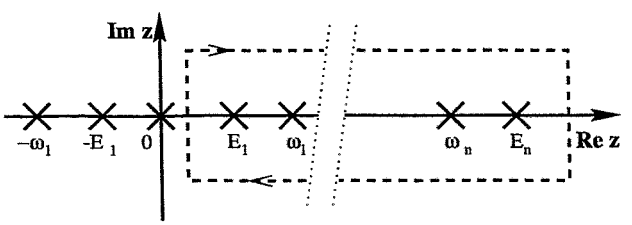

Fig. 1 *A schematic picture of the integration contour (dashed line) in the complex plane. The roots ω_ν and the poles $E_\mu = e_i + e_j$ of the function $F(z)$ are marked with crosses.*

Usually, the integration will be done numerically. The crucial practical advantage of the formula (2) is that we are free to choose the rectangular contour (fig.1) sufficiently distant from the poles such that the spectral function $S(z) = \frac{F'(z)}{F(z)}$ becomes smooth while integrating on this path. Therefore, the necessary grid needs not to be dense for the integration. In practical cases considered so far the integration method turned out to be an extremely effective method for calculating the the RPA correlation energy with the necessary accuracy. The present application concerns the contribution of the pairing vibrations in suprafluid and normal nuclei.

[1] *Joint Institute for Nuclear Research, 141980 Dubna, Russia*

References

[1] F. Dönau, D. Almehed and R.G. Nazmitdinov, Phys. Rev. Lett. **83** (1999) 280

Tilted Axis Cranking with Particle Number Projection [B]

D. Almehed, S. Frauendorf, F. Dönau

The transition of a nucleus from a paired to an unpaired state at high angular momentum is an interesting problem that is studied by means of modern γ-detector arrays. The Tilted Axis Cranking [1] (TAC) model represents the Hartree-Fock-Bogoliubov (HFB) theory of the high-K bands, which permits the calculation of the energies and intra band transition probabilities. The TAC model has been applied to the high-K multi quasiparticle bands in $^{178,179}W$ [2] where the transition from the paired to the unpaired state is found when breaking quasiparticle pairs. The angular momentum was also well reproduced. It is known from investigation at the band heads [3] that the HFB model tends to underestimate the energy distance between the bands. We have used the TAC model in combination with particle number projection to analyze the influence of dynamical pairing correlations in the high-K bands of ^{178}W and their effect on the relative energy, angular momentum and γ-transition ratios. The particle number projection is used together with a static pair field to represent the dynamical pairing correlations which is needed to reproduce the relative energy of the rotational bands. In situations where an unprojected calculation will give totally quenched static pair gap Δ our calculation will give a finite Δ which in this way also accounts for some of the dynamic pair correlation. The calculations show that our model is able to reproduce the experimental [4] values of the relative energy (see fig. 1) as well as angular momentum (see fig. 2) and γ-transition ratios. Our results are also compared with an unpaired calculation ($\Delta = 0$).

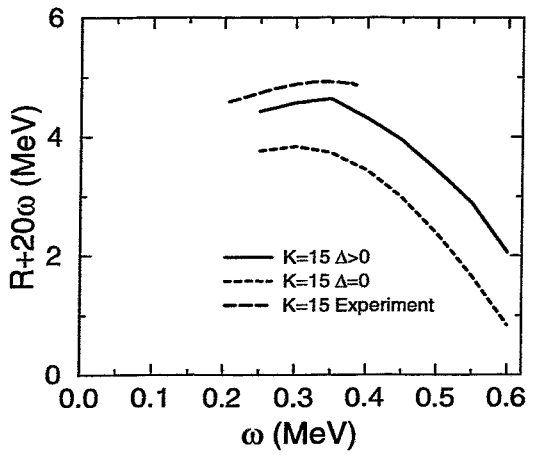

Fig. 1 *The total energy in the rotating frame as a function of the rotational frequency, ω, for the $K^{\pi} = 15^{+}$ band. The experimental values are taken from [4]. A linear term 20ω is added to the energy.*

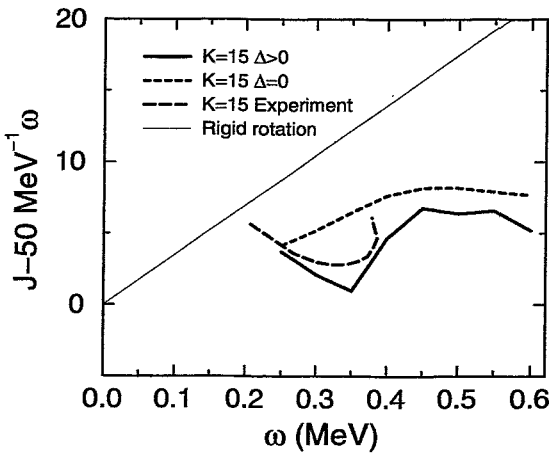

Fig. 2 *The angular momentum as a function of the rotational frequency, ω, for the $K^{\pi} = 15^{+}$ band. The experimental values are taken from [4]. A linear term 50ω is subtracted from the angular momentum.*

References

[1] S. Frauendorf. Nucl. Phys. A 557, 259c (1993)
[2] S. Frauendorf et al., Submitted to Phys. Lett. B
[3] K. Jain et al., Nucl. Phys. A 591, 61 (1995)
[4] C. S. Purry et al., Nucl. Phys. A 632, 229 (1998)

Restoration of Broken Signature Symmetry by Mixing of Mean Field Solutions

F. DÖNAU, JING-YE ZHANG[1] AND L.L. RIEDINGER[1]

The $\Delta I = 1$ staggering effects observed in rotational bands are a consequence of an inherent signature (C2) symmetry of the nuclear wave function against a 180° rotation about the spin direction. This symmetry is naturally broken by the mean field cranking approximation for rotational bands with a non-zero K-value. This is because the nucleus prefers at low rotational frequency in these bands the tilted axis rotation (TAC), i.e. it does not rotate about principal deformation axis. Otherwise, due to the signature symmetry there exist two physically equivalent TAC states which correspond in the potential energy surface to the two symmetry-related degenerate minima with a barrier in between them. The possible tunneling process forth and back between these two minima appears as a typical bifurcation of the rotational band known as signature splitting. We describe this many-body process in which all nucleons participate by diagonalizing an effective nuclear Hamiltonian of the pairing-plus-quadrupole type within a simple set of quasiparticle states. Two of these states have a tilted cranking axis (TAC) and the two other ones correspond to the familiar principal axis rotation (PAC). The practical performance of such a diagonalization is technically ambitious because the PAC and TAC quasiparticle states are complicated many-body states forming in addition a non-orthogonal basis set. The setting up of the Hamiltonian matrix in such a basis and the subsequent calculation of the transition matrix elements were enabled by applying here the tools recently developed [1] in order to derive the overlaps and Hamiltonian kernel for non-orthogonal Hartree-Fock-Bogoliubov (HFB) states. This microscopic approach is able to restore the broken signature symmetry and reproduce the quantum fluctuations between symmetry-related HFB states which emerge as splitting of the band energies and in parallel the staggering in intraband M1 transitions [2]. The beginning of the signature splitting in a K-band can be interpreted as a signal for a smooth transition of the rotational state from the TAC to the PAC regime, the description of which needs to go beyond the selfconsistent mean field approximation.

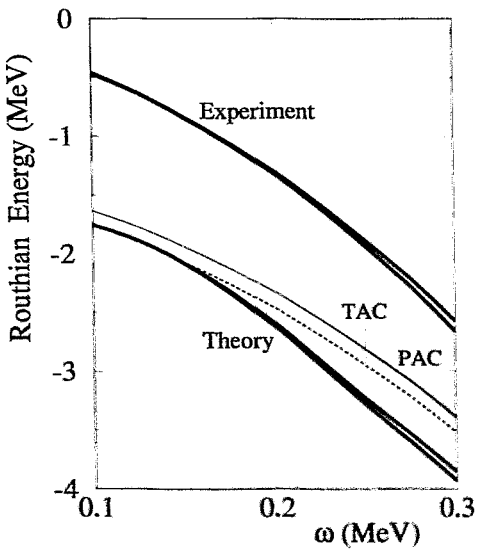

Fig. 1
Calculated and experimental Routhians for the K=7/2 band in ^{175}Hf for frequencies up to 0.3 MeV. In order to be separated from the experimental curve, all the calculated curves have been shifted down as a whole. Among them, thin solid lines are from PAC, dashed ones from TAC and the thick solids from diagonalization.

[1] *Department of Physics and Astronomy, University of Tennessee, TN 37996, USA*

References

[1] F. Dönau, Phys. Rev. **C58** (1998) 872
[2] F. Dönau, Jing-ye Zhang and L.L. Riedinger, Phys. Lett. **B450** (1999) 313

^{73}Br - A World Record in Nuclear Rotational Frequency [B]

H. SCHNARE, R. SCHWENGNER, C. BORCAN, F. DÖNAU, L. KÄUBLER, J. EBERTH[1], T. STEINHARDT[1], O. THELEN[1], M. HAUSMANN[2], A. MÜLLER[2], A. JUNGCLAUS[2], K. P. LIEB[2], D. JENKINS[3], R. WADSWORTH[3], A. WILSON[3], G. DEANGELIS[4], A. GADEA[4], D.R. NAPOLI[4]

Nuclei in the $N \approx Z = 35 - 40$ region display a variety of structural effects. In particular, pronounced angular momentum alignment of a few individual nucleons is characteristic for these neutron deficient isotopes. An experiment was performed at the Laboratori Nazionali di Legnaro to explore these nuclei with the highly-efficient EUROBALL γ-ray spectrometer coupled to the ISIS Si-Ball and the n-Wall for particle identification. High-spin states in the nuclei were populated by a fusion-evaporation reaction of a ^{40}Ca ion beam focussed on a ^{40}Ca target at 185 MeV. A preliminary analysis of the data led to a substantial extension of the previously known level scheme of ^{73}Br [1], with the observation of γ-ray energies greater than 3 MeV (Fig. 1) in three rotational bands (Fig. 2). The γ energy E_γ=3.7 MeV from the top transition in band C corresponds to a rotational frequency of about $\hbar\omega = E_\gamma/2 \approx 1.8$ MeV, which is more than 3 times larger than a typical value in the rare earth region ($\hbar\omega \approx 0.5$ MeV, A=180). A more realistic comparison, considering the different mass regions, is performed by estimating the strength of the Coriolis interaction ($E_c \propto \omega I \propto \omega A^{1/3}$) relative to the shell separation energy ($\Delta E_{sh} \propto A^{-1/3}$). This ratio ($\propto \omega A^{2/3}$) is a factor 2 larger in the case of ^{73}Br compared to the rare earth region. A strong influence of the Coriolis interaction to the single particle motion of the nucleons is expected.

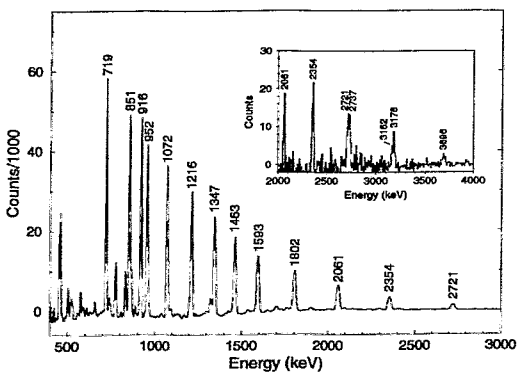

Fig. 1 *Example of a γ-ray spectrum of band C in ^{73}Br, created from a selected sum of $\gamma\gamma\gamma$ coincidence spectra. The inset shows the high energy part of the spectrum, deduced by summing only triple coincidences within the upper members of the band.*

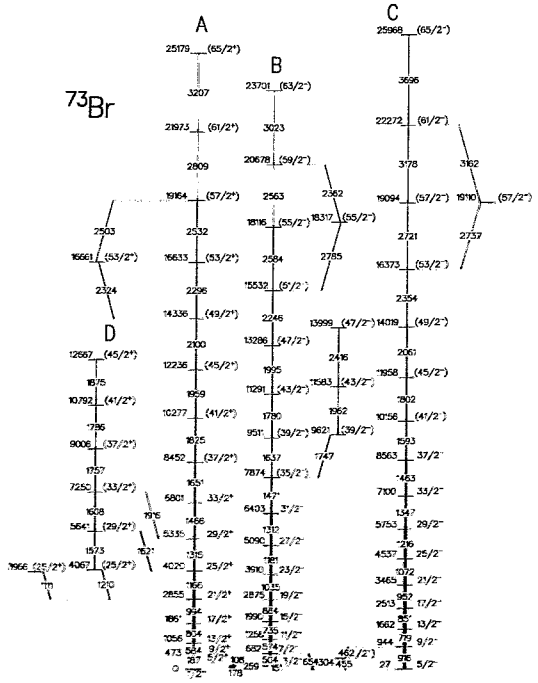

Fig. 2 *Partial level scheme of ^{73}Br*

[1] *IKP, Universität Köln*
[2] *II. Physikalisches Institut, Universität Göttingen*
[3] *University of York, United Kingdom*
[4] *INFN, Legnaro, Italy*

References

[1] J. Heese et al., Phys. Rev. C **36**, 2409 (1987)

Transition Strengths in the N=49 Nucleus ^{87}Sr

C. Borcan, R. Schwengner, H. Schnare, J. Reif, M. Wilhelm[1], A. Fitzler[1], S. Kasemann[1], E. Radermacher[1] and P. von Brentano[1]

In order to understand the nature of the excited states in the N=49 nucleus ^{87}Sr [1] we have continued our study with the determination of level lifetimes using the Doppler shift attenuation method. Mean lifetimes for seven high-spin states have been established. The reduced experimental transition strengths deduced from these lifetimes are given in Table 1.

The experimental states have been interpreted in terms of the shell model, performing the calculations with the RITSSCHIL code [2]. A comparison of experimentally observed levels with predictions of the shell model calculations is shown in Fig. 1. The excitation energies of the experimental states are generally well reproduced by the calculation.

The structure of the positive parity states is mainly determined by the coupling of the proton cluster configuration $((0f_{5/2})(1p_{3/2}))^8_J$, where J has the values $0\hbar$, $2\hbar$ and $4\hbar$ with the two remaining protons in the $g_{9/2}$ orbital, and with one neutron hole in the $g_{9/2}$ orbital. The negative-parity yrast states can be described by the coupling of the $\pi(0g^1_{9/2})\nu(0g^1_{9/2})$ configuration with the remaining 9 protons in the fp shell. The alignment of the protons and neutrons is gradually increasing with the increasing spin, in the $23/2^-$ state they being fully aligned with respect to each other. Experimental and calculated transition strengths are compared in Table 1. The shell model predicts two fast $M1$ transitions between the lowest lying $25/2^+$, $23/2^+$, and $21/2^+$ states. These states have seniority v=5 and are formed by a recoupling of the fully aligned $\pi g^2_{9/2}$ configuration with the protons in the fp subshell and with one neutron hole in the $g_{9/2}$ orbital. This recoupling is the origin of these large $B(M1)$ values.

Table 1 Experimental and calculated transition probabilities in ^{87}Sr, given in Weisskopf units (W.u.)

J^π_i	J^π_f	$\sigma\lambda$	$B(\sigma\lambda)_{\rm EXP}$ (W.u.)	$B(\sigma\lambda)_{\rm SM}$ (W.u.)
$17/2^-_2$	$15/2^-_1$	M1	$0.09^{+0.01}_{-0.01}$	0.08
$23/2^-_1$	$21/2^-_1$	M1	$0.46^{+0.09}_{-0.07}$	0.72
$13/2^+_1$	$9/2^+_1$	E2	$5.4^{+1.6}_{-1.6}$	3.23
$23/2^+_1$	$21/2^+_1$	M1	$0.74^{+0.4}_{-0.2}$	1.06
$25/2^+_1$	$23/2^+_1$	M1	$0.71^{+0.001}_{-0.001}$	1.3
$25/2^+_2$	$23/2^+_1$	M1	$0.024^{+0.0002}_{-0.0001}$	0.015
$25/2^+_2$	$23/2^-_1$	E1	$(5.2^{+5.0}_{-4.6})\times10^{-6}$	
$27/2^+_1$	$25/2^+_1$	M1	$0.01^{+0.08}_{-0.01}$	0.16

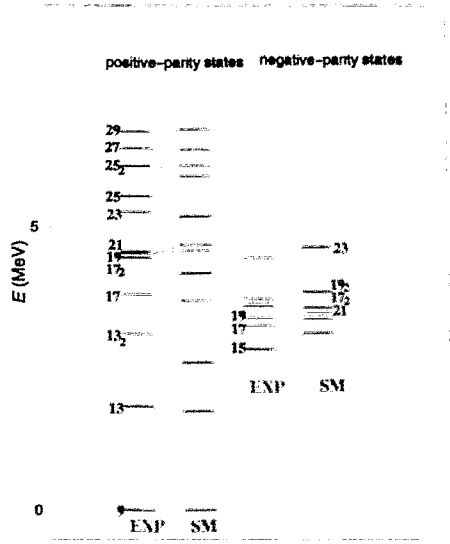

Fig. 1 *Comparison of experimental (EXP) and calculated level energies (SM) for states in ^{87}Sr. Spins are given in units of $1/2\hbar$.*

[1] *Institut für Kernphysik der Universität zu Köln*

References

[1] C. Borcan et al., Annual Report 1997, FZR-215, (1997) 52
[2] D. Zwarts, Comput. Phys. Commun. 38, (1985) 365

High Spin States in the odd-odd ^{72}Br Nucleus

C. Borcan, H. Schnare, R. Schwengner, F. Dönau, L. Käubler, J. Eberth[1], T. Steinhardt[1], O. Thelen[1], M. Hausmann[2], A. Müller[2], A. Jungclaus[2], K. P. Lieb[2], D. Jenkins[3], R. Wadsworth[3], A. Wilson[3], G. de Angelis[4], A. Gadea[4], D.R. Napoli[4], A. Algora[4], S. Lenzi[4]

The odd-odd nuclei in the A = 80 region offer a good opportunity to study the interaction between the unpaired neutron and proton, and the coupling of these quasi-particles with the quadrupole deformed core. The analysis of these nuclei is in general difficult since the nuclear excitations modes depend critically on the proton and neutron numbers and on their specific quasiparticle orbitals involved.

Odd-odd bromine isotopes display complicated low-lying structures, often isomeric, and high-spin rotational bands, built on these isomeric states.

The ^{72}Br nucleus has been studied before in [3]. The present study is based on the analysis of the EUROBALL experiment described in [4] and results in the level scheme presented in Fig. 1. The previously known three rotational bands were extended, reaching the excitation energy of about 13 MeV, and the unfavoured signature-partner of the positive-parity band was identified.

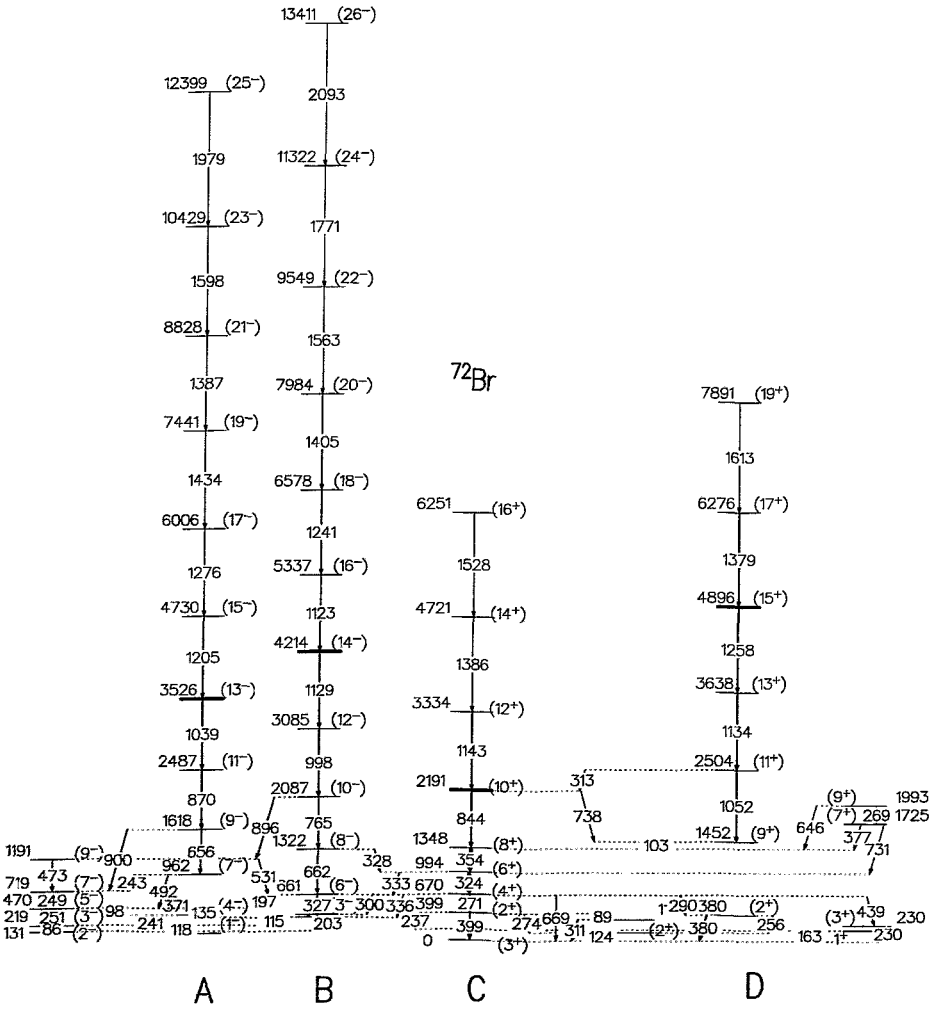

Fig. 1 *The level scheme deduced from the present experiment. The new transitions are figured above the levels having a thicker line.*

The structure at low spins is generated by the single particle excitations of the unpaired proton and neutron, respectively, whilst at higher spins rotational pattern dominates. The same feature is observed in the ^{76}Br nucleus, where the band built on 4^+ isomer shows an irregular pattern at low spins, whereas above spin 9^+ it emerges as a more regular rotational band [1]. This band has been interpreted as a good example for a doubly-blocked $g_{9/2}$ band [2].

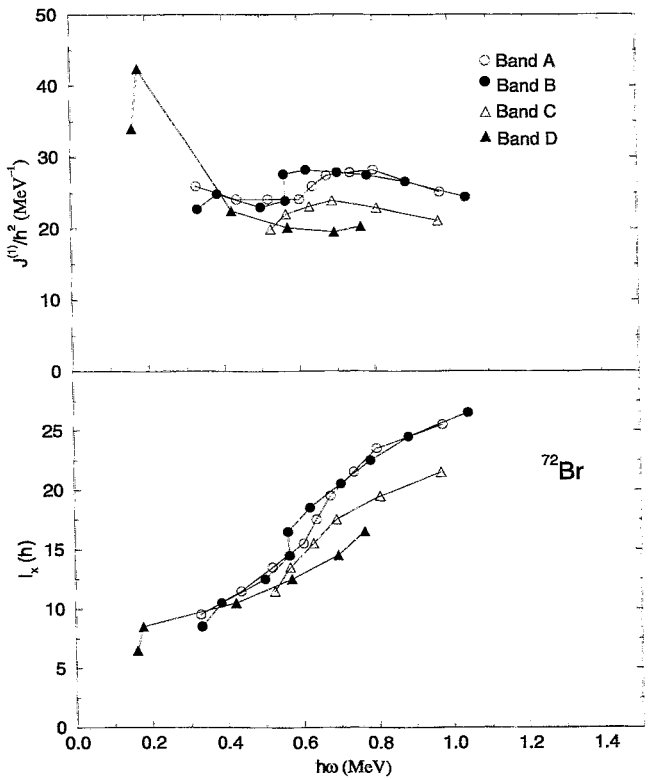

Fig. 2 *Kinematical moment of inertia $J^{(1)}$ (top) and aligned angular momentum I_x (bottom) for the positive and negative parity bands in ^{72}Br as a function of rotational frequency.*

The behaviour of the kinematical moment of inertia for the observed bands in ^{72}Br is shown in Fig. 2. For the positive-parity bands it remains fairly constant at a value which is close to that of rigid rotation for this nucleus (19.3 $\hbar^2 MeV^{-1}$ (Fig. 2-top), and is very similar to that of the positive parity bands in ^{76}Br [2]. This phenomenon of rigid rotation can be discussed in terms of the blocking effect for the $g_{9/2}$ orbitals.

The aligned angular momentum versus rotational frequency is presented in Fig. 2-bottom. For both negative-parity bands an upslope of the angular momentum is occuring at 0.6 MeV frequency, which signals a gradual alignment indicating a change in configuration. This change can be understood in terms of the cranking model with a break-up of a pair of neutrons. The axial deformation is found constant of β=0.3 within this negative-parity bands. The interpretation of the data is in progress.

[1] *IKP, Universität Köln*
[2] *Physikalisches Institut, Universität Göttingen*
[3] *University of York, United Kingdom*
[4] *INFN, Legnaro, Italy*

References

[1] J. Döring et al., Z. Phys. A 305 (1982) 362
[2] S. G. Buccino et al., Phys. Rev. C 41 (1990) 2056
[3] S. Ulbig et al., Z. Phys. A 329 (1988) 51
[4] H. Schnare et al., contribution to this report.

First Experiments with the Rossendorf Si-Ball RoSiB [B]

H. Schnare, R. Schwengner, L. Käubler, C. Borcan, F. Dönau, H.-G. Ortlepp, G. Pausch, H. Prade, H. Grawe[1], J. Eberth[2], S. Skoda[2], T. Steinhardt[2], T. Härtlein[3], F. Köck[3], D. Pansegrau[3], D. Schwalm[3], M. Moszynski[4], D. Wolski[4], A. Axelsson[5], M. Weiszflog[5], R. Wadsworth[6], A. Wilson[6], A. Gadea[7], D.R. Napoli[7],

RoSiB is a 4π Silicon ball consisting of $N = 42$ detector elements [1]. It is designed for the detection of light charged particles inside modern 4π γ-ray spectrometers (e.g. EUROBALL) and exploits the pulse shape discrimination technique for particle identification [2]. Two experiments have been performed at the MP tandem acccelerator of the MPI Heidelberg, using the fusion evaporation reactions ^{58}Ni (220 MeV) + ^{46}Ti and ^{16}O (95 MeV) + ^{58}Ni. The setup consisted of the Rossendorf Cluster detector, three individual HPGe detectors, the Si-Ball RoSiB and a reduced version of the EUROBALL neutron wall [3]. Fig. 1 shows a 2D-plot of zero-crossing time versus energy deposition for one Si-detector. By defining gates in such matrices different exit channels of the fusion evaporation reaction are selected as illustrated in Fig. 2.

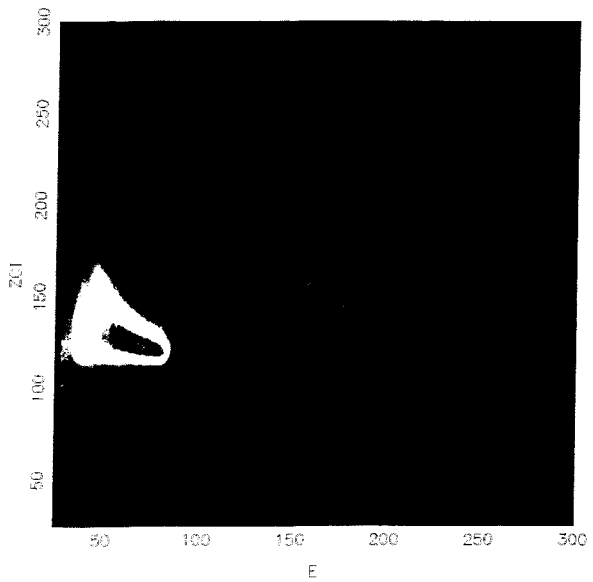

Fig. 1 *Color image of the matrix zero-crossing time (ZCT) versus energy deposition (E) for a Si-detector of RoSiB in forward direction, showing the particle discrimination between protons and alphas. The data has been taken in the reaction ^{16}O + ^{58}Ni at 95 MeV.*

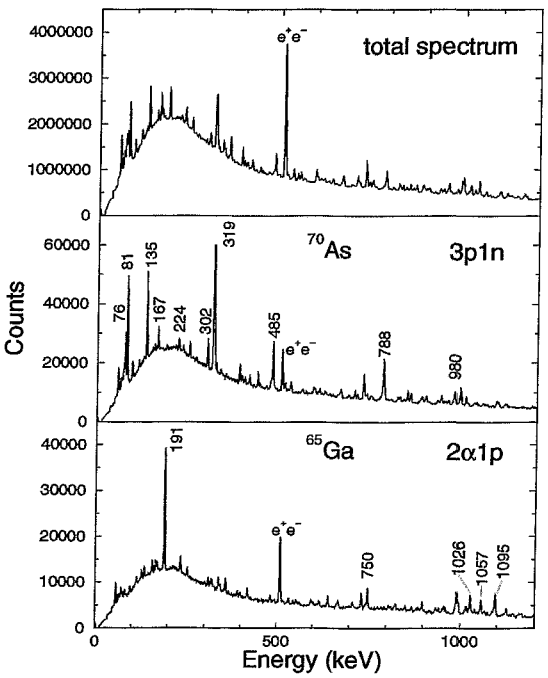

Fig. 2 *Comparison between the total γ-spectrum (top) and particle-gated γ-ray spectra from the reaction ^{16}O + ^{58}Ni at 95 MeV. γ-lines of selected nuclei are labeled by their energies.*

[1] *GSI Darmstadt*
[2] *IKP, Universität Köln*
[3] *MPI Heidelberg*
[4] *Soltan Institute for Nuclear Studies, Swierk, Poland*
[5] *University of Uppsala, Sweden*
[6] *University of York, United Kingdom*
[7] *INFN, Legnaro, Italy*

References

[1] G. Pausch et al., EuroSiB Project description, Rossendorf, 1996
[2] G. Pausch et al., Nucl. Instr. and Meth. A349 (1994) 281
[3] Ö. Skeppstedt et al., Nucl. Inst. and Meth. A421 (1999) 531

Is the 4.742 MeV state in ^{88}Sr really the two-phonon $(2_1^+ \otimes 3_1^-)$ state? [B,D,H]

L. KÄUBLER, H. PRADE, H. SCHNARE, R. SCHWENGNER, M. GRINBERG[3], F. DÖNAU, E. GROSSE, P. v. BRENTANO[1], J. EBERTH[1], J. ENDERS[2], A. FITZLER[1], C. FRANSEN[1], R.-D. HERZBERG[1], H. KAISER[2], P. v. NEUMANN-COSEL[2], N. PIETRALLA[1], A. RICHTER[2], CH. STOYANOV[3], H.-G. THOMAS[1], H. TIESLER[1], D. WEISSHAAR[1], I. WIEDENHÖVER[1] AND A. ZILGES[2]

In even-mass semimagic nuclei with N=82 or Z=50 two-phonon states with J^π=1$^-$ have been observed [1], formed by the coupling of the first quadrupole and octupole phonons $(2_1^+ \otimes 3_1^-)$. It is a longstanding question whether such states can be found also in the semimagic N=50 nuclei [2]. In ^{88}Sr a J=1 state at 4.742 MeV has been observed in a nuclear resonance fluorescence experiment [3]. The parity of this level was not confirmed experimentally. Nevertheless, it is considered to be the 1$^-$ two-phonon state [3]. Therefore, a (γ,γ') experiment on ^{88}Sr has been performed [4] with an electron energy of 6.8 MeV at the S-DALINAC accelerator using two EUROBALL CLUSTER detectors placed at 90° and 127° to the photon beam, where the 90° CLUSTER was used as a Compton polarimeter for the measurement of the γ-ray linear polarisation as described in [5]. Gamma-rays Compton scattered into a direction of 90° with respect to the reaction plane have been sorted into a 90° spectrum, events scattered by 30° or 150° into a 30°+150° spectrum. The asymmetry $A=(I_{90°} - aI_{30°+150°})/(I_{90°} + aI_{30°+150°})$ has been calculated using the fitted intensities I of γ-ray lines of a given energy in the 90° or 30°+150° spectra, respectively. For the normalization factor the theoretical value a=0.5 has been used. The positive A value for the 4.742 MeV transition in ^{88}Sr (Fig. 1) gives together with J=1 [3] very likely multipolarity $M1$, i.e. positive parity for the 4.742 MeV state, in contrast to the hitherto existing assumption of an 1$^-$ two-phonon state [2,3]. Therefore, the existence of such two-phonon states in N=50 nuclei remains an open question. The comparison with quasiparticle-phonon calculations suggests the second 1$^+$ state to be a two phonon state with the structure $(1_1^+ \otimes 2_1^+)$. It is a challenge for the nuclear structure theory to explain the structure of such low-lying $M1$ excitations as the observed J^π=1$^+$ state in ^{88}Sr at 4.742 MeV.

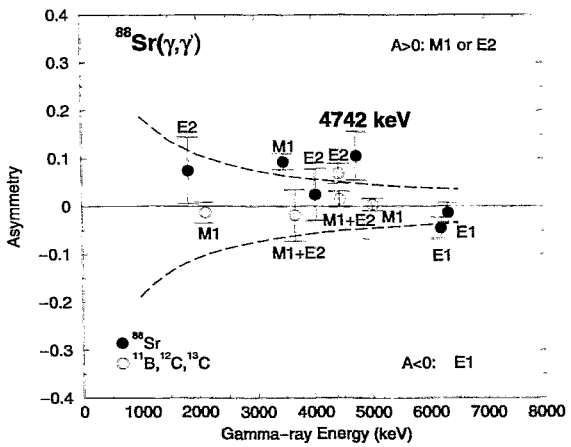

Fig. 1 *Asymmetry A as explained in the text. Transitions with known multipolarities are denoted by σL. The 2.124, 4.444 and 5.019 MeV transitions in ^{11}B are known to be nearly isotropic. The dashed lines represent asymmetry values obtained by means of experimentally calibrated polarisation sensitivity values for the CLUSTER detector.*

[1] *Institut für Kernphysik, Universität zu Köln, D-50937 Köln*
[2] *Institut für Kernphysik, TU Darmstadt, D-64289 Darmstadt*
[3] *Institute of Nuclear Research and Nuclear Energy, Sofia, BG-1784 Sofia*

References

[1] U. Kneissl et al., Prog. Part. Nucl. Phys. 37 (1996) 349
[2] J. Reif et al., Nucl. Phys. A 620 (1997) 1
[3] F. R. Metzger, Phys. Rev. C11 (1975) 2085
[4] L. Käubler et al., Annual report 1997, FZR-219 (1998) 53
[5] D. Weisshaar, Internal Report Inst. f. Kernphysik, Univeristät zu Köln 1996

β Decay of Proton-rich Nuclei near the Doubly Magic ^{56}Ni

A. JOKINEN[1], J. ÄYSTÖ[1], R. BORCEA[2], P. DENDOOVEN[2], M. GIERLIK[3], M. GÓRSKA[2], H. GRAWE[2], M. HELLSTRÖM[4], M. KARNY[3], Z. JANAS[3], R. KIRCHNER[2], M. LA COMMARA[2], P. MAYET[2], A. NIEMINEN[1], H. PENTILLÄ[1], A. PŁOCHOCKI[3], M. REJMUND[2], E. ROECKL[2], M. SAWICKA[3],, C. SCHLEGEL[2], K. SCHMIDT[2], R. SCHWENGNER, F. DÖNAU AND W. SCHULZE

Nuclei with $N \approx Z$ are interesting for the study of the neutron-proton pairing interaction that is expected to be enhanced if neutrons and protons occupy the same orbitals. Moreover, if the particle numbers are near shell closures, these nuclei are of particular interest for tests of nuclear model predictions, since the few nucleons outside the closed shells form relatively simple configurations. These proton-rich nuclei are close to the proton drip line and can hardly be populated in fusion-evaporation reactions. Therefore, decay spectroscopy is often the only way to obtain experimental information on excited states in these nuclei.

We have investigated the β decay of the proton-rich nuclei ^{56}Cu ($T_z = -1$), ^{57}Zn ($T_z = -3/2$) and ^{61}Ga ($T_z = -1/2$) which are near the doubly magic nucleus ^{56}Ni. Radioactive samples of these nuclides were produced at the GSI On-line Mass Separator via the reactions ^{28}Si(^{32}S,$xpyn$) and ^{28}Si(^{36}Ar,$xpyn$). β-delayed protons were measured with a telescope consisting of a ΔE gas detector and an E silicon detector. β-delayed γ rays were detected with the Rossendorf Cluster detector and the GSI Segmented-Clover detector.

The statistics of the data collected for ^{56}Cu and ^{61}Ga has been increased by two orders of magnitude with respect to previous work [1,2]. This will allow us to search for additional β population of daughter levels beyond those observed so far. In addition, more accurate and complete experimental strength distributions for Fermi and Gamov-Teller transitions may be deduced, which are the prerequisites for a stringent test of shell-model predictions.

Experimental data on the decay of ^{57}Zn have previously been obtained from a He-jet measurement [3]. The analysis of the spectrum of β-delayed protons measured in the present experiment reveals a better source purity and a better energy resolution compared with the previous work. This enables us to assign new proton transitions from ^{57}Cu to ^{56}Ni. The analysis of the β-delayed γ-ray spectra is in progress.

The present experiment has shown that heavy-ion induced fusion-evaporation reactions combined with on-line mass separation and efficient detectors for measuring β-delayed protons and γ rays represent a valuable tool to investigate very proton-rich nuclei.

Therefore, we will propose to perform such experiments at the GSI On-line Mass Separator to obtain information on the structure of doubly odd $N = Z$ nuclei in the mass range around $A \approx 70$. Moreover, it is planned to complement these investigations with experiments at the GSI fragment separator.

[1] *University of Jyväskylä*
[2] *GSI Darmstadt*
[3] *Warsaw University*
[4] *Lund University*

References

[1] M. Ramdhane et al., Phys. Lett. B 432 (1998) 22
[2] M. Oinonen et al., Eur. Phys. J. A, in print
[3] D.J. Vieira et al., Phys. Lett. B 60 (76) 261

Sharing of Excitation Energy between Fission Fragments [B]

D.V. KAMANIN[1], V.S. SALAMATIN[1], W. WAGNER, H. FREIESLEBEN[2]

The investigation of excitation energy sharing between fission fragments and probing the time scale of asymmetric binary fission is usually performed by means of a multiplicity analysis of neutrons and light charged particles emitted. The multi-source fit, however, has a number of limitations due to experimental conditions and requires some model assumptions. Utilizing the advantages of the FOBOS 4π-spectrometer [1], a model independent method for this purpose is proposed [2].

The asymmetry of the mass splitting in fission can be appropriately quantified by the parameter $\chi_t = (\beta_t - 1)/(\beta_t + 1)$, where β is the mass ratio of the fission fragments. The index t denotes either the secondary masses measured ("sec") or the primary mass ratio calculated from the fragment velocities ("prim"). By this definition, the parameter χ_{prim} reflects the mass asymmetry at the scission point, and χ_{sec} describes the mass asymmetry after emission of post-scission light particles. On the average, the equilibrium sharing of excitation energy of the fissioning system between the fragments leads to the conservation of the asymmetry ($\chi_{prim} \approx \chi_{sec}$). The parameter $\bar{\zeta}$ defined by $\bar{\zeta} = \beta_{sec}/\beta_{prim}$ is, therefore, close to unity only in the case of thermodynamical equilibrium. It can be shown that $\bar{\zeta} \approx (1 - \nu_1\epsilon_1^*)/(1 - \nu_2\epsilon_2^*)$, where the indices denote the two fission fragments. ϵ_i^* is the excitation energy per nucleon, and ν_i is the average multiplicity of particles per 1 MeV of excitation energy.

The degree of equilibration should be related to the time passed until scission. Indeed, two structures are observed in the mass-asymmetry matrix (Fig. 1). The bump near the equilibrium value $\bar{\zeta} = 1$ for the most mass-symmetric decays relates, obviously, to ordinary fission. The average value of $\bar{\zeta}$ deviates from the equilibrium value with increasing mass asymmetry. A second structure is represented by the peak $\bar{\zeta} \approx 1.8$ at a large asymmetry. It is ascribed to PLF-TLF formation in peripheral collisions, which is known to be much faster than ordinary fission. We defined the excitation energy sharing parameter $\zeta = (\bar{\zeta} - 1)/(\bar{\zeta} + 1)$. Applying the Fermi-gas law $E^* = aT^2$, one roughly gets $\zeta \sim T_2^2 - T_1^2$ for nearly symmetric splitting and moderate temperatures. This relation qualitatively holds also for large asymmetries. Selecting $\chi_{prim} > 0$, a positive value of ζ then means a higher temperature of the lighter fragment. Such a sharing of the excitation energy has been concluded [3] to be essential for PLF-TLF formation. Since similar results have been obtained also for other reactions, the proposed ζ-parameterization turned out to be an effective tool for separating of reaction channels proceeding on different time scales by applying multi-dimensional analyses [2].

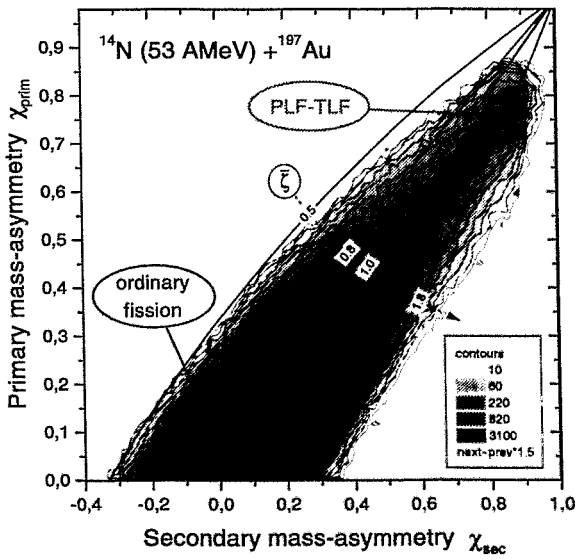

Fig. 1 *The ζ-parameterization of the mass asymmetry matrix (PLF: projectile-like fragments, TLF: target-like fragments).*

[1] *Joint Institute for Nuclear Research Dubna, Russia* [2] *Technical University Dresden, Germany*

References

[1] H.-G. Ortlepp *et al.*, "4π spectrometer FOBOS", Nucl. Instr. and Meth. A 403 (1998) 65.
[2] D.V. Kamanin "Probing the time scale of asymmetric fission", PhD thesis, TU-Dresden, 1999.
[3] G.G. Adamian *et al.*, Physical Review C 53 (1996) 871.

Separation of Different Binary Reaction Channels in Heavy-Ion Collisions [B]

D.V. KAMANIN[1], W. WAGNER, H. FREIESLEBEN[2] AND THE FOBOS COLLABORATION

Heavy-ion induced reactions in the Fermi energy domain are governed by a complicated interplay of different processes. The 4π spectrometer FOBOS [1] is designed especially for the study of fission of highly excited nuclei. Although ordinary fission remains to be a dominating decay mode, evidence has been found for another decay process of heavy composite systems coming into play at high excitation energy. Since this process feeds more asymmetric disintegrations and is supposed to be faster than fission it was called "binary fragmentation" (BF) [2].
The mass of the composite system prior to scission reflects the amount of excitation energy removed from the system by intense light particle emission. Furthermore, the deviation of the excitation energy partition from thermodynamical equilibrium should hint at a faster time scale relative to a decay proceeding after relaxation of initial mass asymmetry or after formation of a compound nucleus [3]. Such non-conventional analysis [4] revealed domains of different processes which significantly differ in excitation energy sharing directorized by the parameter ζ and in mass asymmetry (Fig. 1). The variation of the average ζ with χ_{prim} reflects the contributions of these processes. The parameter matrix for the reaction Ar+Ag (left panel) can be used as a qualitative reference for a short time scale since the contribution of fission is very small. Emission of a PLF as the fastest and most asymmetric process is represented by positive values of ζ, meaning that the temperature of the lighter fragment is higher than that of the heavier one. The ordinary fission of Th-like nuclei (right panel) can be used as an etalon for a slow process. The BF is significantly slower than PLF emission but faster than fission, the most probable temperature of the lighter fragment is lower ($\zeta < 0$). Ordinary fission definitely dominates among most symmetric decays, and it is represented by equilibrated excitation energy sharing.

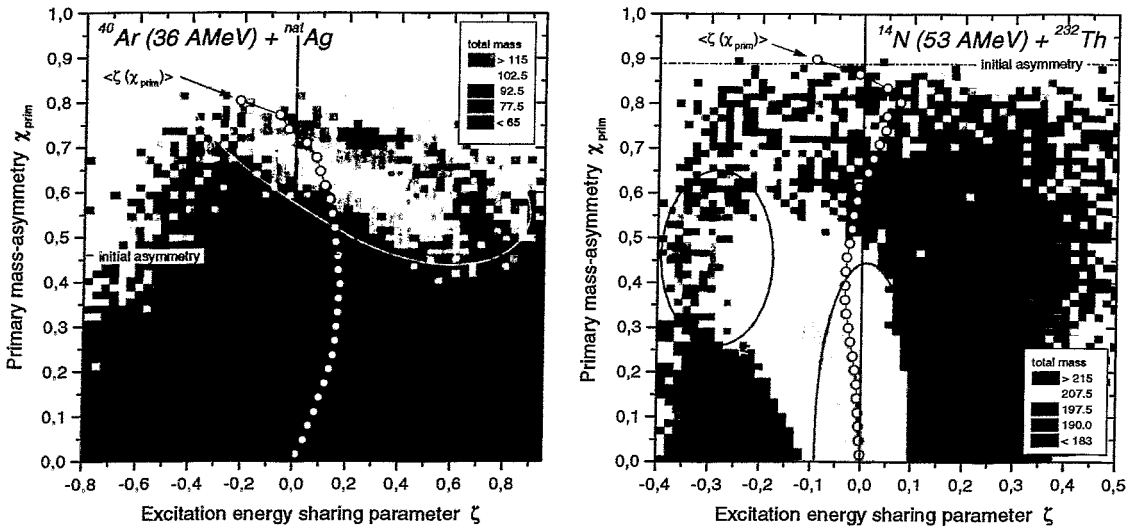

Fig. 1 *Plots of the average total mass of binary reaction products in the ζ-χ-plane. Open circles represent the dependence of the average ζ on χ_{prim}.*

[1] *Joint Institute for Nuclear Research Dubna, Russia* [2] *Technical University Dresden, Germany*

References

[1] H.-G. Ortlepp *et al.*, "4π spectrometer FOBOS", Nucl. Instr. and Meth. A 403 (1998) 65.
[2] W. Wagner and H.-G. Ortlepp, FLNR Sci. Rep. 1995/96, JINR E7-97-206, Dubna 1997, p.243.
[3] D.V. Kamanin "Probing the time scale of asymmetric fission", PhD thesis, TU-Dresden, 1999.
[4] D.V. Kamanin *et al.*, Contribution to this report.

Magnetic Susceptibility of Superconducting Al-Clusters [W]

S. Frauendorf[1], N.K. Kuzmenko [2] and V.M. Mikhajlov[2]

The pair-correlations of Al-clusters in a magnetic field are investigated assuming that the electrons are moving in a spherical potential. In small clusters with less than 1000 atoms the distance between the electronic levels is larger than the pairing gap Δ [1]. This restricts the pair correlations to the degenerate Fermi level. The solution of the Hartree-Fock-Bogolyubov problem becomes possible using nuclear many body methods. It is crucial to use the *canonical* ensemble, i. e. to fix the number of electrons. New features as temperature induced pair-correlation for a magnetic field larger than the critical field of the bulk material (see fig. 1) and oscillations of the susceptibility (see fig. 2) are predicted.

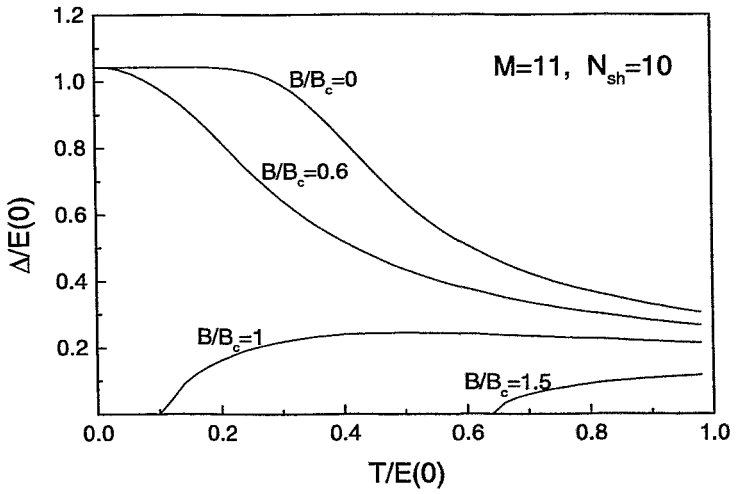

Fig. 1 *The gap parameter of an Al-cluster of about 300 atoms as function of the temperature T (in units of the of the gap in the cluster) for different values of the magnetic field (in units of the critical field of bulk Al)*

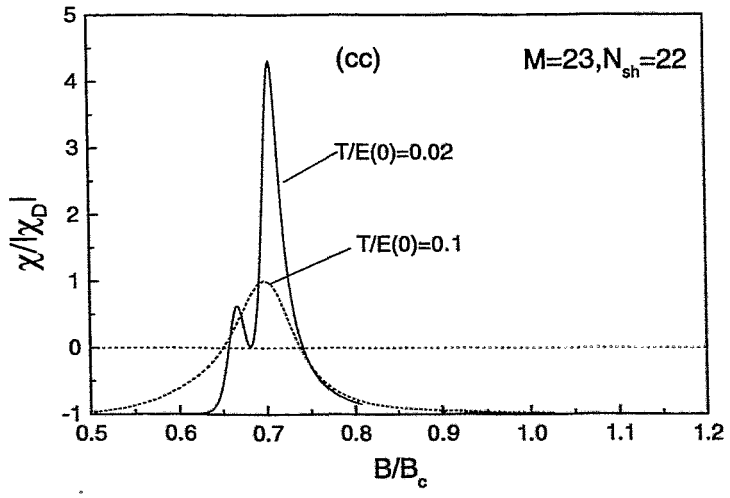

Fig. 2 *The magnetic susceptibility of an Al-cluster of about 3000 atoms as function of the magnetic field (in units of the critical field of bulk Al) for different values of the temperature T (in units of the of the gap in the cluster)*

[1] *on leave of absence at Department of Physics, University of Notre Dame, IN 46556, USA*

[2] *V.G. Khlopin Radium Institute, 194021, St.-Petersburg, Russia*

References

[1] S. Frauendorf, N.K. Kuzmenko and V.M. Mikhajlov , J. of Cluster Science, in print

Biomedical Research

The impact of nuclear physics to biomedicine is traditionally intensive in the fields of radiooncology and radiation biology. The biomedically relevant activities of the institute are devoted to these two topics: on the one hand the contribution to radiooncology is the application of positron emission tomography (PET) to the quality assurance of carbon ion therapy, which has become reality in a clinical form at the experimental heavy ion therapy installation at GSI Darmstadt, and, on the other hand, the use of secondary X-rays produced by means of the ELBE beam for radiobiological experiments with cells, which is still a vision.

The heavy ion cancer therapy facility at GSI Darmstadt, which has been installed in collaboration between the GSI Darmstadt, the University Hospital Heidelberg, the DKFZ Heidelberg and the FZ Rossendorf was set into operation in December 1997 and started continuous patient treatments in August 1998. Up to now 48 patients have been treated with carbon ions, 45 of these treatments were monitored by means of PET, i.e. more than 1000 PET-measurements have been performed during the fractionated irradiations. The main result is a modification of the ^{12}C stopping-power parameterization, which further improved the precision of the dose localization. On the basis of the experience obtained during the clinical application the PET method is further improved with respect to data evaluation methods, the tomographic reconstruction and the biokinetic modelling of the metabolic behaviour of β^+-active fragments in tissue. Furthermore, the first steps on transferring the know-how to a large clinical heavy ion therapy facility that is planned to be built in Heidelberg have been done.

To install a facility for cell irradiations with quasi-monochromatic X-rays at ELBE, it has been shown that channeling of electrons in crystals may provide a sufficiently high dose rate for measuring energy dependent relative biological effectivenesses in an X-ray energy range between 10 and 100 keV. Thus the development of an irradiation device at the ELBE radiation physics beamline has been initiated and a collaboration has been formed for that type of research: it includes the Klinik für Strahlentherapie und Radioonkologie and the Institut für Strahlenschutzphysik of the TU Dresden.

Collaborations

Heavy Ion Tumour Therapy:
- *GSI Darmstadt*
- *Radiologische Klinik of the University Heidelberg*
- *Deutsches Krebsforschungszentrum Heidelberg*
- *Institute of Bioanorganic and Radiopharmaceutical Chemistry (FZ Rossendorf)*
- *NIRS Chiba (Japan)*
- *SINS Swierk (Poland)*

Cell Radiobiology at ELBE:
- *Klinik für Strahlentherapie und Radioonkologie. - Klinik für Nuklearmedizin. - and Institut für Strahlenschutzphysik of the TU Dresden*

The Routine PET Monitoring of Tumour Therapy with ^{12}C Ions [B]

W. Enghardt, J. Debus[1], T. Haberer[2], B.G. Hasch, R. Hinz, O. Jäkel[1], M. Krämer[2], K. Lauckner, J. Pawelke, F. Pönisch

Until September 1999 48 patients mainly suffering from tumours of the head and neck region have been treated with ^{12}C at GSI Darmstadt. Each irradiation has been monitored by means of the in-beam PET scanner BASTEI, because of the close vicinity of organs at risk (optical nerves, brain stem) to the target volume. Thus, 1215 PET-scans have been taken. In order to evaluate the dose localisation, the β^+-activity distributions reconstructed from measured annihilation data are compared with those that have been calculated by means of our Monte Carlo code from the treatment plan. This revealed a high long term stability of the fractionated irradiations and a remarkable reliability of the patient positioning procedure (Fig. 1). However, it shows furthermore deviations between the measured and predicted β^+-activity distributions (Fig. 2). The reasons for such deviations are of different origin: A systematic evaluation of the PET images revealed a range excess of the ^{12}C ions (Fig. 2) indicating a lack of accuracy in the correlation between the Hounsfield units measured by means of X-ray computed tomography and the heavy ion ranges in tissue, which is the basis of heavy ion treatment planning [1]. Range measurements outlined in [1] improved this correlation and a better correspondence has been

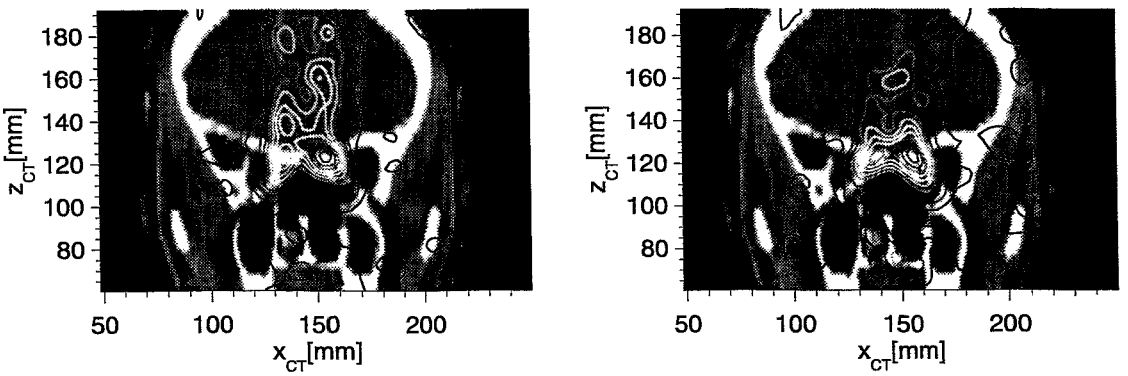

Fig. 1 *Comparison of the β^+-activity distributions reconstructed from simulated (left) and measured (right) PET data. The carbon ions enter the patient's head from cranial. The radiological depth of the target volume is large, however, the penetrated tissue is rather homogeneous. There is a remarkable correspondence between simulation and measurement. The β^+-activity distributions are superimposed onto X-ray computed tomograms as contour plots (levels: 5, 15, ... , 95 % of the maximum activity).*

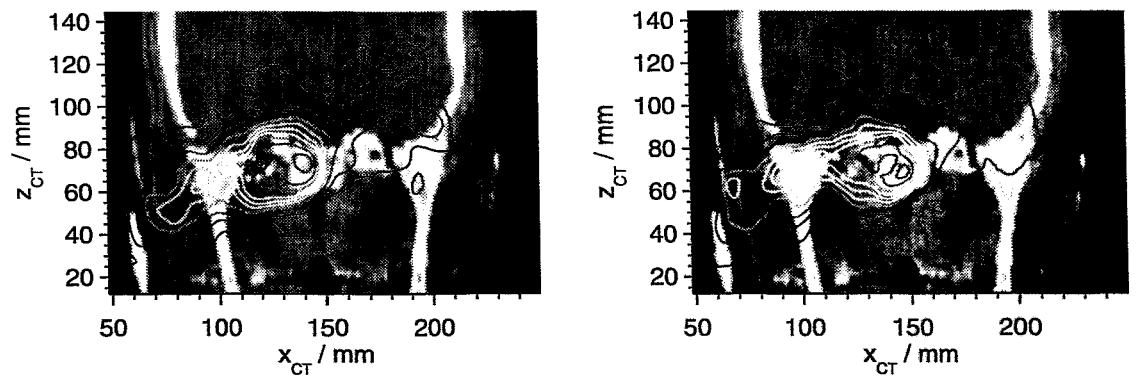

Fig. 2 *As Fig. 1, but for an irradiation where the beam enters the patient's head from the right hand side (left on the picture) and has to penetrate highly inhomogeneous tissue. A considerable difference in the position of the distal edge of the simulated and measured activity distribution was found before the correlation between Hounsfield numbers and ion ranges has been modified.*

[1] *Deutsches Krebsforschungszentrum Heidelberg,* [2] *Gesellschaft für Schwerionenforschung Darmstadt*

achieved between the β^+-activity distributions predicted from the treatment planning and those measured during the therapeutic irradiations (Fig. 3). However, further deviations have been observed by means of PET, which are due to the peculiarities of the stopping process of heavy charged particles in matter, especially to the well defined particle range. Although patient repositioning errors are minimized by means of a stereotactic system and radiographic verification, in cases, where the ^{12}C ions penetrate highly inhomogeneous tissue regions, local fluctuations have been seen at the distal edge of the β^+-activity distribution indicating ion range fluctuations of several millimeters. Furthermore, the condition of the patient may change during the 20 days of fractionated irradiations. This may modify the density distribution within the target volume and, therefore, seriously influence the dose distribution (Fig. 4).

In summary: The PET monitoring of heavy ion therapy essentially contributed to the improvement of the precision of dose localisation by initiating the modification of the treatment planning data base. Furthermore, it provides insight for the peculiarities of the dose delivery by heavy ion beams, where, in contradiction to conventional radiotherapy with photons, minor changes in patient positioning or in the patient's physical condition may cause unavoidable deviations between the planned and the applied dose distributions. These results will feedback to the treatment planning methodology and to the definition of future indications for heavy ion therapy.

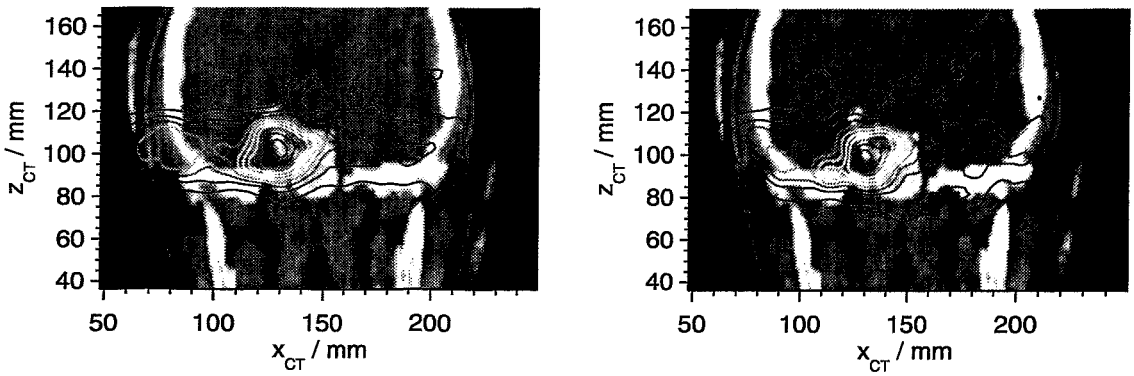

Fig. 3 *As Fig. 1, but for a patient with a similar tumour localisation as that of Fig. 2 after improving the Hounsfield-range correlation.*

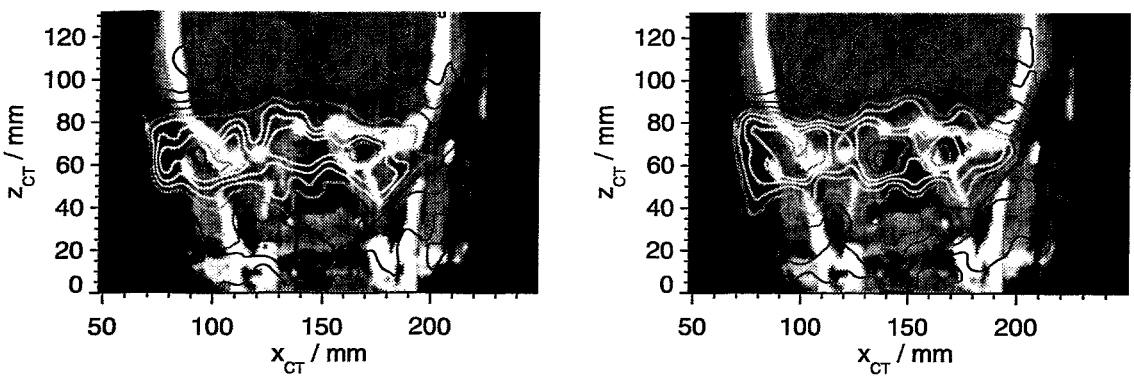

Fig. 4 *The influence of the physical condition of the patient on the maximum particle range. Left: In positron emission tomograms taken for an irradiation field coming from the right hand side of the patient at day 7 of the treatment with 20 fractions in total an unusual high activity concentration in the cavity at $x_{CT} \approx 170$ mm, $z_{CT} \approx 70$ mm, and a correspondingly reduced β^+-activity concentration at $x_{CT} > 180$ mm indicating a reduction of the particle range by ≈ 10 mm was noticed. An magnetic resonance tomogram taken immediately after the irradiation revealed that the cavity was filled with mucus. Right: The normal situation (e.g. at day 11).*

References

[1] O.B. Geiß et al., GSI Scientific Report 1998, GSI 99-1 (1999) 133

The Evaluation of PET-Images obtained during ^{12}C Radiotherapy [B]

F. PÖNISCH, W. ENGHARDT, R. HINZ, O. JÄKEL[1], K. LAUCKNER

The routine monitoring of the radiotherapeutic treatment with ^{12}C ions by means of positron emission tomography (PET) was performed at the GSI in Darmstadt in 1998 for 17 patients [1]. In order to make qualitative statements about the precision of the irradiation for each fraction a comparison of the measured and simulated PET images is required. Therefore the PET images have to be mapped onto the anatomical structures given by X-ray computed tomograms (CT). Since the data are available in different coordinate systems, a transformation of the PET images into the CT coordinate system is necessary. The transformation matrix is generated by multiplying several 4x4 transformation matrices describing the rotation, translation and reflection of the coordinates. The activity value for the resulting position vector is obtained by trilinear interpolation. A C programme executes this transformation and stores the PET data in the CT data format, which consists of a header and a data file. The algorithm and the code have been verified experimentally: A lucite phantom (23 x 15 x 0.5) cm^3 with grooves of 2 mm width and 2 mm depth was imaged by CT. PET data were measured with Cu rods of 0.6 diameter activated in the reactor (leading to the β^+-emitter ^{64}Cu) centered in the grooves. A mapping of the PET data onto the X-ray CT is displayed in Fig. 1. X_{CT} and Z_{CT} are the spatial coordinates in the CT frame. The data processing following the coordinate transform can be performed either by means of the graphics and evaluation tools of the radiotherapy planning programme VIRTUOS [2] or in a more detailed way using our code VIEW_PCT running under IDL. VIEW_PCT (Fig. 2) is capable of displaying β^+-activity as well as dose distributions as coloured contour plots superimposed onto X-ray CTs as frontal, transversal and sagittal planes. It allows a slice by slice visual comparison of two β^+-activity distributions. The code zooms the X-ray CTs for improving the visibility of details within the irradiated volume, it maps the Hounsfield units between -250 and 350 onto the grey scale to enhance the CT-contrast for soft tissue.

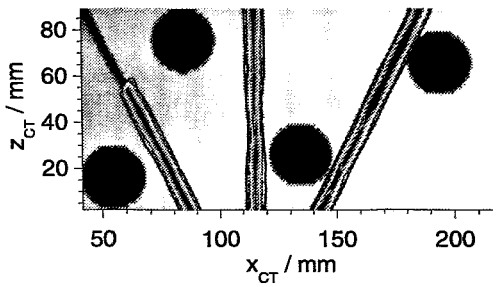

Fig. 1 *X-ray CT of a PMMA-Phantom superimposed with the contour plot of the measured β^+-activity distribution of activated Cu rods (couch angle 60 degrees).*

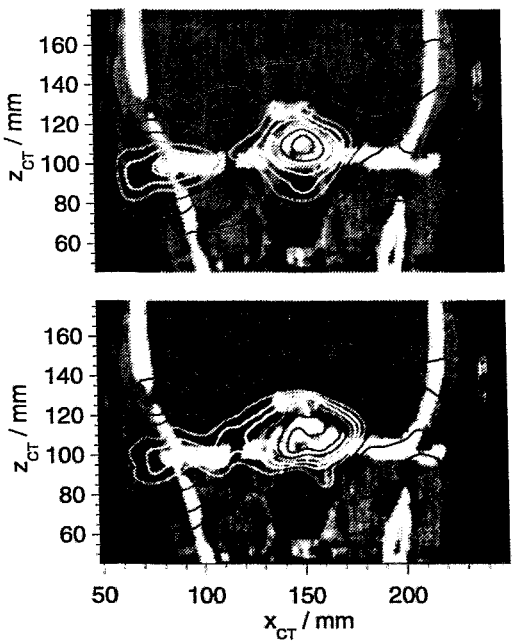

Fig. 2 *X-ray CTs of a patient superimposed with the contour plot of the measured (above) and simulated (lower) β^+-activity distribution.*

[1] *Deutsches Krebsforschungszentrum Heidelberg*

References

[1] W. Enghardt et al., "The routine clinical application of PET to the in-situ monitoring of tumour therapy with ^{12}C ions", this Annual report

[2] W. Schlegel, "VIRTUOS Users Manual", Deutsches Krebsforschungszentrum Heidelberg

Investigations on Transport Processes of ^{11}C Compounds in the Body [B]

R. HINZ, R. BERGMANN, W. ENGHARDT

As reported in [1] the radiotherapeutic treatments of patients with ^{12}C ions go ahead at GSI Darmstadt and are monitored routinely by means of in situ positron emission tomography (PET). Up to now there are no models describing the transport of the radioactive compounds of the β^+-emitters produced by fragmentation reactions between the particles of the stable beam and the nuclei of the tissue within the patient's body. Therefore, we have begun to study the distribution of possible radioactive products in animals and to propose appropriate compartmental models.

In contrast to the application of PET in nuclear medicine, the heavy ion irradiation of organic matter generates simultaneously a mixture of β^+-emitting isotopes of different elements (^{11}C, ^{10}C, ^{9}C, ^{15}O, ^{13}N, ^{8}B and others). The most abundant β^+-emitter is ^{11}C. Depending on the applied dose the hot reactions of ^{11}C in water yield several compounds, mainly $^{11}CO_2$, ^{11}CO, $H^{11}COOH$, $H^{11}CHO$ and $^{11}CH_3OH$ [2]. These radioactive compounds and their metabolites can remain in this region or can be transported out of the target tissue. The resulting radioactivity concentration in the blood is very low. Therefore, the time course of the radioactivity in the target tissue represents the apparent amount of remaining and leaving radioactive isotopes.

To determine typical time constants of these processes we carried out experiments on rats using two radiotracers. Non carrier added $^{11}CO_2$ and $^{11}CH_3I$ dissolved in isotonic sodium chloride solution at pH 7.4 were applied. The $^{11}CO_2$ represents the group of water soluble substances diffusing in the extracellular space and being transported by the blood and the lymph. $^{11}CI_3$ is an example of compounds with a high chemical reactivity which increases the apparent bound radioactivity in the target region. To describe mathematically the ratio of the apparent amount of remaining and leaving radioactivity a three compartment model is introduced (Fig. 1).

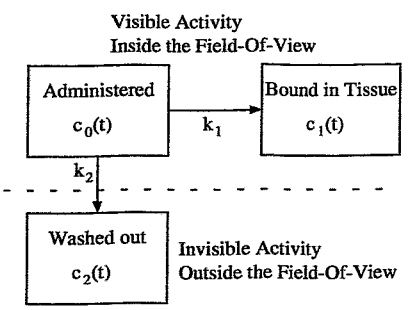

Fig. 1 *Basic three comparment model for wash out processes.*

The k_i are the kinetic parameters of the model: k_1 is the absorption constant and k_2 is the elimination constant. The $c_j(t)$ describe the time dependence of the β^+-emitter concentration in the compartment j, where the initial conditions are $c_0(0) = c_0$ and $c_1(0) = c_2(0) = 0$.

The kinetic model parameters are estimated from the measured time activity curves by graphical plot approaches or non-linear least squares fitting. The obtained k_i values are dependent on the administered tracer volumes. In both cases the half-life of the wash out process is about 100 s. The main difference between the two substances is that more than 99 % of the $^{11}CO_2$ are washed out, wheras approximately 40 % of the $^{11}CH_3I$ remain bound in tissue.

In conclusion, there is much evidence for the importance of the perfusion and chemical binding among the processes contributing to the transport of ^{11}C compounds in the body. Therefore, a perfusion map of the target area and the estimation of the bound radioactivity should be introduced into the computation of the β^+-activity distribution at ^{12}C therapy in order to improve the accuracy of the simulation.

References

[1] W. Enghardt et al., "The routine PET monitoring of tumour therapy with ^{12}C ions", this Annual report

[2] B. Nebeling, "Reaktionen von ^{11}C-Rückstoßatomen mit H_2O", Report, KFA Jülich, JÜL-1973, 1985

Application of a Fully 3D MLE-Algorithm to Patient Data [B]

K. Lauckner, W. Enghardt, R. Hinz and F. Pönisch

The dual-head positron camera BASTEI (Beta$^+$ Activity measurements at the Therapy with Energetic Ions) integrated into the ion beam therapy unit at GSI Darmstadt [1] is used to monitor the irradiation and verify the beam position. Since this PET application is count-limited and the system behavior of BASTEI is strongly shift-variant a fully 3D Maximum Likelihood Estimator (MLE) algorithm has been adapted to BASTEI [2]. The calculation of the normally huge transition matrix has been restricted to that coincidence channels containing events and an image space well adapted to the target volume known from the treatment plan. In this particular implementation a Monte-Carlo simulation is used to incorporate the individual detector response functions which includes furthermore the consideration of the shift-variant non-continuous point response functions and corrections for parallax errors.

Since December 1997 BASTEI has been utilized monitoring the irradiation of 48 patients with heavy ions. Typically about 10,000 to 100,000 and more rarely to 200,000 events were acquired during one dose fraction. The image space is normally defined between 90x50x50 to 256x128x128 voxel (voxel size: 1.6875 mm). The algorithm is fairly fast, capable of reconstructing an image typically between 20 to 120 minutes and sometimes 180 minutes depending on it's size and the number of registered events that contribute to this image space. The results of the patient data show the algorithm's stability recovering β^+-activity distributions from data sets with very low counting statistics. The example displayed in Fig. 1 shows almost artefact-free and distortion-free β^+-activity distributions that has been measured.

The primary aim of the simultaneous radiation therapy control is to ensure that the beam has been stopped inside the target region. The exact localisation of the distal gradients of the β^+-activity distribution is always possible. Additionally in the slices relating to the longitudinal sections of the PET-image (equivalent to the frontal slice in Fig. 1) an exact localisation of the lateral gradients is guaranteed, whereas out of the longitudinal sections (the transverse and sagittal slice in Fig. 1) an interpretation of the lateral gradients should be done by means of a priori information (e.g. the red contour plot marking the target area in Fig. 1)

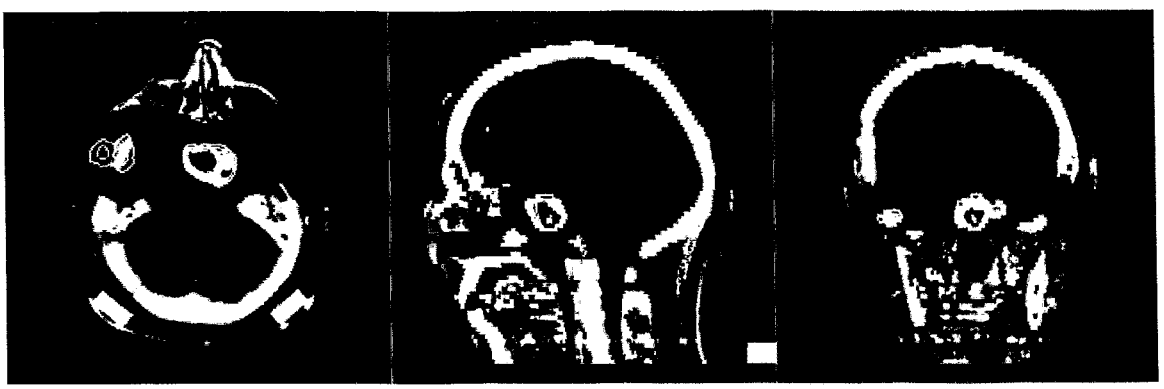

Fig. 1 *Transverse, sagittal and frontal slices of X-ray computed tomograms overlayed with the β^+-activity measured by means of PET(about 30,000 events). The thick red line and points, respectively, mark the target area. The heavy ion beam has entered the patient's head from the right as seen in the transverse and frontal slice (left and right image, respectively).*

References

[1] W. Enghardt et al., "The positron emission tomograph for treatment monitoring at the heavy ion therapy facility at GSI Darmstadt", Annual report 1996, Forschungszentrum Rossendorf

[2] K. Lauckner et al., "Fully 3D PET reconstruction for a spatially-varying system response and very low counting statistics", submitted to Conf. Rec., IEEE MIC, Nov. 12-14, 1998, Toronto, Canada

Calculation of Detour Factors for Positrons

B. Naumann and F. Hensel[1]

For the purpose of a feasibility study of a density measurement technique on the basis of the range of positrons in matter, a Monte Carlo simulation code has been written [1]. This code uses macroscopic parameters as stopping powers and ranges to calculate the spatial distribution of the positron annihilation. Furthermore, detour factors are required as input data, too. The detour factor gives the ratio of a track length (i.e. the continuous slowing down range) to the penetration depth. At first, literature data were used. Unfortunately, the data given in different papers vary by about 50 percent. This variation becomes important, if the simulation program is used to predict densities on the basis of measurements. For positrons with an energy of about 1 MeV (in matter with low effective atomic number Z) some authors published values for the detour factor of about 1.0 [3], others published values of about 1.5 [2]. Therefore, the detour factors were calculated by means of GEANT simulations [4]. In these simulations monoenergetic positrons enter the material (especially polystyrene and polystyrene foam) filling the space with $z > 0$ at the origin of coordinates (Fig. 1). Annihilation points (x,y,z) and track lengths were calculated for several media and densities taking into account 10^5 positrons. The calculated continuous slowing down ranges show very good agreement with values given in the NIST EPSTAR database [5].

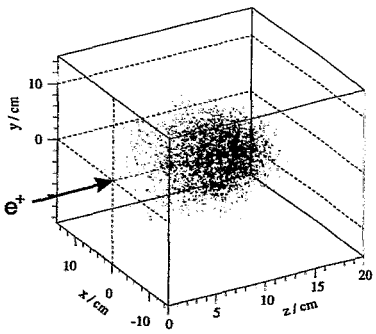

Fig. 1 *Setup for the GEANT Simulations (calculation: N_2, 25 kg/m^3, E=1 MeV).*

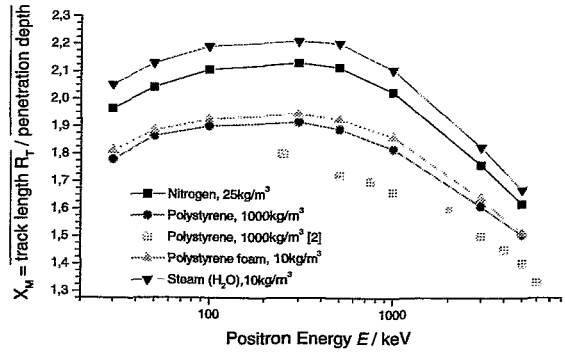

Fig. 2 *Overview on calculated detour factors X_M.*

The detour factor X_M was determined as the ratio of the averaged track length to the averaged penetration depth z. The energy dependence of this factor is shown in Fig. 2. For the same material, the values vary only slightly with changing material density. The detour factors reach the maximum for energies of about 300 keV which is in good agreement with [3]. The values of X_M for polystyrene (density 1000 kg/m^3) obtained with the program GEANT are even higher than those published in [2]. The detour factors used in the density simulation code [1] are taken from the GEANT results described above.

[1] *Institute of Safety Research*

References

[1] F. Hensel, PhD Thesis, in preparation
[2] H.-W. Thümmel, Durchgang von Elektronen- und Betastrahlung durch Materieschichten - Streuabsorptionsmodelle, Akademie-Verlag Berlin, 1974.
[3] H. Krieger, W. Petzold, Anwendungen in der Strahlentherapie und in der klinischen Dosimetrie, Strahlenphysik, Dosimetrie und Strahlenschutz, Band 2, B.G. Teubner Stuttgart, 1989, S. 42-47.
[4] GEANT - Detector Description and Simulation Tool, CERN Prog. Lib. W 5013, March 1994.
[5] S.M. Seltzer, NIST Electron and Positron Stopping Powers of Materials Database (EPSTAR), Version 2, NIST Standard Reference Database 7, 1989.

Dose Consideration for Cell Irradiation by Channeling X-rays

A. Panteleeva, W. Enghardt, U. Lehnert, J. Pawelke

The superconducting electron source ELBE with a maximum electron energy of 40 MeV and a mean beam current of up to 1 mA is being built up. Intense and quasi-monochromatic X-rays tunable within a photon energy range between 10 and 100 keV will be produced by means of electrons channeling in crystals [1].

We consider now the feasibility of a channeling radiation (CR) source for radiobiological experiments especially for the measurement of relative biological effectiveness (RBE) of quasi-monochromatic X-rays by cell survival studies. If we assume a 0.5 mm water equivalent absorbing material in front of the cell monolayer (20 μm thick, water equivalent), a photon beam spot diameter of 1 cm and a photon energy variation through the beam spot of 10 %, and extrapolating the experimental data on the planar channeling in diamond of refs. [1-3] to electron energy range between 12 and 40 MeV, to a beam current of 100 μA and to a crystal thickness of 80 μm. X-rays between 12 and 100 keV with sufficient dose rates of more than about 1 Gy/min will become available (Fig. 1).

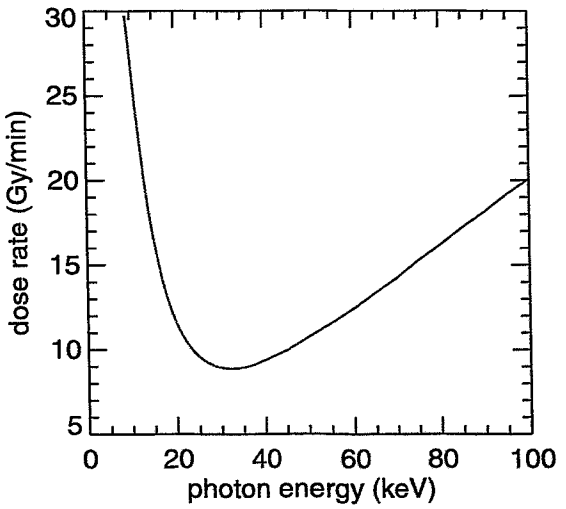

Fig. 1 *Photon energy dependent dose rates expected for a 100 μA ELBE beam (12-40 MeV) for cell irradiations. The X-rays are assumed to be produced by planar channeling at the (110)-plane of diamond and by the transition between the first excited and the ground state of the transverse lattice potential.*

The results of figure 1 are based on the assumption that all photons hit the target area. For a more detailed calculation inhomogenity of the photon flux and energy must be taken into consideration.

According to reference [5] a model of dipole approximation to the quantum theory of CR was applied to obtain the angular distribution of photon yield and energy for channeling conditions as considered for fig. 1. A more homogeneous distribution is obtained when the electron energy and distance between CR source and the target are increased. In the first stage of ELBE electrons with energy range of 12–20 MeV will become available in the radiation physics cave. Practical limitations of the cave construction result in maximum distance of 4.5 m between CR source and the target. A typical example of photon yield and energy spread is shown on fig. 2. Based on these results, together with the energy dependent absorption coefficent we calculated dose-rate distance dependence for given points of the target area (see fig. 3).

In general, dose rate decreases when increasing the distance d following $1/d^2$ law (fig. 3, left). For smaller electron beam energies, the decrease of photon yield is compensated by the increase of photon energy deposition in the target. Therefore, dose rates are close together for both energies shown and sufficient for cell irradiation if distance range is limited to maximum 2 m. However, we have to consider an appropriate dose delivery system in order to achieve homogeneous dose distribution (cf. fig. 3, right).

Future work is devoted to improvement of our calculation by taking into account the contribution of all possible radiative transitions in the crystal and the bremsstrahlung background.

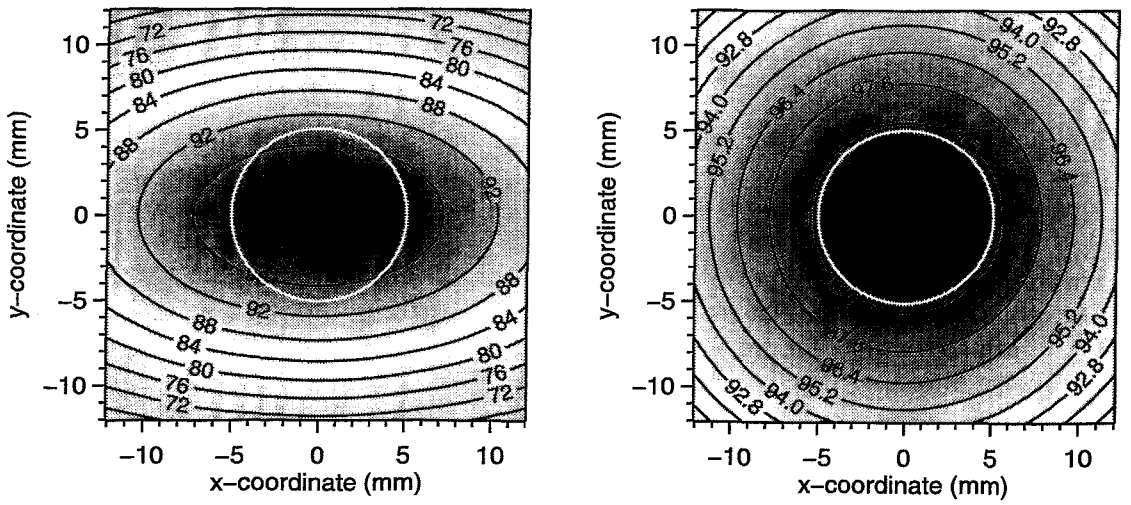

Fig. 2 *Relative photon yield (left) and energy (right) distribution of channeling radiation at a plane perpendicular to electron beam axis and located at a distance of 2 m from diamond crystal. An electron beam of 20 MeV results in maximum photon energy of 31.5 keV. Contour levels are in percentage of the maximum value and the white circle represents the target area.*

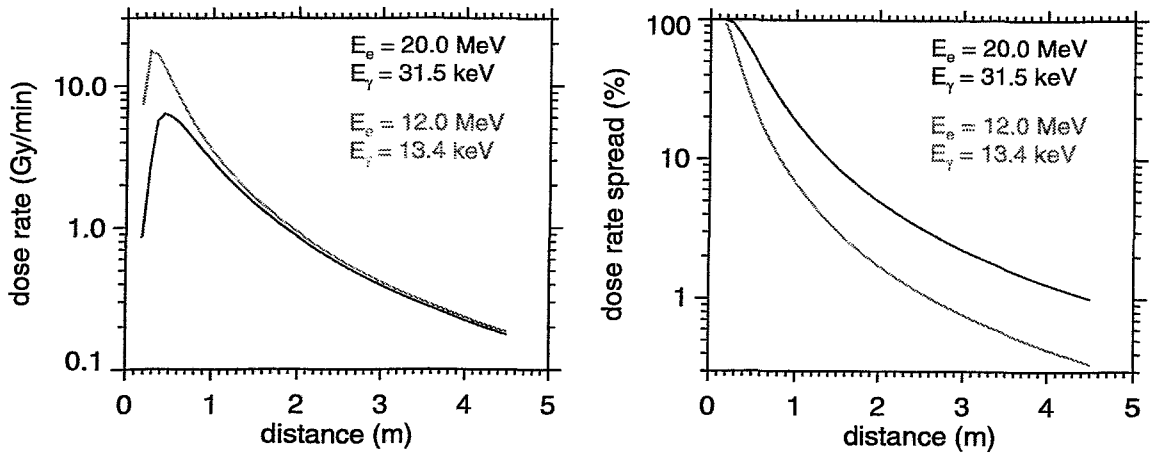

Fig. 3 *Distance dependent dose rates calculated for a 12 MeV (red) and 20 MeV (blue) electron beam. On the left: minimum dose rate in the target, on the right: dose rate difference between minimum and maximum dose rate in the target in percentage of the maximum dose rate.*

References

[1] W. Enghardt et al., Acta Physica Polonica (No. 5) **B30** (1999) 1639–1645

[2] J. Freudenberger et al., Nucl. Instr. Meth. in Phys. Res. **B119** (1996) 123–130

[3] H. Genz et al., Physical Review (No. 14) **B53** (1996) 8922-8936

[4] I. Reitz et al., Verhandl. DPG (VI) **34** (1999) 114

[5] M. Kumakhov and F. Komarov, Radiation from charged particles in solids, American Institute of Physics Translation Series, New York (1989)

Quality Control of Radionuclide Purity of a $^{188}W/^{188}Re$ Generator used for Therapeutic Applications

R. RUNGE[1], M. ANDREEFF[1], J. KROPP[1], G. WUNDERLICH[1], F.F. KNAPP[2], W.-G. FRANKE[1], R. SCHWENGNER AND W. SCHULZE

The nuclide ^{188}Re is well suited for clinical applications such as treatment of cancer with ^{188}Re-labelled antibodies, therapy of bone metastases with ^{188}Re-HEDP and the palliative treatment of arthritis of large synovial joints with ^{188}Re-labelled particles.
The nuclide ^{188}Re decays via β^- decay with a half-life of 17.0 h and a maximum electron energy of 2.12 MeV. The decay is followed by the emission of a 155.0 keV γ ray. ^{188}Re can be produced from the nuclide ^{188}W which decays with a half-life of 69.4 d. A percentage of 99 % of this decay populates the ground state of ^{188}Re [1].
To produce ^{188}Re for therapeutic applications a $^{188}W/^{188}Re$ generator obtained from the Oak Ridge National Laboratory was used. In this generator the daughter nuclide ^{188}Re is separated from the parent nuclide ^{188}W by passing a 0.9 % saline solution through an aluminium oxide adsorbent in which ^{188}W is bound as tungsten acid. The ^{188}Re eluate produced with this procedure may contain impurities of ^{188}W, if this can break through to the collection vessel of the ^{188}Re eluate. Such impurities of ^{188}W have to be avoided in therapeutic applications, since they may lead to a remarkable additional radiation dose caused by the continuing production of ^{188}Re via the decay of ^{188}W with its relatively long half-life. Therefore, the ^{188}Re eluate has to be carefully examined for possible ^{188}W impurities caused by a break through during the elution process. For this purpose, the γ-ray spectrum of the ^{188}Re eluate has been measured three weeks (corresponding to 30 half-lives of ^{188}Re) after the elution. The amount of a contamination with ^{188}W can be derived from the intensity of the characteristic 155.0 keV γ ray which can originate after this time only from a production of ^{188}Re through the decay of the contaminant. An example of a γ-ray spectrum of the ^{188}Re eluate is shown in Fig. 1. The intensity of the 155.0 keV γ ray observed in this spectrum corresponds to a ^{188}W contamination of 1×10^{-3} % per bolus which is within the range accepted for therapeutic applications. The γ rays arising from chemical impurities by ^{191}Os and ^{192}Ir observed in the spectrum are within the accepted range ($< 1.5 \times 10^{-4}$ %) as well.
In conclusion, the used $^{188}W/^{188}Re$ generator meets the requirements of radionuclide purity and can be used to produce ^{188}Re for therapeutic applications.

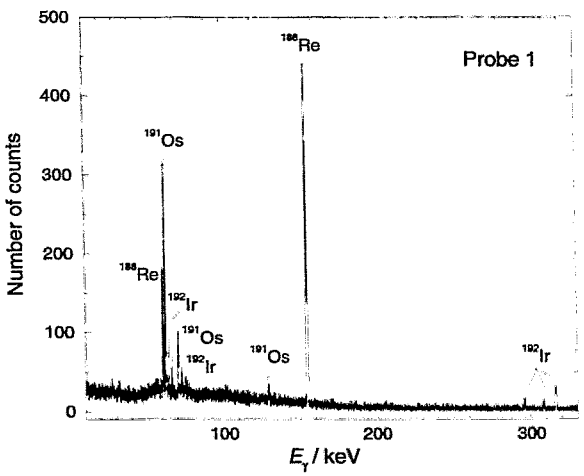

Fig. 1 *γ-ray spectrum of ^{188}Re eluate measured three weeks after the separation from ^{188}W.*

[1] *Klinik für Nuklearmedizin des Universitätsklinikums der TU Dresden*
[2] *Nuclear Medicine Group, Oak Ridge National Laboratory, USA*

References

[1] R. B. Firestone, V. S. Shirley, eds., Table of Isotopes, John Wiley, New York, 1996

PUBLICATIONS AND TALKS

Publications

From the authors printed in **bold** further information can be obtained

A Large Acceptance Multiparticle Spectrometer for 1–3 GeV Proton Beams
(Nucl. Instr. Meth. A 426 (1998) 385-404)

Balestra, F., Y. Bedfer, R. Bertini, L.C. Bland, A. Brenschede, F. Brochard, M.P. Bussa, V. Chalyshev, Seonho Choi, M. Debowski, M. Dzemidzic, J.Cl. Faivre, I.V. Falomkin, L. Fava, L. Ferrero, J. Foryciarz, V. Frolov, R. Garfagnini, D. Gill, A. Grasso, **E. Grosse,** S. Heinz, W.W. Jacobs, W. Kühn, A. Maggiora, M. Maggiora, A. Manara, D. Panzieri, H.W. Pfaff, G. Piragino, G.B. Pontecorvo, A. Popov, J. Ritman, P. Salabura, P. Senger, J. Stroth, F. Tosello, S.E. Vigdor, B. Zalikhanov, G. Zosi

Abstract: A magnetic spectrometer system has been constructed for the study of reactions with multiple charged particles in the final state, induced by polarized proton beams of few GeV energy. The system is based on a large-gap dipole magnet, with a liquid hydrogen target and scintillating fiber tracking detectors embedded inside the magnet. Multiwire proportional chambers, plastic scintillator hodoscopes, and threshold Čerenkov detectors placed outside the magnet provide additional tracking, triggering and particle identification capabilities. The system has been applied to study exclusive hyperon as well as pseudoscalar and vector meson production reactions at bombarding energies below 3 GeV. Additionally, it has been used to monitor the proton beam polarization at Laboratoire National Saturne. The components and performance of the system are reported.

Production of ϕ and ω Mesons in Near Threshold pp Reactions
(Phys. Rev. Lett. 81 (1998) 4572-4575)

Balestra, F., Y. Bedfer, R. Bertini, L.C. Bland, A. Brenschede, F. Brochard., M.P. Bussa, V. Chalyshev, Seonho Choi, **M. Debowski,** M. Dzemidzic, J.-Cl. Faivre, I.V. Falomkin, L. Fava, L. Ferrero, J. Foryciarz, V. Frolov, R. Garfagnini, D. Gill, A. Grasso, E. Grosse, S. Heinz, V.V. Ivanov, W.W. Jacobs, W. Kühn, A. Maggiora, M. Maggiora, A. Manara, D. Panzieri, H.-W. Pfaff, G. Piragino, G.B. Pontecorvo, A. Popov, J. Ritman, P. Salabura, P. Senger, J. Stroth, F. Tosello, S.E. Vigdor, G. Zosi

Abstract: The ratio of the exclusive production cross sections for ϕ and ω mesons has been measured in pp reactions at $T_{beam} = 2.85$ GeV. The observed ϕ/ω ratio is $(3.7 \pm 0.7^{+1.2}_{-0.9}) \times 10^{-3}$. After phase space corrections, this ratio is about a factor 10 enhanced relative to naive predictions based upon the Okubo-Zweig-Iizuka (OZI) rule, in comparison to an enhancement by a factor ~ 3 previously observed at higher energies. The modest increase of this enhancement near the production threshold is compared to the much larger increase of the ϕ/ω ratio observed in specific channels of $\bar{p}p$ annihilation experiments.

Coulomb Effects on Particle Spectra in Relativistic Nuclear Collisions
(Phys. Rev. C 57 (1998) 2536)

Barz, H.W., J.P. Bondorf, J.J. Gaardhøje, H. Heiselberg

Abstract: Coulomb effects on $\pi^{\pm}$ and $K^{\pm}$ spectra in relativistic nuclear collisions are investigated. At collision energies around 1 GeV the ratio of π^- to π^+ is enhanced several times at low transverse momenta but less at ultrarelativistic energies. We describe the ratios at SIS, AGS, and SPS energies with simple analytic models as well as more elaborate numerical models incorporating the expansion dynamics. The Coulomb effect depends on the properties of the source after the violent collision phase and provides information on source sizes, freeze-out times, and expansion velocities. Comparison with results from HBT analyses are made. Predictions for $\pi^{\pm}$ and $K^{\pm}$ at RHIC and LHC energies are given.

Combined Effects of Nuclear Coulomb Field, Radial Flow, and Opaqueness on Two-Pion Correlations
(Phys. Rev. C 59 (1999) 2214-2220)

Barz, H.W.

Abstract: Correlations of two like charged pions emitted from a hot and charged spherically expanding nuclear system are investigated. The motion of the pions is described quantum mechanically using the Klein-Gordon equation which includes Coulomb field and pion absorption. Flow modifies the radial distribution of the source function and rescales the pion wave functions. The radii extracted from the correlation functions are calculated in sideward and outward direction as a function of the pair momentum. Comparison with recent measurements at bombarding energies of 1 GeV and 11 GeV per nucleon is made.

Breakup Conditions of Projectile Spectators from Dynamical Observables
(Phys. Rev. C 58 (1998) 1639-1655)

Begemann-Blaich, M., V. Lindenstruth, J. Pochadzalla, J.C. Adloff, P. Bouissou, J. Hubele, G. Imme, I. Iori, P. Kreutz, G.J. Kunde, S. Leray, Z. Liu, U. Lynen, R.J. Meijer, U. Milkau, A. Moroni, W.F.J. Müller, C. Ngô, C.A. Ogilvie, G. Raciti, G. Rudolf, H. Sann, M. Schnittker, A. Schüttauf, **W. Seidel,** L. Stuttge, W. Trautmann, A. Tucholski

Abstract: Momenta and masses of heavy projectile fragments ($Z \geq 8$), produced in collisions of ^{197}Au with C, Al, Cu, and Pb targets at E/A=600 MeV, were determined with the ALADIN magnetic spectrometer at SIS. Using this information, an analysis of kinematic correlations between the two and three heaviest projectile fragments in their rest frame was performed. The sensitivity of these correlations to the conditions at breakup was verified within the schematic sos model. For a quantitative investigation, the data were compared to calculations with statistical multifragmentation models and classical three-body calculations. With classical trajectory calculations, where the charges and masses of the fragments are taken from a Monte Carlo sampling of the experimental events, the dynamical observables can be reproduced. The deduced breakup parameters, however, differ considerably from those assumed in the statistical multifragmentation models which describe the charge correlations. If, on the other hand, the analysis of kinematic and charge correlations is performed for events with two and three heavy fragments produced by statistical multifragmentation codes, good agreement with the data is found with the exception that the fluctuation widths of the intrinsic fragment energies are significantly underestimated. A new version of the multifragmentation code MCFRAG was therefore used to investigate the potential role of angular momentum at the breakup stage. If a mean angular momentum of 0.75 $\hbar$/nucleon is added to the system, the energy fluctuations can be reproduced, but a the same time the charge partitions are modified and deviate from the data.

Estimates of Production Rates of SUSY Particles in Ultra-Relativistic Heavy-Ion Collisions
(J. Phys. G 24 (1998) 1235-1248)

Beinker, M.W., **B. Kämpfer,** G. Soff

Abstract: We estimate the production rates of supersymmetric particles in central heavy-ion collisions at LHC. The parton cascade model is used to seek for possible collective phenomena which enlarge the production probability of very heavy particles. Even if there is some indication of such cooperative effects, higher energy and higher luminosity of proton beams at LHC disfavour heavy-ion reactions in the search for supersymmetric particles.

Proton-Proton Bremsstrahlung at 797 MeV/c
(Phys. Lett. B 429 (1998) 195)

Bilger, R., A. Böhm, H. Brand, S. Brand, K.-Th. Brinkmann, H. Clement, P. Cloth, M. Dahmen, **S. Dshemuchadse,** W. Eyrich, D. Filges, H. Freiesleben, M. Fritsch, R. Geyer, A. Hassan, J. Hauffe, P. Herrmann, B. Hübner, P. Jahn, K. Kilian, H. Koch, J. Kress, J. Krug, E. Kuhlmann, J.S. Lange, A. Metzger, **P. Michel, K. Möller,** H.P. Morsch, Ch. Nake, H. Nann, **B. Naumann, L. Naumann,** P. Ringe, E. Roderburg, M. Rogge, **A. Schamlott,** P. Schönmeier, A. Schülke, M. Steinke, F. Stinzing, P. Turek, G.J. Wagner, S. Wirth, U. Zielinski

Abstract: At COSY pp-bremsstrahlung was measured at a beam momentum of 797 MeV/c using an external proton beam. Data were taken with a wide angle spectrometer covering a solid angle of approximately 1 sr. The complete data set is presented in a series of c.m. angular distributions as well as a single Dalitz plot. The absence of final state interaction effects is understood as being due to a general insensitivity of the pp γ reaction to the spin-singlet component of the NN interaction. Coplanar angular distributions (in the laboratory system) are well reproduced by recent model calculations; also good agreement is found with the original TRIUMF data [K. Michaelian et al., Phys. Rev. D 41 (1990) 286] when omitting the rescaling factor of 2/3.

Strangeness Production in the Reaction $pp \rightarrow pK^+\Lambda$ in the Threshold Region
(Phys. Lett. B 420 (1998) 217)

Bilger, R., A. Böhm, S. Brand, H.Brand, Brinkmann, K.-Th., H. Clement, P. Cloth, M. Dahmen, M. Dellert, H. Dennert, **S. Dshemuchadse,** W. Eyrich, D. Filges, H. Freiesleben, M. Fritsch, R. Geyer, A. Hassan, J. Hauffe, P. Herrmann, B. Hübner, P. Jahn, K. Kilian, M. Kirsch, H. Koch, J. Kress, J. Krug, E. Kuhlmann, J.S. Lange, A. Metzger, **P. Michel, K. Möller,** H. P. Morsch, M. Moosburger, Ch. Nake, H. Nann, **B. Naumann, L. Naumann,** P. Ringe, E. Roderburg, M. Rogge, **A. Schamlott,** P. Schönmeier, A. Schülke, R. Sperl, M. Steinke, F. Stinzing, P. Turek, G.J. Wagner, S. Wirth, U. Zielinski

Abstract: The reaction $pp \rightarrow K^+\lambda, p$ was measured exclusively at the cooler synchrotron COSY at beam momenta of $p_{Beam} = 2.50$ GeV/c and $p_{Beam} = 2.75$ GeV/c using the TOF detector. Angular and momentum distributions were obtained for the full phase space of the reaction products. Total cross sections were extracted to be (2.7 0.3) μ b and (12.0 0.4) μ b, respectively. The polarization of the Λ-hyperon was determined as a function of its transversal momentum and was found to be negative for transverse momentum transfers of $p_T \geq 0.3$ GeV/c. The results together with existing data are compared with phenomenological parameterizations and model calculations on the basis of meson exchange.

First Identification of Excited States in the N=Z Nucleus ^{70}Br
(Eur. Phys. J. A 5 (1999) 243-246)

Borcan, C., H. Schnare, **R. Schwengner,** L. Käubler, H.G. Ortlepp, **F. Dönau,** H. Grawe, M. Górska, S. Skoda, J. Eberth, T. Härtlein, F. Köck, D. Pansegrau, M. Moszyński, D. Wolski, M. Weiszflog, A. Axelsson, D.R. Napoli, A. Gadea, R. Wadsworth, A. Wilson, W. Andrejtscheff

Abstract: Excited states in the $T_z = 0$ nucleus ^{70}Br have been investigated using the reaction ^{58}Ni(^{16}O, $1p3n$). γ rays were detected with one EUROBALL CLUSTER detector and three single HPGe detectors. Charged particles and neutrons were registered with the Rossendorf silicon ball and six modules of the EUROBALL neutron wall, respectively. The identification of γ transitions in ^{70}Br is based on the analysis of $\gamma\gamma$-proton-neutron coincidences. A level scheme of ^{70}Br has been established for the first time. It shows a multiplet-like structure of probably isospin $T = 0$ while $T = 1$ isobaric analogue states are not observed.

Three-Particle Final States Measured at the Pion threshold with COSY-TOF
(Acta Phys. Polon. B 29 (1998) 2993)

Brinkmann, K.-Th., R. Bilger, A. Böhm, H. Clement, H. Dennert, **S. Dshemuchadse,** H. Dutz, W. Eyrich, C. Fanara, D. Filges, A. Filippi, H. Freiesleben, M. Fritsch, R. Geyer, A. Hassan, J. Hauffe, P. Herrmann, D. Hesselbarth, B. Hübner, P. Jahn, K. Kilian, H. Koch, J. Kress, J. Krug, E. Kuhlmann, S. Marcello, S. Marwinski, A. Metzger, W. Meyer, **P. Michel, K. Möller,** H.P. Morsch, H. Nann, **B. Naumann, L. Naumann,** A. Raimondo, E. Roderburg, M. Rogge, **A. Schamlott,** P. Schönmeier, W. Schröder, M. Schulte-Wissermann, M. Steinke, F. Stinzing, G.Y. Sun, J. Wächter, G.J. Wagner, M. Wagner, S. Wirth, U. Zielinski

Abstract: The production of pions in pp collisions at beam energies of $\leq$ 300 MeV has been studied with the COSY-TOF spectrometer, which was recently extended to flight paths of $\sim$3 m for charged particles through the addition of a barrel section. Together with the bremsstrahlung channel, which was investigated in an earlier experiment, pion production exhausts the inelastic pp cross section at these energies. TOF allows the simultaneous study of all channels, the measurement of $pn\pi^+$ being facilitated by the neutron detector COSYnus. In this contribution, preliminary results on the pionic three-body final states are discussed.

Shears Mechanism in the A $\sim$ 110 Region
(Phys. Rev. Lett. 82 (1999) 3220-3223)

Clark, R.M., S. J. Asztalos, B. Busse, C. J. Chiara, M. Cromaz, M. A. Deleplanque, R. M. Diamond, P. Fallon, D. B. Fossan, D. G. Jenkins, S. Juutinen, N. Kelsall, R. Krücken G. J. Lane, I. Y. Lee, A. O. Macchiavelli, R. W. MacLeod, G. Schmid, J. M. Sears, J. F. Smith, F. S. Stephens, K. Vetter, R. Wadsworth, **S. Frauendorf**

Abstract: Lifetimes of states in a rotational-like $M1$ band in ^{110}Cd have been determined through a Doppler-shift attenuation method measurement performed with the Gammasphere array. The deduced B($M1$) values, which agree well with the predictions of the tilted axis cranking model, clearly confirm that it has the character of a shears band. Using a semiclassical scheme of the coupling of two long j vectors we deduce information on the strength and form of the effective interaction between the constituent nucleons. These results are the first definitive evidence of the shears mechanism and "magnetic rotation" in this mass region.

The Canonical Form of Transition Matrix Elements
(Phys. Rev. C 58 (1998) 872)

Dönau, F.

Abstract: The calculation of complicated transition matrix elements between multi quasiparticle states can be essentially simplified by transforming them in a canonical form. This method allows the extension of the basis space of Generator Coordinate studies aiming to include orthogonal quasiparticle excitations into the commonly considered basis set of collective states. Furthermore, it is shown that the neglect of the exchange contribution of multipole forces may lead to dangerous pole terms in non-diagonal matrix elements.

Restoration of the Broken D2-Symmetry in the Mean Field Description of Rotating Nuclei
(Phys. Lett. B 450 (1999) 313-319)

Dönau, F., Jing-ye Zhang, L.L. Riedinger

Abstract: Signature effects observed in rotational bands are a consequence of an inherent D2-symmetry. This symmetry is naturally broken by the mean field cranking approximation when a tilted (non-principal) axis orientation of the nuclear spin becomes stable. The possible

tunneling forth and back between the two symmetry-related minima in the double-humped potential-energy surface appears as a typical bifurcation of the rotational band. We describe this many-body process in which all nucleons participate by diagonalizing the nuclear Hamiltonian within a selected set of tilted and non-tilted cranking quasiparticle states. This microscopic approach is able to restore the broken D2 symmetry and reproduce the quantum fluctuations between symmetry-related HFB states which emerge as splitting of the band energies and in parallel staggering in intraband M1 transitions.

Integral Representation of the Random Phase Approximation Correlation Energy
(Phys. Rev. Lett. 83 (1999) 280-283)

Dönau, F., D. Almehed, R.G. Nazmitdinov

Abstract: Using the spectral function $\phi'(z)/\phi(z)$ the RPA correlation energy and other properties of a finite system can be written as a contour integral in a compact way. This yields a transparent expression and reduces drastically the numerical efforts for obtaining reliable values. The method applied to pairing vibrations in rotating nuclei as an illustrative example

A Low-Mass Drift Chamber System for the Hades-Spectrometer
(Acta Phys. Polonica B 29 (1998) 3189-3193)

Dohrmann, F., K. Bethge,**W. Enghardt,** O. Fateev, C. Garabatos, E. Grosse, C. Müntz, W. Karig, W. Koenig, L. Smykov, **M. Sobiella,** A. Steigerwald, H. Stelzer, J. Stroth, J. Wüstenfeld, Y. Zanewsky, A. Zentek

Abstract: A new high resolution ($\Delta/M/M < 1$ %) and high acceptance (45 %) di-electron spectrometer (HADES) has been designed to investigate inmedium properties of hadrons. For tracking of all charged particles (in particular with sufficient resolution for electrons) a system of 24 low-mass drift chambers (Helium based counting gas and Aluminium field and cathode wires), arranged in four tracking planes, is used. Design aspects of the chambers are reported. Results of performance optimization using various prototype detectors are discussed, including results of an aging test. Stable operation in the high-multiplicity environment of heavy ion collisions, and a spatial resolution of 70 μm(σ) over 80 % of a cell have been demonstrated in two beam experiments

Photon Scattering Off ^{52}Cr: Two-Phonon E1 Strength at the N=28 Shell Closure?
(Nucl. Phys. A 636 (1998) 139-155)

Enders, J., P. von Brentano, J. Eberth, R.-D. Herzberg, N. Huxel, H. Lenske, P. von Neumann-Cosel, N. Nicolay, N. Pietralla, H. Prade, J. Reif, A. Richter, C. Schlegel, **R. Schwengner,** S. Skoda, H.G. Thomas, I. Wiedenhöver, G. Winter, A. Zilges

Abstract: Results of a ^{nat}Cr(γ,γ') experiment at the S-DALINAC are reported for energies up to 7 MeV utilizing a Euroball Cluster detector. The excitation of a J=1 state at 5544 keV is observed which is believed to belong to ^{52}Cr because of the strength of the signal and the large natural abundance. By a variety of empirical arguments a quadrupole-octupole-coupled two-phonon 1^- character is suggested for this transition. Quasiparticle random-phase-approximation (QRPA) calculations are able to reproduce the energy and B(E1) transition strength remarkably well. The underlying microscopic structure is suggested to be more complex than a pure two-phonon picture. Furthermore, the calculations indicate a pure neutron $(2p_{3/2}^{-1}2p_{1/2})$ magnetic dipole structure for an excitation experimentally seen at 5098 keV which would provide a direct measure of ground-state correlations in ^{52}Cr.

The ELBE Radiation Source Project
(Acta Phys. Polonica B 30 (1999) 1639-1645)

Enghardt, W., F. Gariel, P. Gippner, E. Grosse, H. Guratzsch, D. Janssen, P. Michel, U. Nething, W. Neubert, H. Prade, **K.D. Schilling,** R. Schwengner, W. Seidel, U. Steegmüller, P. vom Stein, W. Wagner, M. Wenzel, A. Wolf, R. Wünsch and the ELBE-crew.

Abstract: The project of the future user facility Radiation Source ELBE is presented, wich is being realized in the Forschungszentrum Rossendorf. After several years of intense planning, the year 1996 has brought the final approval of the project and the groundbreaking started at the end of 1997. The first electron beam is expected until the end of this decade.

The Application of PET to Quality Assurance of Heavy-Ion Tumor Therapy
(Strahlenther. Onkol. 175 Supp II (1999) 33

Enghardt, W., J. Debus, T. Haberer, B.G. Hasch, R. Hinz, O. Jäkel, M. Krämer, K. Lauckner,**J. Pawelke**

Abstract: At the new heavy ion tumor therapy facility of the Gesellschaft für Schwerionenforschung at Darmstadt positron emission tomography (PET) has been implemented for in-beam and in-situ therapy control, i.e. during the tumor irradiation. The components necessary for this dedicated PET-imaging and their integration into the framework of therapy planning and quality assurance of heavy ion cancer treatments are presented. Results of the first application of this PET-method to patient treatments are reported.

Identification of Baryon Resonances in Central Heavy-Ion Collisions at Energies between 1 and 2 AGeV FOPI Collaboration
(European Physical Journal A 4 (1998) 335-349)

Eskef, M., D. Pelte, G. Goebels, E. Häfele, N. Herrmann, M. Korolija, Y. Leifels, H. Merlitz, S. Mohren, M.R. Stockmeier, M. Trzaska, J.P. Alard, A. Andronic , R. Averbeck , Z. Basrak, N. Bastid, I. Belyaev, D. Best, A. Buta, R. Caplar, N. Cindro, J.P. Coffin, P.Crochet, P. Dupieux, M. Dzelalija, L. Fraysse, Z. Fodor, A. Genoux-Lubain, A. Gobbi, K.D. Hildenbrand, B. Hong, F. Jundt, J. Kecskemeti, M. Kirejczyk, **R. Kotte,** R. Kutsche, A. Lebedev, V. Manko, J. Mösner, D. Moisa, W. Neubert, M. Petrovici, C. Pinkenburg, C. Plettner, P. Pras, F. Rami, V. Ramillien, W. Reisdorf, J.L. Ritman, B.de Schauenburg, D. Schüll, Z. Seres, B. Sikora, V. Simion, K. Siwek-Wilczynska, V. Smolyankin, M.A. Vasiliev, P. Wagner, G.S. Wang, K. Wisniewski, D. Wohlfarth , A. Zhilin

Abstract: The mass distributions of baryon resonances populated in near-central collisions of Au on Au and Ni on Ni are deduced by defolding the pt spectra of charged pions by a method which does not depend on a specific resonance shape. In addition the mass distributions of resonances are obtained from the invariant masses of (p, $\pi^{\pm}$) pairs. With both methods the deduced mass distributions are shifted by an average value of -60 MeV/c2 relative to the mass distribution of the free $\Delta(1232)$ resonance, the distributions descent almost exponentially towards mass values of 2000 MeV/c2. The observed differences between (p, π^{-}) and (p, π^{+}) pairs indicate a contribution of isospin I = 1/2 resonances. The attempt to consistently describe the deduced mass distributions and the reconstructed kinetic energy spectra of the resonances leads to new insights about the freeze out conditions, i.e. to rather low temperatures and large expansion velocities.

Supershell Structure of Magnetic Susceptibility
(Phys. Rev. B 58 (1998) 5622-5626)

Frauendorf, S., V.M. Kolomietz, A.G. Magner, A.I. Sanzhur

Abstract: The magnetic susceptibility of electrons confined to a spherical cavity or a circular billiard shows slow oscillations as a function of the number of electrons, which are a manifestation of the supershell structure found in the free energy of metal clusters. The relationship of the oscillations of the two different quantities is analyzed by means of semiclassical calculations, which are in quantitative agreement with quantal results. The oscillations should be observable for ensembles of circular ballistic quantum dots and metal clusters.

Cranked Shell Model and Isospin Symmetry Near N = Z
(Nucl. Phys. A 645 (1999) 509-535)

Frauendorf, S., J.A. Sheikh

Abstract: A cranked shell model approach for the description of rotational bands in N $\approx$ Z nuclei is formulated. The isovector neutron-proton pairing is taken into account explicity. The concept of spontancous breaking and subsequent restoration of the isospin symmetry turns out to be crucial. The general rules to construct the near yrast spectra for rotating nuclei are presented. For the model case of particles in a j-shell, it is shown that excitation spectra and the alignment processes are well described as compared to the exact shell model calculation. Realistic cranked shell model calculations are able to describe the experimental spectra of ^{72,73}Kr and ^{74}Rb isotopes.

Rotational Alignment Near N = Z and Proton-Neutron Correlations
(Phys. Rev. C 59 (1999) 1400-1404)

Frauendorf, S., J. A. Sheikh

Abstract: The effects of the residual proton-neutron interactions on bandcrossing features are studied by means of shell model calculations for nucleons in a high-j intruder orbital. The presence of an odd-nucleon shifts the frequency of the alignment of two nucleons of the other kind along the axis of rotation. It is shown that the anomalous delayed crossing observed in nuclei with aligning neutrons and protons occupying the same intruder subshell can be partly attributed to these residual interactions.

Thermal Dilepton Signal Versus Dileptons from Open Charm and Bottom Decays in Heavy-Ion Collisisions
(Phys. Rev. C 57 (1998) 3276-3283)

Gallmeister, K., B. Kämpfer, O.P. Pavlenko

Abstract: We analyze the opportunity to observe thermal dileptons emitted off deconfined matter resulting in heavy-ion collisions at RHIC and LHC energies. Special kinematical conditions provided by the detector systems PHENIX and ALICE, and the so-called $M_\perp$ scaling behavior of thermal dilepton spectra are taken into account. Our considerations include energy loss effects of the fast heavy quarks in deconfined matter, which for themselves can help to identify the creation of a hot and dense parton medium. Due to a thresholdlike effect for decay leptons we find a window at large transverse pair momentum and fixed transverse mass where the thermal signal can exceed the background of dileptons from correlated semileptonic decays of charm and bottom mesons.

Physical Information in the Thermal Continuum Dilepton Spectrum
(Prog. Part. Nucl. Phys. 42 (1999) 333c)

Gallmeister, K., B. Kämpfer, O.P. Pavlenko

Abstract: We consider the intermediate mass continuum of dileptons (between ϕ and J/ψ) in ultrarelativistic heavy-ion-collisions. The thermal signal depends essentially on thermodynamic

state parameters of the hottest parton stage as $(\tau_i \lambda_i^q T_i^3)^2$ convoluted with an involved detector acceptance function. A refined analysis of the transverse pair momentum spectrum at fixed dilepton transverse mass can reveal the maximum temperature of parton matter.

Can One Discriminate the Thermal Dilepton Signal against the Open Charm and Bottom Decay Background in Ultrarelatistic Heavy-Ion Collisions?
(Eur. Phys. J. C 8 (1999) 473)

Gallmeister, K., B. Kämpfer, O.P. Pavlenko

Abstract: In ultrarelativistic heavy-ion collisions at $\sqrt{s} > 20$ (120) A·GeV a copious production of charm (bottom) production sets in which, via correlated semileptonic $D\bar{D}$ ($B\bar{B}$) decays, gives rise to a dilepton yield at invariant mass $M \approx$ 2-3 GeV in excess of the Drell-Yan yield and the thermal dilepton signal from deconfined matter as well. We show that appropriate single-electron transverse momentum cuts (suitable for ALICE at LHC) cause a threshold like behavior of the dilepton spectra from heavy-quark meson decays and the Drell-Yan process and can allow to observe a thermal dilepton signal from hot deconfined matter.

Die Strahlungsquelle ELBE am Forschungszentrum Rossendorf
(Phys.Bl. 54 (1998) 342-344)

Grosse, E.

Abstract: In einigen Wochen wird der Grundstein für die Strahlungsquelle ELBE am Forschungszentrum Rossendorf (FZR) bei Dresden gelegt. Das Kernstück dieser neuen Anlage wird ein supraleitender Elektronen-Linearbeschleuniger hoher Brillanz sein, der in seiner kombination von hoher Strahlintensität und guter Strahlqualität (d. h. niedriger Emittanz) alle in Europa existierenden Anlagen übertreffen soll (das Akranym ELBE wurde aber nicht nur deshalb gewählt).

Stopping and Radial Flow in Central ^{58}Ni+ ^{58}Ni Collisions between 1A and 2A GeV
(Phys. Rev. C 57 (1998) 244-253)

Hong, B., N. Herrmann, J.L. Ritman, D. Best, A. Gobbi, K.D. Hildebrand, M. Kirejczyk, Y. Leifels, C. Pinkenburg, W. Reisdorf, D. Schüll, U. Sodan, G.S. Wang, T. Wienhold, J.P. Alard, V. Amouroux, N. Bastid, I. Belyev, G. Berek J. Biegansky, A. Buta, J.P. Coffin, P. Crochet, B.de Schauenburg, R. Dona, P. Dupieux, M. Eskef, P. Fintz, Z. Fodor, L. Fraysse, A. Genoux-Lubain, G. Goebels, G. Guillaume, E. Häfele, F. Jundt, J. Kecskemeti, M. Korolija, **R. Kotte,** C. Kuhn, A. Lebedev, I. Legrand, C. Maazouzi, V. Manko, J. Mösner, S. Mohren, **W. Neubert,** D. Pelte, M. Petrovici, P. Pras, F. Rami, C. Roy, Z. Seres, B. Sikora, V. Simion, K. Siwek-Wilczyńska, A. Somov, L. Tizniti, M. Trzaska, M.A. Vasiliev, P. Wagner, D. Wohlfarth, A. Zhilin

Abstract:The production of charged pions, protons, and deuterons has been studied in central collisions of ^{58}Ni on ^{58}Ni at incident beam energies of 1.06A, 1.45A and 1.93A GeV. The dependence of transverse-momentum and rapidity spectra on the beam energy and on the centrality of the collisison is presented. It is shown that the scaling of the mean rapidity shift of protons established for between 10A and 200A GeV at the Brookhaven AGS and the CERN SPS accelerators energies is valid down to 1A GeV. The degree of nuclear stopping is discussed: quantum molecular dynamics calculations reproduce the measured proton rapidity spectra for the most central events reasonably well, but do not show any sensitivity between the soft and the hard equation of state. A radial flow analysis, using the midrapidity transverse-momentum spectra, delivers freeze-out temperatures T and radial flow velocities β_r, which increase with beam energy up to 2A GeV; in comparison to the existing data of Au on Au over a large range of energies, only β_r shows a system size dependence.

Complete Scissors Mode Strength in Heavy Deformed Odd-Mass Nuclei: A Case Study of ^{165}Ho and ^{169}Tm
(Nucl. Phys. A 645 (1999) 239-261)

Huxel, N., P. von Brentano, J. Eberth, J. Enders, R.-D. Herzberg, P. von Neumann-Cosel, N. Nicolay, N. Pietralla, H. Prade, C. Rangacharyulu, J. Reif, A. Richter, C. Schlegel, **R. Schwengner,** S. Skoda, H.G. Thomas, I. Wiedenhöver, G. Winter, A. Zilges

Abstract: The low-energy dipole strength distributions in ^{165}Ho and ^{169}Tm have been studied in nuclear resonance fluorescence experiments at the S-DALINAC utilizing a Euroball Cluster detector. In the energy interval between 2.5 and 4.0 MeV, where the scissors mode is expected, 35 ground state transitions could be observed in ^{165}Ho and 53 in ^{169}Tm. Assuming M1 character for all these transitions corresponds to $\sum B(\mathrm{M1})\uparrow$=1.54(23) μ_N^2 and $\sum B(\mathrm{M1})\uparrow$=2.15(63) μ_N^2 for ^{165}Ho and ^{169}Tm, respectively. A statistical analysis is applied to the measured spectra which is capable of reconstructing the complete strength, including contributions of transitions below the observation limit, with the ratio between M1 and E1 excitations and their total strengths taken as an average over the even-mass neighbours. This results in summed M1 transition strengths of $\sum B(\mathrm{M1})\uparrow=3.54^{+0.75}_{-0.95}\ \mu_N^2$ (^{165}Ho) and $\sum B(\mathrm{M1})\uparrow=3.36^{+100}_{-0.57}\ \mu_N^2$ (^{169}Tm). The large variations of the summed dipole strength and the fragmentation in other deformed odd-mass nuclei can be reproduced by the same statistical ansatz. The total low-lying strength in heavy deformed odd-mass nuclei is in agreement with the findings in the neighbouring even-mass nuclides as well as with sum-rule predictions.

Magnetic Rotation in ^{106}Sn and ^{108}Sn
(Phys. Lett. B 428 (1998) 23-30)

Jenkins, D.G., I.M. Hibbert, C.M. Parry, R. Wadsworth, D.B. Fossan, G.J. Lane, J.M. Sears J.F. Smith, R.M. Clark, R. Krücken, I.Y. Lee, A.O. Macchiavelli, V.P. Janzen, J. Cameron, **S. Frauendorf,**

Abstract: The Nuclei ^{106}Sn and ^{108}Sn have been populated using the ^{54}Fe(^{58}Ni,α2p) and ^{54}Fe(^{58}Ni,4p) reactions, respectively, at a beam energy of 234 MeV and the gamma rays have been detected using the Gammasphere array. Two "rotation-like" structures consisting of magnetic dipole transitions have been observed in each of the nuclei. The bands can be interpreted, using the Tilted Axis Cranking model, as examples of magnetic rotation. The calculations show excellent agreement with the data for ^{108}Sn. However, for the lighter isotope, ^{106}Sn, the model is unable to reproduce the experimental B(M1)/B(E2) ratios. Reasons for this discrepancy are discussed.

Magnetic Rotational Bands in ^{108}Sb
(Phys. Rev. C 58 (1998) 2703-2709)

Jenkins, D.G., R. Wadsworth, J. Cameron, R. M. Clark, D. B. Fossan, I. M. Hibbert, V. P. Janzen, R. Krčken, G. J. Lane, I. Y. Lee, A. O. Macchiavelli, C. M. Parry, J. M. Sears, J. F. Smith, **S. Frauendorf**

Abstract: High-spin states in ^{108}Sb were populated using the ^{54}Fe(^{58}Ni,3pn) reaction at a beam energy of 243 MeV and the subsequent γ decay was studied using the Gammasphere array. A new sequence of magnetic dipole transitions has been observed in addition to a previously known $M1$ band in ^{108}Sb. These bands may be interpreted, within the tilted axis cranking model as magnetic rotational bands with $\pi[{g_{7/2}}^2$ [direct-product] ${g_{(9/2)}}^{-1}]$ [direct-product]$\nu[h_{11/2}]$ and $\pi[h_{11/2}g_{7/2}$ [direct-product] ${g_{(9/2)}}^{-1}]$ [direct-product] $\nu[(g_{7/2}d_{5/2})]$ configurations.

Confirmation of the Shears Mechanism in Near-spherical Tin Nuclei
(Phys. Rev. Lett. 83 (1999) 500-503)

Jenkins, D.G., Wadsworth, R., Cameron, J., Clark, R.M., Fossan, D.B., Hibbert, I.M., Janzen, V.P., Krücken, R., Lane, G.J., Lee, I.Y., Macchiavelli, A.O., Parry, C.M., Sears, J.M., Smith, J.F., **Frauendorf, S.,**

Lifetimes of states of a magnetic dipole band in each of the nuclei ^{106,108}Sn have been obtained using the Doppler shift attenuation method. The deduced B($M1$) transition rates show the characteristic behavior associated with the shears mechanism. A simplified semiclassical analysis yields B($M1$) values in qualitative agreement with those expected for previously assigned configurations. The results suggest extremely low deformations for these dipole structures. In particular, the ^{106}Sn band appears to be the first example of almost pure magnetic rotation in a spherical nucleus.

Lifetime Study of Particle-Hole Excitations in the Semimagic Nucleus ^{94}Ru
(Phys. Rev. C 60 (1999) 014309-1- 014309-12)

Jungclaus, A., D. Kast, K.P. Lieb, C. Teich, M. Weiszflog, T. Härtlein, C. Ender, F. Köck, D. Schwalm, I.P. Johnstone, J. Reif, **R. Schwengner,** R. Peusquens, A. Dewald, J. Eberth, H.G. Thomas, M. Górska, H. Grawe

Abstract: The recoil-distance Doppler-shift technique was employed to determine lifetimes of high-spin states in the semimagic nucleus ^{94}Ru. The nuclei were populated using the reaction ^{58}Ni(^{40}Ca, $4p$) at a beam energy of 145 MeV, and the γ radiation from their decay was detected in six EUROBALL cluster detectors. A total of 23 reduced transition probabilities and limits for fifteen further transitions were extracted and compared to largescale shell model calculations, considering different configuration spaces and residual interactions. The information deduced on transition strengths turned out to be essential for the correct assignment of the calculated to the experimental excited states. The results indicate that the 13^-_2 (6919 keV), 14^-_1 (7970 keV), and the 15^-_1 (8133 keV) levels have pure proton $\pi(f_{5/2})^{-1}\ \pi(g_{9/2})^5$ configurations, whereas all other excited states above 6.3 MeV are built from a neutron $g_{9/2} \rightarrow d_{5/2}$ excitation across the N=50 shell closure, coupled to up to six valence protons. Strong $M1$ transitions were found in a stretched dipole cascade within the sequence of neutron core-excited states at positive parity, while the strengths of the transitions between core-excited and pure proton states were proven to be small, similar as in ^{95}Rh.

Magnetic Moment Measurements in the Semi-Magic Nuclei ^{94}Ru and ^{95}Rh after Recoil Implantation into Iron and Nickel
(Eur. Phys. J. A 6 (1999) 29-36)

Jungclaus, A., D. Kast, K.P. Lieb, C. Lingk, C. Teich, O. Iordanov, T. Härtlein, D. Schwalm, I.P. Johnstone, **R. Schwengner,**

Abstract: The magnetic moments of the 12^+ and 11^- yrast states in ^{94}Ru and of the $25/2^-$, $29/2^+$, and $35/2^+$ levels in ^{95}Rh have been measured via the IMPAD technique. The nuclei were produced in the reaction ^{85}Ni + ^{40}Ca and recoil-implanted into polarized Ni and Fe hosts. The g-factors were deduced from the measured time-integral Larmor precessions. The comparison between the experimental results and large-scale shell model calculations suggests that the 12^+ and 11^- states in ^{94}Ru and the $25/2^-$ level in ^{95}Rh are pure proton states whereas the $29/2^+$ and $35/2^+$ states in ^{95}Rh contain a neutron excitation across the N=50 shell gap. This interpretation supports the conclusion drawn from recent lifetime measurements.

A Method for the Intrinsic Calibration of CsI(Tl) Detectors
(Nucl. Instr. A 413 (1998) 127-137)

Kamanin, D.V., W. Wagner, H.-G. Ortlepp

Abstract: A method for the intrinsic energy calibration of photomultiplier-coupling CsI(Tl) detectors is distributed. A simple empirical model of the scintillation light pulse-shape of CsI(Tl) crystals for light charged particle has been applied to simulate the particle identification matrix as it follows from the pulse-shape analysis method. The calibration procedure for the large-area CsI(Tl) detectors of the scintillator shell of the 4π-array FOBOS for ions with $Z < 4$ at energies below 100 AMeV is based on the energies of the particle punch-through points.

Estimated of Dilepton Spectra from Open Charm and Bottom Decays in Relativistic Heavy-Ion Collisions
(Phys. Lett. B 419 (1998) 412-418)

Kämpfer, B., O.P. Pavlenko, **K. Gallmeister**

Abstract: The spectra of lepton pairs from correlated open charm and bottom decays in ultrarelativistic heavy-ion collisions are calculated. Our approach includes energy loss effects of heavy quarks in deconfined matter which are determined by temperature and density of the expanding parton medium. We find a noticeable suppression of the initial transverse momentum spectrum of heavy quarks due to the energy loss at LHC conditions. Within the central rapidity covered by the ALICE detector system, the dominant contribution from bottom decays to the high invariant mass dielectron spectrum is predicted.

Dileptons, Charm and Bottom in Relativistic Heavy-Ion Collisions
(Prog. Part. Nucl. Phys. 42 (1999) 335c)

Kämpfer, B., O.P. Pavlenko,**K. Gallmeister**

Abstract: The relation of the thermal dilepton signal from deconfined matter, resulting in central ultra-relativistic heavy-ion collisions at RHIC and LHC energies, to the background yiels from the Drell-Yan process and correlated semileptonic decays of open charm and bottom mesons is analyzed. We demonstrate that very stringent kinematical cuts offer a chance to identify the thermal signal in the continuum region.

Elastic Proton-Deuteron Backward Scattering: Relativistic Effects and Polarization Observables
(Phys. Rev. C 57 (1998) 1097)

Kaptari, L.P., **B. Kämpfer,** S.M. Dorkin, S.S. Semikh

Abstract: The elastic proton-deuteron backward reaction is analyzed within a covariant approach based on the Bethe-Salpeter equation with realistic meson-exchange interaction. Lorentz boost and other relativistic effects in the cross section and spin correlation observables, such as tensor analyzing power and polarization transfer, etc., are investigated in explicit form. Results of numerical calculations for a complete set of polarization observables are presented.

Comparison of YAP and BGO for High-Resolution PET Detectors
(Nucl. Instr. Meth. in Phys. Res. A 404 (1998) 413-417)

Kapusta, M., **J. Pawelke,** M. Moszyński

Abstract: The goal of this work was to evaluate the potential of small YAP: Ce crystals, especially designed for a high-resolution PET system. We directly compared the scintillator properties of $3 \times 3 \times 20$ mm^3 crystals YAP with those of BGO. The light output, energy

resolution, detection efficiency and timing properties for the irradiation using ^{137}Cs and ^{22}Na sources were investigated. Special consideration was given to the influence of the reflector coating on the light output as well as on the overall performance of the quality of the studied crystals.

Absolute E1 and E2 Transition Rates in ^{110}Cd
(Eur. Phys. J. A 2 (1998) 269-273)

Kostov, L.K., W. Andrejtscheff, L.G. Kostova, **L. Käubler,** H. Prade, R. Schwengner

Abstract: The lifetimes of several states in ^{110}Cd have been determined by means of the generalized centroid-shift method. The reaction ^{108}Pd(α, 2n) has been used and the following results were obtained: $T_{1/2}$(2879 keV) = 0.60 ± 0.10 ns, $T_{1/2}$(3029 keV) = 0.30 ± 0.10 ns, $T_{1/2}$(3056 keV) = 2.25 ± 0.10 ns, $T_{1/2}$(3611 keV) = 0.45 ± 0.10 ns. Electric dipole and quadrupole transitions are discussed in terms of octupole and quadrupole collectivity. The odd-spin sequence of the semi-aligned structure $\nu(h_{11/2}d_{5/2})$ has been established with the band-head at $J^\pi = 7_2^-$ identified as a new two-quasiparticle isomer, the lower-lying $5^-_{1,2}$ states being of two-quasiproton character.

Nuclear Reaction: ^{108}Pd(α,2n), E = 27 MeV,; measured E_γ, I_γ, γ-r.f. Deduced : $T_{1/2}$, B(αL) in ^{110}Cd. Ge detectors. Generalized centroid-shift analysis.

Pair Correlations and Magnetic Susceptibility of Small Al-Grains
(Journal of Cluster Science 10 (1999) 195-220)

Kuzmenko, N.K., V.M. Mikhajlov, **S. Frauendorf**

Abstract:P air correlations and the magnetic susceptibility of electrons in a spherical cavity are studied both for grand canonical and the canonical ensemble. The coupling constant of the *BCS* Hamiltonian is adjusted to experimental values of the gap parameter. The gap parameter is found to increase for small grains as a consequence of the pronounced shell structure in the spectrum of the spherical cavity. The sharp phase transition at T_c is smeared out for the canonical ensemble. The strong paramagnetic susceptibility of the normal electrons in the cavity is reduced by the superconductivity, but it remains positive.

High-Spin States, Particle-Hole Structure, and Linked Smooth Terminating Bands in Doubly odd ^{112}Sb
(Phys. Rev. C 58 (1998) 127-149)

Lane, G.J., D.B. Fossan, C.J. Chiara, **H. Schnare,** J.M. Sears, J.F. Smith, I. Thorslund, P. Vaska, E.S. Paul, A.N. Wilson, J.N. Wilson, K. Hauschild, I.M. Hibbert, R. Wadsworth, A.V. Afanasjev, I. Ragnarsson

Abstract: Excited states in ^{112}Sb have been observed with the Stony Brook array of six Compton-suppressed HPGe detectors and the ^{103}Rh(^{12}C,3n) reaction at 60 MeV using a thick target. New excited states which decay solely towards the τ_m = 773 ns, I^π=8$^-$ isomer have been identified using time-correlated spectroscopy. The previously known level scheme has also been extended and corrected. In total, five rotational bands are observed, consisting of the two previously known strongly coupled bands based upon one-particle-one-hole (1p-1h) proton excitations across the Z=50 shell gap and tree newly observed decoupled bands based upon 2p-2h proton excitations. The 1p-1h bands are interpreted as deformed rotors, although there is a possibility that a shears mechanism like that observed in the lead region may also play a role. Results from a thin-target measurement using the Eurogam-II spectrometer and the ^{90}Zr(^{31}P,2α,n) reaction at 150 MeV are also presented. These data have been used to extend the decoupled bands up to $I \sim 40\hbar$, a spin regime where the bands exhibit the

features of smooth band termination. The combined results from the two experiments have enabled two of the bands to be connected by discrete γ-ray transitions to the low-spin level scheme, thereby determining their spin and parities. This allows for a definitive comparison with the results of cranked Nilsson-Strutinsky calculations and excellent agreement is obtained. Further confirmation of the terminating band configuration assignments is obtained from an analysis of the relative alignment properties of pairs of bands in the chain $^{110-112}$Sb.

Medium Effects in Kaon and Antikaon Production in Nuclear Collisions at Subthreshold Beam Energies

(Phys. Rev. Lett. 82 (1999) 1640-1643)

Laue, F., C. Sturm, I. Böttcher, **M. Dębowski,** A. Förster, **E. Grosse,** P. Koczoń, B. Kohlmeyer, M. Mang, L. Naumann, H. Oeschler, F. Pühlhofer, E. Schwab, P. Senger, Y. Shin, J. Speer, H. Ströbele, G. Surowka, F. Uhlig, A. Wagner, W. Walus

Abstract: Production cross section of K^+ and K^- mesons have been measured in C + C collisions at beam energies per nucleon below and near the nucleon-nucleon threshold . At a given beam energy, the spectral slopes of the K^- mesons are significantly steeper than the ones of the K^+ mesons. The excitation functions for K^+ and K^- mesons nearly coincide when correcting for the threshold energy. In contrast, the K^+ yield exceeds the K^- yield by a factor of about 100 in proton-proton collisions at beam energies near the respective nucleon-nucleon thresholds.

Observation of a $(\nu 7/2^-[514])^2$ Crossing in ^{118}Os
(Nucl Phys. A 645 (1999) 465-491)

Lieder, R.M., Ts. Venkova, S. Utzelmann, W. Gast, **H. Schnare,** K. Spohr. P. Hoernes. A. Georgiev, D. Bazzacco, R. Menegazzo, C. Rossi-Alverez, G. de Angelis. R. Kaczarowski. T. Rząca-Urban, T. Morek, G.V. Marti, K.H. Maier, **S. Frauendorf**

Abstract: High spin states in ^{118}Os have been populated by means of the ^{150}Nd(^{36}S, 6n) reaction at 177 MeV and studied with the γ-spectrometers OSIRIS and GASP. Eight known bands have been extended to higher spins and a new strongly coupled band has been discovered. Configuration assignment of the bands have been carried out in the framework of the tilted-axis cranking model utilizing experimental ratios of reduced transition probabilities $B(\mathrm{M1})/B(\mathrm{E2})$. The investigation of the alignment behaviour of the bands revealed that besides the well-known first band crossing caused by the alignment of an $i_{13/2}$ quasineutron pair. a second band crossing occurs in four of the bands. The crossing frequency is $\geq$ 0.38 MeV and the alignment gain is fairly small, ranging between 2 and $\leq$ 4 $\hbar$. The crossing can consistently be explained as a two-quasineutron $(\nu 7/2^-[514])^2$ alignm.ent. This crossing has been observed for the first time.

Lifetimes and Collectivity of Low-Lying States in ^{115}Sn
(Phys. Rev. C 59 (1999) 1975-1983)

Lobach, Yu.N., **L. Käubler, R. Schwengner,** A.A. Pasternak

Abstract: The lifetimes of excited states in ^{115}Sn have been measured using the Doppler shift attenuation method in the reaction ^{113}Cd(α,2nγ) at E_α=27.2 MeV. Lifetimes were obtained for 18 states and lifetime limits for 6 states with $E_x \leq 4$ MeV and $J \leq 23/2$. The experimentally obtained $B(\sigma L)$ values for transitions deexciting positive-parity states are compared with calculations in the framework of the Bardeen-Cooper-Schrieffer quasiparticle model and the interacting boson fermion model. whereas the values for transitions between

negative-parity states are discussed qualitatively within a core-particle coupling picture. The value of $B(E2)$=3.5(11) Weisskopf units (W.u.) for the transition linking the $19/2^-$ state of the intruder $\nu h_{11/2}\pi 2p2h$ band to the $15/2^-$ state of the $\nu h_{11/2}\otimes 2_1^+$ multiplet strongly supports the configuration $\nu h_{11/2}\pi(g_{9/2}^{-2}g_{7/2}^2)$ ascribed to this band.

MARS: A Start Detector System for the COSY Time-OF-Flight Spectrometer TOF
(Nucl. Instr. A 408 (1998) 453-467)

Michel, P., K. Möller, B. Naumann, L. Naumann. A. Schamlott, G. Schmidt, A. Schülke, COSY-TOF Collaboration

Abstract: A start detector system (MARS) was developed for the time-of-flight spectrometer TOF at the external beam of the cooler synchrotron COSY. The start detector system is specially tailored to the measurement of the proton-proton bremsstrahlung, but it can also be used for the investigation of other reactions. The MARS detector system consists of two 16-fold segmented rings of plastic scintillators with 500 μm thickness embedded in specially formed hollow light guides. According to simulation calculations and test measurements the light transmission of these light guides amounts to about 40%. The time resolution for minimum ionizing particles was determined to 0.5 ns (FWHM).

High-Spin States in ^{205}Rn: A New Shears Band Structure??
(Phys. Rev. C 59 (1999) R 2989)

Novak, J.R., Beausang, C.W., Amzal, N., Casten, R.F., Cata Danil, G., Cocks, J.F.C., Cooper, J.R., Greenlees, P.T., Hannachi, F., Helariutta, K., Jones, P., Julin, R., Juutinen, S., Kankaanpää, H., Kettunen, H., Krücken, R., Kuusiniemi, P., Leino, M., Liu, B., Muikku, M., Savelius, A., Socci, T., Thomas, J.T., Zamfir, N.V., Zhang, J.-y., **Frauendorf, S.**

Abstract: The high-spin structure of ^{205}Rn has been investigated for the first time following the ^{170}Er(^{40}Ar,5n) and ^{197}Au(^{14}N,6n) reactions at beam energies of 183 MeV and 90-110 MeV, respectively, using the Jurosphere and YRAST Ball arrays. Two new cascades have been identified which dominate the high-spin decay. One of these, consisting of ten stretched M1 transitions with unobserved E2 crossover transitions, is interpreted as a shears structure based on the $\nu i_{13/2}^{-1}$ [direct-product] $\pi i_{13/2}^2$ (or $\nu i_{13/2}^{-1}$ [direct-product] $\pi h_{9/2}i_{13/2}$) configuration.

Fragment Mass Distribution of Fission after Incomplete Fusion in the Reaction ^{7}Li (43A MeV) + ^{232}Th
(Nucl. Phys. A 642 (1998) 407-418)

Ortlepp, H.-G..**W. Wagner,** C.-M. Herbach, P. Gippner, K.D. Schilling, Yu.E. Penionzhkevich

Abstract: Fragment mass distributions of binary fission were measured for the reaction ^{7}Li (43A MeV) + ^{232}Th in dependence on the linear momentum transfer. The excitation energy (E^*) of the compound nuclei produced by incomplete fusion was deduced applying the massive transfer approach and amounted to 57-205 MeV. The analysis procedure avoids distortions due to the acceptance and error correlation. Total fragment masses and single fragment mass dispersions are discussed in terms of E^*, temperature and an effective parameter describing the stiffness against mass asymmetry. Assuming unchanged stiffness, the dispersions at E^* in excess of $\approx$ 70 MeV are found to be considerably smaller than expected. This behaviour is interpreted as a consequence of the remarkably cooling down of the hot nuclei due to neutron emission before the fragment masses are formed in the course of fission. Agreement with the data is achieved supposing a cooling time of (60$\pm$20) $\times$ 10^{-21} s based on the neutron emission time taken from the statistical model. It is concluded that fission remains a relatively slow process up to excitation energies of about 200 MeV.

The 4π-Fragment-Spectrometer FOBOS
(Nucl. Instr. Meth. in Phys. Res. A 403 (1998) 65-97)

Ortlepp, H.-G., **W. Wagner,** C.-M. Herbach, A.A. Aleksandrov, I.A. Aleksandrova, M. Andrassy, B. Budzanowski, B. Czech, M. Danziger, L. Dietterle, V.N. Doronin, S. Dshemuchadse, A.S. Fomichev, W.D. Fromm, M. Gebhardt, P. Gippner, K. Heidel, Sh. Heinitz, H. Homeyer, S.A. Ivanovsky, D.V. Kamanin, I.V. Kolesov, M. Matthies, D. May, S.I. Merzlyakov, W. von Oertzen, Yu.Ts. Oganessian, G. Pausch, Yu.E. Penionzhkevich, Yu.V. Pyatkov, S.V. Radnev, G. Renz, L.A. Rubinskaya, I.D. Sandrev, K.D. Schilling, W. Seidel, D.I. Shishkin, A.P. Sirotin, H. Sodan, O.V. Strekalovsky, V.G. Tishchenko, V.V. Trofimov, I.P. Tsurin, C. Umlauf, D.V. Vakatov, V.M. Vasko, V.A. Vitenko, E. Will, M. Wilpert, R. Yanez, V.E. Zhuchko, P. Ziem, L. Zrodlowski

Abstract: The 4π-fragment-spectrometer FOBOS developed for heavy-ion research at beam energies of 10-100 AMeV has been commissioned for physical experiments at the Flerov Laboratory of Nuclear Reactions of the Joint Institute for Nuclear Research in Dubna. Based on the logarithmic detector principle, it is able to register charged fragments from protons up to heavy residual nuclei in a large dynamical range. Position-sensitive avalanche counters, axial ionization chambers and CsI(Tl) scintillation detectors are arranged in three concentric detectors shells. An array of phoswich detectors is used as a more granular forward detector at narrow polar angles. The modular concept of FOBOS allows for different experimental application in the field of exclusive fragment spectroscopy at medium multiplicities. For illustration, the fragment spectroscopy studies concerning the spontaneous fission process and the fragmentation of hot nuclei by means of the FOBOS set-up are considered.

High-Fold ^{117}I: Coexistence of Collective and Noncollective Structures
Phys. Rev. C 59 (1999) 1984-1998)

Paul, E.S., D.B. Fossan, K. Hauschild, I.M. Hibbert, P.J. Nolan, **H. Schnare,** J.M. Sears, I. Thorslund, R. Wadsworth, A.N. Wilson, J.N. Wilson, I. Ragnarsson

Abstract: High spin states have been populated in $^{117}_{53}$I via the ^{90}Zr(^{31}P.$2p2n$) reaction at 150 MeV, using the EUROGAM II γ-ray spectrometer to record high-fold γ-ray coincidences. A quadruples γ-ray analysis (γ^4) has been used to extend the known level scheme. In addition to several aligned noncollective states, a new high-spin band showing characteristics of smooth termination has been established at and linked into the low-spin level scheme. Its structure has been inferred through comparison with cranked Nilsson-Strutinsky calculations.

One-Loop Self Energies at Finite Temperature
(Ann. Phys. 266 (1998) 162-177)

Peshier, A., K. Schertler, M.H. Thoma

Abstract: The complete one-loop self energies (real and imaginary parts) for photons, gluons, electrons, and quarks at finite temperature are calculated numerically and compared to the results of the hard thermal loop (HTL) approximation used for the resummation technique of Braaten and Pisarski. In this way some light is shed on the validity of the weak coupling limit assumption ($g \ll 1$) or equivalently the high temperature assumption, on which the HTL approximation is based. Furthermore, the gauge dependence of the fermion self energy beyond the HTL approximation is considered. Finally the dispersion relations following from the real part of the self energies are compared to the HTL results.

Thermodynamics of the ϕ^4-Theory in Tadpole Approximation
(Europhys. Lett., 43 (1998) 381-385)

Peshier, A., B. Kämpfer, O.P. Pavlenko, G. Soff

Abstract: Relying on the Luttinger-Ward theorem we derive a thermodynamically self-consistent and scale-independent approximation of the thermodynamic potential for the scalar ϕ^4-theory in the tadpole approximation. With certain approximations the presented approach can be extended to quantum chromodynamics (QCD) and it gives support to parametrize the results of QCD lattice calculations by suitably modified ideal-gas expressions.

Flow Angle from Intermediate Mass Fragments
(Nucl. Phys. A 646 (1999) 367)

Rami, F., P. Crochet, R. Dona, B. de Schauenburg, P. Wagner, J.P. Alard, A. Andronic, Z. Basrak, N. Bastid, I. Belyaev, A. Bendarag, G. Berek, D. Best, R. Caplar, A. Devismes, P. Dupieux, M. Dzelalija, M. Eskef, Z. Fodor, A. Gobbi, Y. Grishkin, N. Herrmann, K.D. Hildenbrand, B. Hong, J. Kecskemeti, M. Kirejczyk, M. Korolija, **R. Kotte**, A. Lebedev, Y. Leifels, H. Merlitz, S. Mohren, D. Moisa, W. Neubert, D. Pelte, M. Petrovici, C. Pinkenburg, C. Plettner, W.Reisdorf, D. Schüll, Z. Seres, B. Sikora, V. Simion, K. Siwek-Wilczynska, G. Stoicea, M. Stockmeier, M. Vasiliev, K. Wisniewski, D. Wohlfarth, I. Yushmanov, A. Zhilin

Abstract: Directed sideward flow of light charged particles and intermediate mass fragments was measured in different symmetric reactions at bombarding energies from 90 to 800 AMeV. The flow parameter is found to increase with the charge of the detected fragment up to Z=3-4 and turns into saturation for heavier fragments. Guided by simple simulations of an anisotropic expanding thermal source, we show that the value at saturation can provide a good estimate of the flow angle, Θ_{flow}, in the participant region. It is found that Θ_{flow}, depends strongly on the impact parameter. The excitation function of Θ_{flow}, reveals striking deviations from the ideal hydrodynamical scaling. The data exhibit a steep rise of Θ_{flow}, to a maximum at around 250-400 AMeV, followed by a moderate decrease as the bombarding energy increases further.

Strange Mesons as Probe for Dense Nuclear Matter
(Prog. Part. Nucl. Phys. 42 (1999) 209c)

Senger, P. et al. (**KaoS** Collaboration)

Abstract: The production and propagation of kaons and antikaons has been studied in symmetric nucleus-nucleus collisions in the SIS energy range. The ratio of the excitation function of K^+ production in Au+Au and C+C collisions increases with decreasing beam energy. This effect was predicated for a soft nuclear equation-of-state. In noncentral Au+Au collisions, the K^+ mesons are preferentially emitted perpendicular to the reaction plane. The K^-/K^+ ratio from A+A collisions at beam energies which are equivalent with respect to the threshold is found to be about two orders of magnitude larger than the corresponding ratio from proton-proton collisions. Both effects are considered to be experimental signatures for a modification of kaon properties in the dense nuclear medium.

Temperatures of Exploding Nuclei
(Phys. Rev. Lett. 80 (1998) 3928-3931)

Serfling V., C. Schwarz, R. Bassini, M. Begemann-Blaich, S. Fritz, S.J. Gaff, C. Groß, G. Immé, I. Iori, U. Kleinevoß, G.J. Kunde, W.D. Kunze, U. Lynen, V. Maddalena, M. Mahi, T. Möhlenkamp, A. Moroni, W.F.J. Müller, C. Nociforo, B. Ocker, T. Odeh, F. Petruzzelli, J. Pochodzalla, G. Raciti, G. Riccobene, F.P. Romano, A. Saija, M. Schnittker, A. Schüttauf, **W. Seidel,** C. Sfienti, W. Trautmann, A. Trzcinski, G. Verde, A. Wörner, Hongfei XI, B. Zwieglinski

Abstract: Breakup temperatures in central collisions of ^{197} Au + ^{197}Au at bombarding energies E/A = 50 to 200 MeV were determined with two methods. Isotope temperatures, deduced from double ratios of hydrogen, helium, and lithium isotopic yields, increase monotonically with bombarding energy from 5 to 12 MeV, in qualitative agreement with a scenario of chemical freeze-out after adiabatic expansion. Excited-state temperatures, derived from yield ratios of states in ^{4}He, ^{5,6}Li, and ^{8}Be, are about 5 MeV, independent of projectile energy, and seem to reflect the internal temperature of fragments at their final separation from system.

Self-Consistent Pushing and Cranking Corrections to the Meson Fields of the Chiral Quark-Loop Soliton
(Int. J. Mod. Phys. E 7 (1998) 121-138)

Schleif. M., **R. Wünsch,** T. Meissner

Abstract: We study translational and spin-isospin symmetry restoration for the two-flavor chiral quark-loop soliton. Instead of a static soliton at rest we consider a boosted and rotating hedgehog soliton. Corrected classical meson fields are obtained by minimizing a corrected energy functional which has been derived by semi-classical methods (*variation after projection*). We evaluate corrected meson fields in the region 300 MeV $\leq M \leq$ 600 MeV of constituent quark masses M and compare them with the uncorrected fields. We study the effect of the corrections on various expectation values of nuclear observables such as the root-mean square radius. the axial-vector coupling constant, magnetic moments and the delta-nucleon mass splitting.

Thermodynamic Properties of the SU(2)$_f$ Chiral Quark Loop Soliton
(Eur. Phys. J. A 1 (1998) 171)

Schleif, M., **R. Wünsch**

Abstract: We consider a chiral one-loop hedgehog soliton of the bosonized SU(2)$_f$ Nambu & Jona-Lasiniomodel which is embedded in a hot medium of constituent quarks. Energy and radius of the soliton are determined in self-consistent mean-field approximation. Quasi-classical corrections to the soliton energy are derived by means of the pushing and cranking approaches. The corresponding inertial parameters are evaluated. It is shown that the inertial mass is equivalent to the total internal energy of the soliton. Corrected nucleon and isobar masses are calculated in dependence on temperature and density of the medium. As a result of the self-consistently determined internal structure of the soliton the scaling between constituent quark mass, soliton mass and radius is noticeably disturbed.

Enhanced Out-of-Plane Emission of K^+ Mesons Observed in Au + Au Collisions at 1A GeV
(Phys. Rev. Lett. 81 (1998) 1576-1579

Shin, Y., W. Ahner, R. Barth, P. Beckerle, D. Brill, M. Cieślak, **M. Dębowski, E. Grosse,** P. Koczoń, B. Kohlmeyer, M. Mang, D. Miśkowiec, C. Müntz, H. Oeschler, F. Pühlhofer, E. Schwab, R. Schicker, P. Senger, J. Speer, H. Ströbele, C. Sturm, K. Völkel, A. Wagner, W. Walus

Abstract: The azimuthal angular distribution of K^+ mesons has been measured in Au + Au collisions at 1A GeV. In peripheral and semicentral collisions, K^+ mesons are emitted preferentially perpendicular to the reaction plane. The strength of the azimuthal anisotropy of K^+ emission is comparable to the one of pions. No in-plane flow was found for K^- mesons near projectile and target rapidity

Bremsstrahlung in Intermediate-Energy Nucleon Reactions within an Effective One-Boson Exchange Model
(Nucl. Phys. A 628 (1998) 255-274)

Shklyar, V.V., **B. Kämpfer,** B.L. Reznik, A.I. Titov

Abstract: Within a covariant effective one-boson exchange model for the T matrix of NN interactions we present detailed calculations of bremsstrahlung cross sections for proton-proton and proton-neutron reactions at beam energies in the 1 GeV region. Besides pure bremsstrahlung processes we consider photons from Δ decays and contributions from $\eta \to \gamma\gamma$ process. At beam energies above 700 MeV the Δ decay channel dominates the spectra at large photon energies, where the interference between non-resonance processes and the Δ decay channel becomes also important. Low energy photons stem from pure bremsstrahlung processes. The available experimental data at 730 MeV beam energy is well described. We extrapolate the model down to 280 MeV, where more detailed experimental data exist, and find agreement with angular distributions.

Identification of Excited States in the $N = Z$ Nucleus ^{68}Se with Cluster Detectors
(Phys. Rev. C 58 (1998) R5-R9)

Skoda, S., B. Fiedler, F. Becker, J. Eberth , S. Freund, T. Steinhardt, O. Stuch, O. Thelen, H.G. Thomas, L. Käubler, J. Reif, H. Schnare, **R. Schwengner,** T. Servene, G. Winter, V. Fischer, J. Jungclaus, D. Kast, K.P. Lieb, C. Teich, C. Ender, T. Härtlein, F. Köck, D. Schwalm, P. Baumann

Abstract: A first level scheme of ^{68}Se with states up to 4.2 MeV excitation energy and tentative spins 6^+ and 7^- has been established from $\gamma\gamma\gamma$ coincidences measured with six EUROBALL Cluster detectors in close geometry. The level scheme is interpreted in comparison with neutron deficient nuclei of the $A \approx$70 region and cranking model calculations. In a similar experiment a triple coincidence between the ^{72}Kr transitions 710, 611, and 792 keV has been proven.

First Evidence of Magnetic Rotation in the $A = 80$ Region
(Phys. Rev. Lett. 82 (1999) 4408-4411)

Schnare, H., **R. Schwengner,** S. Frauendorf, F. Dönau, L. Käubler, H. Prade, A. Jungclaus, K.P. Lieb, C. Lingk, S. Skoda, J. Eberth, G. de Angelis, A. Gadea, E. Farnea, D.R. Napoli, C.A. Ur, G. Lo Bianco

Abstract: Rotational bands with strong magnetic dipole transitions have been observed in the doubly odd nuclei ^{82}Rb and ^{84}Rb. These bands show the characteristic features of magnetic rotation. They are the first evidence of this new kind of nuclear excitation in the $A \approx$ region. The results are well reproduced within the framework of the tilted axis cranking model on the basis of four-quasiparticle configurations of the type $\pi(fp)$-$\pi(g_{9/2}^2)$-$\nu(g_{9/2})$.

States of Seniority 3 and 5 in the N=48 Nucleus ^{48}Y
(Phys. Rev. C 57 (1998) 2892-2902)

Schwengner, R., J. Reif, H. Schnare, G. Winter, T. Servene, L. Käubler, H. Prade, M. Wilhelm, A. Fitzler, S. Kasemann, E. Radermacher, P. von Brentano

Abstract: Excited states of the nucleus ^{87}Y were investigated via the reaction ^{80}Se(^{11}B, $4n$) at 45 MeV. γ rays were detected with the six-detector array OSIRIS CUBE. The level scheme of ^{87}Y has been extended up to J^π=$33/2^{(-)} \approx 7$ MeV. Mean lifetimes of eight levels have been deduced using the Doppler-shift-attenuation method. The structure of ^{87}Y has been interpreted in terms

of the shell model. The calculation performed in the model space $\pi(0f_{5/2},1p_{3/2},1p_{1/2},0g_{9/2})$ well reproduce experimental excitation energies and transition strengths in ^{87}Y, especially the large $B(M1)$ values of up to 1.8 W.u. between yrast states with J >21/2. Structural differences between ^{87}Y and the isotone ^{85}Rb are discussed on the basis of the shell-model calculations.

Polarization Observables in the Reaction NN $\longrightarrow$ NN ϕ
(Phys. Rev. C 59 (1999) 999)

Titov, A.I., **B. Kämpfer,** V. V. Shklyar

Abstract: The sensitivity of polarization observables in the reaction NN NN slightly above the threshold is studied with respect to the details of the one-boson exchange model and a possible admixture of hidden strangeness in the nucleon. It is shown that the finite-energy predictions differ strongly from the threshold predictions. A measurement of the beam-target asymmetry and the decay anisotropy can help to disentangle the role of various reaction mechanisms.

Particle-Hole Induced Electric and Magnetic Rotation in ^{111}In
(Phys. Rev. C 57 (1998) 1634-1647)

Vaska, P., D.B. Fossan, D.R. LaFosse, **H. Schnare**, M.P. Waring, S.M. Mullins, G. Hackmann, D. Prévost, C. Waddington, V.P. Janzen, D. Ward, R. Wadsworth, E.S. Paul

Abstract: The high-spin structure of ^{111}In has been investigated with γ-ray spectroscopic methods using the ^{96}Zr(^{19}F,4n) reaction with thin and backed targets. A comprehensive level scheme has been constructed which exhibits interesting collective as well as novel single-particle excitations. Unambiguous evidence of proton particle-hole excitations is found for the first time in a Z <50 nucleus in the form of decoupled bands involving proton $g_{7/2}(d_{5/2})$ and $h_{11/2}$ orbitals above the Z=50 spherical shell gap. The high-spin structure of ^{111}In also involves the recently discovered magnetic rotation mechanism which is manifest as high-spin ΔI=1 bands with no signature splitting and large $B(M1)$ strengths, but only a small associated deformation.

Lowest Four-Quasiparticle Magnetic Dipole Band in ^{128}Ba
(Phys. Rev. C 56 (1998) 1338-1343)

Vogel, O., D. Dewald, P. von Brentano, J. Gableske, R. Krücken, N. Nicolay, A. Gelberg, P. Petkov, A. Gizon, J. Gizon, D. Bazzacco, C. Rossi Alvarez, S. Lunardi, P. Pavan, D.R. Napoli, **S. Frauendorf, F. Dönau**

Abstract: The four-quasiparticle magnetic dipole band in ^{128}Ba has been investigated with the ^{96}Zr(^{36}S,4n)^{128}Ba reaction at the GASP spectrometer of the Laboratori Nazionali di Legnaro. Linking transitions to the previously known positive parity states have been observed for the first time in this mass region and new transitions on top of the band have been found. The experimental results are compared to previously made tilted axis cranking calculations.

Contribution of the Massive Photon Decay Channel to Neutrino Cooling of Neutron Stars
(Journal of Exp. and Theor. Phys. 87 (1998) 211-217)

Voskresensky, D.N., E.E. Kolomeitsev, **B. Kämpfer**

Abstract: We consider massive photon decay reactions via intermediate states of electron-electron -holes and proton-proton-holes into neutrino-antineutrino pairs in the course of neutron star cooling. These reactions may become operative in hot neutron stars in the region of proton

pairing where the photon due to the Higgs-Meissner effect acquires an effective mass m_γ that is small compared to the corresponding plasma frequency. The contribution of these reactions to neutrino emissivity is calculated; it varies with the temperature and the photon mass as $T^{3/2}m^{7/2}$ exp(-m_γ/T) for T < m_γ. Estimates show that these processes appear as extra efficient cooling channels of neutron stars at temperatures T $\simeq 10^9$-10^{10} K.

Evidence for Different Freeze-Out Radii of High- and Low-Energy Pions Emitted in Au+Au Collisions at 1 A·GeV
(Phys.Lett. B 420 (1998) 20-24)

Wagner, A., C. Müntz, H. Oeschler, C. Sturm, R. Barth, M. Cieślak, M. Dębowski, E. Grosse, P. Koczoń, M. Mang, D. Miśkowiec, R. Schicker, E. Schwab, P. Senger. P. Beckerle, D. Brill, Y. Shin, H. Ströbel, W. Waluś, B. Kohlmeyer, F. Pühlhofer, J. Speer, K. Völkel

Abstract: Double differential production cross sections of π^- and π^+ mesons and the number of participating protons have been measured in central Au+Au collisions at 1 A·GeV. At low pion energies the π^- yield is strongly enhanced over the π^+ yield. The energy dependence of the π^-/π^+ ratio is assigned to the Coulomb interaction of the charged pions with the protons in the reaction zone. The deduced Coulomb potential increases with increasing pion c.m. energy. This behavior indicates different freeze-out radii for different pion energies in the c.m. frame.

Detailed Angular Correlation Analysis with 4π Spectrometers: Spin Determinations and Multipolarity Mixing Measurements in ^{128}Ba
(Phys. Rev. C 58 (1998) 721-728)

Wiedenhöver, I., O. Vogel, H. Klein, A. Dewald, P. von Brentano, J. Gableske, R. Krücken, N. Nicolay, A. Gelberg, P. Petkov, A. Gizon, J. Gizon, D. Bazzacco, C. Rossi Alvarez, G. de Angelis, S. Lunardi, P. Pavan, D.R. Napoli, S. Frauendorf, **F. Dönau,** R.V.F. Janssens, M.P. Carpenter

Abstract: We analyze for the first time the full $\gamma\gamma$ directional correlations from oriented states (DCO) in an experiment performed with the GASP detector array. Our analysis based on a transformation of the directional information into expansion coefficients of an orthogonal basis. With this method, which we call SpeeDCO (spectral expansion of DCO), the complete DCO information is concentrated in 12 $\gamma\gamma$ coincidence spectra. The analysis is applicable to all detector arrays which uniformly cover the solid angle. We show that the complete DCO information can be used for a reliable and unique determination of spins and multipolarity mixing ratios in weakly populated bands. We were able to establish the spins and the positive parity of the Δ I=1 "$M1$ band" in ^{128}Ba and multipolarity mixing ratios of $M1/E2$ in-band transitions were derived as well. The measured values are in good agreement with those expected for a high-K rotational band.

Thermal Particle Production at SIS
(Prog. Part. Nucl. Phys. 42 (1999) 157c)

Wolf, Gy., **H.W. Barz, B. Kämpfer**

Abstract: In a transport model calculation we study some of the basic assumptions of thermal models. We find at SIS energies the particles are mainly produced in a highly non-equilibrium situation. At freeze-out only nucleons are thermalized.

Conference Contributions
Laboratory Reports and Patents

Andronenko, L.N., M.N. Andronenko, D.M. Selivestrov, **W. Neubert**:
Measurement of Fragment Production Cross Sections in 1 GeV Proton Interactions with Carbon
Preprint PNPI NP-3-1998

Auberger, T., M. Benedikt, P. Bryant, A. Colotto, **W. Enghardt**, D. Georg, E. Griesmayer, R. Hartl, U. Haverkamp, E. Hensler, H.G. Löw, A. Maier, H. Pernegger, K. Plojanc, F. Primik, H. Rabitsch, H. Rahim, T. Rauth, M. Regler, S. Reimoser, N. Schreuder, H. Schönauer, U. Wolff:
Med-AUSTRON - Machbarkeitsstudie, Band II: Der Med-AUSTRON-Beschleuniger ein europäisches Konzept zur Protonen- und Ionentherapie - Aspekte der Beschleunigerphysik und der Medizinphysik
Wiener Neustadt, Dec. 1998

Barz, H.W., J.P. Bondorf, J.J. Gaardhoje, H. Heiselberg:
Coulomb Effects on Particle Spectra in Relativistic Nuclear Collisions
Preprint NORDITA-98/18 NP

Barz, H.W., J.P. Bondorf, J.J. Gaardhoje:
Coulomb Mean Field Effects in Relativistic Heavy-Ion Reactions on One- and Two-Particle Spectra
Verhandl. DPG (VI), 33, 447 (1998)

Barz, H.W.:
Combined Effect of Nuclear Coulomb field and radial Flow on Two-Pion Correlations
Proc. of CHRIS'98 - 2nd Catania Relativistic Ion Studies, Acicastello, Italy, June 8-12, 1998, in print

Barz, H.W.:
Combined Effects of Nuclear Coulomb Field, Radial Flow, and Opaqueness on Two-Pion Correlations
e-Print archive, nucl-th/9808027

Barz, H.W.:
Coulomb Effects in Pion Interferometry
Proc. Int Workshop "Nonequilibrium Physics at Short Time Scales"
Morawetz, P. Lipavsky, V. Spicka, Rostock 1998, p. 128

Barz, H.W., R. Kotte:
Excitation Energies of Clusters from Light Fragment Correlations
Proceedings of the International Workshop XXVII on Gross Properties of Nuclei and Nuclear Excitations Hirschegg, Austria, January 17-23, 1999

Beinker, M.W., B. Kämpfer, G. Soff:
Estimates of Production Rates of SUSY Particles in Ultra-Relativistic Heavy-Ion Collisions
FZR-213 (1998)

Borchert, G. A.K. Kacharava, V.I. Komarov, A.V. Kulikov, M.S. Nioradze, G.G. Macharasgvili, **H. Müller**, A. Yu. Petrus, S.V. Yaschenko
Feasibility to Study the Inclusive Production of Fast Nuclear Fragments At ANKE Spectrometer, Dubna E1-98-342

Böhm, A., K.-Th. Brinkmann, **S. Dshemuchadse,** J.S. Lange, H. Freiesleben, P. Herrmann, B. Hübner, E. Kuhlmann, P. Michel, K. Möller, A. Schamlott, P. Schönmeier, A. Schülke, M. Steinke, G.Y. Sun, M. Würschig-Pörsel, U. Zielinski:
Performance of the Barrel-Detector for the COSY-TOF-Spectrometer
Verhandl. DPG (VI), 33, 497 (1998)

Borcan, R., R. Schwengner, H. Schnare, L. Käubler, T. Servene, M. Wilhelm, A. Fitzler, S. Kasemann, E. Rademacher, P. Brentano:
Particle Excitations in the N=49 Nuclei ^{88}Y and ^{87}Sr
Verhandl. DPG (VI), 33, 452 (1998)

Clark, R.M. S.J. Aszatalos, B. Busse, C. Chirara, M. Cromaz, M.A. Deleplaneque, R.M. Diamond, P. Fallon, D.B. Fossan D.G. Jenkins, S. Juutinen, N. Kelsall, R. Krucken, G. Lane, I.Y. Lee, A.O. Macchiavelli, R.W. MacLeod, G. Schmid, J. Sears, J. Smith, F.S. Stephens, K. Vetter, R. Wadsworth, **S. Frauendorf:**
The Shears Mechanism in the A $\sim$ 110 Region
Contrib. Nuclear Structure 98, Gatlinburg, p. 146 (1998)

Debus, J., M. Wannenmacher, D. Ertner, M. Fuss, P. Heeg, F. Wenz, H. zur Hausen, R. Bendel, T. Bortfeld, G. Hartmann, O. Jäkel, C.P.Karger, A. Kriessbach, C. Lappe, M. Massimino, U. Ölfke, W. Schlegel, H.J. Specht, N. Angert, W. Badura, W. Becher, D. Böhne, H. Brand, C. Brusasco, A. Dolinskij, H. Eickhoff, H.G. Essel, B. Franzcak, O. Geiss, Th. Haberer, J. Hoffmann, M. Krämer, G. Kraft, W. Kraft-Weyrather, U. Krause, N. Kurz, B. Langenbeck, W. Ott, M. Pavlovic, K. Poppensieker, M. Richter, D. Schardt, A. Schempp, B. Schlitt, M. Scholz, P. Spiller, R. Steiner, H. Stelzer, B. Voss, U. Weber, F. Pobell, **W. Enghardt**, B. Hasch, R. Hinz, K. Lauckner, J. Pawelke, M. Sobiella:
Proposal for a Dedicated Ion Beam Facility for Cancer Therapy
Radiologische Universitätsklinik Heidelberg, DKFZ Heidelberg, GSI Darmstadt in cooperation with FZ Rossendorf, Sept. 1998

Dohrmann, F., W. Enghardt, C. Garabatos, E. Grosse, C. Muentz, W. Karig M. Sobiella, H. Stelzer, J. Stroth, J. Wuestenfeld P. Zumbruch:
A Low-Mass Drift Chamber System for the HADES-Spectrometer: Status Report
Verhandl. DPG (VI), 33, 471 (1998)

Dohrmann, F., K. Bethge, W. Enghardt O. Fateev, C. Garabatos, E. Grosse, C. Müntz, W. Karig, W. Koenig, L. Smykov, M. Sobiella, A. Steigerwald, H. Stelzer, J. Stroth, J. Wüstenfeld, Y. Zanewsky, A. Zentek
A Low-Mass Drift Chamber System for the Hades-Spectrometer
Conference MESON'98, Cracow, Poland, May 26-June 2, 1998

Dohrmann, F., E. Grosse, B. Kämpfer:
Seltsame Kaonen, hadronische Materie und kosmische Phasenübergänge
FZR-Jahresbericht 1998 (1999)

Dönau, F.:
Elementare Kernanregungen
Phys. Bätter H. 2 (1998)

Dönau, F.:
Medium-Mass Nuclei
Miniworkshop, FZ-Rossendorf, February 25-26, 1999

Enders. J., P. von Brentano, J. Eberth, A. Fitzler, C. Fransen, R.-D. Herzberg, H. Kaiser, L. Käubler, P. von Neumann-Cosel, N. Pietralla, V.Yu. Ponomarev, H. Prade, A. Richter, H. Schnare, **R. Schwengner**, S. Skoda, H.G. Thomas, H. Tiesler, D. Weisshaar, I. Wiedenhöver, A. Zilges:
Photon Scattering Off ^{204,206,208}Pb up to 6.5 MeV
Verhandl. DPG (VI), 33, 502 (1998)

Enghardt, W., J. Debus, T. Haberer, B.G. Hasch, R. Hinz, O. Jäkel, M. Krämer, K. Lauckner, J. Pawelke:
Positron Emission Tomography for Quality Assurance of Cancer Therapy with Light-Ion Beams
Verhandl. DPG (VI), 33, 510 (1998)

Enghardt, W., J. Debus, T. Haberer, B.G. Hasch, R. Hinz, O. Jäkel, M. Krämer, K. Lauckner, J. Pawelke:
Positron Emission Tomography for Quality Assurance of Cancer Therapy with Light-Ion Beams
International Nucl. Phys. Conference, Aug. 1998, Paris France, Book of Abstracts, p. 823

Enghardt, W., T. Haberer, R. Hinz, O. Jäkel, M. Krämer, K. Lauckner, J. Pawelke, M. Sobiella:
Positronen Emissions Tomographie für die Qualitätskontrolle der Strahlentherapie mit ^{12}C-Ionen;
Med. Physik 1998, Tagungsband der 29. Wissenschaftlichen Tagung der Deutschen Gesellschaft für Medizinische Physik e.V., p. 126

Enghardt, W., F. Gabriel, P. Gippner, E. Grosse, H. Guratzsch, D. Janssen, P. Michel, U. Nething, W. Neubert, H. Prade, K.D. Schilling, R. Schwengner, W. Seidel, U. Steegmüller, P. vom Stein, **W. Wagner,** M. Wenzel, A. Wolf, R. Wünsch:
Poster-contribution presented at the International Workshop on Radiation Physics with Relativistic Electrons
Tabarz, Germany, June 9-12, 1998

Enghardt, W., T. Haberer, B. Hasch, R. Hinz, O. Jäkel, M. Krämer, K. Lauckner, J. Pawelke, M. Sobiella:
Positronen Emissions Tomographie für die Qualitätskontrolle der Strahlentherapie mit ^{12}C-Ionen
29. Tagung der Deutschen Gesellschaft. für Med. Phys. Dresden 14.-17. Oktober 1998

Enghardt, W., F. Gabriel, P. Gippner, E. Grosse, H. Guratzsch, D. Janssen, P. Michel, U. Nething, W. Neubert, H. Prade, **K.D. Schilling**, R. Schwengner, W. Seidel, U. Steegmüller, P. vom Stein, W. Wagner, M. Wenzel, A. Wolf, R. Wünsch:
The Elbe Radiation Source Project
Int. Conference, Warszawa, Poland, June 30-July 4, 1998

Enghardt, W., U. Lehnert, B. Naumann, W. Neubert, J. Pawelke, H. Prade, W. Wagner:
Quasi-Monochromatic X-Rays from the ELBE Radiation Source
18th Int. Conf. on X-ray and Shell Processes, Chicago, Aug. 1999

Frauendorf, S.
Mesoskopische Quanteneffekte in Atomkernen
Jahresbericht 1997, FZ Rossendorf, 36-42 (1998)

Frauendorf, S.
Magnetic Rotation
Workshop on Physics at the Coulombbarrier, Yale University, USA, June, 9 - 11, 1999

Frauendorf, S.
Isospin Symmetry Breaking by T=1 p-n Pairing
Gordon Research Conference on Nuclear Chemistry, New London, USA, June, 13 - 18, 1999

Frauendorf, S.
Isospin Symmetry Breaking by T=1 Pairing
International Conference on Achievements and Perspectives in Nuclear Structure, Crete, Greece, July 1999

Fransen, C., R.-D. Herzberg, P. von Brentano, J. Eberth, J. Enders, A. Fitzler, H. Kaiser, L. Käubler, P. von Neumann-Cosel, N. Pietralla, H. Prade, A. Richter, H. Schnare, **R. Schwengner**, O. Thelen, H.G. Thomas, H. Tiesler, D. Weisshaar, I. Wiedenhöver, A. Zilges:
Dipole Excitations in ^{138}Ba Studied in Photon Scattering Experiments with Two Cluster Detectors
Verhandl. DPG (VI), 33, 475 (1998)

Fritz, S., C. Schwarz, R. Bassini M. Begemann,-Blaich, S.J. Gaff-Ejakov, D. Gourio, C. Groß, G. Imme, I. Iori, U. Kleinevoß, G.J. Kunde, W.D. Kunze, U. Lynen, V. Maddalena, M. Mahi, T. Möhlenkamp, A. Moroni, W.F.J. Müller, C. Nociforo, B. Ocker, T. Odeh, F. Petruzzelli, J. Pochodzalla, G. Raciti, G. Riccobene, F.P. Romano, A. Saija, M. Schnittker, A. Schüttauf. **W. Seidel,** V. Serfling, C. Sfienti, W. Trautmann, A. Trzcinski, G. Verde, A. Wörner
Breakup Density in Spectator Fragmentation
GSI-Preprint-99-17, June 1999

Gabriel, F. P. Gippner, **E. Grosse,** D. Janssen, P. Michel, P. Prade, A. Schamlott, W. Seidel, U. Steegmüller, M. Wenzel, A. Wolf, R. Wünsch, and the ELBE-Crew
The FEL Projects at the Rossendorf Radiation Source ELBE
Proc. 20^{th} Int. Conf. On Free Electron Lasers, Williamsburg, USA, Aug. 1998

Gallmeister, K., B. Kämpfer, O.P. Pavlenko:
Can One Discriminate the Thermal Dilepton Signal against the Open Charm and Bottom Decay Background in Ultrarelativistic Heavy-Ion Collisions?
FZR-235 (1998)

Gallmeister, K., B. Kämpfer, O.P. Pavlenko:
Dileptons from Open Charm and Bottom: Signal or Background in High-Energy Heavy-Ions Collisions?
Verhandl. DPG (VI), 33, 505 (1998)

Gallmeister, K., B. Kämpfer:
Dileptons and Charm & Bottom in Relativistic Heavy-Ion Collisions

Proc. XXXVII Int. Winter Meeting on Nucl. Phys., (Ed.) I. Iori, 1999, p. 139

Gippner, P.:
Strahlführung zum MIR-FEL Projekt Strahlungsquelle ELBE
Maschinentechn. Konzept (Design Report), 1998

Grosse, E.:
In-Medium Properties of Kaons and Antikaons as Studied by Threshold Production in Nuclear Collisions
INPC, Paris 1998

Grosse, E., B. Kämpfer:
2^{nd} Workshop on Kaon Production
FZR-249 (1999)

Grosse, E., B. Kämpfer:
Mini-Workshop "Electromagnetic Radiation off Colliding Hadron Systems: Dileptons and Bremsstrahlung"
FZR-258 (1999)

Herzberg, R.-D., J. Bryssinck, L. Govor, D. Belic, F. Bauwens, O. Beck, P. von Brentano, D. de Frenne, J. Eberth, T. Eckert, J. Enders, A. Fitzler, C. Fransen, K. Govaert, E. Jacobs, L. Käubler, H. Kaiser, U. Kneissl, A. Linnemann, H. Maser, P. Matschinsky, P. von Neumann-Cosel, A. Nord, N. Pietralla, H.H. Pitz, V.Yu. Ponomarev, H. Prade, E. Rademacher, A. Richter, H. Schnare, **R. Schwengner,** O. Thelen, H.G. Thomas, H. Tiesler, V. Werner, D. Weisshaar, I. Wiedenhöver M. Wilhelm, A. Zilges:
Electric Dipole Excitations in Semi Magic Nuclei Studied in Photon Scattering Experiments
Verhandl. DPG (VI), 33, 511 (1998)

Hinz, R., J. Debus, W. Enghardt, T. Haberer, B. Hasch, O. Jäkel, K. Lauckner, M. Krämer, J. Pawelke, M. Sobiella:
Simultaneous Control of the Radiation Therapy with Heavy Ions by Positron Emission Tomography
1998 IEEE Medical Imaging Conference, Nov. 12-14, 1998, Toronto, Canada

Hinz, R., W. Enghardt, B.G. Hasch, K. Lauckner, J. Pawelke, M. Sobiella, R. Freyer
Simultankontrolle der Strahlentherapie mit Schwerionen durch Positronen-Emissions-Tomographie
Biomedizinische Technik 43/1 (1998) 28

Iwasa, N., F. Boue, G. Surowka, T. Baumann, B. Blank, S. Czajkowski, A. Förster, M. Gai, H. Geissel, **E. Grosse,** M. Hellström P. Koczon, B. Kohlmeyer, R. Kulessa, F. Lane, J. Speer, T. Motobayashi, H. Oeschler, A. Ozawa, M.S. Pravikoff, E. Schwab, W. Schwab, P. Senger, K. Sümmerer, C. Sturm, W. Walus, A. Surowiec, T. Teranishi, F. Uhlig, A. Wagner:
Coulomb Dissociation of ^{8}B at 254 A MeV
Verhandl. DPG (VI), 33, 480 (1998)

Jokinen, A., J. Aysto, R. Borcea, P. Dendooven, M. Gierlik, M. Gorska, H. Grawe, M. Hellstrom, M. Karny, Z. Janas, R. Kirchner, M. La Commara, P. Mayet, A. Nieminen, H. Penttila, A. Plochocki, M. Rejmund, E. Roeckl, M. Sawicka, C. Schlegel, K. Schmidt, **R.**

Schwengner:
Beta Decay of ^{57}Zn
GSI 99-1, p.18 (1999)

Kamanin, D.V., C.-M. Herbach, H.-G. Ortlepp, K.D. Schilling, V.G. Tichtchenko, W. Wagner, R. Yanez:
Light Charged Particles Accompanying ^{14}N (34 and 53 AMeV) and ^{40}Ar (38 AMeV) Induced Fission
Verhandl. DPG (VI), 33, 478 (1998)

Kaiser, H., P. von Brentano, J. Eberth, J. Enders, A. Fitzler, C. Fransen, R.-D. Herzberg, L. Käubler, H. Lenske, P. von Neumann-Cosel, N. Pietralla, H. Prade, A. Richter, H. Schnare, **R. Schwengner**, S. Skoda, H.G. Thomas, H. Tiesler, D. Weisshaar, I. Wiedenhöver, A. Zilges:
Inelastic Photon Scattering Off the Semi-Magic Nucleus ^{51}V
Verhandl. DPG (VI), 33, 440 (1998)

Kaptari, L.P., **B. Kämpfer,** S.M. Dorkin, S.S. Semikh:
Pion Exchange Effects in Elastic Backward Proton-Deuteron Scattering
FZR-246 Jan. 1999

B. Kämpfer, K. Gallmeister, O.P. Pavlenko:
Thermal Dilepton Signal and Dileptons from Correlated Open Charm and Bottom Decays in Ultrarelativistic Heavy-Ion Collisions
Proceedings of the 14th Wintershop on Nuclear Dynamics, held January 31 - February 7, 1998, in Snowbird, Utah

B. Kämpfer:
Kaon Workshop, FZ-Rossendorf, December 10 - 11, 1998

B. Kämpfer, O.P. Pavlenko:
On the Ter-Mikaelian and Landau-Pomeranchuk Effects for Induced Gluon Radiation in a QCD Medium
hep-ph/9906248

B. Kämpfer:
Medium Mass Nuclei - their Properties and their Importance
Workshop, FZ-Rossendorf, Febr. 25.26, 1999

B. Kämpfer:
Electromagnetic Radiation off Colliding Hadron Systems: Dileptons & Bremsstrahlung:
Miniworkshop, FZ-Rossendorf, April 16-17, 1999

Käubler, L., P. von Brentano, J. Eberth, J. Enders, A. Fitzler, M. Grinberg, E. Grosse, R.-D. Herzberg, H. Kaiser, P. von Neumann-Cosel, N. Pietralla, H. Prade, A. Richter, Schnare, R. Schwengner, Ch. Stoyanov, H.G. Thomas, H. Tiesler, D. Weisshaar, I. Wiedenhöver, A. Zilges:
Two and Three-Phonon States in ^{88}Sr
Verhandl. DPG (VI), 33, 453 (1998)

Kotte, R.:
Proton-Proton Correlations in Central Heavy-Ion Collisions at SIS Energies and the Space-Time Extent of the Emission Source
CRIS'98, 2nd Catania Relativistic Ion Studies, Measuring the Size of Things in the Universe: HBT Interferometry and Heavy Ion Physics
Acicastello, Italy, June 1998, to be published in World Scientific, Singapore

Kotte, R., H.W. Barz:
On the Sequence of Proton and Composite Particle Emission in Central Collisions of Ru(Zr)+Ru(Zr) at 400 A·MeV
Proceedings of the International Workshop XXVII on Gross Properties of Nuclei and Nuclear Excitations Hirschegg, Austria, January 17-23, 1999

Lane, G.J., D.B. Fossan, C.J. Chiara, **H. Schnare,** J.M. Sears, J.F. Smith, I. Thorslund, P. Vaska, E.S. Paul, A.N. Wilson, J.N. Wilson, K. Hauschild, I.M. Hibbert, R. Wadsworth, A.V. Afanasjev, I. Ragnarsson:
Smooth Band Termination in the A = 110 Region: Recent Results for ^{112}Sb
Contrib. Nuclear Structure '98, Gatlinburg, p.74 (1998)

Lauckner, K., W. Enghardt, R. Hinz, J. Pawelke:
Fully 3D PET Image Reconstruction for a Spatially-Varying System Response and Very low Counting Statistics
IEEE Medical Imaging Conference, November 2-14, 1998. Toronto, Canada

Lauckner, K., W. Enghardt, R. Hinz, R. Freyer:
Ein 3D MLE-Algorithmus für die Positronen-Emissions-Tomographie während der Strahlentherapie mit Schwerionen
Biomedizinische Technik 43/1 (1998) 28

Naumann, B., W. Neubert, D. Pröhl:
Entwicklung von Strahlfängern für maximale Elektronenenergie am Beschleuniger ELBE
FZR-267, July 1999

Novak, J.R., C. W. Beausang, N. Amzal, R.F. Casten, G. Cata Danil, J.F. C. Cocks, J.R. Cooper, P.T. Greenlees, F. Hannachi, K. Helariutta, P. Jones, R. Julin, S. Juutinen, H. Kankaanpaa, H. Kettunen, R. Kruecken, P. Kuusiniemi, M. Leino, B. Liu, M. Muikku, A. Savelius, T.J. Thomas, N.V. Zamfir, J.-Y. Zhang, **S. Frauendorf**:
High Spin States in ^{205}Rn: A New Magnetic Rotor
JYFL Ann. Rep. 1998, p.34 (1999)

Pawelke, J.:
Positronen-Emissions-Tomographie zur in-situ Kontrolle der Tumorbehandlung mit Strahlen schwerer Ionen
Mitteilungen aus der Wissenschaftsgemeinschaft Gottfried Wilhelm Leibnitz, WGL Journal 2/1998, 12

Pawelke, J.:
Interview with a Foreign Researcher
Rad. Sci 41 (1998) 524

Pawelke, J., W. Enghardt, B.G. Hasch, R.Hinz, K. Lauckner, K. Yoshikawa, T. Tomitani, M. Kanazawa, T. Kanai, H. Tsuji:
Comparison between the In-Beam and the Out-Of-Beam Methods for PET Control of Carbon Ion Therapy
Oncol. 51/1 (1999) S7

Peshier, A., B. Kämpfer, O.P. Pavlenko, G. Soff:
The Equation of State of the Quark-Gluon Plasma
Verhandl. DPG (VI), 33, 506 (1998)

Peshier, A., B. Kämpfer, O.P. Pavlenko, G. Soff:
Thermodynamics of the ϕ^4 Theory in Tadpole Approximation
FZR-208 (1998)

Peshier, A.:
Quasiparticle Description of Strongly Coupled Plasma
Proc. 5th Int. Workshop on Thermal Field Theories and Their Applications
Regensburg, Aug. 1998 , hep-ph/9809379

Peshier, A., B. Kämpfer, G. Soff:
Thermodynamics of Deconfined Matter at Finite Chemical Potential in a Quasiparticle Description
hep-ph/9906305

Peshier, A., M.H. Thoma:
Quark Dispersion Relation and Dilepton Production in the Quark-Gluon Plasma
hep-ph/9907268

Peshier, A., B. Kämpfer:
Quasiparticle Description of Deconfined Matter at Finite mu and T
Proceedings of ECT* International Workshop on Understanding Deconfinement in QCD, Trento, Italy, 1-13 Mar 1999, hep- ph/9906258

Pönisch, F., J. Debus, W. Enghardt, T. Haberer, B.G. Hasch, R. Hinz, O. Jäkel, M. Krämer, K. Lauckner, J. Pawelke, K. Poppensieker:
PET bei der Krebstherapie mit ^{12}C-Strahlen: Resultate der ersten klinischen Anwendungen
Verhandl. DPG (VI), 34, 114 (1999)

Prade, H. L. Käubler, R. Schwengner:
Das Zyklotron K-120 - langjährige Basis der Rossendorfer Kernstrukturforschung
FZR-234, 1-12 (1998)

Pyatkov, Yu.V., A.A. Alexandrova, V.V. Pashkevich, Yu.E. Penionzhkevich, V.G. Tishenko, A.V. Unzhakova, V. A. Maslov, I.P. Tsurin, H.-G. Ortlepp, P. Gippner, C.-M. Herbach, K.D. Schilling, **W. Wagner,** B.I. Mitsofanov:
The Two-Sn Mode Observed in Cold Fission of Cm and Cf Isotopes
VI. Intern. School-Seminar on the Heavy Ion Physics, Dubna, Russia, World Scientific 1998, p 720-723, ed. by Yu.Ts. Oganessian and R. Kalpakchia

Rami, F. et al. (**FOPI** Collaboration):
Isospin Tracing: a Probe of Nonequilibrium in Central Heavy-Ion Collisions

Schnare, H., R. Schwengner, S. Frauendorf, F. Dönau, L. Käubler, H. Prade, E. Grosse, A. Jungclaus, K.P. Lieb, C. Lingk, S. Skoda, J. Eberth, G.de Angelis, A. Gadea, E. Farnea, C.A. Ur, G.Lo Bianco:
Magnetic Dipole Bands in ^{82}Rb,^{83}Rb and ^{84}Rb
Contrib. Nuclear Structure '98, Gatlinburg, p.117 (1998)

Schnare, H.:
Magnetic Rotation in the Odd-Odd Nuclei ^{82,84}Rb
Proc. 1st Int. Conf. on Experimental Nucl. Physics in Europe, Sevilla, Publ. by American Inst. of Physics, 1999

Seidel, W.
MIR-FEL an Elbe, Projekt Strahlungsquelle ELBE
Maschinentechn. Konzept (Design Report), 1998

Seidel, W.
Production of Terahertz Radiation at ELBE
Meeting about Characterization of Biological System with Far Infrared and Terahertz Radiation, ENEA-Frascati, Italy, May 1999

Skoda, S., B. Fiedler, F. Becker, J. Eberth, S. Freund, T. Steinhardt, O. Stuch, O. Thelen, H.G. Thomas, L. Käubler, J. Reif, H. Schnare, **R. Schwengner,** T. Servene, G. Winter, V. Fischer, A. Jungclaus, D. Kast, K.P. Lieb, C. Teich, C. Ender, T. Hartlein, F. Kock, D. Schwalm, P. Baumann:
Identification of Excited States in ^{68}Se with a EUROBALL Cluster Detector CUBE
Contrib. Nuclear Structure '98, Gatlinburg, p.123 (1998)

Schwengner, R., H. Schnare, S. Frauendorf, L. Käubler, F. Dönau, H. Prade, E. Grosse, A. Jungclaus, K.P. Lieb, Ch. Lingk, S. Skoda, J. Eberth, G. de Angelis, A. Gadea, E. Farnea, C.A. Ur, G. lo Bianco:
Magnetic Dipole Bands in ^{82}Rb,^{83}Rb and ^{84}Rb
Verhandl. DPG (VI), 33, 452 (1998)

Schwengner, R.:
Magnetic Dipole Bands in ^{82}Rb, ^{83}Rb and ^{84}Rb
2nd International Conference on Exotic Nuclei and Atomic Masses,
Bellaire, Michigan, USA, 23.6. - 27.6. 1998, Poster

Schwengner, R., H. Schnare, S. Frauendorf, F. Dönau, L. Käubler, H. Prade, A. Jungclaus, K.P. Lieb, C. Lingk, S. Skoda, J. Eberth, G. de Angelis, A. Gadea, E. Farnea, D.R. Napoli, C.A. Ur, G. Lo Bianco.
Study of Magnetic Rotation in ^{82}Rb, ^{83}Rb and ^{84}Rb within the TAC Model
LNL-INFN 139/99, (Ann. Rep. Legnaro 1998), p. 19

Tichtchenko, V.G., **C.-M. Herbach,** H.-G. Ortlepp, P. Gippner, D.V. Kamanin, Yu.E. Penionzhkevich, K.D. Schilling, W. Wagner:
Mass-Symmetric Tripartition Studied in the Reactions ^{40}Ar(36 AMeV) + ^{248}Cm and ^{232}Th
Verhandl. DPG (VI), 33, 478 (1998)

Venkova, Ts., R.M. Lieder, St. Utzelmann, W. Gast, H. Schnare, G.V. Marti, K. Spohr, P. Hoernes, A. Georgiev, D. Bazzacco, R. Menegazzo, C. Rossi-Alvarez, G. de Angelis, R. Kaczarowski, T. Rzaca-Urban, T. Morek, K.H. Maier **S. Frauendorf:**
Beobachtung einer $\nu h_{9/2}$ Bandenkreuzung in ^{180}Os
Verhandl. DPG (VI), 33, 501 (1998)

Wadsworth, R., I.M. Hibbert, D. Jenkins, N. Kelsall, C.M. Parry, D.B. Fossan, G.J. Lane, J.M. Sears, J.F. Smith, R.M. Clark, R. Krucken, I.Y. Lee, A.O. Macchiavelli, V.P. Janzen, J. Cameron, S. Juutinen, **S. Frauendorf**:
Magnetic Rotation in the A $\sim$ 108 Mass Region
Contrib. Nuclear Structure '98, Gatlinburg, p.146 (1998)

Patent:

Haberer, T. M. Krämer u.a.
J. Pawelke, R. Hinz, W. Enghardt.

Ion Beam Therapy System and a Method for operating the System
Europäische Patentanmeldung 98117256.-2-2-2208, 11. Sept. 1998

Theses

Habilitations

F.-M. Dittes
The decay of quantum systems with a small number of open channels
TU Dresden, 1998

PhD - Theses

K. Lauckner
Entwicklung eines iterativen 3D Rekonstruktionsverfahrens für die Kontrolle der Tumorbehandlung mit Schwerionen mittels der Positronen-Emissions-Tomographie
FZ Rossendorf, FZR-264, 1998

A. Peshier
Zur Zustandsgleichung stark-wechselwirkender Materie
FZ Rossendorf, FZR-239, 1998

C. Plettner
Strangenessproduktion bei kleinen transversalen Impulsen und mittleren Rapiditäten an der Reaktion Ru+Au bei 1.69 AGeV
TU Dresden, 1998

M. Schleif
Solitonische Feldkonfigurationen des NJL-Modells im Medium
FZ Rossendorf, FZR-211, 1998

T. Servene
Magnetische und kollektive Rotation im N=44 Kern ^{79}Br
TU Dresden, 1998

Lectures and Seminars

Almehed, D.:
High K Rotational Bands Described with Tilted Axis Cranking and Particle Number Projection; IKH/FZ Rossendorf, June 1998

Almehed, D.:
High K Rotation Bands Described with Tilted Axis Cranking and Particle Number Projection
Seminar on Balkan Nucl. Phys. School, Istanbul, Sept. 1998

Almehed, D.:
RPA Correlation Energy in Nuclear Physics
Seminar, TU Dresden, Febr. 1999

Almehed, D.:
RPA Correlation Energy Calculations
Int. Miniworkshop on Medium Mass Nuclei, FZ Rossendorf, Febr. 1999

Almehed, D.:
Tilted Axis Cranking with Particle Number Projection
DPG Frühjahrstagung, Freiburg, March 1999

Almehed, D.:
RPA Correlation Energy Calculations in Rotating Nuclei
Int. Workshop on Collective Excitations in Nuclei and other Finite Fermi Systems, JINR Dubna, June 1999

Barz, H.W.:
Relativistische Streu- und Reaktionstheorie
Course, TU Dresden, WS 1998/99

Barz, H.W.:
Coulomb Effects in Pion Interferometry
V. Workshop on Nonequilibrium Physics at Short time Scales, Rostock, April 27-30, 1998

Barz, H.W.:
Excitation Energies of Cluster from Light Fragment Correlations
Int. Workshop XXVII on Gross Properties of Nuclei and Nuclear Excitations
Hirschegg, Jan. 1999

Barz, H.W.:
Raum-Zeit-Folge der Bildung leichter Fragmente in Schwerionenreaktionen
DPG Freiburg, March 1999

Barz, H.W.:
Relativistische Schwerionenreaktionen
TU Dresden, March-May 1999

Barz, H.W.:
Coulomb Mean Field Effects in Relativistic Heavy-Ion Reactions on One- and Two-Particle Spectra
Nuclear Physics Spring Meeting, Bochum, Germany, March 16-20, 1998

Barz, H.W.:
Combined Effect of Nuclear Coulomb field and radial Flow on Two-Meson Correlations
CRIS98-2nd Catania Relativistic Ion Studies, Acicastello, Italy, June 8-12, 1998

Borcan, C.:
Particle Excitations in N=49 Nuclei ^{88}Y and ^{87}Sr
DPG Frühjahrstagung, Bochum, March 1998

Borcan, C.:
Spectroscopy of the N=Z Nucleus ^{70}Br
Int. Miniworkshop on Medium Mass Nuclei , FZ Rossendorf, Febr. 1999

Borcan, C.:
First Identification of Excited States in the N=Z Nucleus ^{70}Br
1^{st} Int. Conf. On Experimental Nucl. Phys. in Europe, Sevilla, June 1999

Debowski, M.:
Medium Effects in Kaon and Anti-Kaon Production in Nuclear Collisions
Bormio, Winter Meeting 1999

Dittes, F.-M.:
Intensive Channeling-Strahlung an ELBE (Theorie);
IKH/FZ Rossendorf, Feb. 1998

Dohrmann, F.:
Drell-Yan Mechanism, HADES Collaboration Meeting
Krakow, Poland, Febr. 20, 1998

Dohrmann, F.:
HADES MDC III at FZR - Status Report, HADES Collaboration Meeting
Krakow, Poland, Febr. 20 1998

Dohrmann, F.:
Bericht über HADES-Arbeitstreffen in Krakau;
IKH/FZ Rossendorf, March 1998

Dohrmann, F.:
A Low-Mass Drift Chamber System for the HADES Spectrometer: Status Report;
DPG, Bochum, March 1998

Dohrmann, F.:
Das neue Dileptonen-Spectrometer HADES am SIS;
Institutsseminar TU Dresden, May 1998

Dohrmann, F.:
A Low-mass Tracking System for the HADES-Spectrometer
Meson 98, Krakow, Poland, May 30 - June 2 1998

Dohrmann, F.:
Status Report on HADES Drift Chambers MDC III, HADES Collaboration
Meeting, GSI Darmstadt, Dec. 1998

Dohrmann, F.:
Mesonenspektroskopie bei SIS-Energien mit HADES
Arbeitstreffen Kernphysik, Schleching, May 1999

Dohrmann, F.:
Das Elektronenpaar-Spektrometer HADES: Statusbericht
DPG, Freiburg, March 1999

Dohrmann, F.:
The HADES Project
Workshop on "Electromagnetic Radiation Off Colliding Hadron Systems: Dileptons & Bremsstrahlung" FZ Rossendorf, Apr. 1999

Dohrmann, F.: Strange Particles and Dileptons as Probes for the Properties of Hadrons and Hadronic Matter
Seminar, MIT, Cambridge, USA, May 1999

Dohrmann, F.:
Strange Particles and Dileptons as Probes for the Properties of Hadrons and Hadronic Matter
Seminar, Argonne Nat. Lab. , Chicago, USA, May 1999

Dohrmann, F.:
Medium Effects in Kaon and Antikaon Production in Nuclear Collisions at Subthreshold Beam Energies
Particles and Nuclei Int. Conference 1999 (PANIC99), Uppsala, Sweden, June 1999

Dönau, F.:
Transitional Pair Expansion in the Fock Space
Miniworkshop Quantum fluctuations and configuration mixing
FZ Rossendorf April 15 -17, 1998

Dönau, F.:
Vorlesungen zur Struktur des Atomkerns
Universität Göttingen, June/July 1998

Dönau, F.:
Cranking und Symmetriebrechung
Universität Göttingen, June 1998

Dönau, F.:
Die Magnetische Rotation - ein neues Phänomen der Kernanregung
Universität Stuttgart, July 1998

Dönau, F.:
Search for Proton-Neutron Pairing in Nuclei with Mass number A$\approx$ 70
EUROBALL PAC meeting, Legnaro, Italy, July 1998

Dönau, F.:
Tilted Cranking and Symmetry Restoration
Invited lecture at Istanbul School on Nuclear Physics

Istanbul, Turkey, Sept. 1998

Dönau, F.:
RPA on Excited States
Int. Miniworkshop on Medium Mass Nuclei, FZ Rossendorf, Febr. 1999

Dönau, F..:
RPA on Excited States
Seminar, Centre des Recherches Nucleaires, Strasbourg, April 15, 1999

Dshemuchadse, S:
TOF-Barrel: Einsatz und erste Experimente
COSY FFE-Treffen, FZJ, May 1999

Enghardt, W.:
Physikalische Grundlagen tomographischer Verfahren
Course, TU Dresden, WS 197/98

Enghardt, W.:
PET in der Schwerionentherapie - eine ganz besondere Anwendung nuklearer Technologie
FZ Rossendorf, Feb. 1998

Enghardt, W.:
Positron Emission Tomography for Quality Assurance of Cancer Therapy with Light-Ion Beams
Nucl. Phys. Spring Meeting Bochum, March 1998

Enghardt, W.:
Positronen Emissions Tomographie zur Qualitätssicherung der Schwerionentherapie
Institut für Strahlenschutzphysik der TU Dresden, Apr. 1998

Enghardt, W.:
Tomographische Rekonstruktion bei PET I: Analytische Verfahren
Klinik und Poliklinik für Nuclearmedizin des Universitätsklinikims Carl Gustav Carus der TU Dresden, Apr. 1998

Enghardt, W.:
Tomographische Rekonstruktion bei PET II: Algebraische Verfahren
Klinik und Poliklinik für Nuclearmedizin des Universitätsklinikums Carl Gustav Carus der TU Dresden, Apr. 1998

Enghardt, W.:
Tomographische Rekonstruktion bei PET III: Rebinning Verfahren
Klinik und Poliklinik für Nuclearmedizin des Universitätsklinikums Carl Gustav Carus der TU Dresden, May 1998

Enghardt, W.:
Radiotherapie mit Photonen und Elektronen (Teletherapie)
Institut für biomedizinische Technik an der Fakultät Elektrotechnik der TU Dresden, May 1998

Enghardt, W.:
Positron Emission Tomography for Quality Assurance of Cancer Therapy with Light-Ion Beams

Int. Nucl. Phys. Conf. Paris, Aug. 1998

Enghardt, W.:
Krebstherapie mit Schwerionenstrahlen
Lehrerfortbildung 1998:
Moderne kernphysikalische Methoden in der Medizin
FZ Rossendorf, Aug. 1998

Enghardt, W.:
Positronen Emissions Tomographie für die Qualitätskontrolle der Strahlentherapie mit ^{12}C-Ionen
29. Wiss. Tagung der Deutschen Gesellschaft für Medizinische Physik e.V., Dresden, Oct. 1998

Enghardt, W.:
PET: Grundlagen, nuklear-medizinische Anwendungen und Einsatz bei der Schwerionentherapie
Fortbildung med.-techn. Röntgenassistenten auf der 29. Wiss. Tagung der Deutschen Gesellschaft für Medizinische Physik e.V., Dresden, Oct. 1998

Enghardt, W.:
Positronen-Emissions-Tomographie zur Qualitätssicherung bei der Tumortherapie mit schweren Ionen
Virchow-Kolloquium Radio-/Thermotherapie, Berlin, Dec.1998

Enghardt, W.:
PET in der Schwerionen-Tumortherapie
FZ Rossendorf, Zentrumsseminar March 1999

Enghardt, W.:
Die Anforderungen der Strahlungsphysik an die ELBE-Strahlführung
FZ Rossendorf, ELBE-Seminar, June 1999

Enghardt, W.:
Radiotherapie mit Photonen und Elektronen (Teletherapie)
Inst. Für Biomedizinische Technik, Fakultät Elektrotechnik, TU Dresden, June 1999

Enghardt, W.:
Positronen Emissions Tomographie zur retrospektiven Dosislokalisation bei der Schwerionen-Tumortherapie
Wiss. Konferenz zur Jahrestagung 1999 der Wissenschaftsgemeinschaft Gottfried Wilhelm Leibnitz, München, Oct. 1999

Frauendorf, S.:
Isospin Symmetry and Pairing in N=Z Nuclei
Spring Meeting Holzhau, April 1998

Frauendorf. S.:
Marshak Lecture: Magnetic Rotation
Spring meeting of the American Physical Society, Miniworkshop on Magnetic Rotation, Columbus, USA, 1998

Frauendorf. S.:

Kernphysik
University of Notre Dame/USA, Jan. 1999

Frauendorf. S.:
Magnetic Rotation
Invited Lecture at Workshop on Physics at the Coulombbarrier
Yale University, June 1999

Frauendorf. S.:
Isospin Symmetry Breaking by T=1 p-n Pairing
Invited Lecture at Gordon Research Conf. on Nuclear Chemistry, New London, June 1999

Frauendorf. S.:
Quantenmechanik
University of Notre Dame/USA, SS 1999

Gallmeister, K.:
Dileptons from Open Charm and Bottom: Signal or Background in High-Energy Heavy-Ion Collisions?
DPG, Bochum, March 1998

Gallmeister, K.:
Diatonenspektren in relativistischen Schwerionenreaktionen
IKH/FZ Rossendorf, June 1998

Gallmeister, K.:
Charm, Bottom, Dileptonen bei RHIC und LHC
GSI-Theorietreffen, June 1998

Gallmeister, K.:
Charm, Bottom, Dileptonen bei RHIC und LHC
ISHEPP XIV, Dubna, Aug. 1998

Gallmeister, K.:
Physical Information in the Thermal Continuum Dilepton Spectrum
Erice/Italien: Meeting on Nucl. Physics, Sept. 1998

Gallmeister, K.:
Dileptonen von offenen Charm und Bottom in ultrarelativistischen Schwerionenstößen
Theorie-Seminar, TU Dresden, March 1999

Gallmeister, K.:
Dileptonen von offenen Charm und Bottom in ultrarelativistischen Schwerionenstößen
DPG Freiburg, March 1999

Gallmeister, K.:
Dileptons in Ultrarelativistic Heavy-Ion Collisions
WDS 99, Charles University Prague, June 1999

Gippner, P.:
Überlegungen zum ELBE-Seminar

IKH/FZ Rossendorf, Sept. 1998

Gippner, P.:
Strahlführung zum MID-IR FEL
ELBE Seminar FZ Rossendorf, Jan. 1999

Grosse, E.:
Experimentelle Methoden der Kern- und Teilchenphysik
Course, TU Dresden SS 1998

Grosse, E.:
The FEL Projects at the Rossendorf Radiation Source ELBE
Proc. 20^{th} Int. Conf. On Free Electron Lasers, Williamsburg, USA, Aug. 1998

Grosse, E.:
Überlegungen zum ELBE-Seminar
IKH/FZ Rossendorf, Sept. 1998

Grosse, E.:
Die Strahlungsquelle ELBE im Forschungszentrum Rossendorf:
Berlin, BESSY II-Projektteam, Jan. 1998

Grosse, E.:
Bericht über HADES-Arbeitstreffen in Krakau;
IKH/FZ Rossendorf, March 1998

Grosse, E.:
Relativistische Schwerionenreaktionen
TU Dresden, March-May 1999

Hasch, B.G.
Die physikalischen Grundlagen einer Verifikation des Bestrahlungsplanes in der Schwerionen-Tumortherapie mit der Positronen-Emissions-Tomographie
GSI Darmstadt, Jan, 1999

Herbach, C.-M.:
Spaltung schwerer Kerne in drei Fragmente mit annähernd gleicher Masse:
Institutsseminar TU Dresden, Dez. 1998

Hinz, R.:
Positronen-Emissions-Tomographie als Monitor der räumlichen Präzision der Dosisapplikation bei der Schwerionentherapie
GSI Darmstadt, Jan. 1998

Hinz, R.:
Positronen-Emissions-Tomographie zur Kontrolle der Schwerionen-Tumortherapie
Inst. für Biomedizinische Technik, Fakultät Elektrotechnik, TU Dresden. Apr. 1998

Hinz, R.:
Positronen-Emissions-Tomographie zur Kontrolle der Schwerionen-Tumortherapie
Seminar am Inst. für Kern- und Teilchenphysik, Fakultät Math. und Naturwissenschaften, TU

Dresden, June 1998

Hinz, R.:
In-Situ PET Monitoring of Heavy-Ion Therapy at GSI Darmstadt
Medical Research Council Cyclotron Unit, London, July 1998

Hinz, R.:
Simultankontrolle der Strahlentherapie mit Schwerionen durch Positronen-Emissions-Tomographie
32. Jahrestagung der Deutschen Gesellschaft für Biomedizinische Technik, Dresden, Sept. 1998

Hinz, R.:
The In-Situ PET Monitoring of the ^{12}C Therapy at GSI
XXIX PTCOG Meeting, Heidelberg, Sep. 1998

Hinz, R.:
PET Monitoring of Heavy-Ion Therapy
ECAT Technical Users Meeting, Amsterdam, Apr. 1999

Kamanin, D.V.:
Light Charged Particles Accompanying ^{14}N(34 and 53 AMeV) and ^{40}Ar(38 AMeV) Induced Fission
DPG Frühjahrstagung, Bochum, March 1998

Kämpfer, B.:
Quantenfeldtheorie
Course, TU Dresden, WS, 1997/98

Kämpfer, B.:
Charm and Bottom and Dileptons in Ultrarelativistic Heavy-Ion Collisions
Winter Workshop on Nuclear Dynamics, Snowbird Utah, USA, Febr. 1998

Kämpfer, B.:
Quasiparticle Equation of State for Deconfined Matter
Seminar, LBNL Berkeley, Febr. 1998

Kämpfer, B.:
Transverse Flow in Relativistic Heavy-Ion Collisions
Seminar, LBNL Berkeley, Febr. 1998

Kämpfer, B.:
Dileptons, Charm and Bottom in Ultrarelativistic Heavy-Ion Collisions
Spring Meeting Holzhau, April 1998

Kämpfer, B.:
Quasiparticle Model of the Quark-Gluon Plasma
Workshop "Phase Transitions" in Less Houches, Apr. 1998

Kämpfer, B.:
Kosmische Phasenübergänge
Kosmologie-Kurs, Bad Honnef, July, 1998

Kämpfer, B.:
Dileptons, Charm and Bottom in URHICS
Erice/Italien: Int. Meeting on Nucl. Physics, Sept. 1998

Kämpfer, B.:
Comparison of Benchmark Tests
2^{nd}Workshop on Strangeness Production, Dez. 1998

Kämpfer, B.:
General Theory of Relativity
Course, TU Dresden, WS 1998/99

Kämpfer, B.:
Deconfined Matter
Theorieseminar Uni Heidelberg, Jan. 99

Kämpfer, B.:
Dileptons and Charm and Bottom
Bormio. Winter Meeting, Jan. 99

Kämpfer, B.:
Bericht über die Konferenz "Quark-Matter 99 "
IKH/FZ Rossendorf, May 1999

Kämpfer, B.:
Bericht über PANIC 99
FZ Rossendorf, July 15, 1999

Kämpfer, B.:
Quantenfeldtheorie
Course, TU Dresden, SS 1999

Käubler, L.:
Two and Three-Phonon States in ^{88}Sr
DPG Frühjahrstagung, Bochum, March 1998

Käubler, L.:
The Structure of the 4.743 MeV State in ^{88}S
DPG Frühjahrstagung, Freiburg, March 1999

Kotte, R.:
p-p Correlations in Central Collisions of Ru(Zr)+Ru(Zr) at 400 and 1530 AMeV. Search for systematic N/Z dependencies
FOPI collaboration meeting, Darmstadt, March 1998

Kotte, R.:
Proton-Proton Correlations in Central Heavy-Ion Collisions at SIS Energies and the Space-Time Extent of the Emission Source
CRIS98 2^{nd} Catania Relativistic Ion Studies, Acicastello, Italy, June 1998

Kotte, R.:
On the Time Sequence of Proton and Composite Particle Emission in Central Collisions of Ru(Zr)+Ru(Zr) at 400 AMeV
FOPI collaboration meeting, Warsaw, Poland, Sept. 1998

Kotte, R.:
On the Sequence of Proton and Composite Particle Emission in Central Collisions of Ru(Zr)+Ru(Zr) at 400 AMeV
Int. Workshop XXVII on Gross Properties of Nuclei and Nuclear Excitations, Hirschegg, Jan. 1999

Kotte, R.:
Phi's in the Helitron
FOPI Collaboration Meeting, Darmstadt, March 1999

Kotte, R.:
K± und ϕ-Erzeugung in Schwerionenstößen
IKH/FZ Rossendorf, Sept. 1, 1999

Lauckner, K.:
Ein 3D MLE-Algorithmus für die Positronen-Emissions-Tomographie während der Strahlentherapie mit Schwerionen
32. Jahrestagung der Deutschen Gesellschaft für Biomedizinische Technik, Dresden, Sept. 1998

Lauckner, K.:
Comparison between the In-Beam and the Out-Of-Beam Methods for PET Control of Carbon Ion Therapy
5th Biennial ESTRO Meeting on Phys. for Clinical Radiotherapy, Göttingen, Apr. 1999

Lauckner, K.:
Performance of the 3D MLE Algorithm Adapted to the Positron Camera BASTEI with Limited Angle Geometry
ECAT Technical Users Meeting, Amsterdam, Apr. 1999

Naumann, B.:
Konzepte zu den Beam dumps im Elbe-Projekt;
IKH/FZ Rossendorf, Okt. 1998

Naumann, L.:
Application of a Two-Dimensional Vertex Cut for Effective Separation of Kaon
KaoS Workshop, Cracow, June 2 1998

Naumann, L.:
Der Nachweis von Antiprotonen mit dem KaoS-Spektrometer
KaoS Workshop, GSI Darmstadt, Oct. 1998

Naumann, L.:
Differential Cross Section of Inclusive Kaon Production at 1 AGeV Au+Au Scattering
KaoS Workshop, at FZR, Dec. 1998

Neubert, W.:

Energy Spectra of Light Charged Particles in 1 AGeV Au+Au Collisions
FOPI meeting, Warsaw Sept. 1998

Pawelke, J.:
PET for Quality Assurance of Cancer Th4erapy with Heavy-Ion Beams
National Inst. of Radiological Sciences, Research Center of Charged Particle Therapy, Feb. 20 1998

Pawelke, J.:
PET-Monitoring for Control of Heavy-Ion Treatment at HIMAC
National Inst. of Radiological Sciences, Research Center of Charged Particle Therapy, May 1998

Pawelke, J.:
Positron Emission Tomographie at the Forschungszentrum Rossendorf
National Inst. of Radiological Sciences, Division of Advanced Technology for Medical Imaging, Aug. 1998

Pawelke, J.:
How Useful is the Method of PET Autoactivation Measurement for Control of Carbon Ion Therapy HIMAC?
Nat. Institute of Radiological Sciences, Research Center of Charged Particle Therapy, Apr. 1999

Pawelke, J.:
Study of Biological Activity Wash-Out by Irradiation of Rabbits with ^{11}C-Beams
Nat. Institute of Radiological Sciences, Division of Radiation Research, March 1999

Pawelke, J.:
Bericht zum Arbeitsaufenthalt am National Institute of Radiological Sciences in Chiba, Japan June 21, 1999

Peshier, A.:
Quasiparticle Description of Strongly Couplet Plasma
5th Int. Workshop on Thermal Field Theories and Their Applications, Regensburg, Aug. 1998

Peshier, A.:
Quasiparticle Description of Deconfined Matter at Finite Mu and T, ECT Int. Workshop on Understanding Deconfinement in QCD, Trento, Italy, March 1999

Peshier, A.:
Quasiteilchenmodell für stark gekoppelte Plasmen
DPG Freiburg, March 1999

Peshier, A.:
Thermofeldtheorie
Course, TU Dresden, SS 1999

Plettner, C.:
Kaonen-Nachweis mit dem FOPI-Detektor an der GSI;
Hadronenseminar TU Dresden, Dec. 1998

Plettner, C.:

Kaonenspektren bei mittleren Rapiditäten an FOPI
Seminar, FZ Rossendorf, Dec. 1998

Pönisch, F.:
PET bei der Krebstherapie mit ^{12}C-Strahlen: Resultate der klinischen Anwendungen, Gruppenbericht, DPG Frühjahrstagung, Hadronen und Kerne, Freiburg, March 1999

Scheinast, W.:
pA Runs at KaoS
Kaon Workshop at FZR, Dec. 1998

Scheinast, W.:
Kaon and Antikaon Production in Proton-Nucleus Collisions
WDS FFE-Treffen, May 1999

Schneider, Ch.:
K-Meson Production in p + C Interactions at the COSY-ANKE Spectrometer
Seminar, Argonne, July 1998

Schnare, H.:
Untersuchung mittelschwerer Kerne mit neuen Methoden der Gamma-Spektroskopie;
TU Dresden, Jan. 1998

Schnare, H.:
Magnetic Rotation in ^{82,84}Rb (s)
Int. Miniworkshop on Medium Mass Nuclei, FZ Rossendorf, Febr. 1999

Schnare, H.:
Magnetic Rotation in the Odd-Odd Nuclei
1^{st} Int. Conf. On Experimental Nucl. Phys. in Europe, Sevilla, June 1999

Schneider, Ch.:
ANKE @ COSY, Status and Proposals;
Hadronenseminar TU Dresden, Nov. 1998

Schneider, Ch.:
Bericht über die großen Drahtkammern für ANKE
COSY FFE-Treffen, May 1999

Seidel, W.,:
Freie Elektronen-Laserstrahlung - eine Perspektive für Rossendorf - möglicher Nutzen für Naturwissenschaft, Technik und Medizin?
Seminar TU Dresden, May 1998

Seidel, W.:
Angewandte Naturwissenschaft
Bergakademie/Freiberg, May 1998

Seidel, W.:
Freie Elektron-Laser
IFW/FZ Rossendorf, July 1998

Seidel, W.:
ELBE-Projekt mit FEL
TU Dresden, Jan. 1999

Seidel, W.:
Undulatoren für MIR-Bereich an ELBE
ELBE-Seminar/FZ Rossendorf, March 1998

Seidel, W.:
Freie Elektronen Laserstrahlung - Prinzip und mögliche Anwendungen
FWB/FZ Rossendorf, March 1999

Seidel, W.:
Undulatoren für MIR Bereich an ELBE
ELBE Seminar FZ Rossendorf, March 1999

Seidel, W.:
Projekt eines Frei-Elektronen-Lasers im FZR und mögliche Anwendungen
FWR/FZ Rossendorf, Apr. 1999

Seidel, W.:
Production of THz Radiation at ELBE
Meeting on Biological Systems, ENEA/Frascati, May 1999

Seidel, W.:
Stand der Arbeiten am "Gepulsten Injektor"
DESY- und Frascati - Undulatoren und ihr Aufbau an ELBE
FZ Rossendorf, June 7, 1999

Seidel, W.:
DESY-und Frascati-Undulatoren und ihr Aufbau an ELBE
ELBE-Seminar FZ Rossendorf, June 1999

Servene, Th.:
Untersuchungen der magnetischen Dipolbande in Br-79;
Hadronenseminar TU Dresden, Jan. 1998

Schnare, H.:
Untersuchung mittelschwerer Kerne mit neuen Methoden der Gamma-Spektroskopie;
TU Dresden, Jan. 1998

Schwengner, R.:
M1 bands in Heavy Rb Isotopes
Workshop on Applications of High-Precision Gamma-Spectroscopy,
University of Notre Dame, Notre Dame, Indiana, USA, July 1998

Schwengner, R.:
Magnetic Rotation in the Mass 80 Region
Special Physics Division Seminar, Argonne National Laboratory, Argonne, Illinois, USA, 7.7. 1998

Schwengner, R.:
Das Zyklotron U-120 - langjährige Basis der Rossendorfer Kernstrukturforschung
Kolloquium "40 Jahre Rossendorfer Zyklotron U-120", FZ Rossendorf, Sept. 1998

Schwengner, R.:
Planned Spectroscopy in Medium Mass Nuclei
Int. Miniworkshop on Medium Mass Nuclei, FZ Rossendorf, Febr. 1999

Schwengner, R.:
Stand der Arbeiten am "Gepulsten Injektor"
Planungen für den Kernphysik-Meßplatz
FZ Rossendorf, June 7, 1999

Wagner, A.
Coulomb-Aufbruch von ^{8}B
FZ Rossendorf, June 29, 1999

Wagner, W.:
Intensive Channeling-Strahlung an ELBE (Messungen);
IKH/FZ Rossendorf, Feb. 1998

Wolf, Gy.:
Vektor-Mesonen-Erzeugung in Schwerionenstößen;
IKH/FZ Rossendorf, March 1998

Wolf, Gy.:
Abschätzungen von Dileptonenraten für HADES-Experimente;
IKH/FZ Rossendorf, Sept. 1998

Wünsch, R.:
Grundlagen des FEL (Besonderheiten des planaren Undulators);
IKH/FZ Rossendorf, Jan. 1998

Wünsch, R.:
Undulatoren für ELBE
ELBE Seminar FZ Rossendorf, March 1999

Talks of Visitors

Auerhammer, J., IFW Dresden:
Experimente mit FELIX: Nichtlineare Optik-Laserablation an biologischem Gewebe
Apr. 20, 1999

Balabanski, D., Univertsity Sofia :
Study of the Quadrupole Deformation of the K=35/2 Isomer in ^{179}W with the Level Mixing Spectroscopy (LEMS) Method
Dez. 7, 1998

Bakker, R., BESSY Berlin:
Das Beschleunigerkontroll-System von BESSY II
Apr. 6, 1998

Blaschke, D., University Rostock:
Hadron Properties and Deconfinement in the Quark Matter Phase Diagram
Nov. 30, 1998

Berndt, O., MBI Berlin:
Zweifarben-Pump- und Kontinuum-Probe-Experiment - Transientenspektroskopie an Molekülen mit ausgedehnten π-Elektronensystemen
March 3, 1999

Bertsch, G., University of Washington Seattle:
Physics of Atomic Clusters
May 28, 1999

Birse, M., University Manchester:
Chiral Symmetry and QCD Sum Rules
May 27, 1999

Birse, M., University Manchester:
Seeing the Lighter Side of Quarks?
May 31, 1999

Birse, M., University Manchester:
Renormalization Group Approach to Two-Body Scattering
June 1, 1999

Bohn, C., TJNAF Virginia:
Commissioning Jefferson Laboratory's Superconducting Free-Electron Laser: Trials, Tribulations, and Successes
Jan. 18, 1999

Braun, D., Montanuniversity Leoben:
Modellrechnungen zu selektiv oxidierten VC-Lasern
Jan. 4, 1999

Cassing, W., University Giessen:
Mesonen-Erzeugung in pp-, pA- und AA-Reaktionen nahe an der Schwelle
June 14, 1999

Cleymans, J., University of Cape Town, South Africa
Particle Ratios at SIS, AGS and SPS: Unified Description of Freeze-Out Parameters
July 26, 1999

Cleymans, J., University of Cape Town, South Africa
Diskussion der dynamischen Ausfrierbedingungen in Schwerionenreaktionen
July 27, 1999

Ciofi degli Atti, C., University Perugia:
Semi-Inclusive Deep-Inelastic Scattering off Nuclear Systems
Dez. 14, 1998

Crosson, E., HEPL Stanford University:
Electron Beam Bunch Measurements at Stanford
May 4, 1999

Csernai, L.P., University Bergen:
Can we Observe Disoriented Chiral Condensates
Jan. 26, 1998

Dietrich, J., FZ Jülich:
Strahldiagnose am Synchrotron mit externer Strahlanregung
Jan. 25, 1999

Dressler, R., PSI Villigen:
Bies Methode zur Auswertung von Experimenten
Sept. 10, 1998

Dressler, R., TU Dresden:
Synthese neutronenreicher Isotope schwerster Elemente in xn- und α-xn-Reaktionen - Läßt sich die Produktionsrate vorhersagen?
May 17, 1999

Dudek, J., University Strasbourg:
Pseudospin in Nuclear Structure
July 5, 1999

Düren, M., University Erlangen:
Neue Resultate vom HERMES-Experiment bei DESY
Jan. 29, 1999

Enders, J., TU Darmstadt:
Scissors Mode: Status und neuere Resultate
june 28, 1999

Gallerano, G.P., ENEA Rom:
Investigation of the Effect of Energy-Phase Correlation on the Coherent Emission from a Bunched Electron Beam
June 29, 1998

Gontchar, I.I., State Railway University Omsk:

A Langevin Model for Fission
Febr. 4, 19999

Gover, A., University Tel-Aviv:
Innovative Free Electron Radiation Schemes
March 17, 1999

Grigoryan, L.Sh., Inst. of Applied Problems of Phys. NAS, Yerevan, Armenia:
Influence of Acoustic Waves on Channeling Radiation
Aug. 16, 1999

Hayn, R., TU Dresden:
Optische Eigenschaften von Hochtemperatursupraleitern
March 8, 1999

Hilscher, D., HMI Berlin:
Nukleare Untersuchungen zur Spallations-Neutronen-Quellen für Strukturforschung, Transmutation und Energieezeugung
May 4, 1998

Hildenbrand, K., GSI Darmstadt:
Stopping, Equilibration and Directed Flow in Heavy-Ion Collisions of Symmetric Systems between 0.1 and 2 A·GeV
June 15, 1998

Jing-Ye Zhang, University of Tennesee (USA):
Lack of Additivity in Mass-190 Superdeformed Bands
June 8, 1998

Jokinen, A., University Jyväskylä:
Spectroscopy of Proton Rich Nuclei in sd and fp-Shells
June 2, 1998

Junghans, A., GSI Darmstadt:
Untersuchungen zur Kollektivität von Kernanregungen in der Fragmentation relativistischer Uranprojektile
Oct. 5, 1998

Kalionska, D., Inst. f. Org. Chemie, Sofia:
Biomolecular Studies with IR
July 20, 1999

Kilian, K., FZ Jülich:
Resultate und Perespektiven der Hadronenphysik an COSY
June 22, 1998

Knoll B., MPI für Biochemie Martinsried:
Vibrationskontrast in der Infrarot-Nahfeldmikroskopie
May 5, 1999

Kotte, R., FZR Rossendorf:

Analyse von Φ-Mesonenausbeuten an FOPI
May 3, 1999

Köster, U., LMU München:
Experimente mit der ISOLDE Laserionenquelle
June 2, 1998

Krappe, J., HMI Berlin:
Pairing in Cold Fission
May 12, 1998

Krause-Rehberg, R., University Halle
Untersuchung von Kristalldefekten mit Positronen
July 12, 1999

Lehnert, U., State University Kansas:
Erzeugung von Röntgen-Strahlung in Ion-Oberflächen-Stößen
Dez. 21, 1998

Marian, M.-A., Bucharest, Romania:
Industrial and Medical Application of Solid State Lasers Operating in Near-Infrared Region
Apr. 20, 1999

Mikaihailov, A., Institute for Nucl. Research, Sofia, Bulgaria:
One Some Recent Developments of the Semiconducor Detector Laboratory of the Institute for Nuclear Research at Sofia that might be used in FZ-Rossendorf
July 8, 1999

Morokhovskii, V., TU Darmstadt:
Untersuchung der parametrischen Röntgenstrahlung am S-DALINAC
May 11, 1998

Nölle, D., University Dortmund:
Status der Beschleunigeranlage DELTA und die aktuellen Ergebnisse der Inbetriebnahme des Free-Electron-Laser Experiments FELICITA I
Jan. 20, 1999

Oeschler, H., TU Darmstadt:
Pionen-Emission - eine Sonde für die Zeitevolution von Schwerionenreaktionen
July 20, 1998

Panteleeva, A.C. , Inst. for Nucl. Research and Nucl. Energy Sofia:
Influence of Low-Dose gamma-ray Irradiation on Mitosis and Adaptive Response of Pea Cells
Jan. 13, 1999

Pavlenko, O.P., ITP Kiev:
Electromagnetic Radiation of Fast Electrons Passing through Matter: Ter-Mikaelian-Effect
May 19, 1998

Pavlenko, O.P., ITP Kiev:
Scaling Properties of Dilepton Spectra in Ultrarelativistic Heavy Ion Collisions

Oct. 19, 1998

Pavlenko, O.P., ITP Kiev/FZR:
Zur Analyse der Dileptonendaten im NA38-Experiment
Apr. 12, 1999

Pavlenko, O.P., ITP Kiev/FZR:
Interpreting the Intermediate-Mass Continuum Dilepton Spectra in HICs at SPS Energies
May 7, 1999

Pfaff, H.-W., University Giessen:
Schwellennahe Mesonen-Erzeugung in pp-Stößen
Apr. 20, 1998

Pellemans, H., FOM Rijnhuizen:
FIR Spectroscopy at FELIX: Techniques and Applications
Nov. 2, 1998

Pflüger, J., DESY Hamburg:
Undulatoren für Strahlungsquellen der 4. Generation
Feb. 8, 1999

Piot, P., TJNAF, Virgina:
Controlling, Measuring and Monitoring Bunch Length in an Electron Linac
Jan. 11, 1999

Redlich, K., GSI Darmstadt:
Thermal Model and SIS-Doscopy of Proton Rich Nuclei in sd and fp-Shells
June 2, 1998

Rösler, S., CERN Genf:
Rechnungen mit dem Programmpaket FLUKA zur Abschätzung von Strahlenrisiken - dargestellt für das Cern-Experiment ALICE
April 9, 1999

Schmidt, R., TU Dresden:
Dynamik metallischer Cluster und von Fullerenen
June 30, 1999

Senger, P., GSI Darmstadt:
Pionen- und Kaonen-Produktion in Schwerionenstößen bei SIS-Energien
Jan. 19, 1998

A. Sibirtsev, A., University Giessen:
Strangeness-Production in pp-Collisions
Nov. 16, 1998

Stachel, J., University Heidelberg:
Hydrodynamische Expansion und kollektiver Fluß in Schwerionenreactionen
Jan. 14, 1998

Stöcker, H., University Frankfurt/Main:
Relativistische Schwerionenreaktionen: Analysen und Vorhersagen von Observablen
Okt. 12, 1998

Sturm, C., TU Darmstadt:
Produktion von Kaonen und Antikaonen in dichter Kernmaterie
July 6 , 1999

Schwettmann, A., Stanford University:
Recent Developments of the HEPL-ps-FEL
Apr. 23, 1999

Trautmann, W. , TU Darmstadt:
Experimente zum Flüssig-Gas-Phasenübergang in Kernmaterie
April 27, 1998

Wagner, A., East Lansing, Michigan, State University (USA):
Neue Detektionssysteme für die Mittelenergiephysik am NSCL
Okt. 6, 1998

Waschull, J., TU Berlin und Dresden:
Hochauflösende IR-Spektroskopie am gasförmigen Benzol
March 5, 1999

Wiedenhöver, I., Argonne National Laboratory (USA):
Experimente mit GAMMASPHERE am ANL
Sept. 21, 1998

Wolf, Gy., KFKI Budapest:
Coupled Channel Method for Meson-Nucleon Interaction
Apr. 20, 1999

Wolter, H., LMU München:
Zustandsgleichung von Kernmaterie und in Schwerionenstößen
Nov. 9, 1998

Yang, Ji-Ping, University Jena:
Kurze Laserpulse in der Forschung - ps- und fs-Dynamik mit Molekülen
March 1, 1999

Zakharov, B., FZ Jülich:
Landau-Pomeranchuk-Migdal Effect in QED and QCD
Nov. 23, 1998

THE INSTITUTE OF NUCLEAR AND HADRON PHYSICS

Departments of the Institute

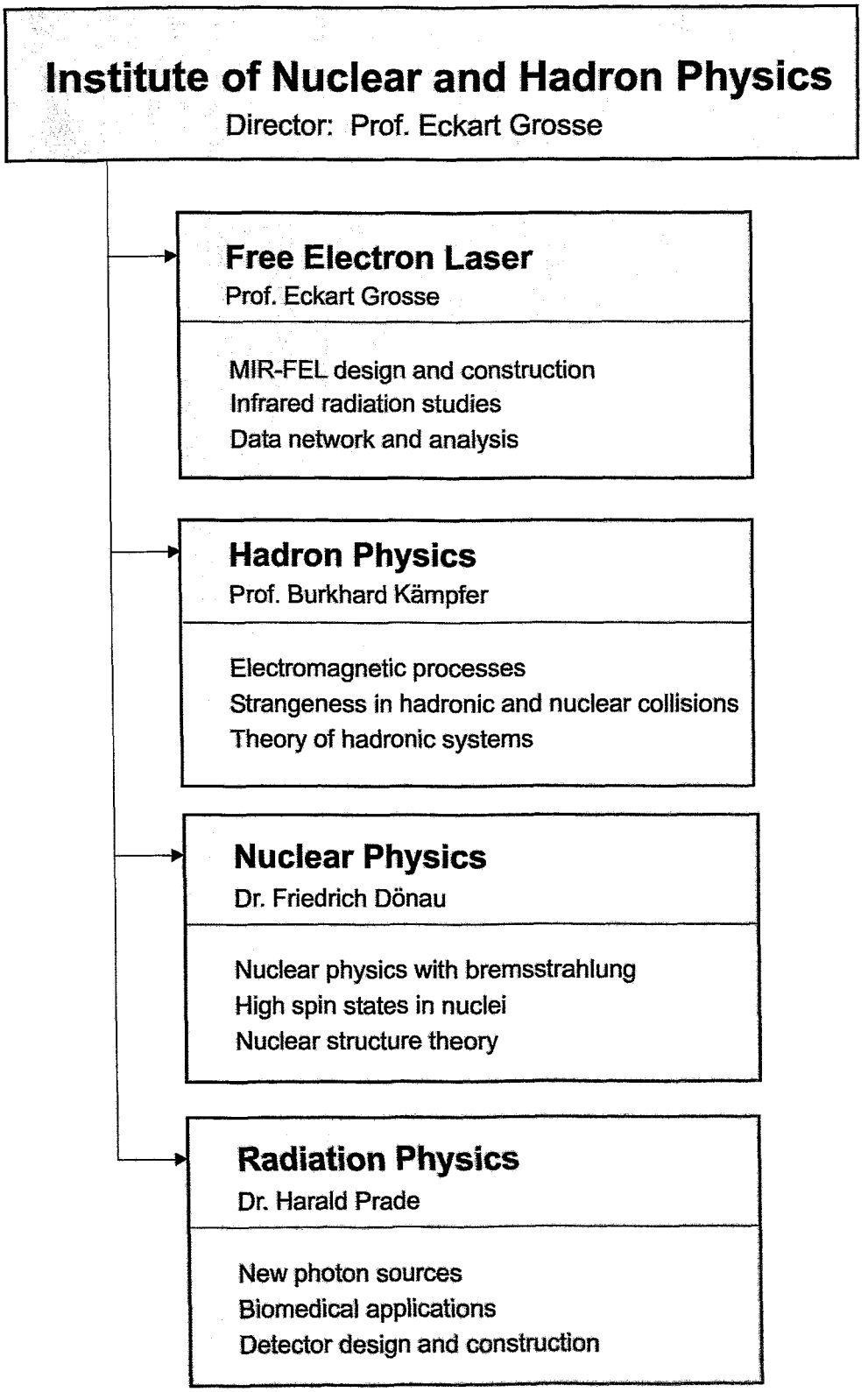

Personnel of the Institute for Nuclear and Hadron Physics

Director: Prof. E. Grosse[1]

Scientific Personnel

Dr. H.W. Barz
Dr. F.M. Dittes
Dr. M. Debowski
Dr. F. Dönau
Dr. F. Dohrmann
Dr. S. Dshemuchadse
Dr. W. Enghardt
Dr. S. Frauendorf
Dr. P. Gippner
Dr. B. Hasch
Dr. C.-M. Herbach
Dr. B. Kämpfer
Dr. L. Käubler
Dr. R. Kotte
Dr. K. Lauckner
Dr. u. Lehnert
Dr. P. Michel
Dr. K. Möller
Dr. H. Müller
Dr. B. Naumann
Dr. L. Naumann
Dr. W. Neubert
Dr. H.-G. Ortlepp
Dr. J. Pawelke
Dr. A. Peshier
Dr. H. Prade
A. Schamlott
Dr. K.D. Schilling
Dr. H. Schnare
Dr. M. Schlett
Dr. C. Schneider
Dr. R. Schwengner
Dr. W. Seidel
Dr. U. Steegmüller
Dr. A. Wagner
Dr. W. Wagner
Dr. M. Wenzel
D. Wohlfarth
Dr. R. Wünsch

PhD Students

D. Almehed
Ch. Borcan
K. Gallmeister
R. Hinz
D. Kamanin
A. Panteleeva
C. Plettner
F. Pönisch
D. Reppel
W. Scheinast
M. Schleif
Th. Servene

Technical Personnel

M. Altus
H. Angermann
U. Baumann
J.U. Berlin
M. Boeck
M. Böse
J. Fiedler
R. Förster
M. Freitag
K. Heidel
L. Heinrich
K.H. Hermann
J. Hutsch
J. Kerber
E. Kluge
D. Krüger
M. Langer
U. Oehmichen
M. Paul
B. Prietzschk
I. Probst
B. Rimarzig
H. Römer
M. Scheinpflug
Chr. Schneidereit
W. Schulze
J. Schwarzenau
M. Sobiella
U. Wolf

[1]also TU Dresden

Guest Scientists

Prof. Andrejtscheff, W.	INRNE Sofia
Dr. Alekseev, V.K.	JINR Dubna, Russia
Dr. Andronenko, M.	Inst. of Physics, St. Petersburg/Russia
Prof. Aslanyan, H. A.	Inst. of Physics,Yerevan/Armenien
DP Atamas, N.	University Kiew/Ukraine
DP Bakker, R.	BESSY II, Berlin
DP Balabanski, D.	University Sofia/Bulgaria
DP Berndt, O.	Max-Born-Institut Berlin
Prof. Birse, M.	University of Manchester/Great Britain
Prof. Blaschke, D.	University Rostock
Dr. Bohn, C,	T.Jefferson Laboratory, Newport News/Virginia
Dr. Braun, D.	Montanuniversity Leoben/Austria
Prof. Cassing, W.	Justus-Liebig-Universität Giessen
Prof. C. Ciofi degli Atti	University of Perugia/Italy
Dr. Chmel, C.	University Bonn
Dr. Crosson, E.	Stanford University/USA
Prof. Csernai, L.	University Frankfurt
Dr. Dietrich, J.	FZ Jülich
Prof. Dimitrov, V. I.	University Sofia/Bulgaria
Prof. Djolos, R.	JINR Dubna, Russia
Dr. Düren, M.	DESY Erlangen
DP Enders, J.	Inst. F. Kernphysik, TU Darmstadt
Dr. Franczak, B.	GSI Darmstadt
Dr. Gallerano, G. P.	ENEA Frascati and University Rom/Italy
Dr. Gettinger, A.	Omsk State Railway University/Russia
Dr. Gontchar, I. I.	Omsk State Railway University/Russia
Dr.Grinberg, M.	INRNE Sofia/Bulgaria
Dr. Hildenbrand, K.	GSI Darmstadt
Dr. Hilscher, D.	HMI Berlin
Prof. Jing-ye Zhang	University of Tennessee,Knoxville/USA
Dr. Jokinen, A.	CERN Genf
Prof. Kamys, B.	Institute of Physics, Krakow/Poland
Dr. Kaptari, L. P.	JINR Dubna, Russia
DP Kapusta, M.	Soltan Institute for Nuclear Studies, Swierk/Poland
Prof. Kilian, K.	FZ Jülich
Prof. Köster, U.	TU München
Prof. Knoll, B.	MPI f. Biochemie, Martinsried
Dr. Krappe, H. J.	HMI Berlin
Dr. Magner, A. G.	Institute for Nuclear Research, Kiew/Ukraine
DP Marian, M.-A.	Nat. Inst. Bucharest/Romania
DP Meier, Peter	University Regensburg
Prof. Mkrtchyan, A. R.	Physics Institute,Yerevan/Arm.
Dr. Mrktchyan, A.H.	Physics Insitute, Yerevan/Arm.
Dr. Mehrabyan, K.	Physics Institute, Yerevan/Arm.
Dr. Mirzoyan, V.	Physics Institute, Yerevan/Arm.
Dr. Morokhovskii, V.	TU Darmstadt
Dr. Moroz, V.D.	JINR Dubna, Russia
Dr. Nazmitdinov, R.	JINR Dubna, Russia
Dr. Nölle, D.	University Dortmund

Dr. Pavlenko, O .P.	Institute for Theor. Physics, Kiev/Ukraine
Prof. Dr. Paskevich, V.V.	JINR Dubna, Russia
Dr. Pellemans, H.	Inst. for Plasmaphysics, Rijnhuizen/The Netherlands
DP Pfaff, H.W.	University Giessen
Dr. Piot, Pr.	TJNAF CEBAF, Newport News/VA
Prof. Dr. Quasil, J.	University Prague/Czech. Rep.
Prof. Redlich, K.	GSI Darmstadt
Dr. Rösler, S.	CERN
Dr. Salamatin, V.	JINR Dubna
Prof. Schwettmann,A.	Stanford University/USA
Dr. Senger, P.	GSI Darmstadt
Dr. Semikh, S.S.	JINR Dubna, Russia
Dr. Sibirtsev, A.	JINR Dubna/University Giessen
Prof. Dr. Stachel, J.	University Heidelberg
Prof. Stöcker, H.	University Frankfurt
Tichtchenko, V.G.	JINR Dubna, Russia
Prof. Dr. Titov, A.I.	JINR Dubna, Russia
Dr. Toni, K.	Physics Institute, Yerevan/Arm.
Dr. Trautmann, W.	GSI Darmstadt
Dr. Wiedenhöver, I.	University Frankfurt
Dr. Wolf, G.	KFKI Budapest/Hungary
Dr. Wolski, D.	Soltan Institute for Nuclear Studies, Swierk/Poland
Prof. Dr. Wolter, H.	University München
Dr. Zakharov, B.	FZ Jülich

Awards

Forschungspreis des FZR 1998

Dr. W. Enghardt, Dr. B. Hasch, Dipl.- Ing. R. Hinz, Dipl.- Ing. K. Lauckner, Dr. J. Pawelke, Dipl.- Ing. M. Sobiella

Entwicklung und Aufbau der Positronen-Emissions-Tomographie (PET) in der Schwerionen-Tumortherapie

Doktorandenpreis des FZR 1998

Dr. A Peshier

Zur Zustandsgleichung heißer stark wechselwirkender Materie - konsistente Beschreibung stark gekoppelter Quantensysteme

Beste Auszubildende 1999

D. Krüger

Meetings organized by the Institute

Topic	Period	Number of participant
ELBE-Undulatoren	20.02.1997	20
Workshop on a Superconducting Photoelectron RF-Gun	20.05.1997	20
FEL-Nutzertreffen	10.12. - 11.12.1997	60
Holzhau-Meeting on Infrared Light and Secondary Radiation as well as on Electromagnetic Processes in Nuclei and Hadrons	30.03. - 04.04.1998	96
Workshop on Kaon Production	10.12. - 11.12.1998	52
Workshop on Medium Mass Nuclei	25.02. - 26.02.1999	48
Workshop on Electromagnetic Radiation of Colliding Hadron Systems	16.04. - 17.04.1999	48
FEL Workshop on Research with Infrared Radiation	30.08. - 31.08.1999	60